PB86-110210

REPORT NO.
UCB/EERC-83/14
JUNE 1985

EARTHQUAKE ENGINEERING RESEARCH CENTER

SHAKING TABLE TESTS OF LARGE-PANEL PRECAST CONCRETE BUILDING SYSTEM ASSEMBLAGES

by

M.G. OLIVA
R.W. CLOUGH

Report to the National Science Foundation

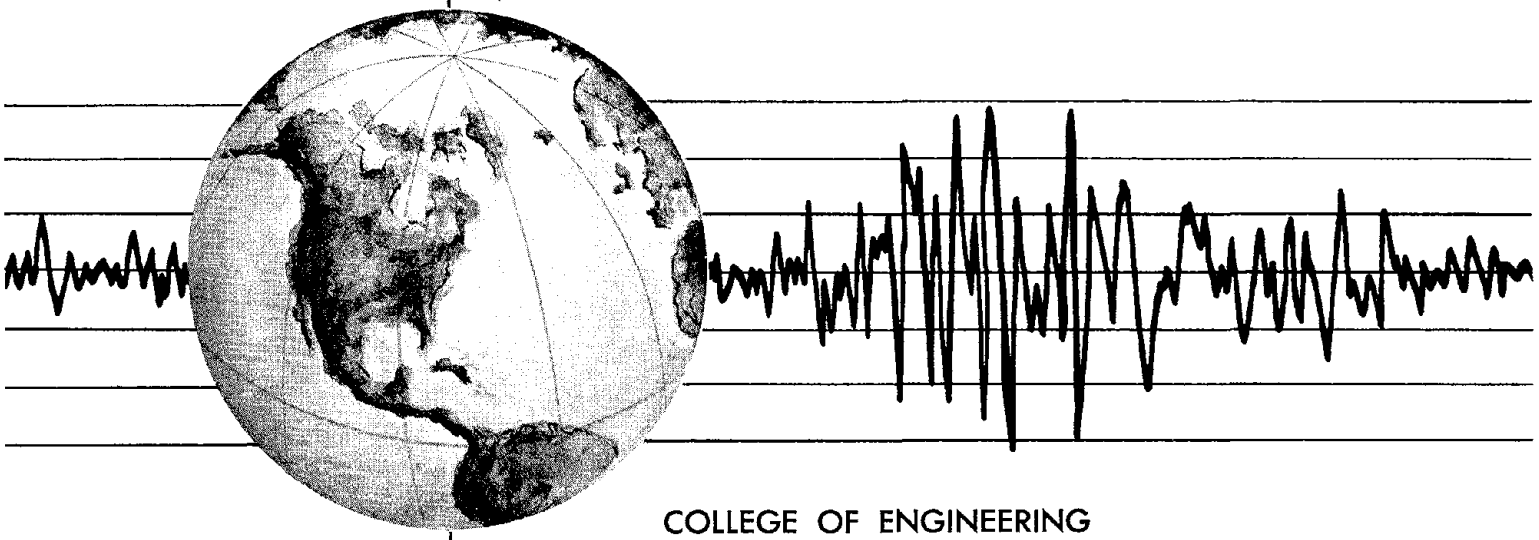

COLLEGE OF ENGINEERING

UNIVERSITY OF CALIFORNIA · Berkeley, California

50272-101

REPORT DOCUMENTATION PAGE	1. REPORT NO. NSF/CEE-83018	2.	3. Recipient's Accession No. PB86 110210/AS

4. Title and Subtitle

"Shaking Table Tests of Large-Panel Precast Concrete Building System Assemblages"

5. Report Date June 1985

6.

7. Author(s)

M. G. Oliva and R. W. Clough

8. Performing Organization Rept. No. UCB/EERC-83/14

9. Performing Organization Name and Address

Earthquake Engineering Research Center
University of California, Berkeley
1301 So. 46th Street
Richmond, Calif. 94804

10. Project/Task/Work Unit No.

11. Contract(C) or Grant(G) No.

(C)

(G) CEE-77-22527

12. Sponsoring Organization Name and Address

National Science Foundation
1800 G Street, N.W.
Washington, D.C. 20550

13. Type of Report & Period Covered

14.

15. Supplementary Notes

16. Abstract (Limit: 200 words)

This report presents the experimental studies of the first large scale shaking table tests of three panel wall structures. The experiments were performed at the University of California Earthquake Simulator Laboratory as part of a joint U.S.-Yugoslavia research project.

The test models consisted of a single bay simple wall, a single bay simple wall with door openings at each level, and a single bay flanged wall. The experimental results were examined to determine the relative importance of the controlling mechanisms, i.e., rocking and slip. The data was further studied to evaluate the degree of stiffness degradation and system ductility.

17. Document Analysis a. Descriptors

b. Identifiers/Open-Ended Terms

c. COSATI Field/Group

18. Availability Statement	19. Security Class (This Report)	21. No. of Pages
Release Unlimited		226
	20. Security Class (This Page)	22. Price
		A10

(See ANSI-Z39.18) *See Instructions on Reverse*

OPTIONAL FORM 272 (4-77)
(Formerly NTIS-35)
Department of Commerce

SHAKING TABLE TESTS OF LARGE-PANEL PRECAST CONCRETE BUILDING SYSTEM ASSEMBLAGES

by

M. G. Oliva

and

R. W. Clough

Report to the

National Science Foundation

Report No. UCB/EERC-83/14
Earthquake Engineering Research Center
University of California
Berkeley, California

June 1985

ABSTRACT

This report presents the experimental studies of the first large scale shaking table tests of three panel wall structures. The experiments were performed at the University of California Earthquake Simulator Laboratory as part of a joint U.S.-Yugoslavian research project.

The tests models consisted of a single bay simple wall, a single bay simple wall with door openings at each level, and a single bay flanged wall. The experimental results were examined to determine the relative importance of the controlling mechanisms, i.e., rocking and slip. The data was further studied to evaluate the degree of stiffness degradation and system ductility.

ACKNOWLEDGEMENTS

This investigation is part of an overall research program concerning the seismic response of concrete high rise residential buildings involving cooperative research between the University of California and the University "Kiril and Metodij", Skopje, Yugoslavia. The research described here was primarily sponsored by the National Science Foundation under grant No. CEE-77-22527 with additional travel assistance provided by the U.S. National Academy of Science and the Macedonian Academy of Science.

The authors wish to acknowedge the aid provided by Mr. Predrag Gavrilovic of the University "Kiril and Metodij", and by Mr. Dan Chen, a visiting scholar from the People's Republic of China, which was a significant contribution toward construction of the test specimens. Assistance during the testing program was received from Mr. Zhu Zhengkui, a visiting scholar from the People's Republic of China, and Mr. Bahram Mojaddad-Shahrooz, a student from the University of Wisconsin. Considerable additional assistance and advice was provided by the staff of the Earthquake Engineering Research Center, University of California.

TABLE OF CONTENTS

TABLE OF CONTENTS (Cont'd)

TABLE OF CONTENTS (Cont'd) Page

LIST OF TABLES

LIST OF FIGURES

LIST OF FIGURES (Cont'd)

LIST OF FIGURES (Cont'd)

LIST OF FIGURES (Cont'd)

LIST OF FIGURES (Cont'd)

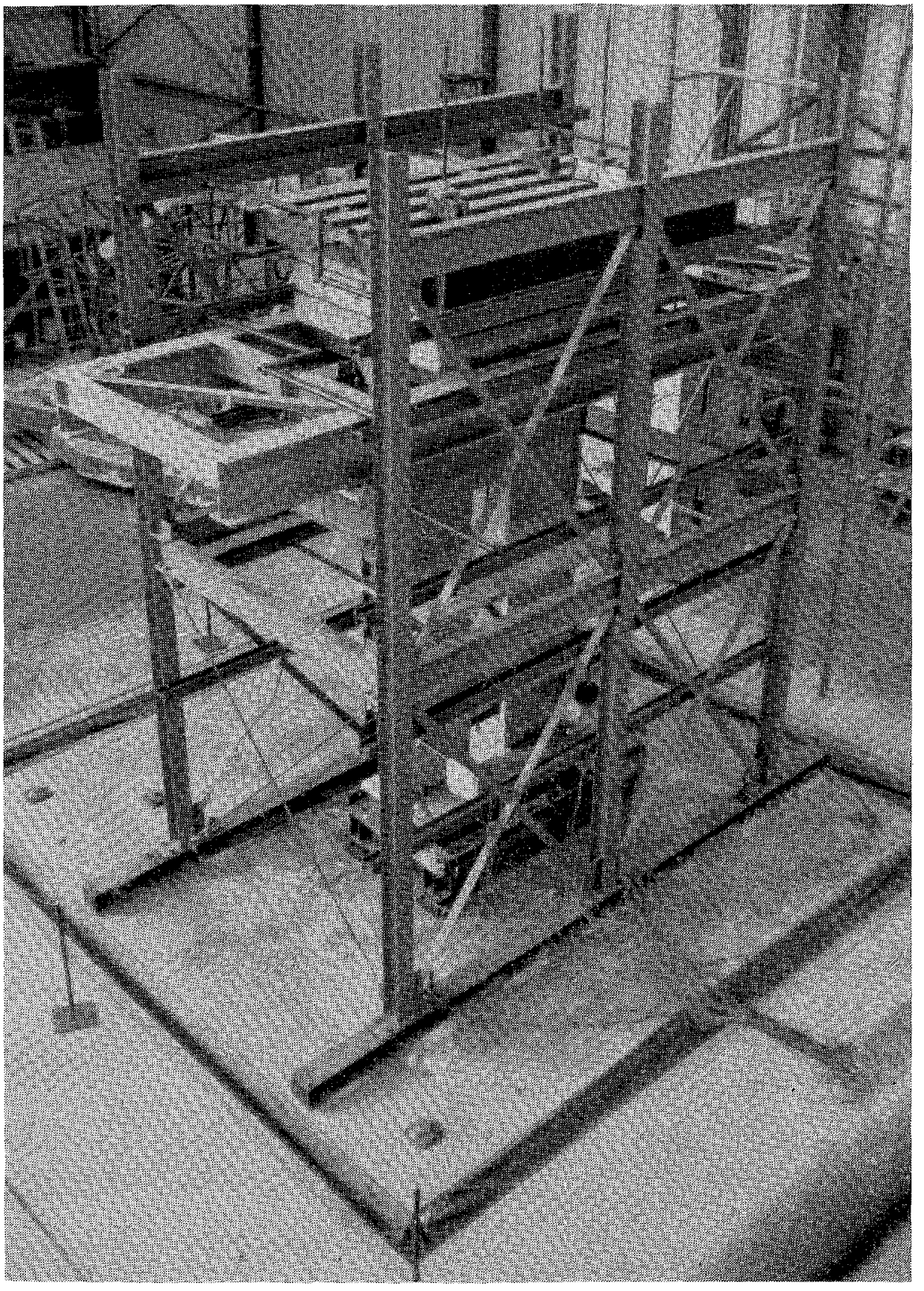

Figure 1.1 Precast panel wall model mounted on the shaking table with added mass system above and a lateral support frame on either side.

I. INTRODUCTION

1.1 Background of the Research Program

The research project described in this report is one phase of a continuing cooperative research program in earthquake engineering between the Institute of Earthquake Engineering and Engineering Seismology (IZIIS) of the University "Kiril and Metodij", Skopje, Yugoslavia and the Earthquake Engineering Research Center (EERC) of the University of California, Berkeley. In 1975, previous activities were extended with the principal thrust of the cooperative research directed toward "Seismic Stability of High-Rise Residential Buildings Constructed as Precast and Monolithic Reinforced Concrete Systems". The present project is the final phase of that research effort; it deals with the earthquake performance of high-rise apartment buildings constructed by assembling large precast concrete panels.

This investigation is an integrated research project using the structural test facilities and computers of both EERC and IZIIS. The test specimens were contributed by and also produced by the RAD Construction Company of Belgrade, Yugoslavia. The RAD Company supplied one-third scale model concrete panels, typical of their high-rise building system, to both EERC and IZIIS and similar full scale panels to IZIIS. The reduced scale panels were assembled into three different types of three-story assemblages, representing portions of high-rise buildings. The resulting specimens were tested on the shaking table at EERC, and at IZIIS by a pseudo-static test method. In this report, the shaking table test program carried out at EERC is described, and the test results presented. The parallel pseudo-static test program carried out at IZIIS is described in a separate report [6]*. Correlation of the results

*Numbers in brackets refer to the sources listed in the References.

from the two test procedures will be the subject of an additional report.

1.2 Seismic Response Mechanisms of Large Panel Buildings

The use of large precast concrete structures in housing has expanded within the last twenty years and should continue to grow. This growth has been due to a tremendous demand for housing, to economic and material limitations, to the need for non-labor-intensive construction methods, and to the desire to use factory quality-controlled labor rather than relatively low-skilled field labor.

Panel buildings are composed of vertical wall panels supporting horizontal floor panels to form the complete structure. Vertical panels are stacked and joined to create load bearing shear walls while horizontal panels act as diaphragms and gravity load collecting floor and roof systems. In reference 16 Zeck reviews the basic systems of large panel precast concrete structures and some of the typical joint types.

Initially, panel construction was limited to low-rise structures in non-seismic regions. However, since such construction is now used for high-rise buildings in regions of high seismic risk, its safe design is of great importance. For low amplitude motions, the behavior of panel buildings is similar to that of any other bearing wall structure. Under such ultimate loads as those induced by earthquake motion, however, their behavior changes in a distinctive fashion. The performance is different from that of cast-in-place construction because of (1) the different pattern and density of reinforcement due to construction and economic constraints, and (2) damage mechanisms concentrated in the connection region with subsequent softening of the overall structural stiffness.

In a simple wall system, which is a vertical stack of solid panels with only horizontal joints, two types of damage are likely to occur; overturning

moment distortion and shear slip. Overturning moment response, usually referred to as rocking motion, is the continual opening and closing of the horizontal joint. Because of this motion, panels do not remain plane at their horizontal edges, but undergo severe strain at the panel corners. Horizontal shear slip along the cracked joint is associated with the transfer of shear forces across the connection. Figure 1.2 illustrates these two mechanisms.

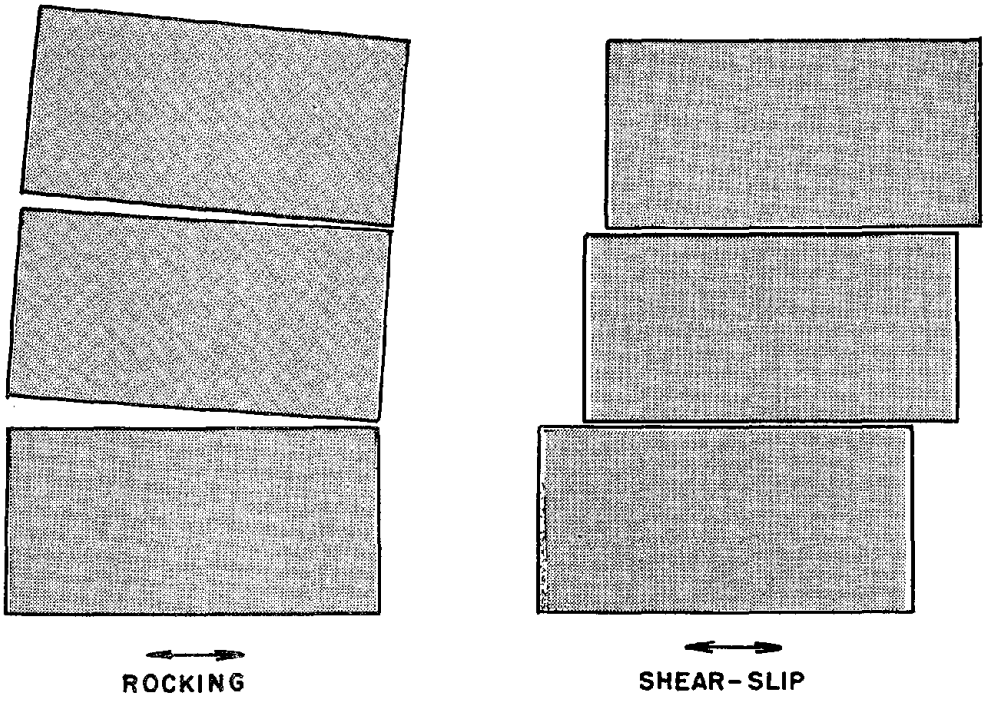

Figure 1.2 Overall wall deformation mechanisms

The crack opening and stress-concentration associated with rocking response can cause progressive deterioration of the panel corners and of the closed portion of the joint. The resulting crushing failure increases the amount of gap opening during a reversed cycle and induces cross sectional rotations with subsequent increases in the lateral deflections. Thus, rocking response can seriously threaten the overall stability of the structure. In spite of this, rocking response may exhibit moment-limiting behavior and

correspondingly lower force levels than for linear elastic response. This mechanism can also be a source of energy dissipation if the vertical reinforcement provides adequate continuity to develop yielding. Llorente [11] has examined this moment limiting effect and the energy dissipation of rocking response in a series of analytical studies.

Shear-slip response is controlled by the shear strength of the joint. If the shear force exceeds the shear strength, shear slip occurs. Shear transfer across the connection may be accomplished by (i) cohesion, (ii) Coulomb friction, (iii) shear friction and dowel action with vertical reinforcement, and (iv) direct bearing in the shear keys. It is typical, however, to assume that Coulomb friction mechanisms and direct bearing in the shear keys determine the ultimate shear strength of a connection since shrinkage and creep may destroy bond in the joints and a number of studies indicates that there is little influence from dowel action. On this basis, after the shear keys crush, the maximum shear force that can be transferred is $\mu(A_s f_y + N)$, where μ is the coefficient of friction, A_s is the area of vertical reinforcing steel, f_y is the yield strength of reinforcing steel, and N is the compressive normal load due to dead weight. The term in parenthesis represents the total compressive normal force that could possibly be developed. ACI Code [1] recommends $\mu = 1.0$ for plain connections, but under cyclic loading, values as low as 0.4 and even 0.2 have been suggested [4,9]. The reinforcement term, $A_s f_y$, needs significant shear displacement (slip) in order to be active. Shear resistance initially is provided by direct bearing on shear keys and by Coulomb friction neither of which require relative slip to be mobilized. It should be noted that the total compressive normal force is not constant but varies with the amplitude of overturning moment and the amplitude of slip; therefore, shear slip occurs at different shear force levels. In other words, if the normal load in the compression region of the connection drops, the amount of shear

force which can be transferred decreases and slip can occur at a lower force level.

In a series of analytical studies, Llorente [11] considered the potential of shear slip as a source of force isolation and energy dissipation. These studies concluded that shear slip cannot be counted upon as a reliable mechanism for two major reasons. First, as the discussion in the last paragraph clearly indicates, it is unlikely that shear slip will occur unless the normal load is small (e.g., in the upper levels of a building), the coefficient of friction is low, or the reinforcing bar mechanism does not clamp the section together. Thus, it is questionable whether shear slip movement can effectively be mobilized. The second reason concerns the stability of the entire building. Shear slip degrades the strength of horizontal joints which are the primary load bearing elements. Damage to the connection and the consequent shear slip, therefore, may lead to eccentricity in the shear wall and this could threaten the stability and integrity of the building.

In summary, rocking response and shear-slip movement are generally influenced by coefficients of friction across the joint, transverse loads, the clamping effect of reinforcement crossing the cracked connection, the amount of coupling action between tension reinforcement and compression concrete (depending on their strength and stiffness), and the existence of shear keys. Therefore, the energy dissipation that can develop as a result of these two joint deformation mechanisms may vary considerably.

For simple walls with both door openings and end flange walls, the aforementioned mechanisms can also be expected to prevail, and this would lead to subsequent degradation of the horizontal connection. However, there will also be a coupling effect through the door lintels and/or through the vertical connections between the wall panel and the end flanges. Such coupling mechanisms modify the stiffness of the walls and provide a potential for energy

dissipation in their inelastic response. Thus they improve the seismic behavior of the walls. Any premature shear-slip movement in a horizontal connection, however, may adversely affect the possible energy dissipation of the coupling mechanism; therefore, in order to ensure better seismic resistance, a weak vertical connection or a weak lintel with a strong horizontal connection has been suggested [12,13]. This design philosophy is intended to avoid degradation of the load bearing horizontal connections, which may threaten the overall stability of the building. It should, however, be noted that this deformation concept assumes the vertical connections or door lintels to have adequate deformability or energy dissipation capacity.

The seismic behavior of panel structures has been studied analytically by several authors. For example, Llorente [11] has investigated the response of simple precast concrete walls, while Mueller and Becker [12] have studied the effects of vertical joints in the seismic behavior of I-shaped composite walls. Unfortunately, these analytical studies cannot, as yet, be practically applied because they are based on the very limited experimental data currently available. Most existing experimental studies involve only low amplitude vibration tests, static equivalent tests of subassemblages, and ambient vibration [3,5,13,15] monitoring.

1.3 The RAD Large Panel Building System

The RAD Construction Company of Belgrade, Yugoslavia specializes in design and construction of all types of high rise buildings both nationally and internationally. Toward the end of the 1960's, a great demand for the construction of residential buildings in Yugoslavia induced RAD to direct a considerable part of its capacity to the construction of residential buildings. A factory for the production of residential building components was completed in the late 1970's, and to date four and a half thousand residential units in

buildings of various story heights have been constructed.

Almost 90% of Yugoslavia is seismically active, so from the beginning, theoretical and experimental studies were initiated to assess the characteristics and behavior of these building systems under seismic conditions. Improvements in design, production processes, assemblage details and construction followed. In general, previous large panel construction had been conceived for non-seismic areas and therefore required modification for economical and structurally desirable construction in seismic areas.

A prefabricated large panel system consists of vertical bearing panels, nonbearing walls, and horizontal floor planks industrially produced and then assembled into a building structure at the site. The particular system used by RAD is characterized by methods of connecting prefabricated elements using cast-in-place 'wet' joints.

1.3.1 Description of the Structural System

Structural vertical bearing panels in both of the building's orthogonal directions form the basis of the structural system, with prefabricated floor planks resting on the walls. Particular walls may be non-structural elements depending on location and system requirements. The prefabricated elements are erected and jointed at the construction site. The distribution of structural walls in a typical building plan is shown in Figure 1.3.

Buildings constructed with this system typically have structural walls oriented so that uniform stiffness results along both of the building's orthogonal axes. The walls are placed in a modular pattern and receive vertical dead and live loads from the floor planks according to the plan of the wall system and the sequence in which the floor planks are assembled into a monolithic floor system.

1.3.2 Vertical Wall Panels

The vertical wall panels of the prefabricated wall system are reinforced monolithic units. The panels are cast with all the reinforcement required for panel strength and the connections to form joints with adjacent elements. The panel thickness is 16 cm, 19 cm or 22 cm, depending on the location of the panel in the building.

The basic characteristics of a typical vertical bearing panel without openings are shown in Figure 1.4, and include the following:

a) side denticulation of the panel with protruding stirrup reinforcing for connection with adjacent panels of the same story,

b) wire fabric mesh in the middle of the panels with deformed bars along the edges,

c) bolt connections for joining to adjacent panels above and below,

d) flat area at panel top for supporting floor planks,

e) denticulation of edge at the base of the panel.

Reinforcement at the ends of the panels is welded to a steel box housing a bolt connection, see Figure 1.5. The bolt connection is installed during erection to provide continuity between panels above and below resulting in some vertical continuity over the height of the building. A large key is cast at the end of each wall together with the cast-in-place joint concrete below the wall. In Figure 1.5 such a key is evident below the joint between the two vertical wall panels. Vertical reinforcement is also provided in the cast-in-place vertical joints between panels. The continuous reinforcing in the vertical joints and reinforcing bolted together between upper and lower panels are intended to improve the structural characteristics and deformability of the system during seismic motion significantly.

Many different combinations of walls are possible. Solid panels as shown in Figure 1.4 are available as well as panels with various door and window openings.

1.3.3 Floor Planks

Floors are made of industrially produced planks in widths of 120 cm, 180 cm, 240 cm and 300 cm (4 ft to 10 ft). The planks are simply-supported one way units which rest, during construction, on the wall panels; the planks are then joined to provide a monolithic two way multi-span floor diaphragm system to carry subsequent loads. Supporting the planks on the wall panels during construction allows casting of joint concrete without formwork, as is evident in Figure 1.6. Continuity between planks in one span and planks in the next span is provided by reinforcing the cast joint above the wall panel. Looped reinforcement protruding from each plank is overlapped and additional stirrups and belt reinforcement running lengthwise under the wall are placed in the joint. Then the joint can easily be cast from above.

1.3.4 Vertical Connection between Wall Panels

Vertical connections between wall panels run the full height of the building. A cross sectional detail of such a connection is shown in Figure 1.7. The adjoining panels provide all the forming needed for the joining grout. The cast-in-place concrete of the joint is confined by stirrups protruding from each of the adjoining panels. Two 14 mm bars are placed in the joint to provide some vertical continuity over the building height. The contact surface of the panels in the joint is denticulated for extra shear transfer. These connections link all adjacent wall panels, and the behavior of the wall system as a whole depends on the strength and deformability of the joint 'links'.

1.3.5 Connections between Floor Slabs

The connection which runs lengthwise between two adjacent floor planks is depicted in Figure 1.8. The protruding loops from the planks overlap and lengthwise reinforcing bars are added. The connection makes the floor system

act as a monolithic two way slab and diaphragm for subsequent loading.

1.3.6 System Development

Special teams from RAD collaborated with Civil Engineering Faculty of the Institute for Materials and Structures in Belgrade and the Institute of Earthquake Engineering and Engineering Seismology of the University "Kiril and Metodij", Skopje (see § 1.3) to plan a long term study of large panel prefabricated systems. Theoretical and experimental results from this program were first obtained in 1977 and continue today. The main topics under investigation are the following:

(a) The behavior of joint elements in prefabricated units when subjected to the static forces present in actual structures.

(b) The behavior of models of three-story sections of the structure, in particular the interaction of joined prefabricated panels under static and dynamic loads.

(c) The behavior of actual buildings evaluated through instrumentation of finished buildings to observe the dynamic characteristics of the structure under service conditions with motion resulting from natural phenomena or induced by means of eccentric vibration generators.

(d) Definition of characteristics of sites proposed for construction of buildings using the RAD large panel system.

1.4 Objectives and Scope

The general objective of this research program is to evaluate and improve the seismic performance of high-rise residential buildings assembled from large precast panel units. The RAD precast building system was selected as the specific type of construction to be investigated, and the RAD Construction Company provided the one-third scale panel units from which the

test structures were assembled. Parallel test programs on similar test models are being carried out by EERC and IZIIS, using the shaking table and pseudo-static test facilities of the two laboratories, respectively. In each laboratory, three types of test structure were constructed; each structure consisted of a model shear wall, three stories high, with floor plank elements at each level. The basic configurations of the three models were: (a) simple wall without openings, (b) simple wall with door opening at each level, and (c) wall without openings but with flanges at the edges.

In this report, the measured responses of the three test models to the shaking table excitation are described; results are presented in graphical form in such a way that the controlling response mechanisms (rocking and shear slip) may be identified and the ductility and damage mechanisms may be evaluated.

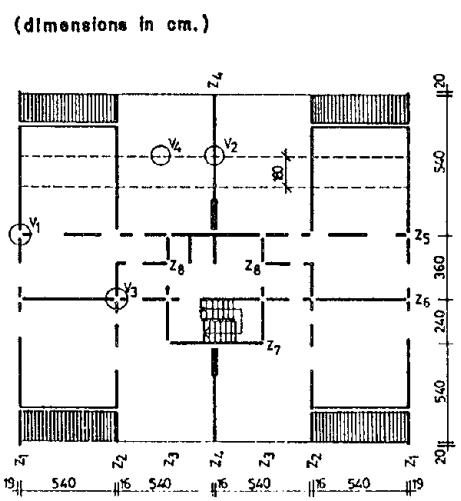

Figure 1.3 Typical plan of a high-rise panel building.

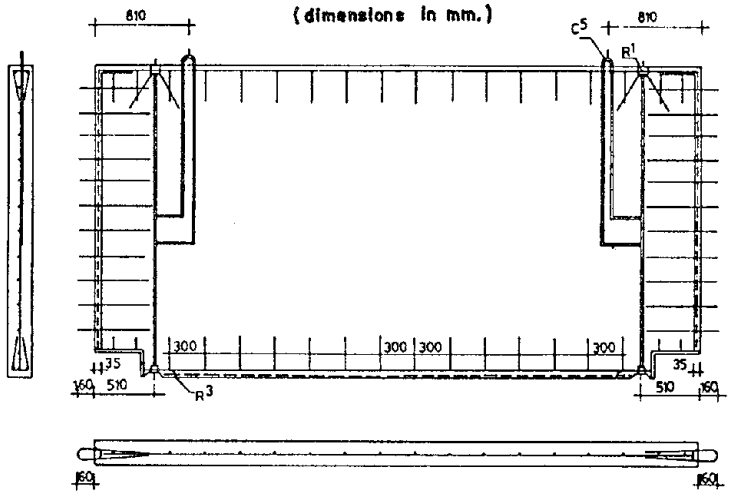

Figure 1.4 Detail of vertical bearing panel with ties and cast-in-place keys.

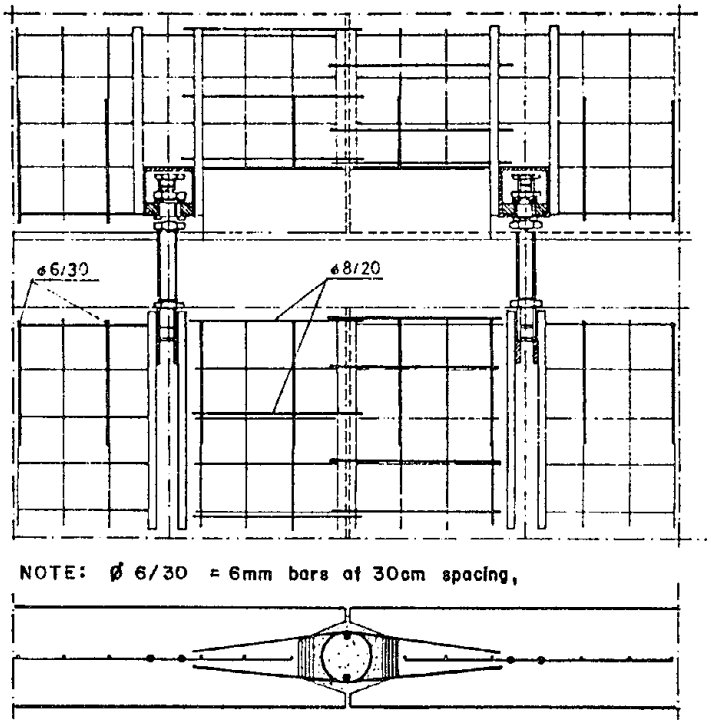

Figure 1.5 Detail of steel tie between vertical bearing panels.

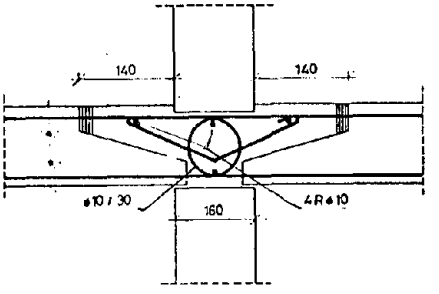

Figure 1.6 Horizontal connection between vertical panels.

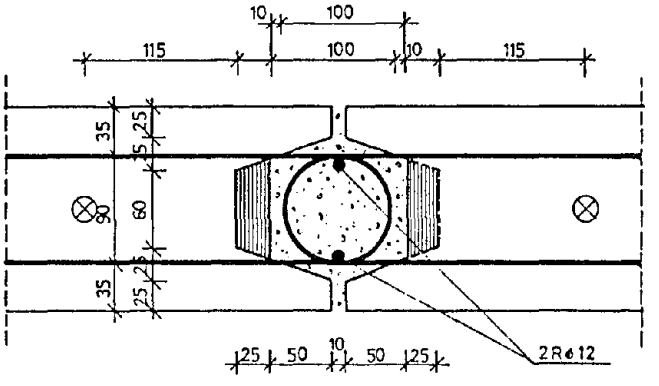

Figure 1.7 Vertical connection between bearing panels.

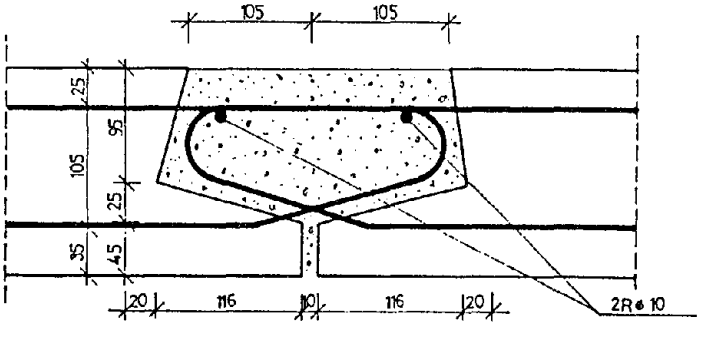

Figure 1.8 Horizontal connection between floor planks (mm. units).

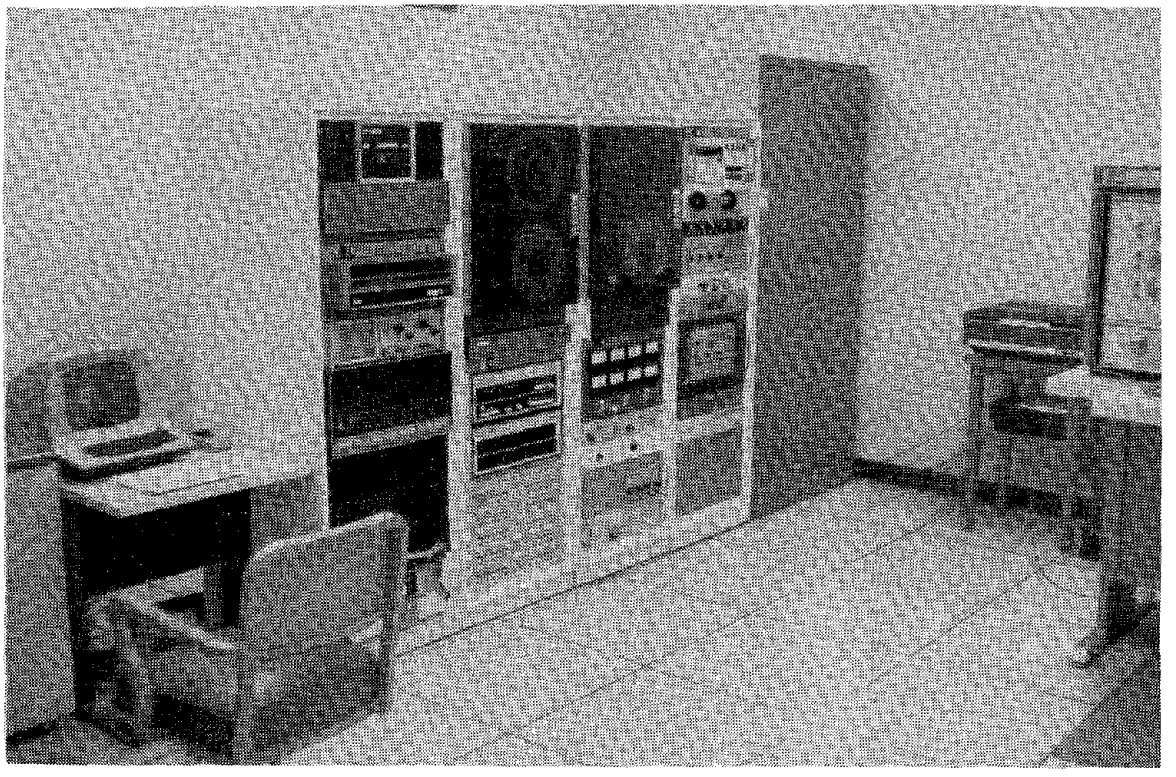

Figure 2.1 Control room with data acquisition computer.

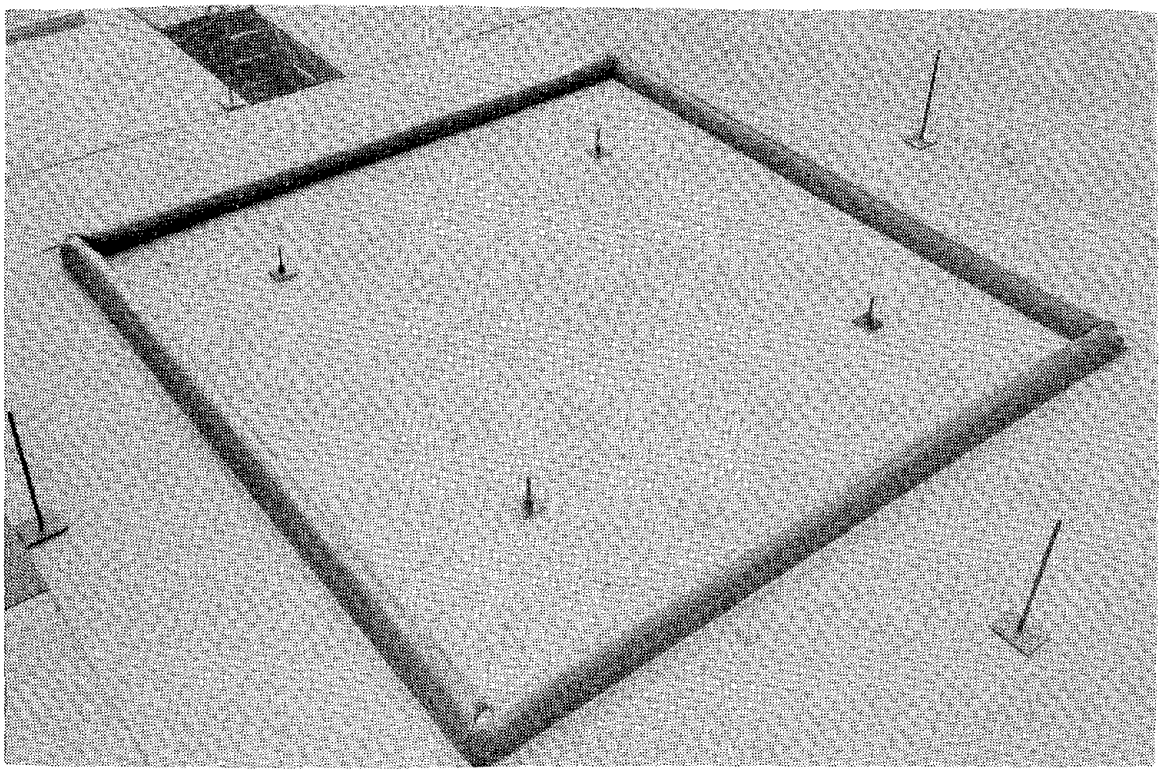

Figure 2.2 Shaking table, 20 ft x 20 ft (6.1 m x 6.1 m).

2. TEST FACILITIES

The experiments were performed at the Richmond Field Station Earthquake Simulator Laboratory of the University of California. This chapter briefly describes the primary testing facilities consisting of the shaking table and the data acquisition system, shown in Figures 2.1 and 2.2.

2.1 Earthquake Simulator

The 20 ft square shaking table is a 1 ft thick reinforced and post-tensioned concrete slab. This electronically controlled table simultaneously allows one horizontal and one vertical motion. The horizontal motion is achieved by three 50-kip hydraulic actuators; four 25-kip hydraulic actuators drive the table in the vertical direction. The vertical and horizontal capabilities of the shaking table are shown in Figure 2.3. These limitations are imposed by the capacity of the actuators and pumping system (see Rea and Penzien [14]). The shaking table itself weighs 100 kips and is able to subject structures weighing up to 100 kips to horizontal accelerations up to 0.67g. The table motion duplicates actual displacement time histories within capacity limitations.

2.2 Data Acquisition System

The primary function of the data acquisition system is the collection of data during tests. It is also used to generate the input command signals that drive the shaking table. The system consists of a NOVA 1200 mini-computer which operates with a Diablo 31 magnetic disk unit and a NEFF System 620 Analog-Digital processor. The mini-computer is capable of acquiring data from up to 128 data channels at rates up to 155 samples per second, per channel. The analog signals from the transducers are converted to digitized data through the analog-digital processor. The digitized data are

initially stored on magnetic disks, from which they can be transferred to magnetic tapes for permanent storage.

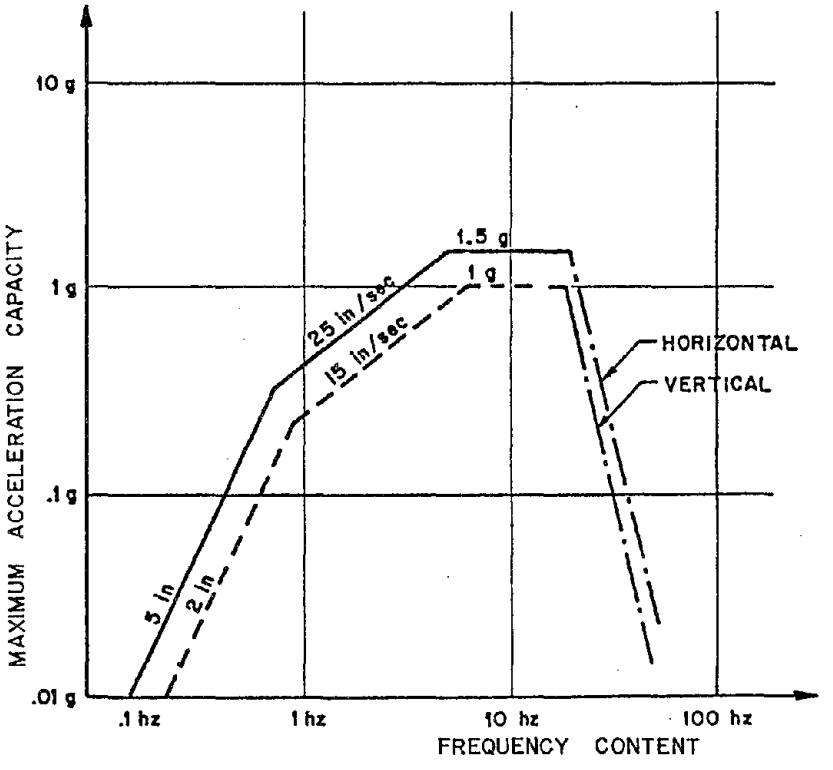

Figure 2.3 Shaking table motion capabilities

3. TEST STRUCTURES

The test models were true one-third scale three-story walls. They included a single bay simple wall (PZ-I), a single bay simple wall with door opening at each level (PZ-II) and a single bay composite wall (PZ-III), i.e., a simple wall with attached end flange walls. Throughout the rest of this report these models are referred to as PZ-I, PZ-II, and PZ-III, respectively. From tests of PZ-I it was possible to study the major failure mechanisms of an isolated wall. Observations of PZ-II and PZ-III provided additional insight into these mechanisms as well as the opportunity to investigate the effect of door lintels and vertical connections on the seismic behavior of such walls.

It was necessary to restrain lateral displacements of the wall system in order to prevent out-of-plane failure. Displacements in this direction were prevented using a special lateral restraint mechanism. This chapter describes the test fixture and the test models. The lateral support system is also explained briefly.

3.1 Test Fixture

The overall test setup consisted of the precast test panels, two steel platforms with mass blocks, lateral support frame, and a set of lateral linkages, as shown in Figures 3.1(a) and (b). The individual components are illustrated in Figures 3.2(a) and (b). This section explains the different parts and their purpose.

The steel frame provided support for the lateral linkage mechanism. The frame was stiffened in the longitudinal direction by angle X-braces and in the lateral direction by rod-turnbuckle X-braces. The lateral linkages were attached at the two ends of the test specimen at the second and the

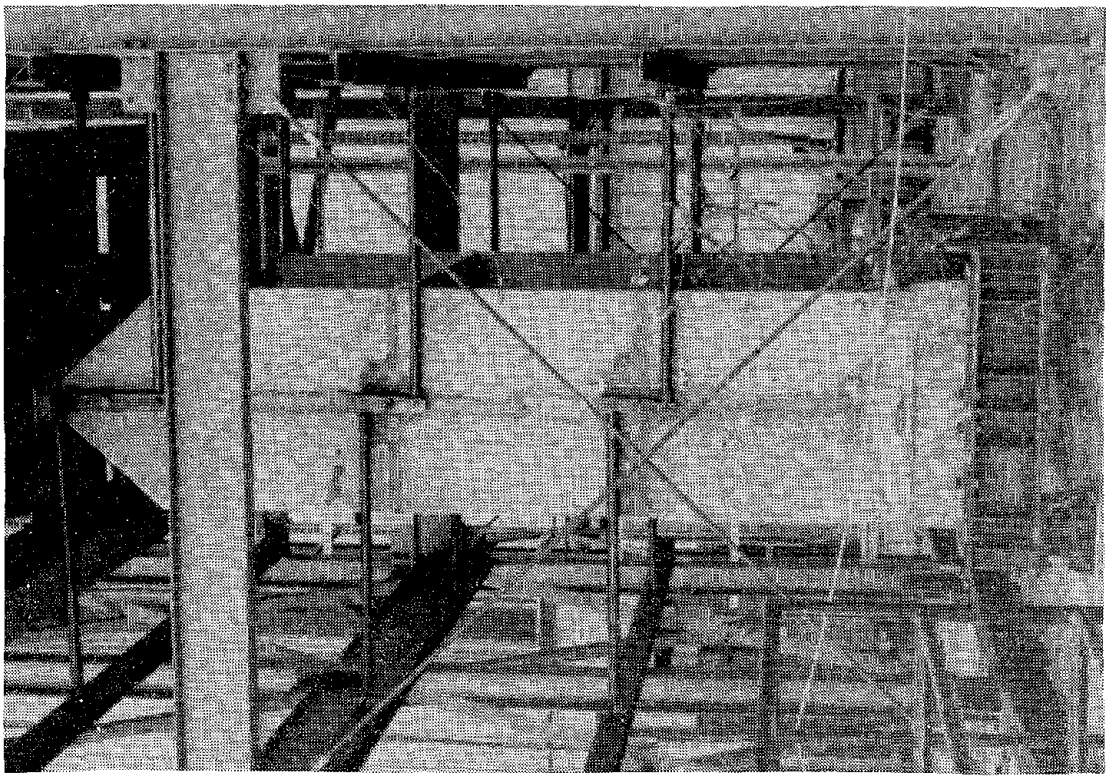

Figure 3.1a Front view, model and lateral support frame.

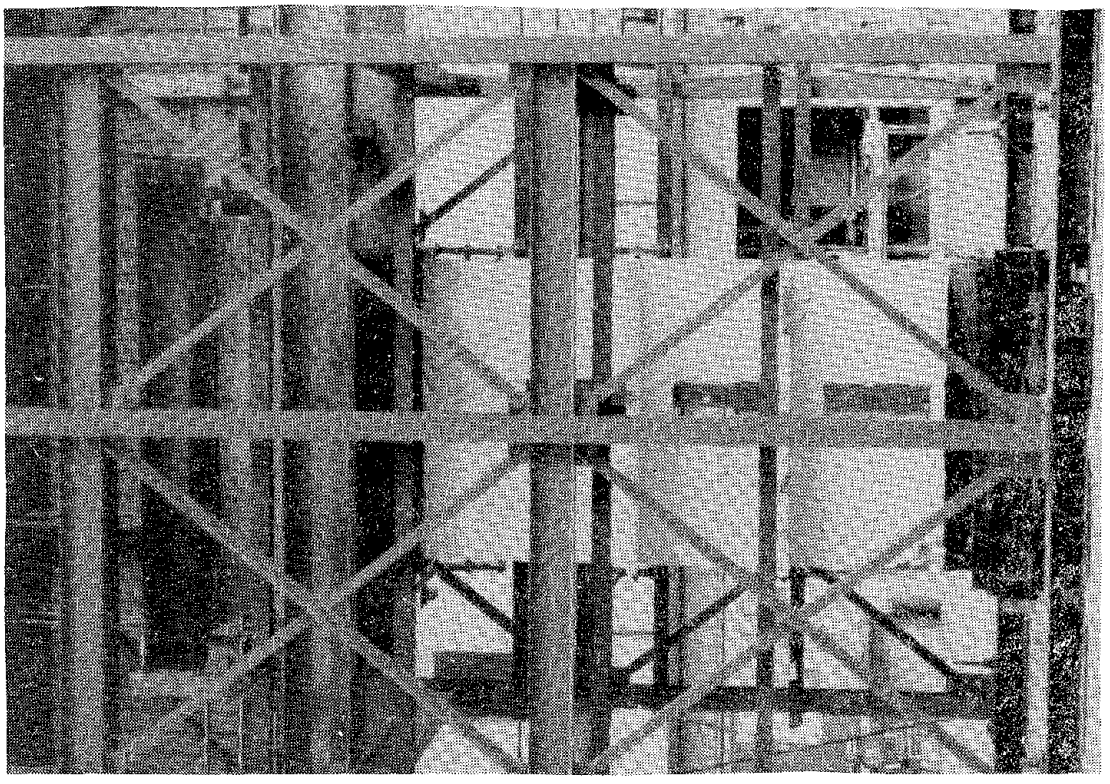

Figure 3.1b Side view, lateral bracing through linkage system.

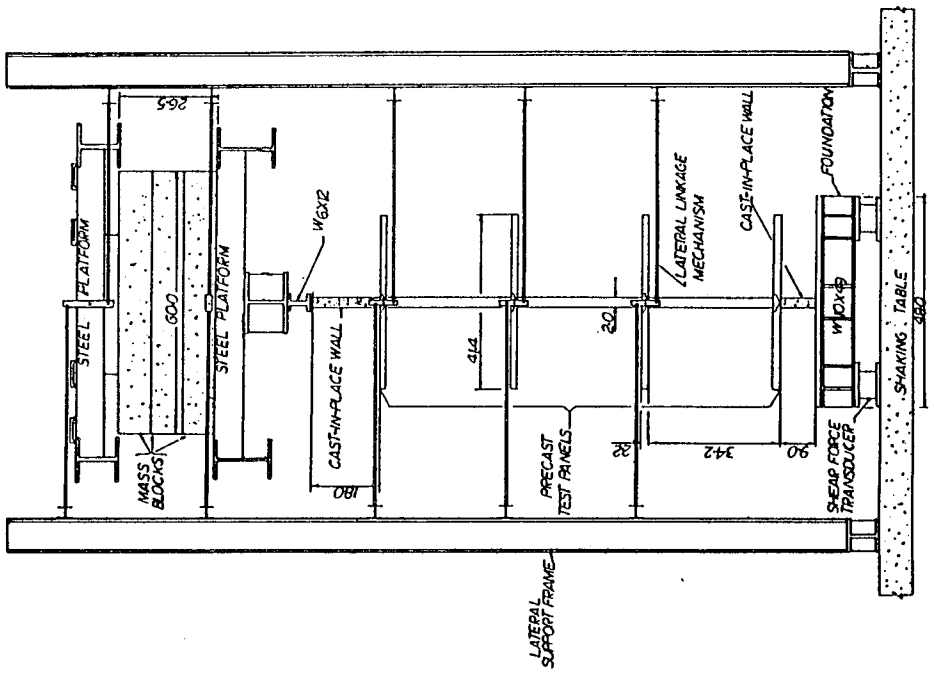

Figure 3.2b Side elevation of the test specimen layout.

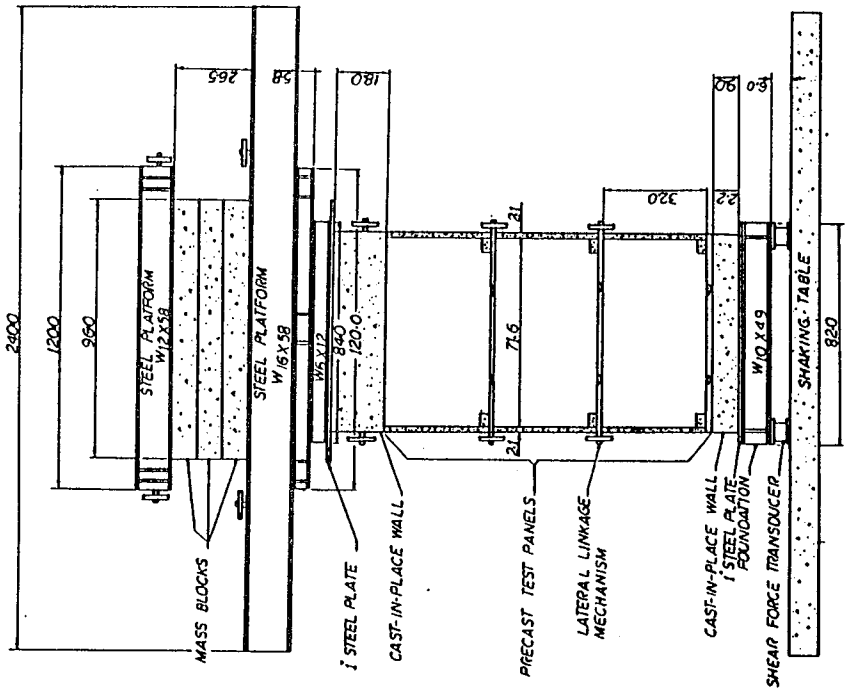

Figure 3.2a Front elevation of the test specimen layout.

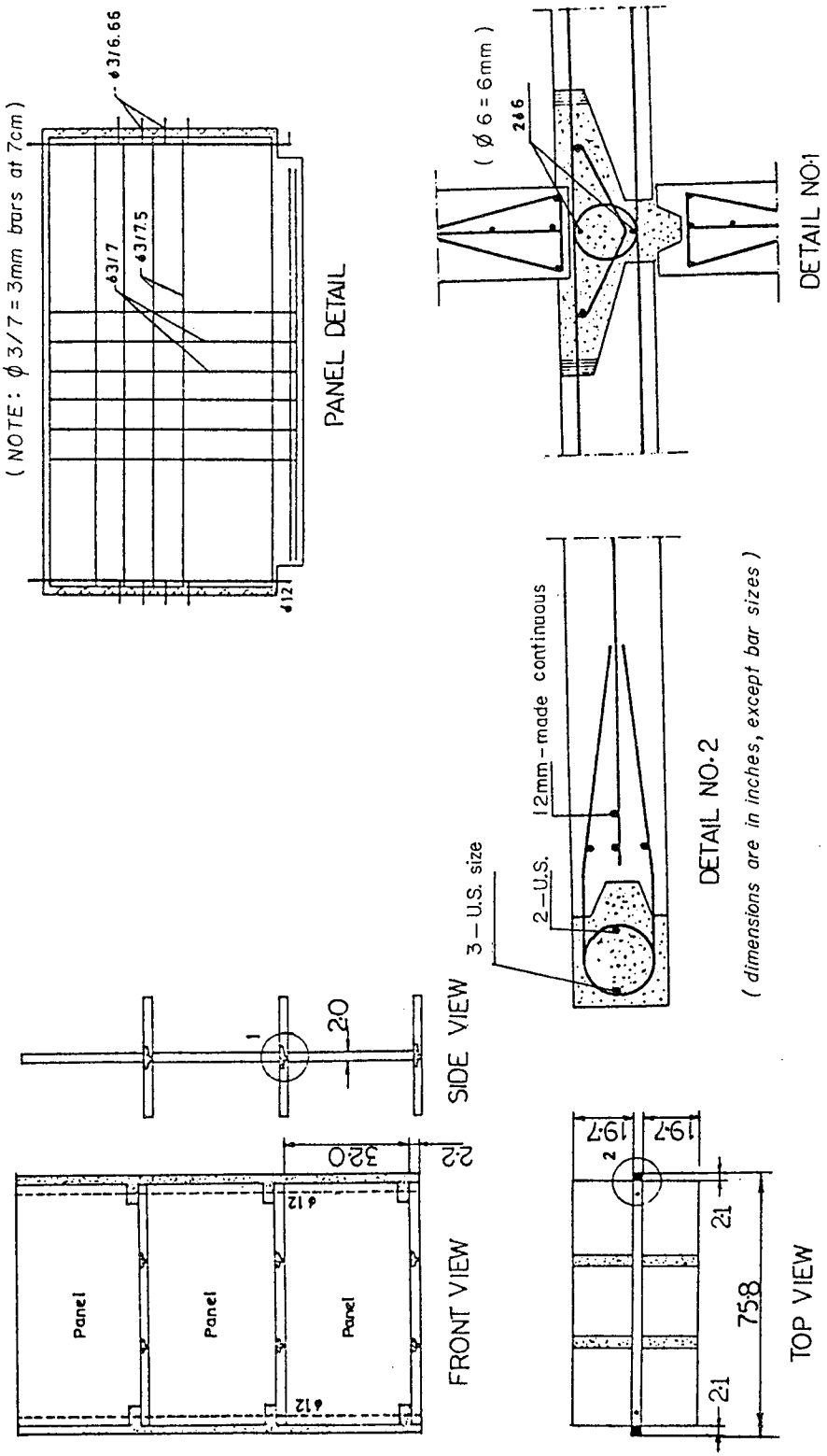

Figure 3.3 Configuration of model PZ-I, simple wall.

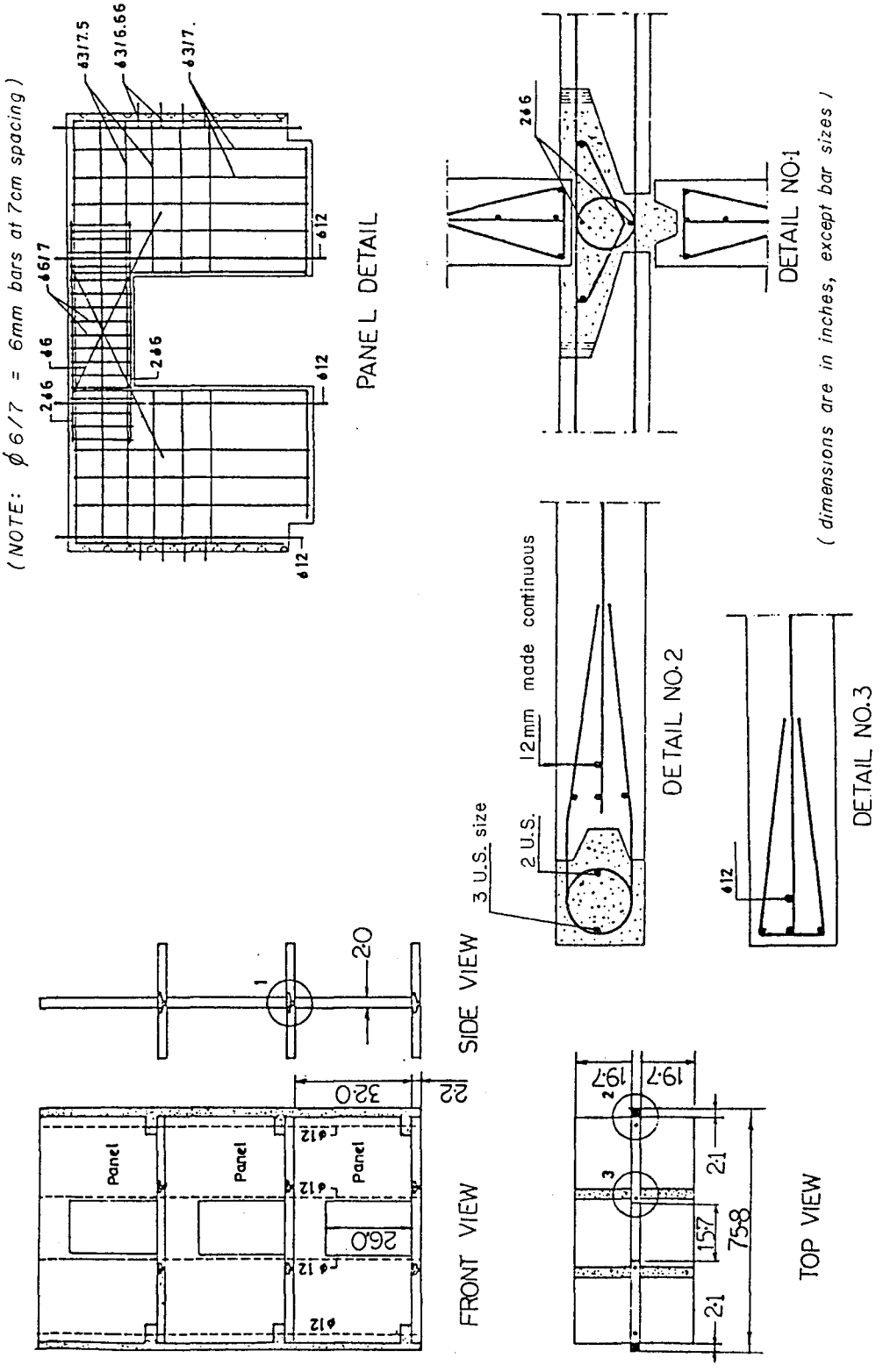

Figure 3.4 Configuration of model PZ-II, with doors.

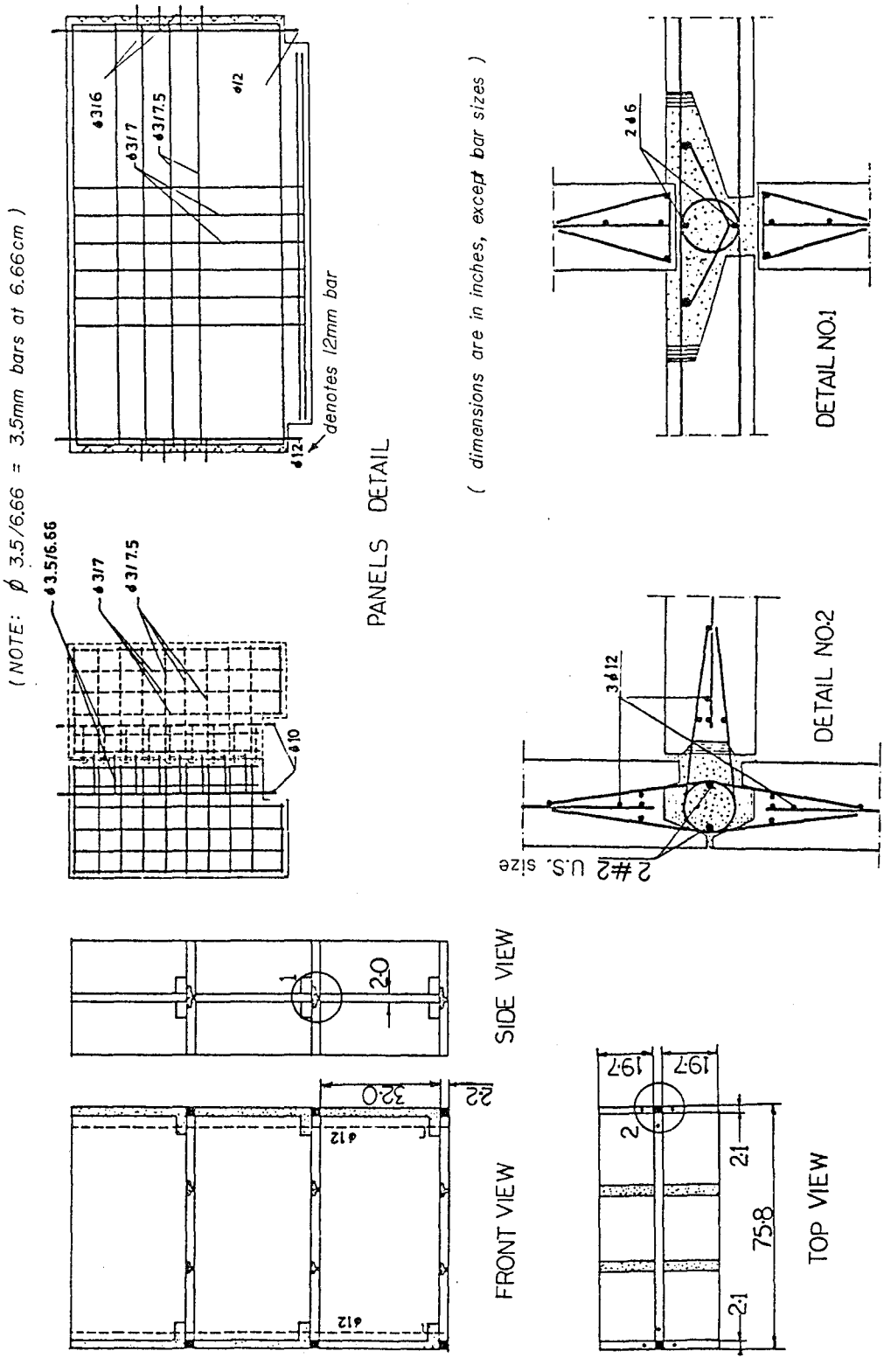

Figure 3.5 Configuration of model PZ-III, flanged wall.

third floor levels, at the top of the specimen, and below and above the mass blocks. These linkages were intended to prevent lateral displacement of the test model and to restrain lateral rocking of the blocks. Figures 3.2(a) and (b) show the location of these linkages. Ghanaat [8] describes the lateral support linkage system and its operational mechanism. Two concrete walls were cast in place at the top and the bottom of the precast panel walls. The top 18-inch cast-in-place wall was intended to distribute the axial loads to the wall system and particularly to the flanges of the flanged wall. The bottom wall was cast to connect the precast walls to the foundation. One-inch steel plates, welded to the vertical reinforcement, were bonded to the cast-in-place concrete at the base and the top of the model. The bottom steel plate was bolted to the W10x49 foundation, and the foundation was stressed down to the shaking table.

It was necessary that out-of-plane bending of the wall caused by lateral rocking or asymmetric placement of the added top masses be prevented, and it was also necessary to transfer the axial and induced longitudinal shear loads to the wall model. To achieve these results the top steel plate was bolted to a W6x12 girder. This small section provided "hinging" action about the axis parallel to the wall because of its thin laterally flexible web. The W6x12 girder was attached to a double W14x22 section which was intended to distribute the axial load uniformly.

The double section supported the 20 ft long steel platform. The lower surface of this platform had a 1.5 inch clearance above the top beams of the lateral restraint frame. This permitted its free movement but would prevent its dropping on the shaking table should collapse occur. This lower platform with another 10 ft long upper platform was used to prestress the mass blocks together as shown in Figures 3.2(a) and (b).

The selection of the mass blocks was based upon the desired load levels and the capabilities of the shaking table. By considering the total estimated axial stress expected in the middle of a typical 15 story building, the approximate overturning moment capacity of the wall system based on previous tests [6], and the necessary acceleration to develop such moment, an additional mass of approximately 18 kips was estimated to be necessary. The 20 ft and 10 ft long steel platforms weighed 4.5 kips and 2.5 kips, respectively. The additional axial load was provided using three 8 ft x 5 ft x 8 in. concrete blocks with a total weight of 12.2 kips. Therefore, a total weight of 19.1 kips of axial load was added to the wall system.

3.2 Test Models

The true one-third scale models represent walls with axial stresses similar to those near mid-height of a ten to twenty-story building. At this height the gravity axial loads are relatively small, so the walls are more susceptible to shear-slip failure. Furthermore, at this portion of a building there may be significant overturning moment which can induce rocking behavior. Thus, the tests enabled these two failure mechanisms to be investigated. The overall configuration and the geometry of the test models are illustrated in Figures 3.3, 3.4, and 3.5.

The particular panel connection system was of the wet-joint type; that is, the joint elements were cast-in-place concrete with reinforcement and precast elements arranged to eliminate formwork (see § 1.3.3). Vertical continuity was achieved using vertical reinforcement at the two ends of the wall with cast-in-place concrete surrounding them and bars within the panels spliced at the horizontal joint. Specific details of the joints and the design of the panels were developed from work at IZIIS in Skopje, the University of Belgrade and the RAD Company, Yugoslavia. A brief description

of the horizontal joints and the panel reinforcement is given in § 1.3; a complete description can be found in Reference 6. The test models, however, had minor differences in the vertical reinforcement at their two end joints. The size and the number of reinforcing bars were changed. Furthermore, during construction of PZ-III in order to close the joint properly, it was necessary to cut the horizontal hoops extending out of the wall panels. These cut hoops were welded shut before the concrete was cast.

As mentioned before, the test specimens were true one-third scale models made of the same material to be used in the prototype. Thus, the experimental results can be extrapolated to define prototype response, using the standard similitude ratios. The scale factors are summarized in Table 3.1.

TABLE 3.1

Scale Factors

Parameter	Model/Prototype
Length	r^*
Area	r^2
Stress	1
Mass	r^2 (due to added mass)
Force	r^2
Strain	1
Displacement	r
Acceleration	1
Time	$\sqrt{r}$
Period	$\sqrt{r}$
Moment	r^3

*$r = \frac{1}{3}$ geometric similitude of model/prototype.

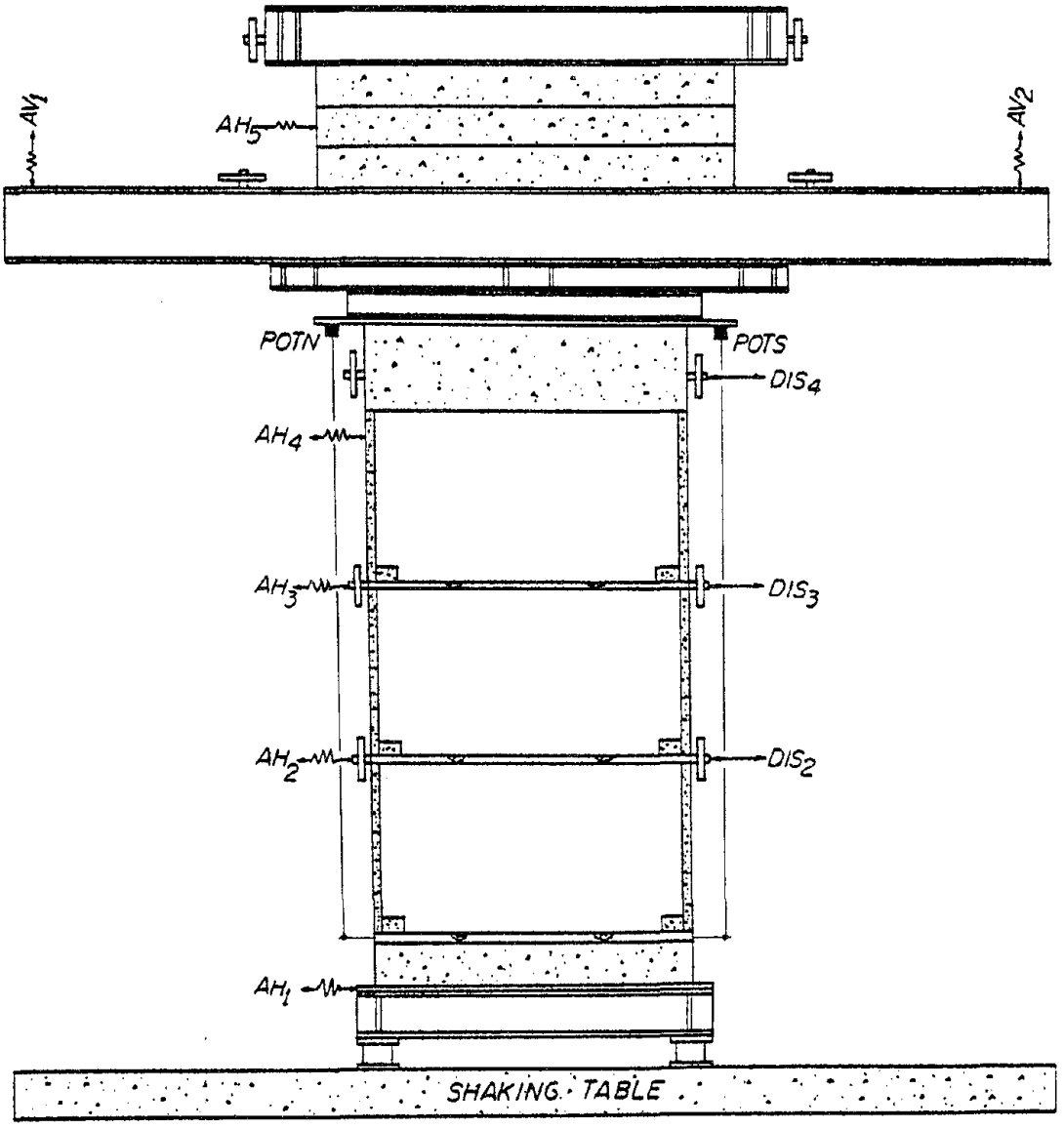

Figure 4.1 Locations of accelerometers and displacement measuring potentiometers placed on all three of the test models.

4. INSTRUMENTATION

Instrumentation used in these experiments was intended to monitor three types of dynamic response: (1) the shaking table motion, (2) the global response of the test models, and (3) the local deformations occurring in each model. Fifteen data channels were devoted to measuring the shaking table quantities. Global and local responses of models PZ-I, PZ-II, and PZ-III were monitored through 65, 73, and 70 channels of instrumentation, respectively. During all the tests, the scanning rate of the data acquisition system was set to 100 samples per second, per channel.

The measured dynamic responses included displacements and accelerations at all floor levels, horizontal and vertical accelerations of the added mass blocks, base shear force, slip and uplift of the wall panels along the horizontal joints, deformations in the wall panels, and strains in selected reinforcing bars. In the following sections, the measurement procedures are discussed, and the significance of the monitored responses is explained. A list of all the data channels for each wall model is included in Appendix A.

4.1 Acceleration Measurement

Setra accelerometers were used to quantify the accelerations during the tests. At foundation level, second and third floor level, the top of the panel system, and the middle of the added mass blocks accelerometers were mounted to measure horizontal accelerations up to $\pm$ 2.5 g in the direction of horizontal acceleration of the shaking table. In addition, an accelerometer was placed at each end of the 20 ft long steel platform to monitor the vertical accelerations. The vertical accelerometers were set to measure a data range of $\pm$ 1 g. Figure 4.1 illustrates the location of

accelerometers. Measurements from the accelerometers AH1, AH2, AH3, AH4, and AH5 were used to calculate the inertia forces (horizontal accelerations at floor levels times the appropriate masses allocated properly). These factors in turn were used to calculate values of base shear force and overturning moment. Vertical accelerometers recorded rocking movement of the added mass blocks. Thus, it was possible to determine the additional moment due to rigid-body rotation of the mass blocks and the attached platforms.

4.2 Local Deformation Measurement

Direct Current Differential Transformers (DCDTs) were employed at different locations to monitor the local behavior of each test model. The choice of location, type, and number of DCDTs was governed by: (1) measurement of responses which would lead to conclusions about the controlling mechanisms, (2) necessary accuracy for measured quantities based on their importance, (3) data acquisition system capacity for number of DCDT channels, (4) maximum expected displacements at each location, and (5) availability of DCDTs of different ranges. On the basis of these considerations, 35 DCDTs were mounted on PZ-I and 40 DCDTs monitored the behavior of PZ-II and of PZ-III. Figures 4.2, 4.3, 4.4 and 4.5 show the DCDT locations.

In particular, DCDT measurements were used in the following ways.

1. The uplift measurements were used to monitor rocking behavior.
2. DCDTs measuring wall-slab and wall-key displacements were used to investigate shear-slip mechanism.
3. Panel deformations detected by diagonal DCDTs and those labelled "B3" and "B4" were used to determine any bending or shearing nonlinearity in the wall panels.
4. Two sets of DCDTs on flange panels were used to find the extent of the compressive zone in these panels.

5. DCDTs labelled "WF" were placed to monitor any possible degradation in the vertical connection between flange panel and wall panel.

Figures 4.6, 4.7, and 4.8 show typical DCDT arrangements to monitor horizontal shear slip, panel bending, diagonal deformation in the wall panel, slab panel uplift, vertical connection degradation; uplift of slab panel relative to foundation; and bending in the flange panel, respectively. The exact location of all the instrumentation is included in Appendix C.

4.3 Strain Measurement

Resistance wire strain gauges were welded to reinforcing bars at certain critical locations. Each gauge had a nominal strain capacity of $\pm$ 20 mil/in., so ductile deformations could be recorded. At the first and second floor levels gauges were placed on both the outside and inside vertical reinforcing bars in the two end cast-in-place columns. A gauge was attached to the single panel bar which extended through the horizontal connection at each panel end. Two additional gauges were mounted on top at the middle of the horizontal longitudinal reinforcing bars in the horizontal connection at the first and the second floor levels. Figure 4.9 illustrates the location of strain gauges for PZ-I and PZ-III. Three extra gauges were welded to the reinforcing bars around the door opening in model PZ-II (see Figure 4.10). These were placed to obtain additional information regarding possible coupling behavior that could develop in this type of wall system. Two additional strain gauges were mounted on the reinforcing bar in the connection at the second and the third floor levels near the middle of the wall. These were welded under the door opening to monitor the effect of the opening on the bar.

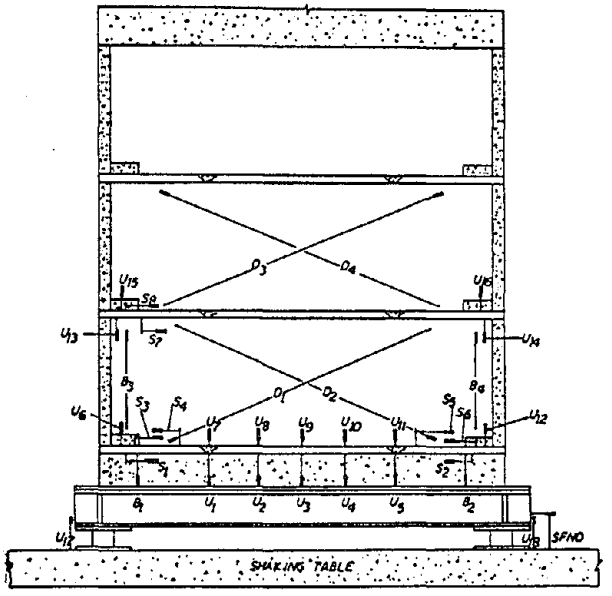

Figure 4.2 DCDT arrangement on PZ-I.

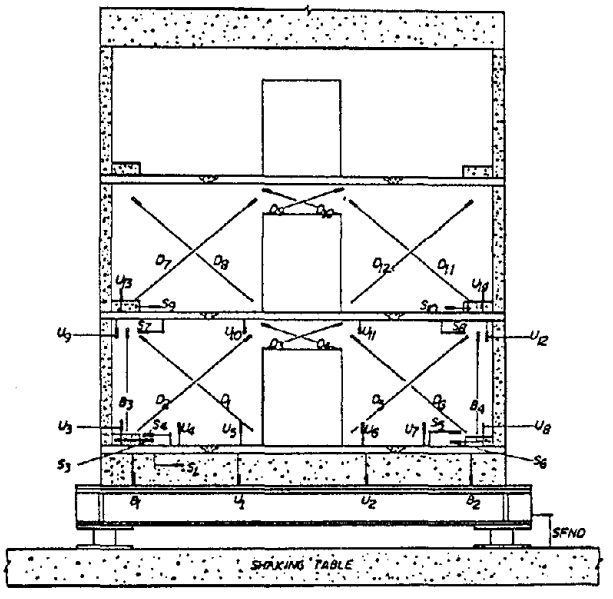

Figure 4.3 DCDT arrangement on PZ-II.

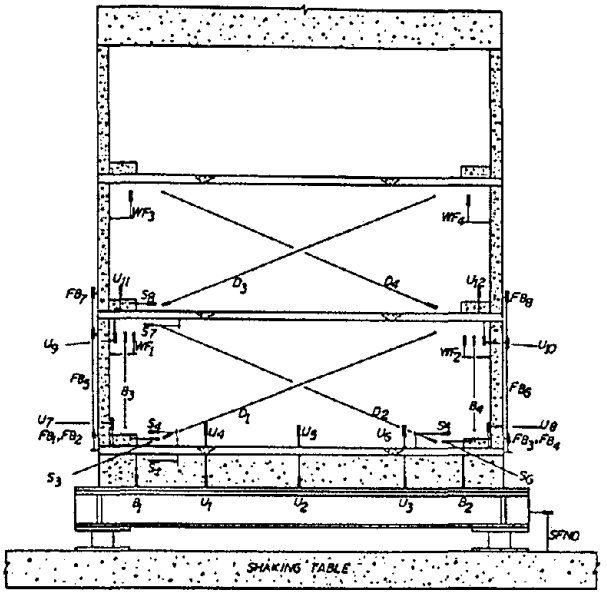

Figure 4.4 DCDT arrangement on PZ-III.

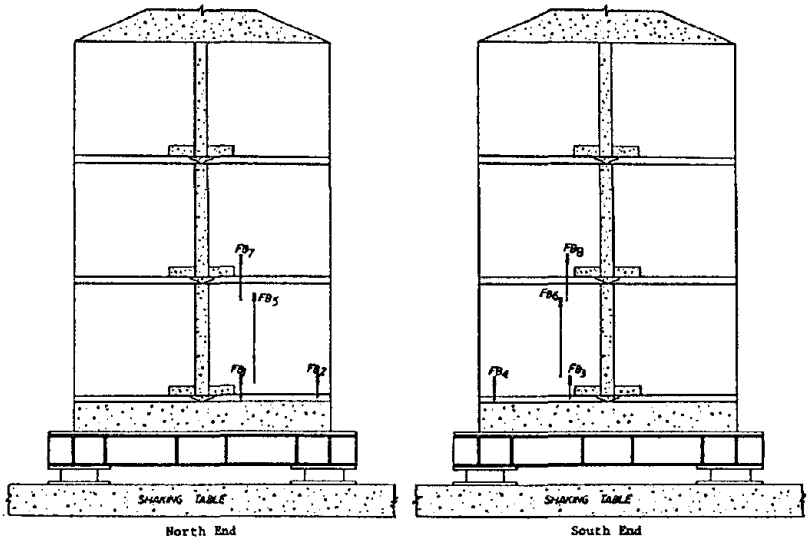

Figure 4.5 DCDT arrangement on flanges, PZ-III.

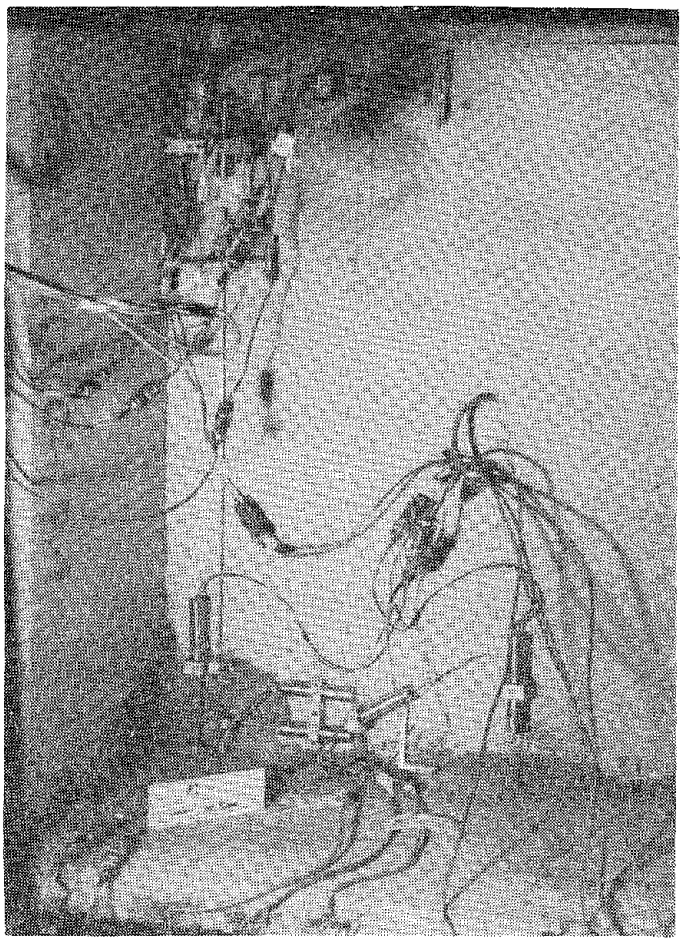

Figure 4.6
Typical DCDT mountings on the wall panel.

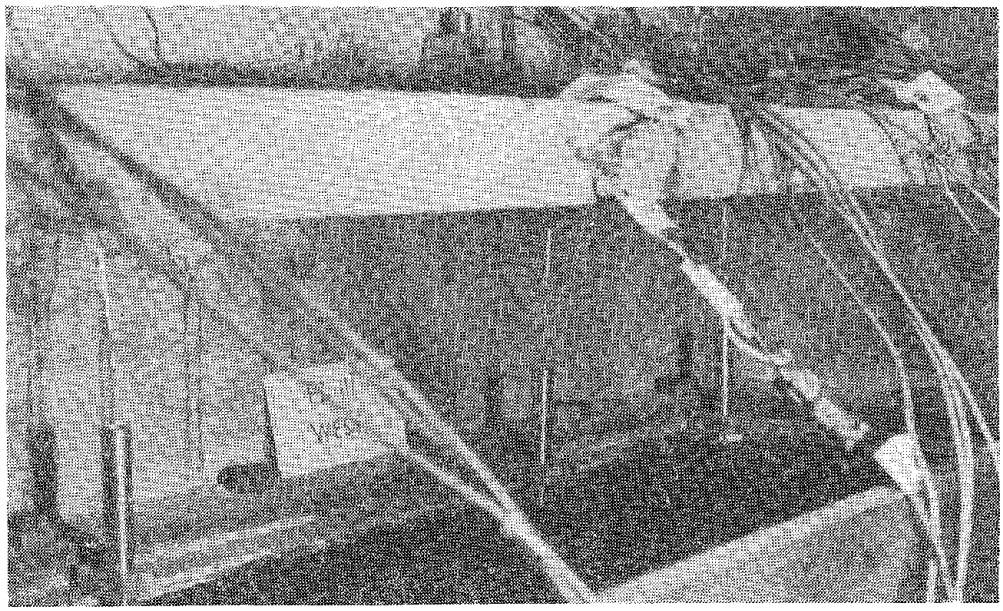

Figure 4.7 DCDT configuration for measurement of floor uplift.

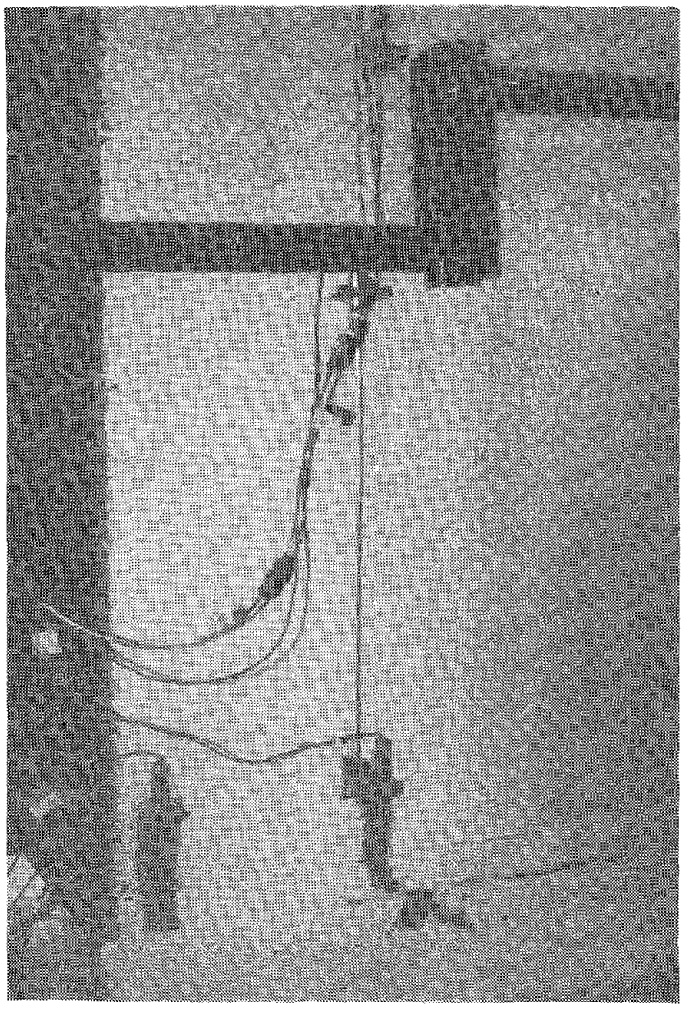

Figure 4.8 DCDTs mounted on flange wall to measure extension and uplift across floor joint.

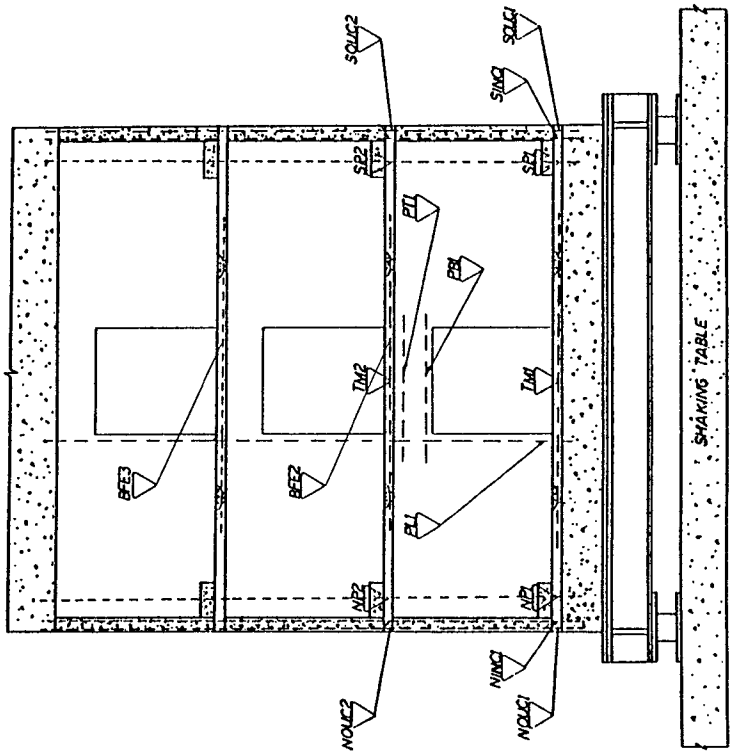

Figure 4.10 Location of strain gauges, PZ-II.

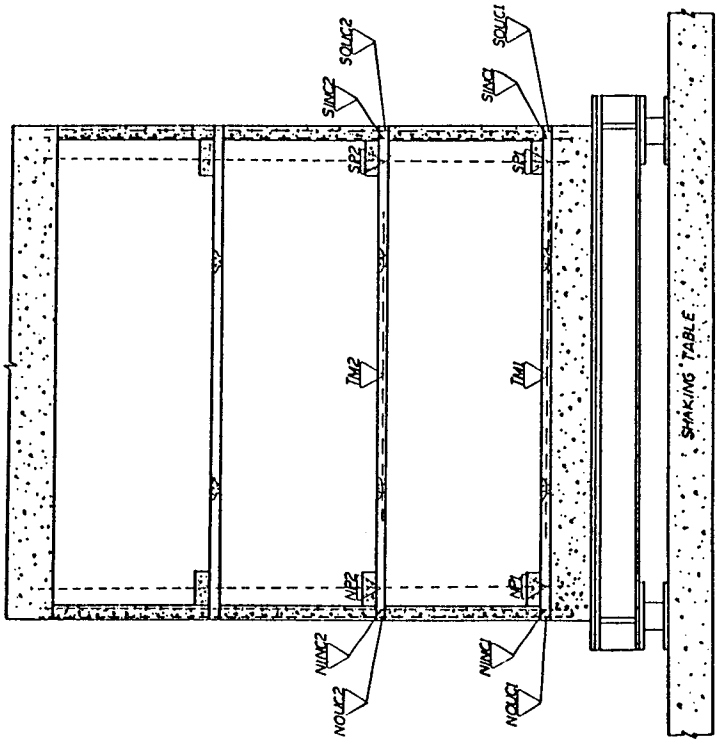

Figure 4.9 Location of strain gauges on PZ-I and PZ-III.

4.4 Displacement Measurement

Although the foundation had been prestressed to the table, in order to define the wall base motion accurately it was desirable to monitor any possible horizontal displacements that might occur. For this purpose, a DCDT capable of recording horizontal displacements of up to $\pm$ 0.1 in. was placed between the foundation and table. The location of this DCDT, labelled "SFND", is shown in Figures 4.2, 4.3 and 4.4.

Potentiometers were employed to measure the horizontal displacements at floor levels. These were mounted on a fixed reference frame outside the table, and their connecting wires were attached at different levels, see Figure 4.1. This set of potentiometers was calibrated to measure a displacement range of $\pm$ 8 in. Two additional potentiometers, labelled POTN and POTS in Figure 4.1, were used to determine the relative displacement between the first floor slab and the top of the 18 in. cast-in-place wall. From this measurement it was possible to calculate an overall curvature for the entire wall system. Potentiometers POTN and POTS could monitor displacements within a range of $\pm$ 2 in.

4.5 Force Measurement

Four force transducers, each with a 10 kip measurement capacity, were installed at the corners of the foundation to determine base shear force; their location is shown in Figures 3.2(a) and (b). A comparison of the measured shear force and the calculated inertial value was thus possible and was used to check the accuracy of the calculated inertia forces and overturning moment (see Chapter 7).

TABLE 5.1

Test Sequence

Test Model	Test No	Earthquake Signal	Max. Table Acc. (g)	Signal Identification
PZ-I	1	El Centro Span 150	0.179	EC-150
	2	El Centro Span 700	0.666	EC-700
	3	El Centro Span 500	0.495	EC-500
PZ-II	1	El Centro Span 100	0.123	EC-100
	2	El Centro Span 700	0.668	EC-700
PZ-III	1	El Centro Span 200	0.223	EC-200
	2	El Centro Span 750	0.689	EC-750
	3	El Centro Span 1000	1.081	EC-1000

TABLE 5.2

Measured Natural Frequencies

(low amplitude natural frequency in first mode)

Test Model	Sequence of Frequency Measurement	Frequency (Hz)
PZ-I	Prior to test	5.20
	Post EC-150	5.10
	Post EC-700	3.90
PZ-II	Prior to Test	5.00
	Post EC-100	4.72
PZ-III	Prior to test	6.30
	Post EC-750	4.32

5. TEST PROGRAM

The experimental program involved shaking table tests of three panel wall systems. The actual earthquake motions were applied at progressively increasing amplitudes to cause elastic, inelastic, and after-shock response. Frequencies of the original and the damaged walls were measured to evaluate the frequency and stiffness degradation experienced by each model during the earthquake excitation.

5.1 Earthquake Excitation

Throughout this experiment nine different shaking table tests were performed. PZ-I, PZ-II, and PZ-III were subjected to three, two, and four excitations, respectively. The input displacement to the earthquake simulator was derived from the S00.0E component of the 1940 Imperial Valley earthquake recorded at El Centro and scaled in amplitude and time. This signal was applied to each test model at different intensities. Table 5.1 summarizes the excitations which were considered significant. The number indicated after each signal represents "span setting" which is the control console dial setting that governs the input displacement. The first excitation of PZ-III had low intensity and was applied to check the instrumentation.

In order to simulate elastic response of the test models without any premature inelastic behavior or any unexpected damage, low intensity signals were first applied, and then the input displacement signals were increased to a higher amplitude to cause inelastic response. This made it possible to monitor the behavior of the test specimen in the inelastic region. Models PZ-I and PZ-III were finally subjected to another signal to simulate the after-shock response of the damaged wall.

5.2 Frequency Measurement

Free vibration frequencies of the test models were measured before each test and after completion of tests which had induced inelastic response. The frequencies were monitored to provide information about the structural stiffness degradation associated with different damages. "White noise" shaking was employed to determine the free vibration frequency. This method is described below.

The shaking table with the structure on it was vibrated by very small amplitude motion considered as white noise -- i.e., uniform motion over a frequency range of 0.3 to 20 Hz. The response from the accelerometer on the mass blocks (AH5) was used by a spectrum analyzer to determine the dominant response frequencies. These frequencies are considered to be the real frequencies of the test models on an actual "soft" foundation. The so-called soft foundation is provided by the shaking table with its hydraulic actuators and its air cushion. Table 5.2 summarizes the measured frequencies.

6. DAMAGE OBSERVATIONS

As explained in Chapter 4, extensive instrumentation was employed to obtain complete quantitative data concerning the response of the wall systems. Furthermore, the damage patterns and visual observations provide additional information which helps to identify the controlling mechanisms. Accordingly, the structures were inspected carefully after each test for pattern and extent of damage. A summary of these observations is presented in this chapter.

6.1 Model PZ-I - Simple 3-Story Wall

Under the low amplitude ground shaking of 0.18g (EC-150 test), there was no visual damage. However, the structure experienced rather extensive damage when the input signal was amplified to have a maximum ground acceleration of 0.67g (EC-700 test). The most prominent mechanism during the test was rocking. Any shear-slip behavior was not large enough to be visible.

Rocking motion opened the first-floor horizontal joint over at least half its length. The compression force induced by rocking spalled part of the south-end cast-in-place column and part of the shear key in the joint. This was followed by buckling failure of the two vertical reinforcing bars in this side. The panel bar in the same side ruptured at 0.75 in. above the floor slab. Subsequent to these damages, the amount of joint opening increased causing spalling of the south-end panel corner. Figures 6.1(a) and 6.1(b) illustrate the extent of the damage. Meanwhile, the north-end corner appeared to be intact with minor cracks, see Figure 6.1(c).

Signal EC-500, which was intended to simulate after-shock excitation, did not introduce any new visible damage. Again, the most visible motion was rocking.

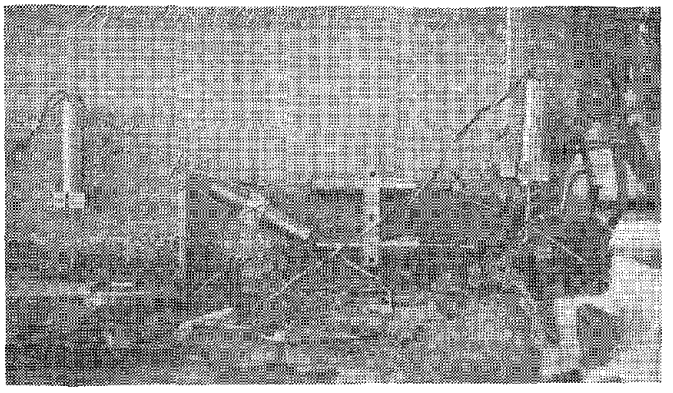

(a) South-west corner

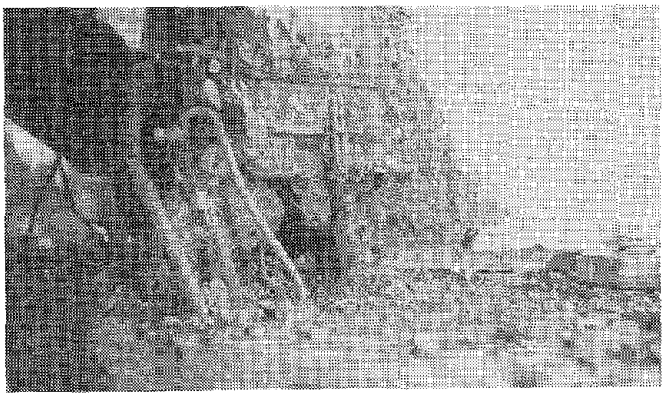

(b) South-east corner

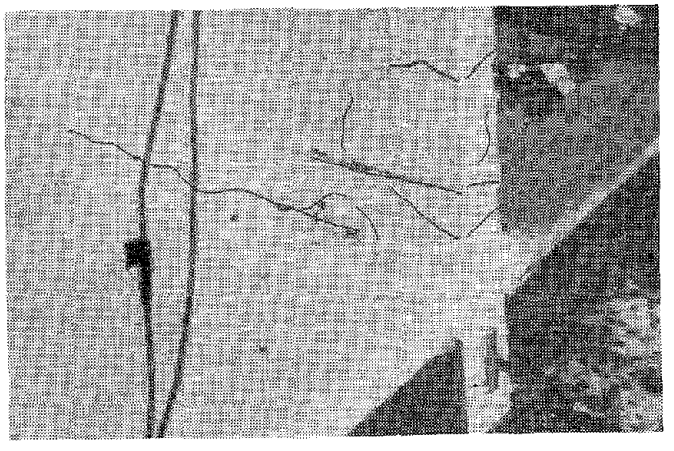

(c) North end

Figure 6.1 First floor joint of simple wall (PZ-I) after EC-500, 0.67g.

6.2 Model PZ-II

The behavior of this model was similar to that of the simple wall. That is, under small amplitude motion no visible damage occurred. It is, however, believed that because frequency measurements after this test indicated a drop of 0.28 Hz in the natural frequency, there were some minor damages which reduced the stiffness of the wall. This unexpected damage was due to a sudden malfunctioning of the table control system which caused a single high acceleration spike during the otherwise low amplitude test.

Under the higher amplitude 0.67g base motion (EC-700), rocking behavior dominated the visual response. The primary failure occurred at the south end, and the extent of damage in this side was of the same degree as that for the simple wall. The two vertical reinforcing bars failed by buckling, but the panel bar did not rupture, in contrast to the simple wall. (See Figures 6.2(a) and (b).) The north corner again suffered moderate spalling with more visible cracks. Figures 6.2(c) and (d) illustrate the location of cracks.

It was intended that significant coupling would occur through the action of the door lintels. Unfortunately the stiff added mass system at the top of the specimen provided the major component of coupling and door lintels were not heavily loaded. There was no sign of damage from this action, i.e., no diagonal cracks in the door lintels. Minor cracking occurred around the door opening of the first floor as presented in Figure 6.3. On account of the coupling effect of the top mass system the behavior of this wall was very similar to that of the simple wall PZ-I. Because of this similarity the response data from the PZ-II wall with doors will not be included in the subsequent data analysis chapters.

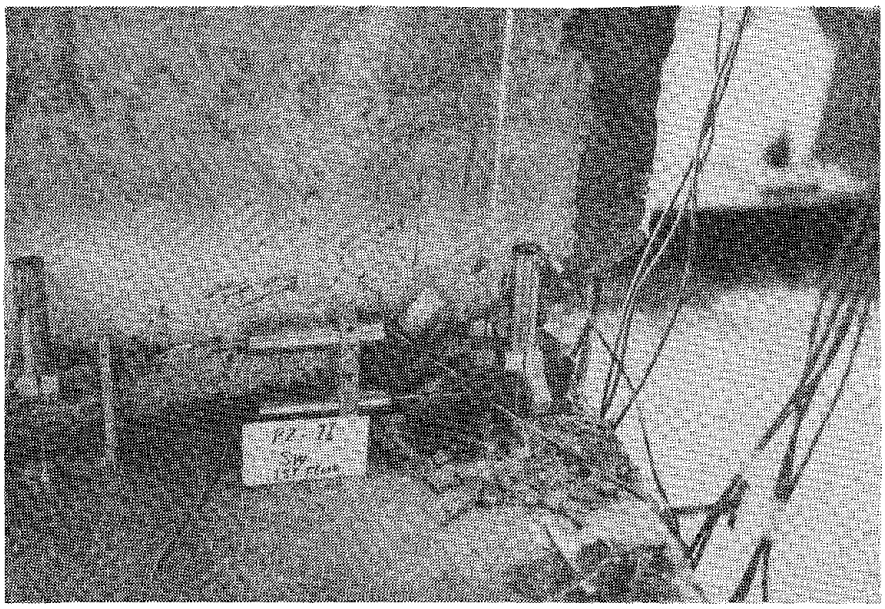

(a) South-west corner

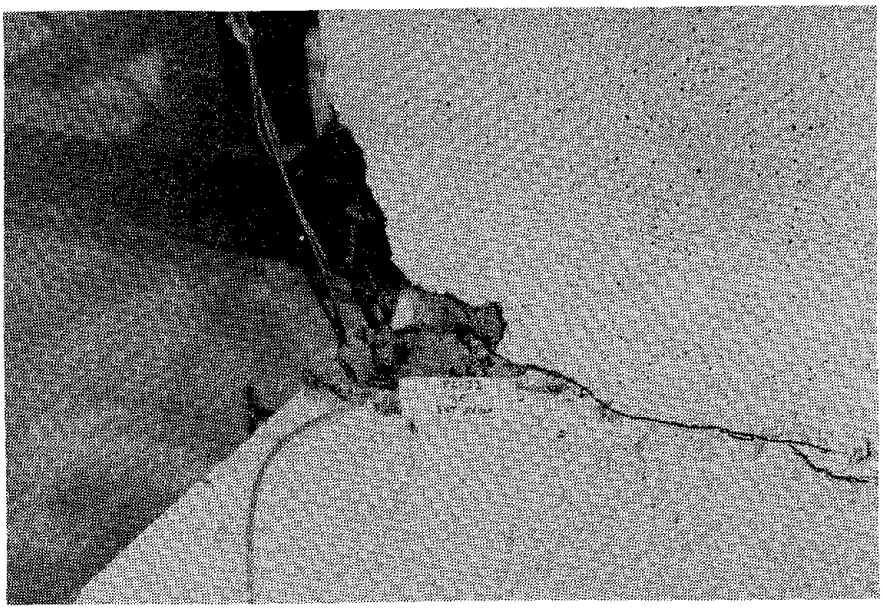

(b) South-east corner

Figure 6.2 First floor joint of panel with door (PZ-II) after EC-700, 0.67g.

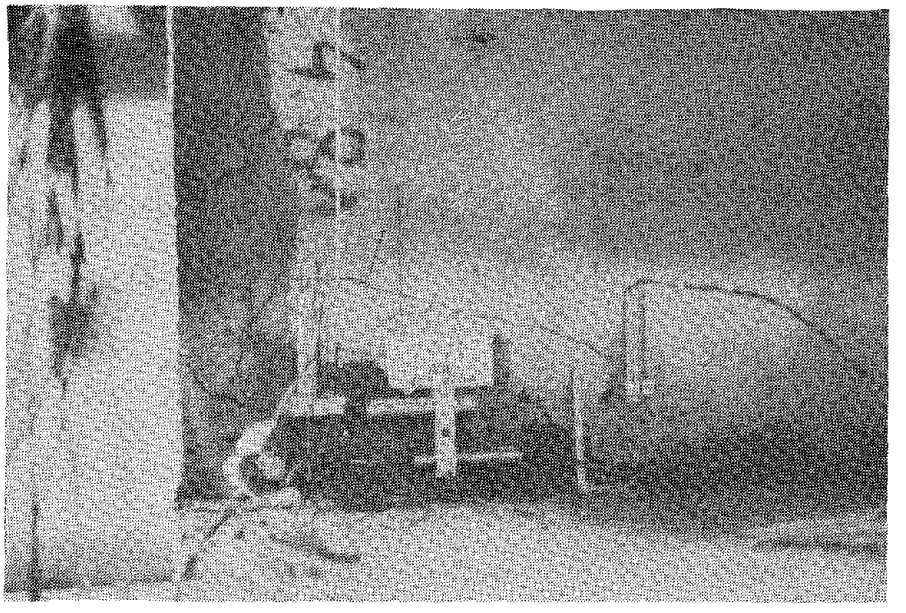

(c) North-west corner

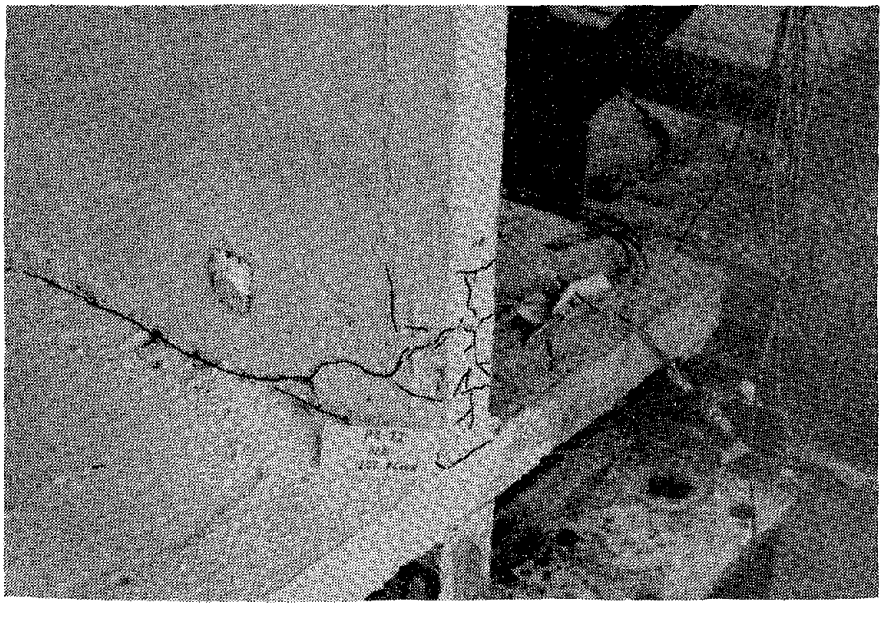

(d) North-east corner

Figure 6.2 (Continued)

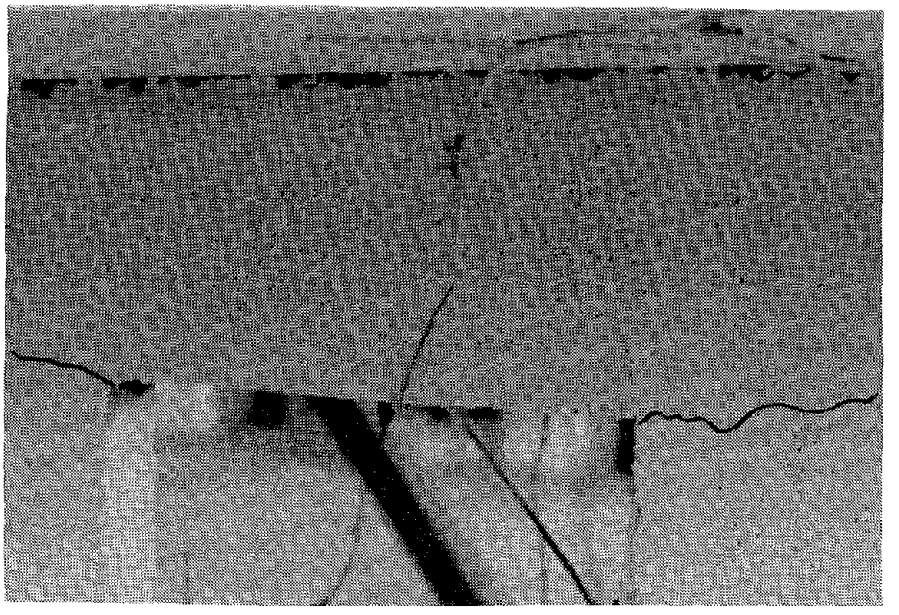

Figure 6.3 First floor panel near door opening (PZ-II) after EC-700, 0.67g (east side).

6.3 Model PZ-III

As in the tests of the PZ-I and PZ-II models rocking motion appeared to dominate the visible behavior of the flanged wall. When exposed to 0.69g (EC-750) and 1.08g (EC-1000) ground motion this model experienced uplift along the horizontal connection and at the flange-floor intersection. Subsequently, the shear key at the south end of the first floor spalled and crushed almost completely, and the north-end shear key was damaged to a lesser degree. The wall and flange panels spalled at these two ends near the connection region. At the south end the panel spalled to 7 in. up the wall; the damage at the north side extended to 5 in. Figures 6.4(a) and (b) demonstrate the degree of damage.

A careful examination of the model showed that the outside column bar at the south end had ruptured at 1.375 in. above the floor, and the inside bar had buckled. The flange and wall panel bars had ruptured at 2.25 in. above the floor and at the top of the welding point, respectively. The

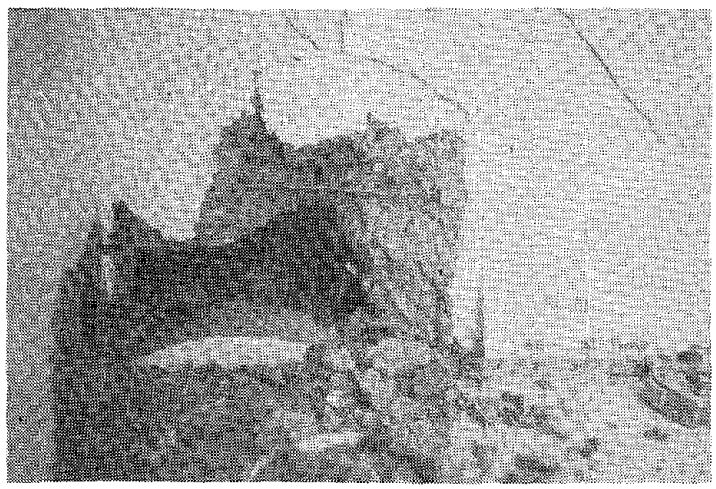

Figure 6.4(a)
First floor joint of flanged wall (PZ-III) after EC-1000, 1.08g (south end).

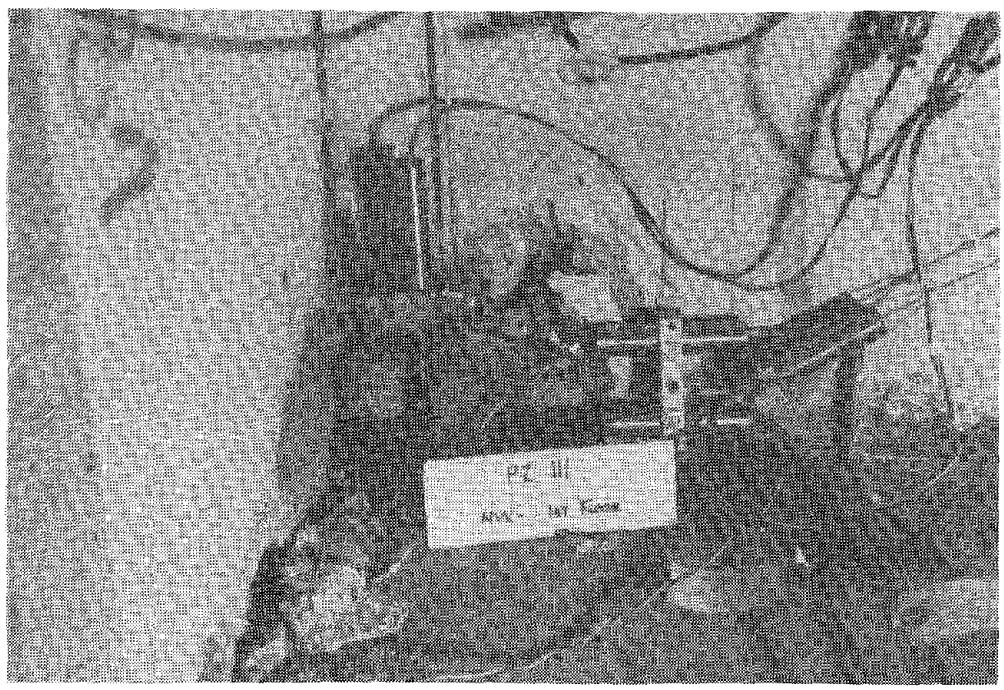

Figure 6.4(b) First floor inside corner joint of flanged wall after EC-1000, 1.08g (north end).

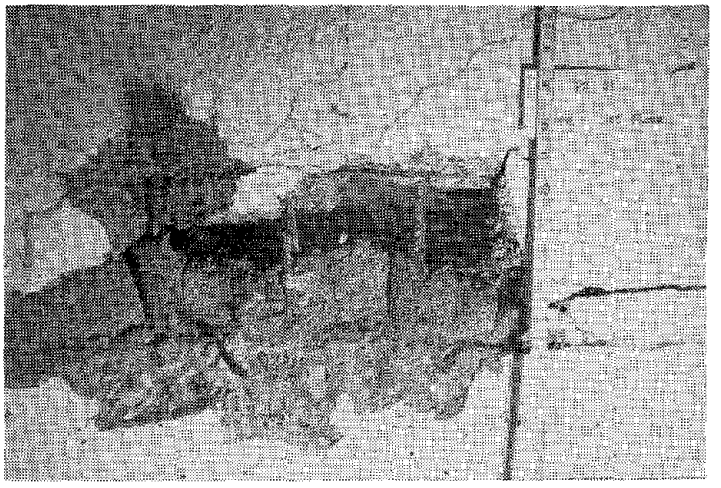

Figure 6.5(a)
Failure of reinforcing bars at the south end of the flanged wall (PZ-III).

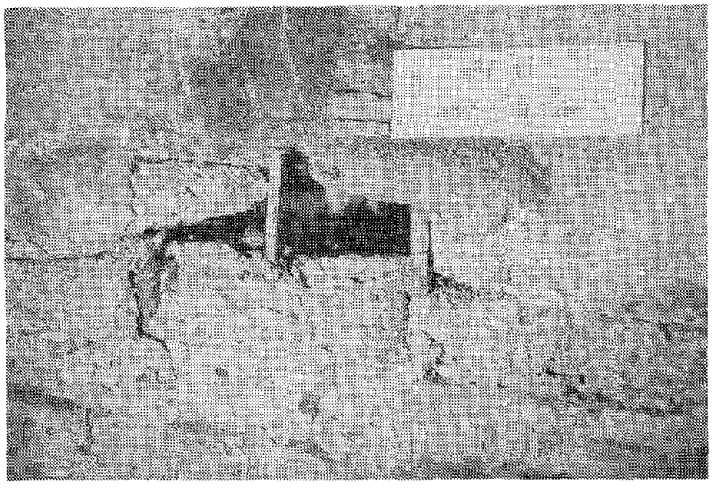

Figure 6.5(b)
Failure of reinforcing bars at the north end of the flanged wall.

reinforcing bars at the north end were damaged to a lesser extent. Both of the column bars had buckled, and one of the flange panel bars had ruptured at the top of the welding point. The ruptured and buckled bars are shown in Figures 6.5(a) and (b).

7. TEST RESULTS FOR SIMPLE WALL

This chapter presents the test results of the simple wall (PZ-I) in graphical form. As mentioned in the previous chapters, this wall was subjected to three different base motions, namely, EC-150, EC-700, and EC-500 (0.18g, 0.67g and 0.50g, respectively). The last test (EC-500) was applied to simulate an aftershock response. The results from the first two tests are considered in this chapter.

The preliminary steps involved in the data reduction, identical for all three wall systems, are followed by the results from each test. Instruments which malfunctioned or exceeded their calibration limit were detected and noted. The selected data were then used to determine the behavior of the structure. All of the data presented are in the original unfiltered form.

7.1 Separation of Data Channels

It was obvious that the test results would have a base line shift due to initial offsets in the instrumentation. Therefore, data were corrected before any further steps. Second floor accelerations were plotted against time to examine the magnitude of the offset. From Figure 7.1, it was decided that the first 150 data points (1.5 seconds) from each channel would be used to account for the initial offsets. A similar process was used in subsequent tests.

7.2 Results from El Centro at 0.18g (EC-150) - PZ-I Wall

7.2.1 Introduction

This test was intended to demonstrate the behavior of the wall system in the elastic region. Thus, the input signal was applied at a relatively low amplitude producing a maximum horizontal displacement of -0.756 in. and a maximum horizontal acceleration of 0.179g in the table motion. Figure 7.2

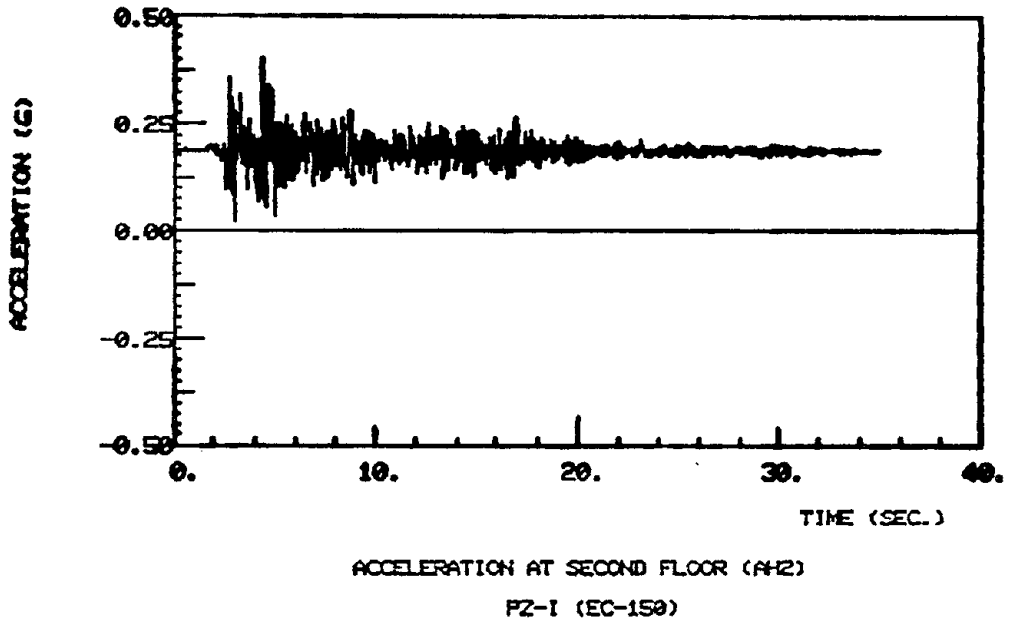

Figure 7.1 Channel 16 before base line correction.

illustrates the horizontal components of table displacement and table acceleration.

Because of the low amplitude input for this test, it was necessary to check whether the monitored data were of significant value to be detected by the instrumentation. Hence, the data channels to be used in the next steps were carefully inspected. It was found that the slip values at the base of the wall were of such small magnitude that the instruments were not able to measure them. Figure 7.3 illustrates this point. The scale on the vertical axes was exaggerated to show the relative magnitude between the different DCDTs (Direct Current Differential Transformers). Values detected by S2, S4, S5, and S6 were, however, too small to be measured accurately by the DCDTs. The displacements indicated, in the range of 2 to 4 ten thousandths of an inch, have a form which could be electronic "noise" or the result of sticking cores and mechanical "noise". The maximum value was measured by S3 which

reached a peak of 0.0012 in. This value of slip was rather insignificant. The expected accuracy of the DCDTs S2, S4, S5 and S6 because of instrument limitations was $\pm$ 0.00125 in.; the accuracy of the instruments S1 and S3 was $\pm$ 0.00025 in. (see Figure 4.2 for instrument locations). Consequently, no attempt was made to calculate an average slip value.

7.2.2 Accelerometer Results

Accelerations measured by different accelerometers are presented in Figure 7.4. The added concrete blocks experienced the maximum acceleration, which was -0.405g. It is interesting to note that the rocking motion of the 20 ft long steel platform produced a vertical acceleration measured by AV1 of -0.346g which is greater than the acceleration at the top of the wall. Thus, this motion was considered to be a significant source of overturning moment in calculating the base moment. Table 7.1 summarizes the maximum accelerations from the different accelerometers.

7.2.3 Lateral Displacements

As was explained in Chapter 4, the purpose of the potentiometers labelled DIS2, DIS3, and DIS4 was to measure lateral displacements of the wall. The measured data, however, were the actual displacements including the horizontal table motion. Hence, to obtain relative displacements it was necessary to subtract the table displacement. Figure 7.5 illustrates the variation in lateral displacement at different locations. The plots from the second floor and the third floor indicate that these two displacements still contain some table motion. The overall magnitude of the motion is less than 0.10 in. with an apparent residual table motion amplitude of 0.04 in. This might be due to slightly inaccurate amplification set for the potentiometers labelled DIS2 and DIS3 which had a total measurement range of $\pm$ 8 inches. The wall

TABLE 7.1

Extreme Values from EC-150 Test, PZ-I
(table motion of 0.18g)

Quantity	Extreme Value
Acceleration at foundation	-0.174g
Acceleration at second floor	0.215g
Acceleration at third floor	0.253g
Acceleration at top of wall	0.285g
Acceleration at concrete blocks	-0.405g
Acceleration at steel platform at AV1	-0.346g
Acceleration at steel platform at AV2	-0.333g
Top of wall lateral displacement	0.325 cm (0.128 in.)
Base shear force	33.48 kN (7.44 kips)
Base bending moment	172.3 kN-m (1525 in-kips)
Strain in south-end panel bar of first floor	0.082%
Strain in south-end outside column bar of first floor	0.059%
Strain in south-end inside column bar of first floor	0.080%
Strain in north-end panel bar of first floor	0.069%
Strain in north-end outside column bar of first floor	0.103%
Strain in north-end inside column bar of first floor	0.056%
North-end uplift	0.51 mm (0.020 in.)
South-end uplift	0.43 mm (0.017 in.)
Average wall curvature	0.58×10^{-6} rad/cm (1.48×10^{-6} rad/in.)

experienced a maximum relative displacement of 0.12 in. at its top. This value is almost 1.5 times greater than that of the second floor.

7.2.4 Base Shear Force and Bending Moment

Using the data from each force transducer placed between the foundation and the shaking table, it was possible to find the total shear force at this level by summing the forces measured in the four force transducers. However, there was no direct approach for obtaining the bending moment at this or any other level. Since the accelerations at specific levels were known, it was decided to use inertia forces to calculate the bending moment. For this purpose, it was necessary to model the structure as a series of lumped masses and to have accelerations at some intermediate values and particularly at the location of the lumped masses. Accelerations had been measured only at the locations of the accelerometers.

A bilinear variation in acceleration was assumed for the upper wall segment and the mass system, i.e., two different straight lines below and above the W6x12 connecting beam (see Figure 7.6) were used to define accelerations in the masses at the top of the wall system. Using this assumption, acceleration at any point beyond 0 can be evaluated from equation (1) in Figure 7.6. The accuracy of this assumption was checked by using vertical accelerations from AV1 and AV2 (see Figure 7.6) to define the angular acceleration, α, and then predicting the lateral acceleration at the location of accelerometer AH5. The predicted and measured accelerations from AH5 are compared in Figure 7.7. The closeness of the match justifies the interpolation assumption for accelerations of the upper mass system. Alternatively, equation (2) in Figure 7.6 can be used to calculate the rotational acceleration of the mass blocks using the bilinear assumption and accelerations AH3, AH4 and AH5. The resulting value was plotted against that

computed from readings of accelerometers labelled AV1 and AV2, i.e., $\frac{AV2-AV1}{x}$. Figure 7.8 illustrates the match between the two different methods. Variation between the records is due in part to local vibrations of the steel frame itself at a higher frequency. This indicates that a close approximation for the angular acceleration of the top masses can be obtained by using values measured by the accelerometers labelled AH3, AH4, and AH5.

Then since accelerations beyond the W6x12 girder can be found at any level, the structure was idealized according to Figure 7.9. The following assumptions were made in selecting the masses and the rotational inertia:

1. Masses from the lower floor slab, the 9 in. cast-in-place wall, half of the wall panel plus the end columns, and the foundation were considered as M1.
2. M2 and M3 consisted of the mass of a wall panel plus the end columns and the mass of a floor slab.
3. Half of the mass of a wall panel plus the end columns and the mass of the 18 in. cast-in-place wall were lumped together as M4.
4. Masses from the 20 ft long steel platform were assumed to be M5.
5. The mass of the concrete blocks was considered to be M6.
6. M7 consisted of the mass of the 10 ft long steel platform.
7. The mass moment of inertia of the steel platforms and the concrete blocks, all prestressed together, was included assuming that they act as a rigid rotating body.

It was assumed that the accelerations corresponding to M1, M2, M3, M4, and M6 were those measured by accelerometers labelled AH1, AH2, AH3, AH4, and AH5 (see Figure 4.1). The lateral accelerations at the center of gravity of M5 and M7 was calculated using equation (1) in Figure 7.6. These accelerations were assumed to operate on M5 and M7.

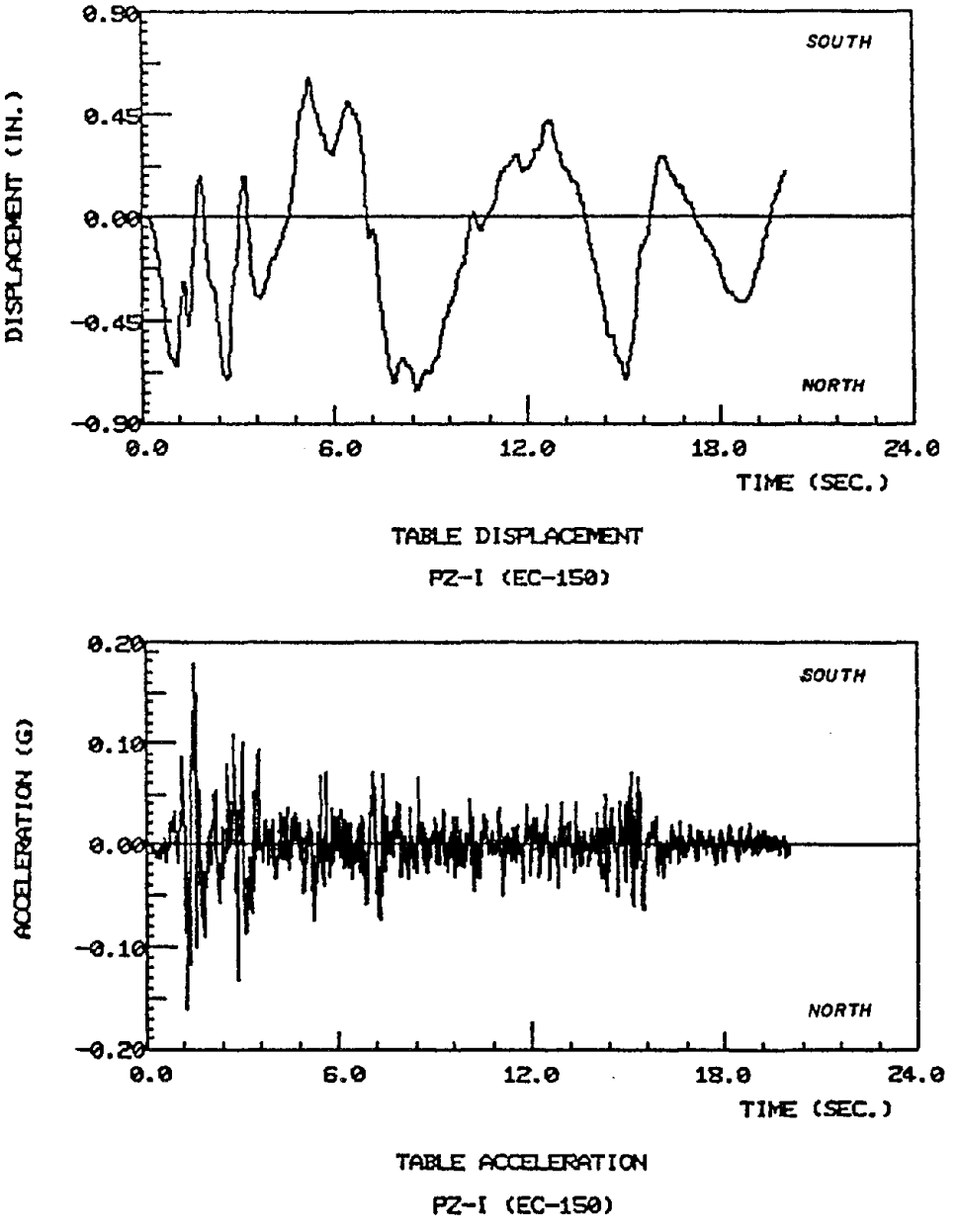

Figure 7.2 Horizontal displacement and acceleration of the shaking table (EC-150, 0.18g).

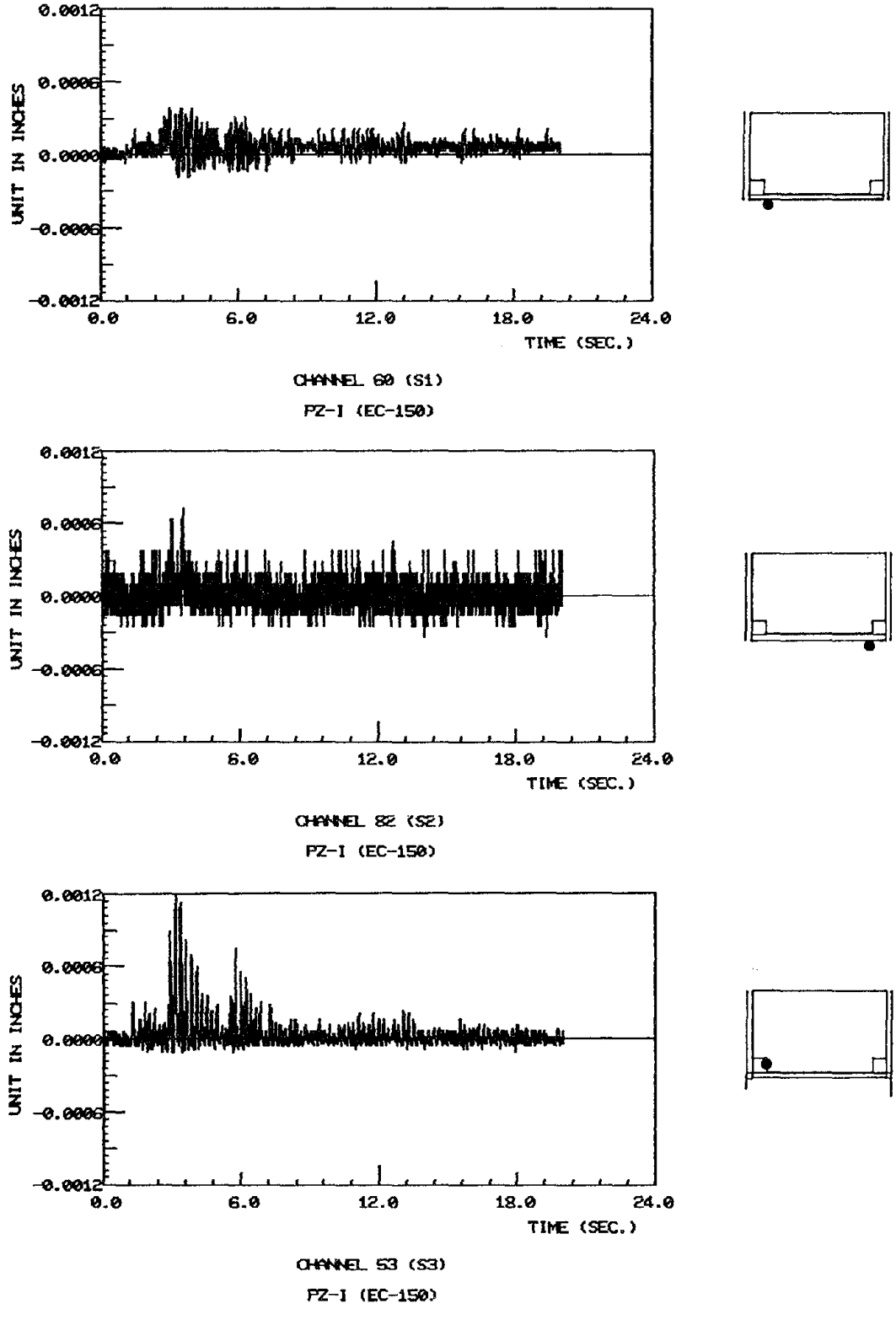

Figure 7.3 Time histories of DCDTs for slip measurement.

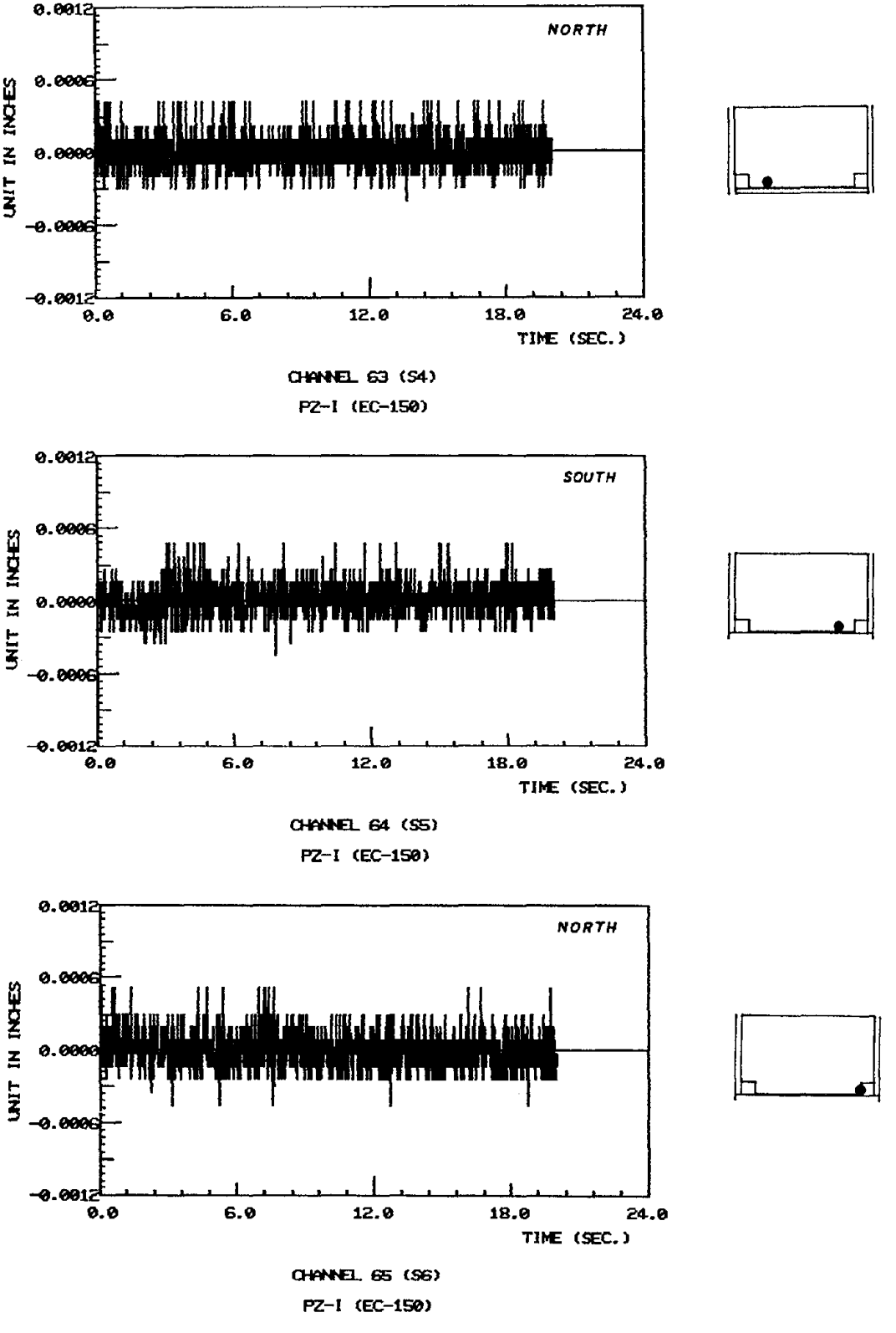

Figure 7.3 Continued.

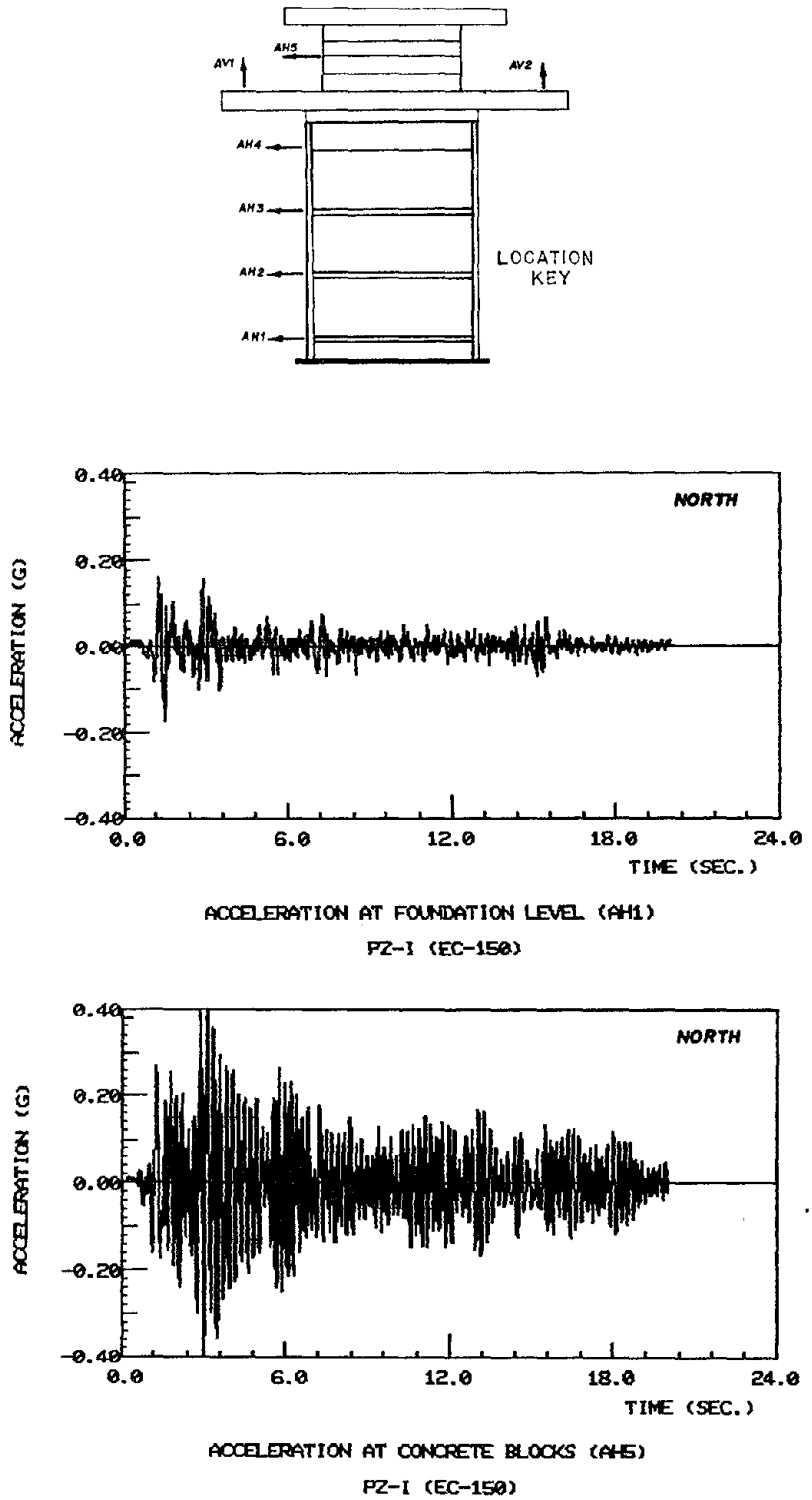

Figure 7.4 Accelerations at different locations, simple wall, EC-150, 0.18g.

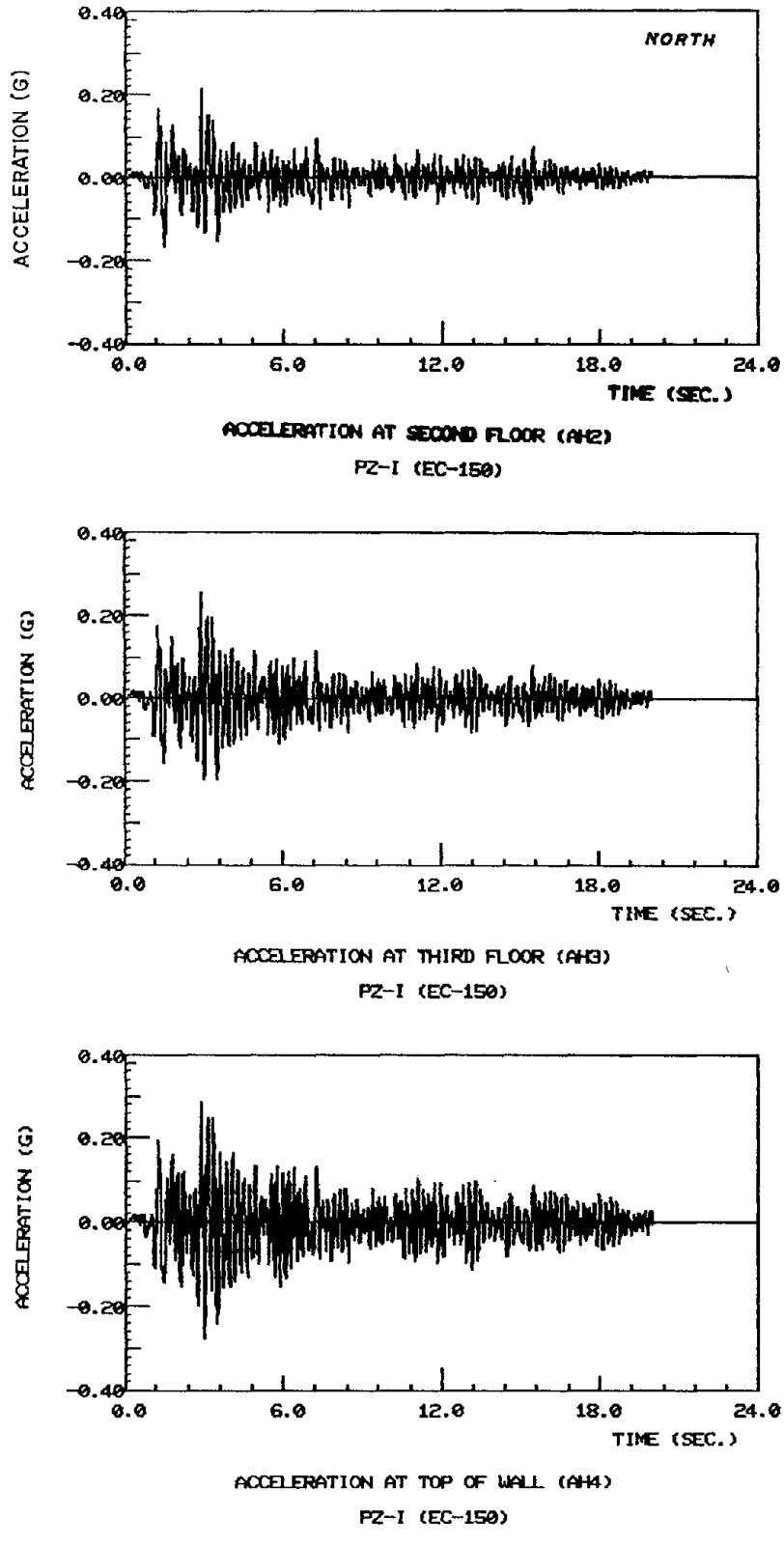

Figure 7.4 Continued.

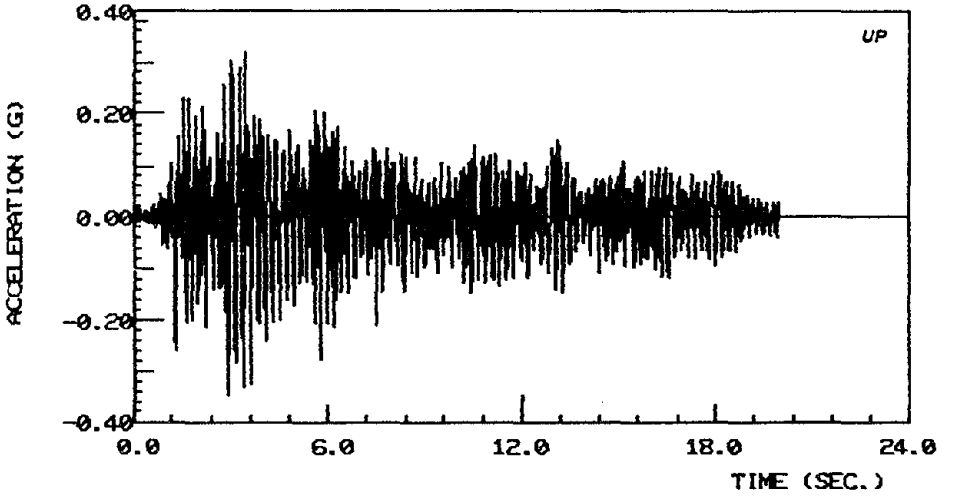

ACCELERATION AT STEEL PLATFORM (AV1)

PZ-I (EC-150)

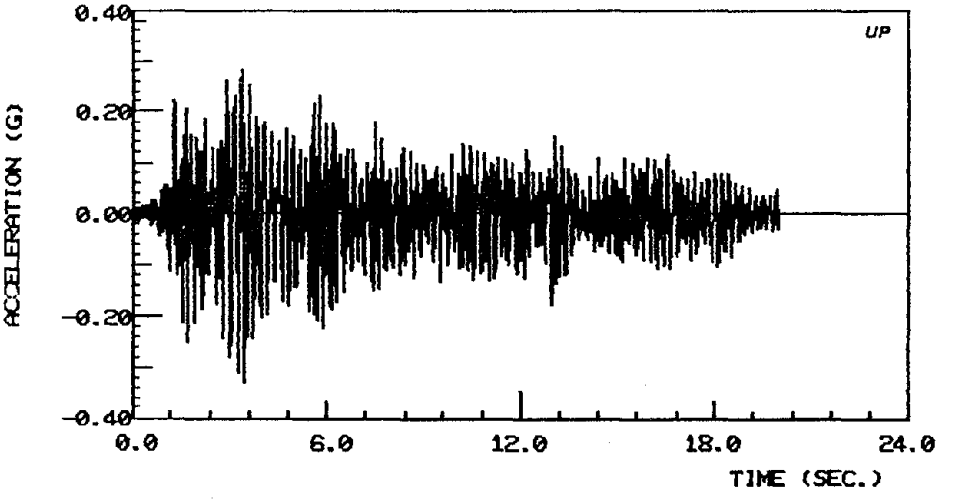

ACCELERATION AT STEEL PLATFORM (AV2)

PZ-I (EC-150)

Figure 7.4 Continued.

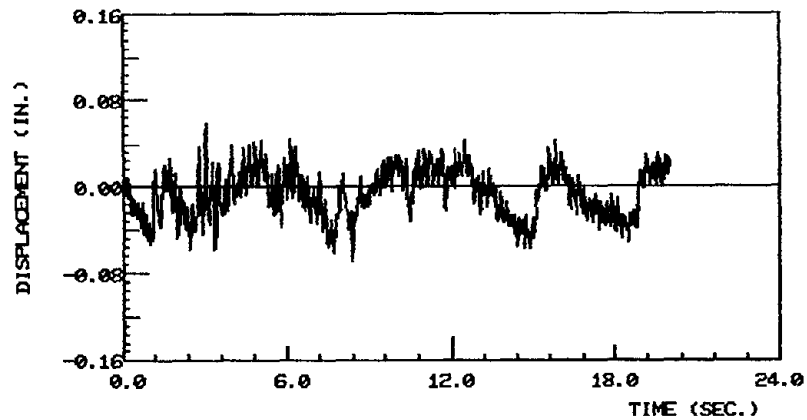

LATERAL DISPLACEMENT AT SECOND FLOOR

PZ-I (EC-150)

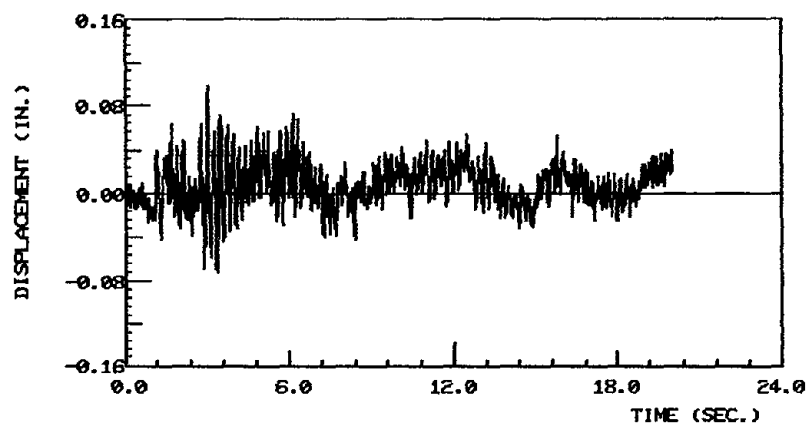

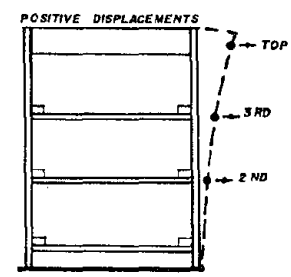

LATERAL DISPLACEMENT AT THIRD FLOOR

PZ-I (EC-150)

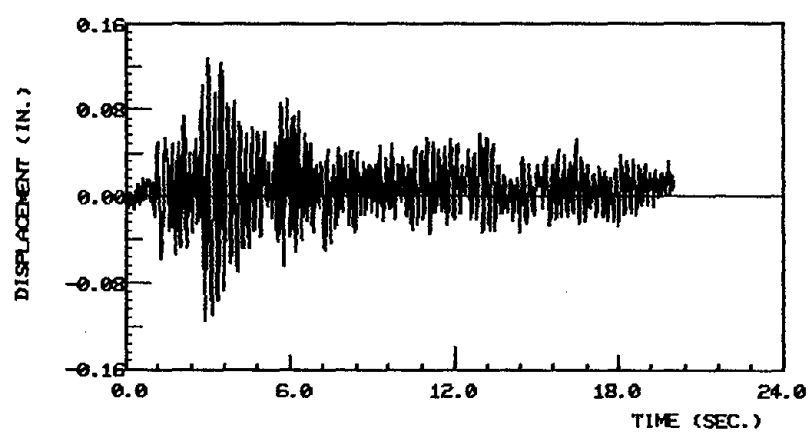

LATERAL DISPLACEMENT AT TOP OF WALL

PZ-I (EC-150)

Figure 7.5 Relative lateral displacements, simple wall, EC-150, 0.18g.

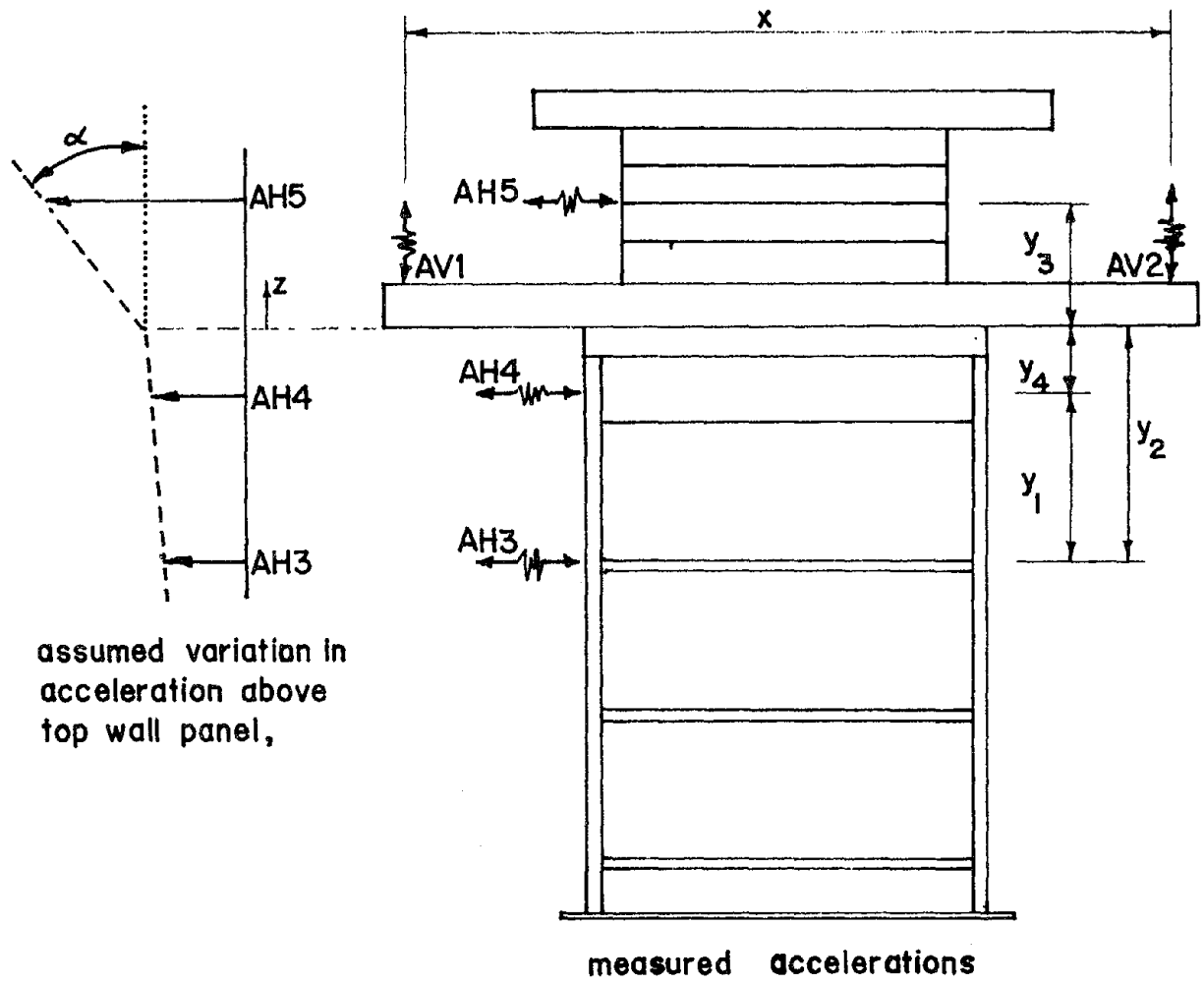

$$(1.) \quad AHz = y_4 \cdot (AH_4 - AH_3) / y_1 + AH_4 + \alpha \cdot z$$

$$(2.) \quad \alpha = (AH_5 - y_4 \cdot (AH_4 - AH_3) / y_1 - AH_4) / y_3$$

AHZ = lateral acceleration at any distance , Z , above the top of wall (+ to North).

α = angular acceleration of added mass defined by measured lateral accelerations and the assumed bilinear shape (+ CCW).

Figure 7.6 Mathematical model for acceleration.

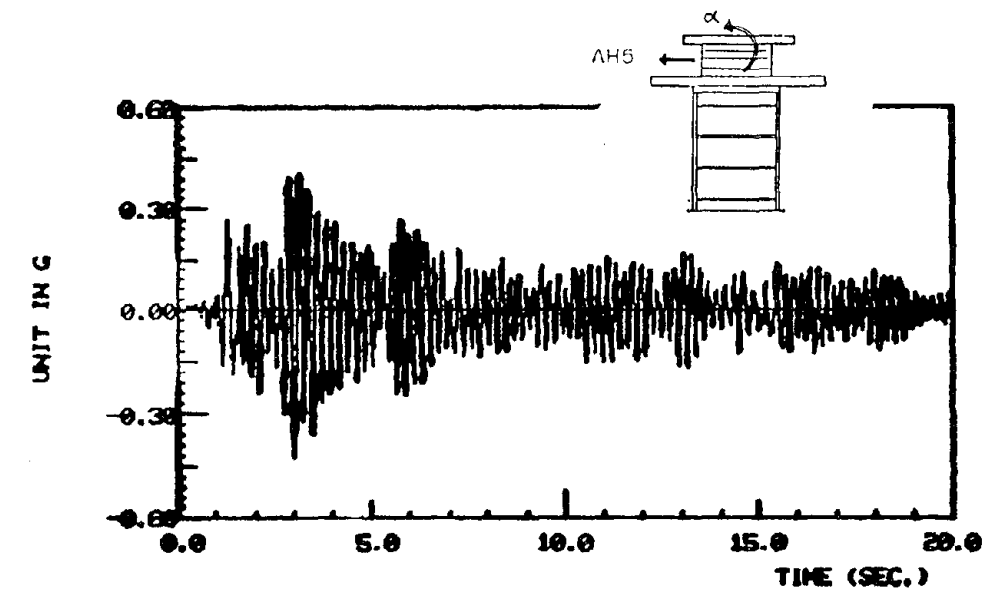

COMPUTED AND MEASURED AH5
PZ-I (EC-150)

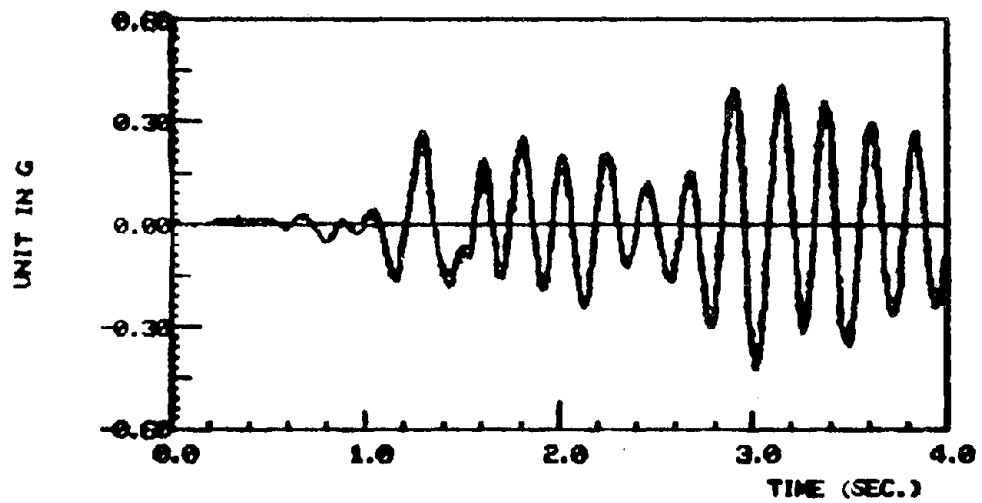

COMPUTED AND MEASURED AH5 (1ST 4 SECONDS)
PZ-I (EC-150)

———— = measured results

- - - - = computed using Eq. 1, Fig. 7.6, α = (AV2-AV1)/X

Figure 7.7 Comparison between measured and computed acceleration at concrete blocks.

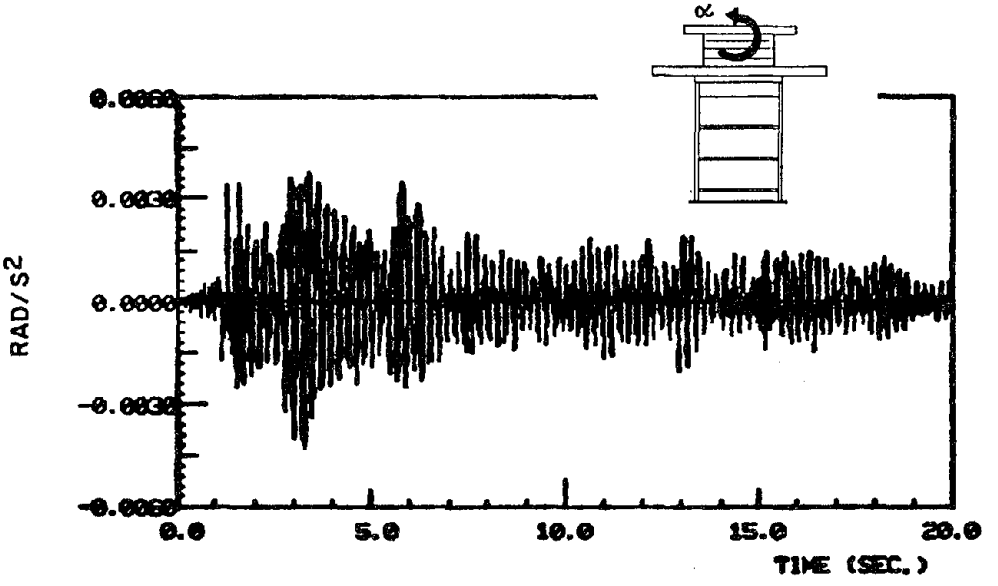

COMPUTED AND MEASURED ANGULAR ACCELERATION OF TOP MASS
PZ-I (EC-150)

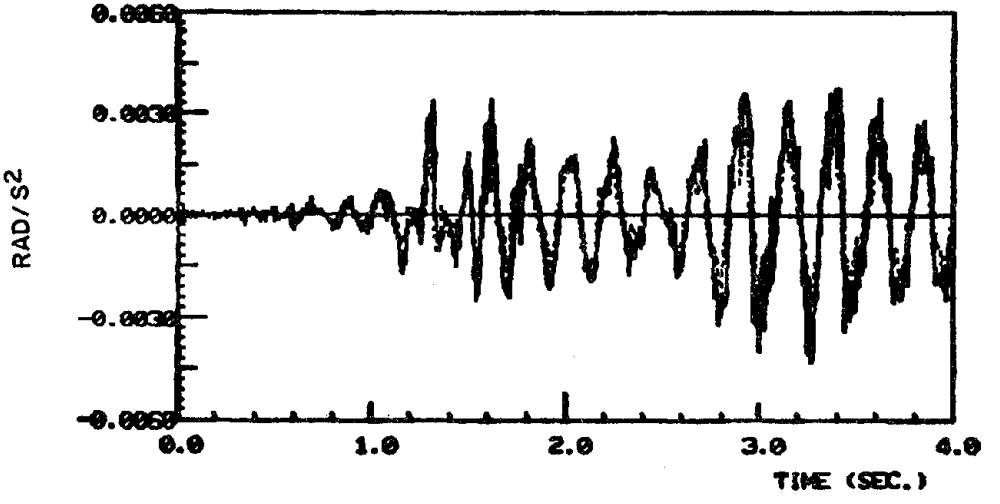

COMPUTED AND MEASURED ANGULAR ACCELERATION OF TOP MASS
PZ-I (EC-150) (1ST 4 SECONDS)

- - - - = measured

———— = computed using Eq. 2, Fig. 7.6

Figure 7.8 Comparison between computed and experimental rotational acceleration.

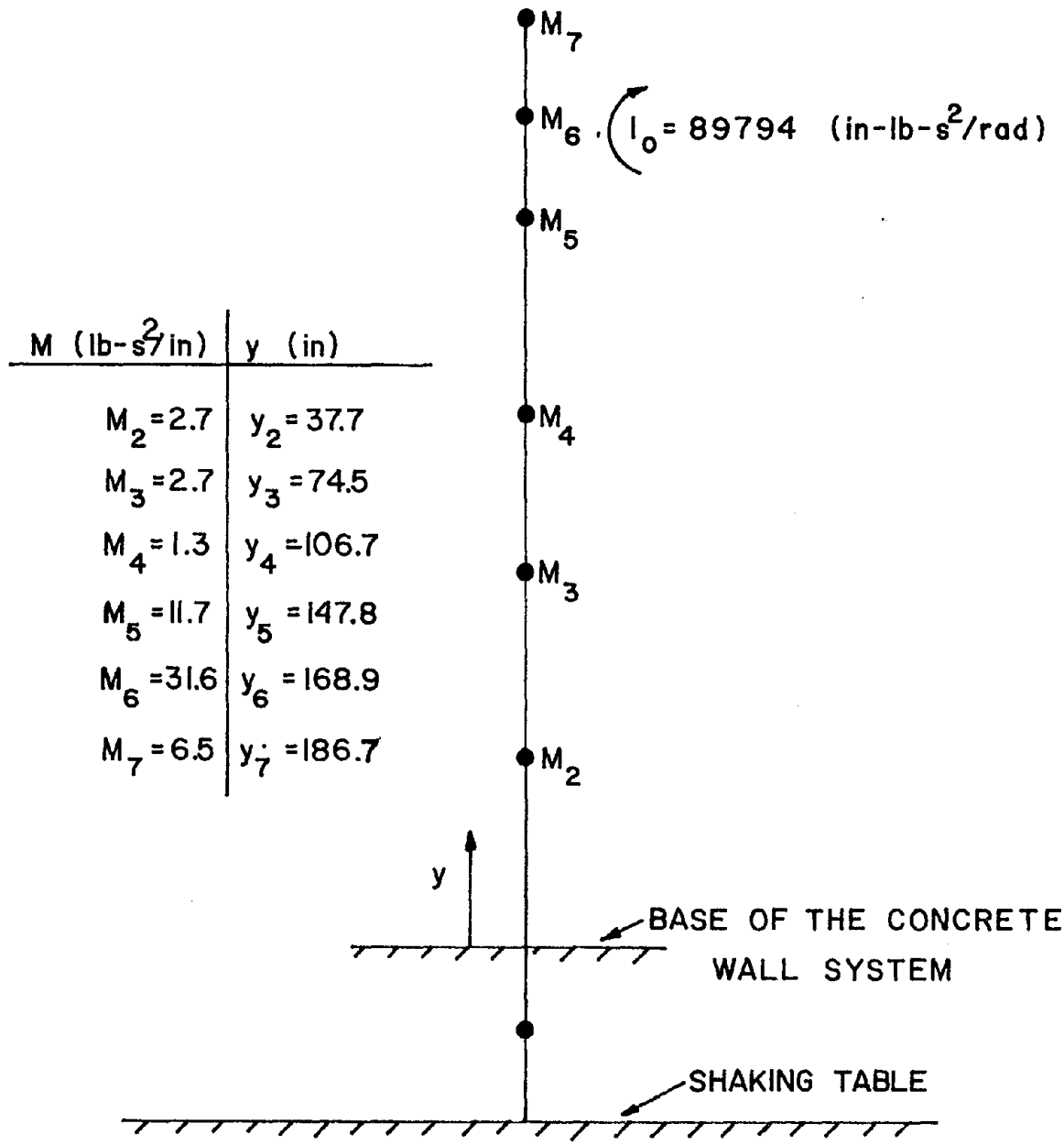

M (lb-s²/in)	y (in)
M_2 = 2.7	y_2 = 37.7
M_3 = 2.7	y_3 = 74.5
M_4 = 1.3	y_4 = 106.7
M_5 = 11.7	y_5 = 147.8
M_6 = 31.6	y_6 = 168.9
M_7 = 6.5	y_7 = 186.7

Figure 7.9 Allocation of lumped masses.

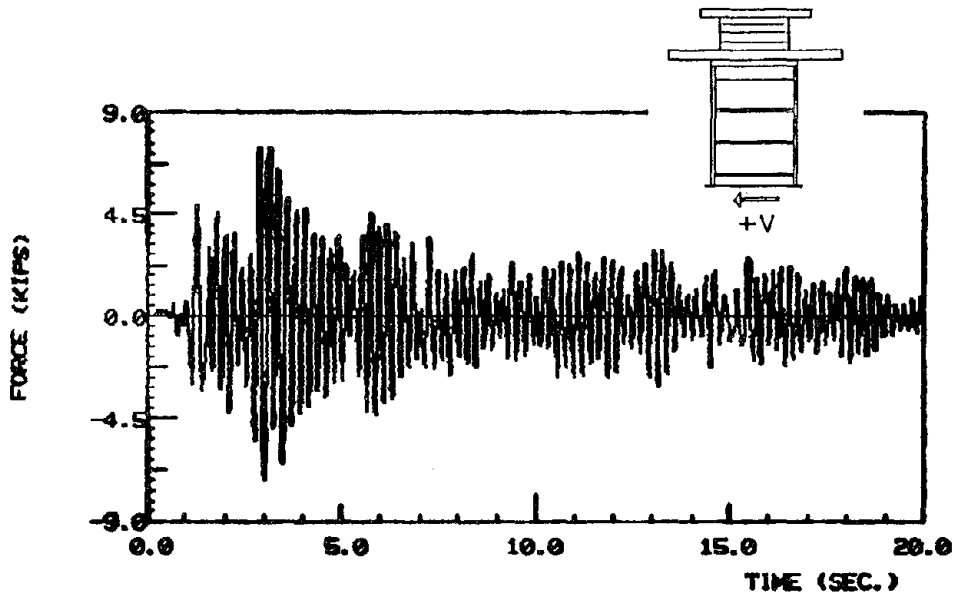

COMPUTED AND EXPERIMENTAL SHEAR FORCE AT FOUNDATION
PZ-I (EC-150)

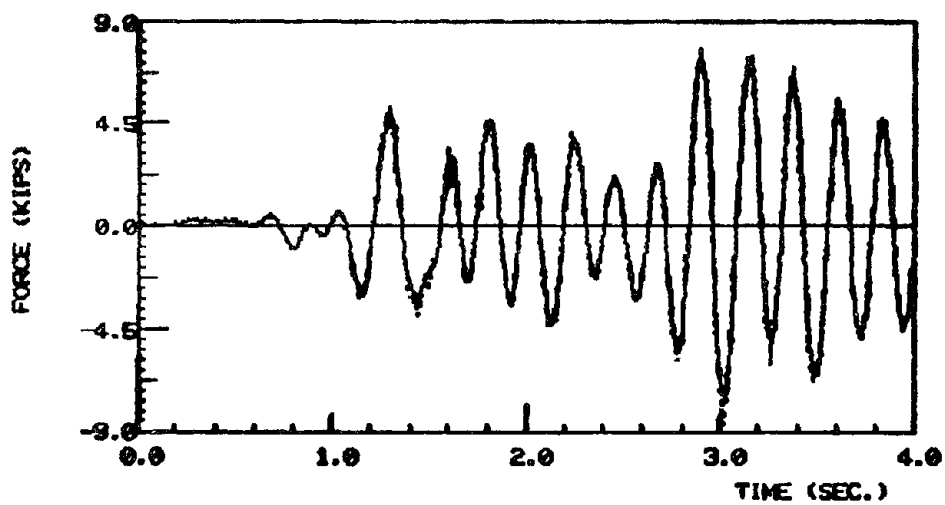

COMPUTED AND EXPERIMENTAL SHEAR FORCE AT FOUNDATION (1ST 4 SECONDS)
PZ-I (EC-150)

——— = measured from force transducers

- - - - = computed inertial force summation

Figure 7.10 Comparison between computed and measured experimental base shear.

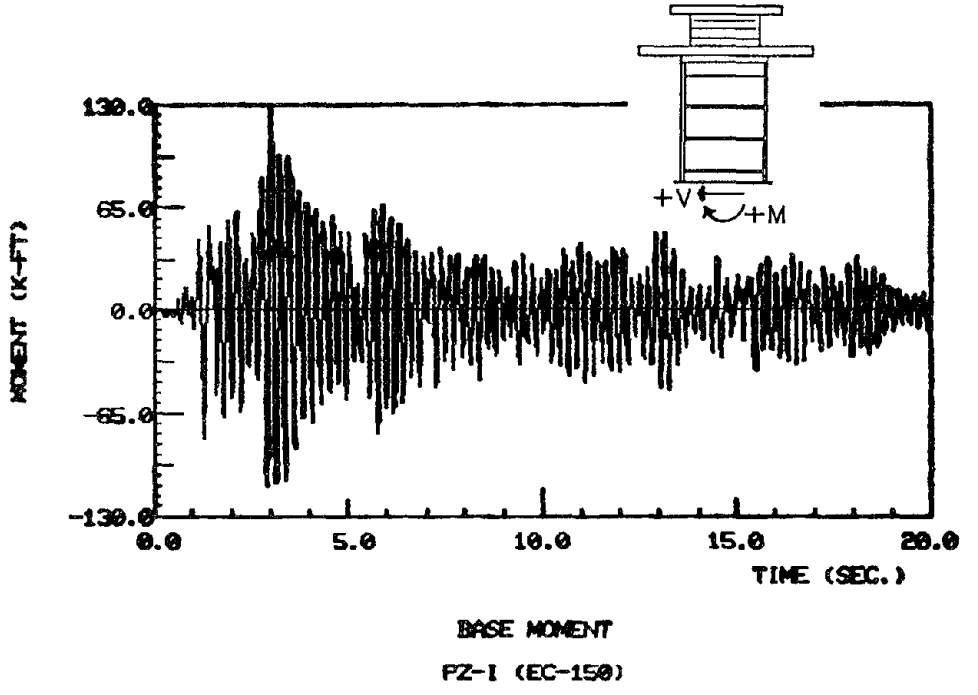

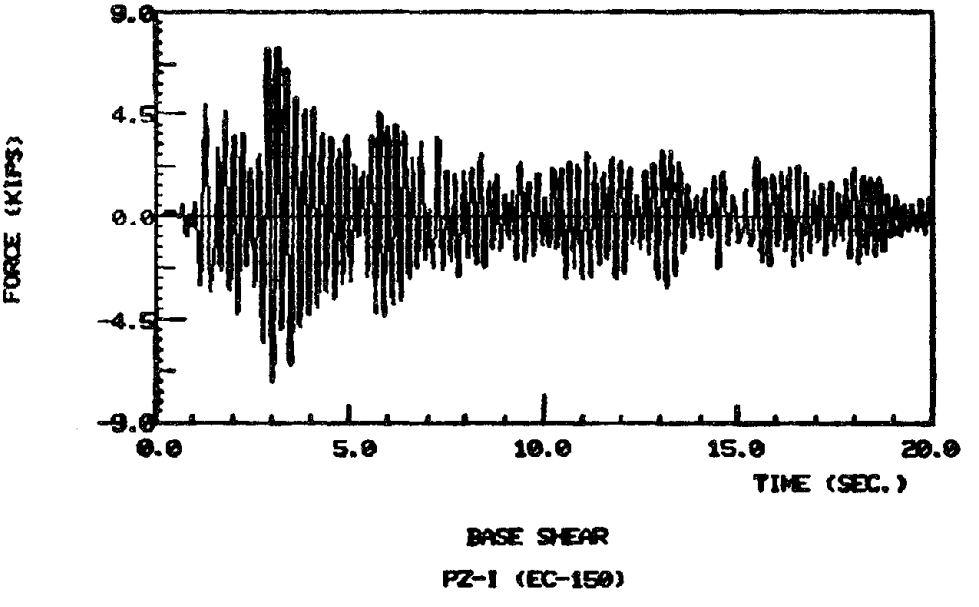

Figure 7.11 Base shear and base bending moment, simple wall, EC-150, 0.18g. Moment calculated from inertial forces and shear measured by transducers and adjusted to correct value at base of precast wall.

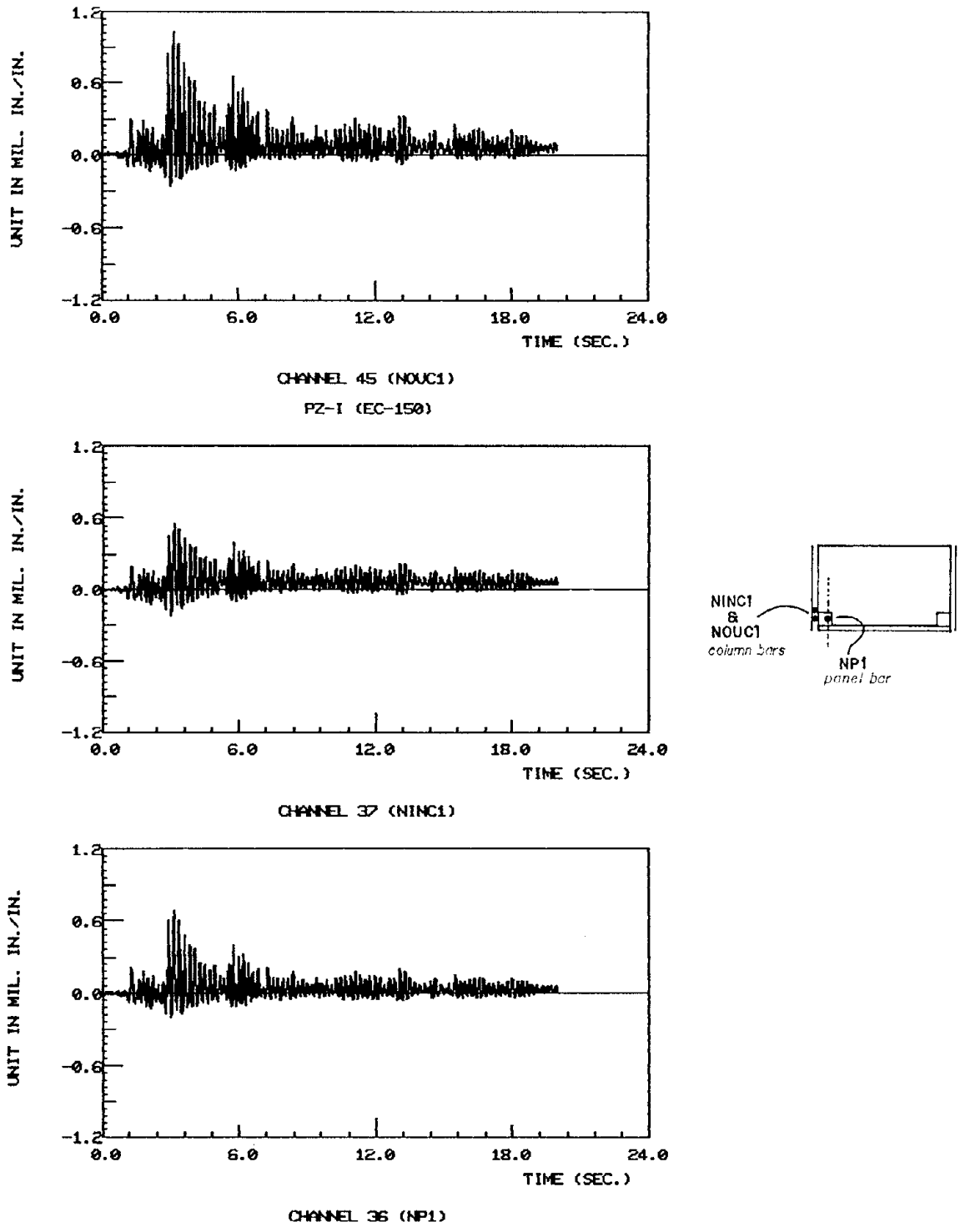

Figure 7.12 Strains in reinforcing bars, simple wall, EC-150, 0.18g. (positive = tensile strain)

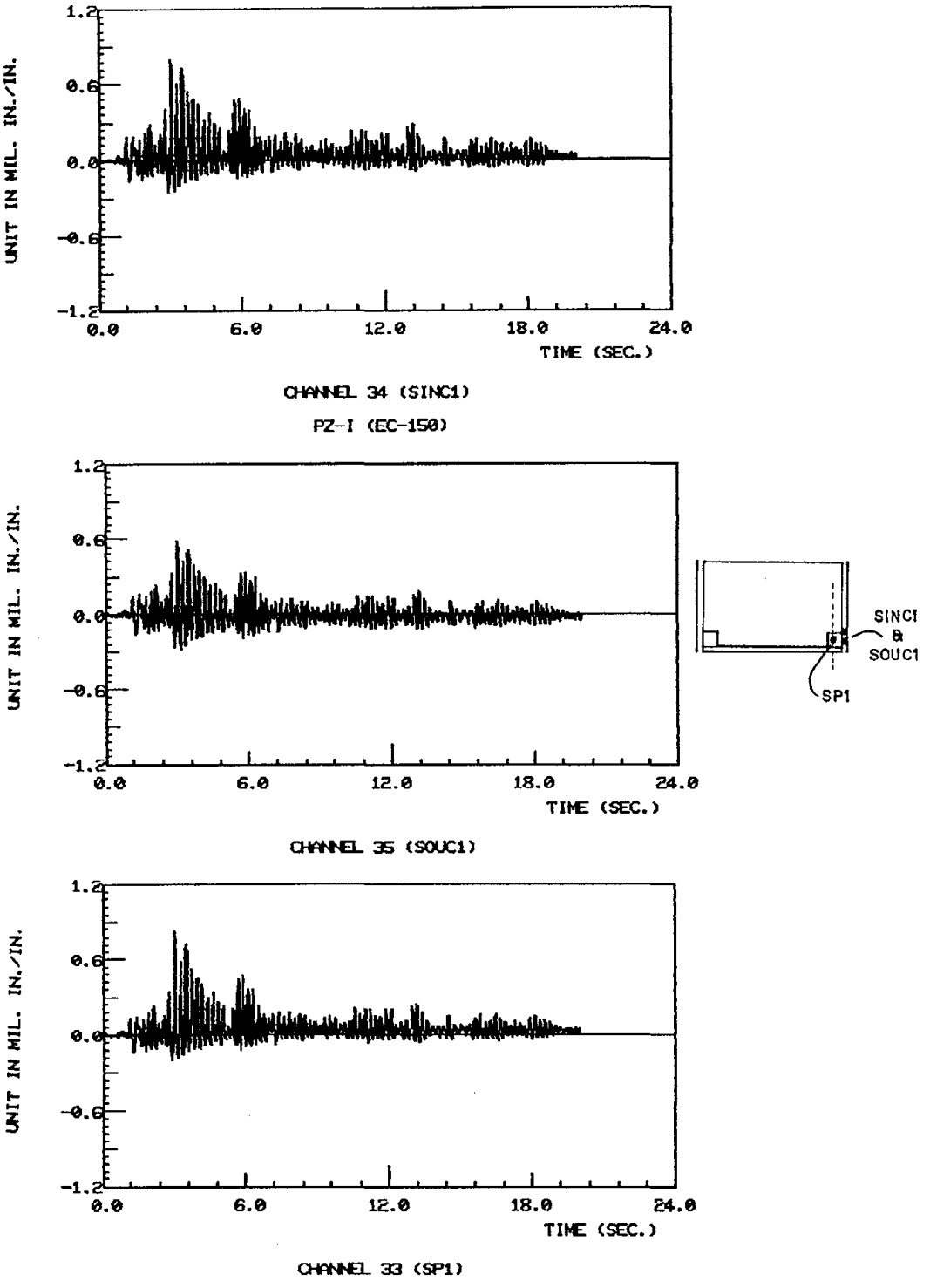

Figure 7.12 Continued.

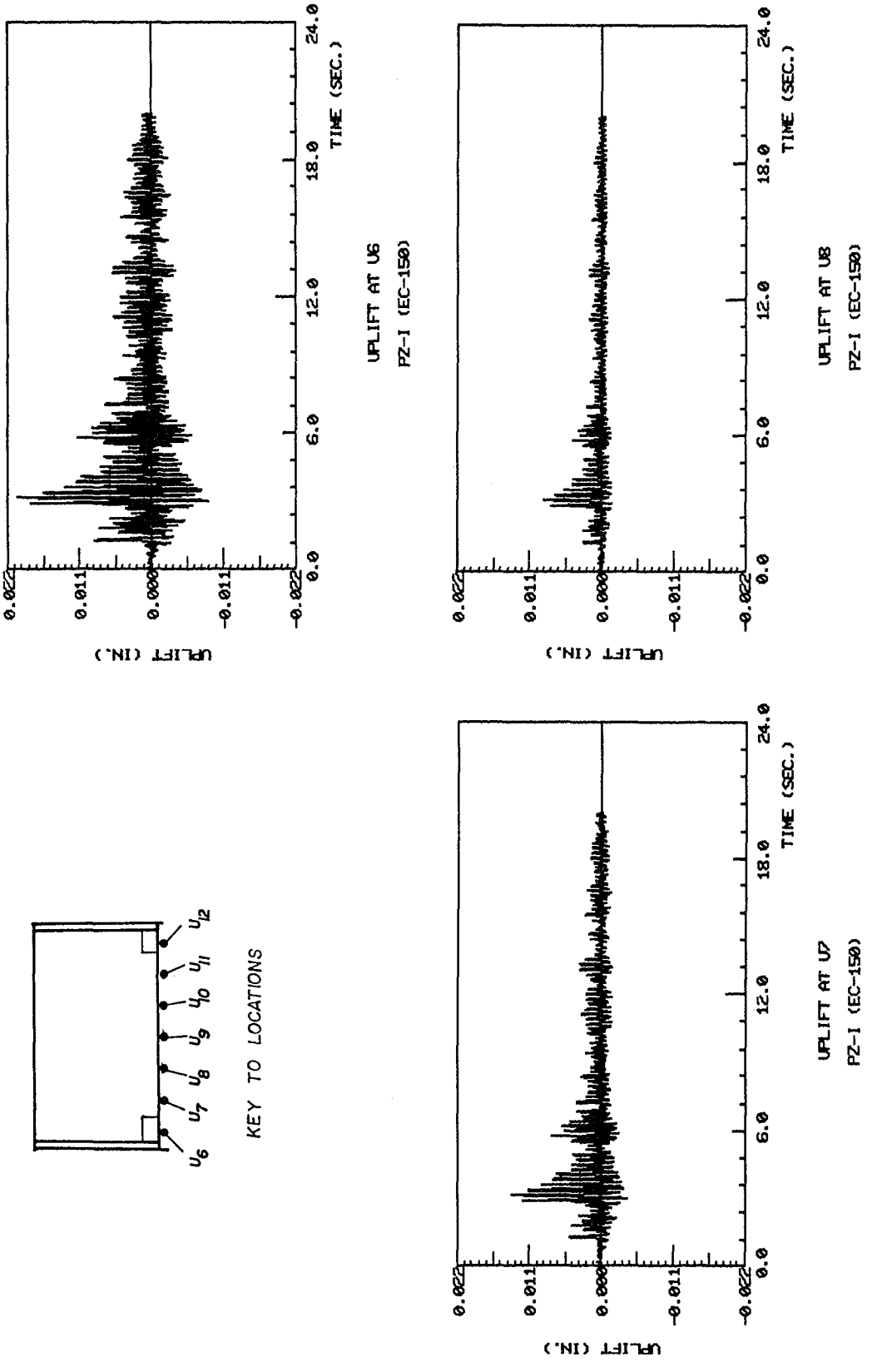

Figure 7.13 Total uplift, simple wall, EC-150, 0.18g.

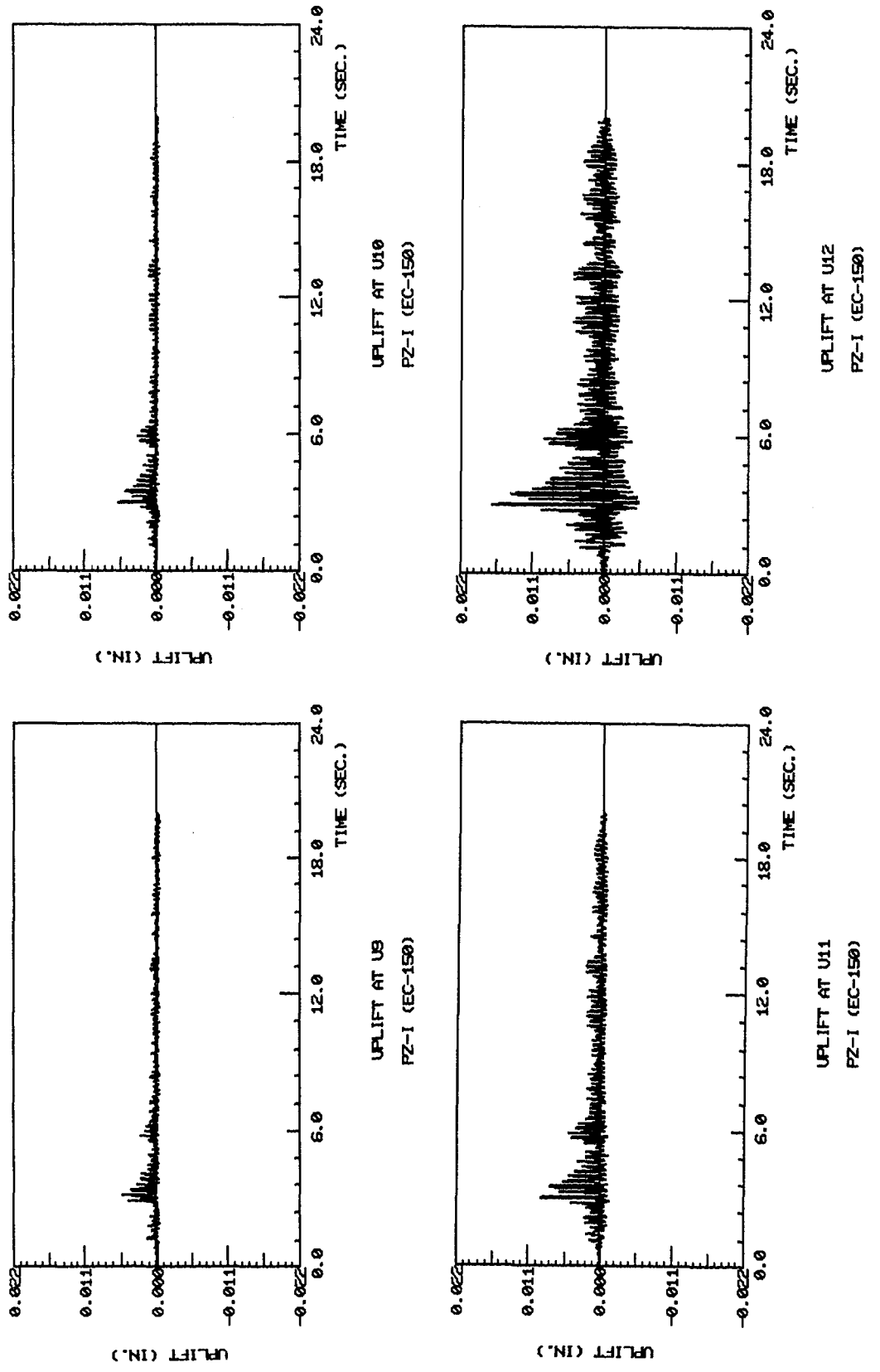

Figure 7.13 Continued.

The resultant inertia forces were added at the foundation level and the total compared with the sum of the measured force transducer shears in Fig. 7.10. These two quantities are compared over the entire record and, in particular, during the first four seconds since the maximum shear force occurred in this period; the results were almost identical. The force transducers registered a maximum value of 7.5 kips though the base shear was computed as 8.6 kips when the inertia forces were added; the variation occurred in the peak at 3.01 seconds. Nevertheless, it can be concluded that the assumptions regarding allocation of the masses and the corresponding accelerations were fairly accurate.

After the accuracy of the lumped masses was checked, the bending moment was calculated at the first floor level. The inertia force resulting from M1 and AH1 was ignored. At 3.01 seconds, the bending moment reached its maximum value of 127.1 kips-ft. Figure 7.11 shows its variation with time.

The experimental shear force measured by the force transducers was modified to obtain the shear force at the first floor level. It was assumed that the foundation, and a portion of the lower walls having a mass of 3.5 lb sec^2/in. were vibrating with the table acceleration. The resulting inertia force was subtracted from the shear value at the foundation level to obtain the wall base shear force. Figure 7.11 illustrates the base force at the first floor level which reached a maximum value of 7.4 kips.

7.2.5 Strains in Reinforcing Bars

Time-history plots of the strains in the reinforcing bars are shown in Figure 7.12. These plots indicate that the bars remained within the elastic limit. For example, the maximum strain experienced by the outside column bar at the north side was 1.03 mil/in. Channels 37 and 45, however, show some small amount of offset at the end of the signal. This is not permanent strain

due to yielding of the bars since they remained in the elastic range. The offset is believed to be because of microcracking in the concrete. It is interesting to note that at the time when the south-end bars were stretched to their maximum values, the north-end bars were compressed to their minimum values. Table 7.1 includes the maximum and minimum strains for the different reinforcing bars.

7.2.6 Uplift Values of the First-Floor Joint

The uplift value of the wall panel with respect to the floor panel and that of the floor panel with respect to the foundation had been measured by the DCDTs placed specifically for this purpose, i.e., B1,B2,U1,U2,...,U12. However, it was desirable to have the total uplift value of the wall panel in order to study the behavior of the joint at this level. For this purpose, the individual values from B1,U1,...,B2 were added to those from U6,U7,...,U12. The resulting total uplift values are presented in Figure 7.13. At the time when the south end had opened to its maximum value (0.017 in.), the north end showed a compression (0.009 in.). The maximum uplift was experienced by the north end which opened 0.020 in. It is interesting to note that the maximum opening at the south end corresponds to the maximum negative overturning moment (-127.1 k-ft). A complete list of the maximum uplifts at the two ends of the wall can be found in Table 7.1.

7.2.7 Overall Behavior of the Wall System

The average stiffness and curvature of the entire wall can provide information regarding the overall behavior of the system. The average strains in the two ends of the wall are obtained from potentiometers POTN and POTS which measured the overall extension or compression at the ends of the wall. The resulting strains are then divided by the distance between the two

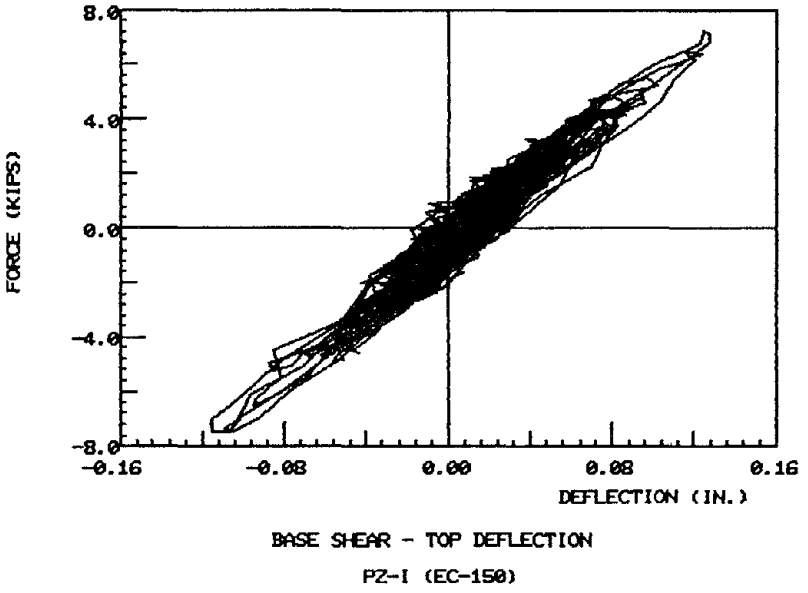

Figure 7.14 Overall behavior of the system, simple wall, EC-150, 0.18g top deflection and simultaneous base shear.

potentiometers in order to determine an average curvature.

Base shear force is plotted against top deflection in Figure 7.14; an average stiffness of 54 kips/in. can be approximated from this plot. The plot clearly indicates that the entire wall remained in the elastic region.

The base shear is plotted against the curvature measured in the lower panel in Figure 7.15. The bilinear stiffness apparent in the plots is probably due to slight cracking in the panel, reducing the effective section.

7.3 Results From El Centro at 0.67 (EC-700) - PZ-I Wall

7.3.1 Introduction

In contrast to the first test (EC-150), this test was performed at a high amplitude. The increase in intensity was in order to investigate the inelastic behavior of the entire wall and, in particular, the horizontal joint. The horizontal table acceleration and displacement of this amplified signal are illustrated in Figure 7.16. From this figure, it can be seen that the table reached its peak horizontal displacement of -3.553 in. at 8.45 sec,

and that the maximum horizontal acceleration of the shaking table was -0.666g at 1.22 second.

The high amplitude motion during this test caused deformations beyond the range of a few of the monitoring instruments and damaged instrument mounts or made instruments inoperable in other cases. The mountings of the slip measuring DCDTs - S4 and S6 were damaged. S4 produced no meaningful data and S6 was damaged shortly into the test resulting in limited data as shown in Figure 7.17. The mounting for one of the diagonal DCDTs on the lower wall panel, channel D1, broke away during the test. Low range instruments ($\pm$ 0.10 in.) were used to measure wall uplift at positions U9 and U10. However, the magnitude of the uplift exceeded those anticipated limits and the instrument amplifiers reached this peak output resulting in the flat tops of cut-off uplift peaks visible in Figure 7.18. A similar situation developed in the vertical accelerometers mounted on the steel platform above the wall, AV1 and AV2. None of the bad channels resulted in a serious loss of data.

7.3.2 Accelerometer Results

Figure 7.19 illustrates the time-history plots of accelerations at different locations. It is interesting to note that the maximum acceleration was measured by the accelerometer located at the foundation. This value is almost three times greater than the acceleration at the added concrete blocks and coincides with an acceleration pulse in the table motion, see Figure 7.16.The maximum acceleration at the foundation occurred simultaneously (at 1.45 sec) with the first major crack opening at the south side and the rupture of the south panel bar. At this instant, DCDTs labelled U11 and U12 registered 0.25 in. and 0.31 in. of crack, respectively. The large

TABLE 7.2

Extreme Values from EC-700 Test (PZ-I)

Quantity	Extreme Value	
Acceleration at foundation	2.47g	
Acceleration at second floor	-1.87g	
Acceleration at third floor	-1.10g	
Acceleration at top of wall	0.80g	
Acceleration at concrete blocks	0.84g	
Second-floor lateral displacement	1.17 cm	(0.46 in.)
Third-floor lateral displacement	2.26 cm	(0.89 in.)
Top of wall lateral displacement	3.76 cm	(1.48 in.)
Base shear force	-70.7 kN	(-15.7 kip)
Base bending moment	-397.3 kN-m	(-3516 in-k)
Strain in north-end panel bar of first floor	3.92%	
Strain in north-end outside column bar of first floor	2.29%	
North-end uplift	0.86 cm	(0.34 in.)
South-end uplift	1.78 cm	(0.70 in.)
Shear-slip of first floor joint	0.10 cm	(0.04 in.)
Average wall curvature	2.76×10^{-5} rad/cm	(6.998×10^{-5} rad/in.)
Curvature of first-floor wall panel	0.62×10^{-5} rad/cm	(-1.57×10^{-5} rad/in.)

acceleration spike was apparently caused by a shock wave originating with the bar rupture. Plots at increasing height above the rupture location show a decreasing size of acceleration spike.

7.3.3 Lateral Displacements

Relative lateral displacements were obtained from the absolute wall displacements and table motion as before. Figure 7.20 illustrates the time-history plots of these quantities. The displacement of the wall's steel foundation beam relative to the shaking table was directly measured and is also shown in Figure 7.20. The maximum lateral deflection was 1.5 in. and occurred at the top of the wall. This value is almost 13 times larger than the similar deflection in the previous test. The second and the third floor displacements are 8 and 9 times larger than those values measured during the first test. Table 7.2 lists the maximum deflections in both directions.

7.3.4 Base Shear Force and Bending Moment

As mentioned earlier, accelerometers AV1 and AV2 exceeded their calibration limit or the corresponding amplifiers were saturated. Therefore, it was not possible to use the resulting accelerations to obtain the rotational acceleration of the added mass system. The method developed in Section 7.2.4, i.e., using equation (2) from Figure 7.6 provides an alternate way to determine rotational acceleration; then, a similar approach to that in Section 7.2.4 is possible. From the force transducers the force at the foundation level reached a maximum of 16.4 kips. The theoretical shear force at this level was computed by using inertial force and Equation 2. This force reached a maximum value equal to 17.3 kips. Both maximum magnitudes occurred at 1.42 seconds. The comparison in Figure 7.21 of the experimental and calculated results for the first four seconds in addition to the entire record, illustrates the

closeness of the two shear forces. For moment computation the inertial forces are seen to be sufficiently accurate, though overturning moments will not be exact.

Using the same lumped masses and ignoring the inertia force resulting from AH1, the bending moment at the base of the wall was computed. Figure 7.22 indicates that the bending moment reached an approximate maximum of 3516 in.-k at 1.45 sec.

Similar adjustments as in the first test were made on the measured shear force at the foundation level in order to present it at the base of the wall. Its variation with time is shown in Figure 7.22. The base of the wall underwent a maximum shear force equal to -15.7 kips, the magnitude of which is twice that of the base shear of the low amplitude test.

7.3.5 Strains in Reinforcing Bars

Because of the high intensity of this test, the reinforcing bars experienced large strains, particularly those at the south end. Figure 7.23 illustrates the level of strains which caused severe damage in the bars. Although the bars at the south end suffered more extensive damage, the first yield was detected by the strain gauges at the north end. At 1.23 sec when the overturning moment was 218 ft-kip, the outside bar in the north end column was strained to 2.33 mil/in. The strain gauges labelled SP1, SINC1, SOUC1, NP1 and NINC1 (prefix 'S' indicates a south bar, 'N' indicates a north bar) at this time registered -0.405 mil/in., -0.520 mil/in., -0.534 mil/in., 1.80 mil/in. and 1.472 mil/in., respectively. (The strain gauges were rated for a maximum strain of 20 mil/in.)

From Figure 7.23 it is seen that at 1.43 sec the panel bar at the south end (SP1) was strained beyond its calibration limit, i.e., 42.1 mil/in. The measured data after this point cannot be reliable. A time-history plot from

the strain gauge mounted on this bar indicates that after 2.84 sec, the strain gauge registered a constant negative strain. This constant value can be either due to a damaged strain gauge or because of a ruptured reinforcing bar with residual strain. It seems most likely that the former was the reason since at the end of the test this bar was found ruptured very close to the strain gauge location causing strains considerably beyond the gauge's rated limit.

Variation in the strain for the column bars at the south end indicates that they also had exceeded their limits. At 1.49 sec, the inside column bar experienced a strain of 42.5 mil/in. and 0.04 sec later the outside column bar passed beyond its maximum rated value. A similar state of constant strain can be observed for both of these bars. As mentioned earlier, this behavior might have been due to a damaged strain gauge or a ruptured bar - probably the former since the post-test examination did not show any rupture, and also because of the closeness of the buckling point and the strain gauge location. In other words, it is believed that the buckling action damaged the gauges so they were not capable of registering any more strain. This would explain the constant state of strain.

According to Figure 7.23, the bars at the north end of the wall did not strain as much as the south-end bars. The inside column bar at this side, however, exceeded its calibration limit at 7.45 sec. Thus, the data beyond this point cannot be reliable. The maximum strain at this side was experienced by the panel bar which was strained to 39.2 mil/in. Table 7.2 summarizes the maximum strain values for strain gauges which did not exceed their calibration limits.

7.3.6 Uplift Values of the First-Floor Joint

The total uplift of the first-floor wall panel from the foundation was found at different locations. The resulting net uplift values have been illustrated in Figure 7.24.

Because of the higher intensity of the input signals, all the uplift values show a considerable increase over those measured in the previous test. The south end experienced a maximum uplift of 0.70 in., almost 40 times greater than the corresponding value for the first test. At 7.15 sec, 0.01 sec before the maximum uplift was detected, the top of the wall deflected north to its maximum lateral displacement. The north end of the wall opened to a maximum of 0.34 in. at 1.82 second (17 times greater than the corresponding value in the previous test EC-150), concurrent with the maximum deflection towards the south.

It is interesting to note that the first significant uplift at the south end occurred at 1.43 sec when the wall was lifted from 0.006 in. to 0.11 in. at its extreme end. This sudden increase of uplift corresponds to an excessive straining of the panel bar at this side. At this instant, the south-end panel bar was strained from 2.98 mil/in. to 42.3 mil/in., at which the strain gauge welded onto this bar exceeded its calibration limit and it is likely that bar rupture followed.

The time-history plots in Figure 7.24 illustrate a very distinctive behavior--that there are no significant negative values of uplift. Some small negative values were detected at the beginning of the test, but these gradually disappeared toward the end of the tests. These plots, in other words, indicate that the gap which was opened during the uplift motion did not ever close. It is believed that the crushed concrete pieces prevented the complete closure of the gap. The entire wall thus experienced a rigid-body

uplift. That is, although the lifted portions of the wall should be closed by the rocking motion, the instrumentation did not register negative displacement-compression.

The abovementioned rigid-body uplift of the entire wall should be taken into consideration in any attempt to find the location of the neutral axis. This is because the positive sign of the uplift values imply that the deformed cross section of the wall never shows compression and hence there is no neutral axis within the extent of the joint.

7.3.7 Shear-Slip at the First-Floor Joint

In contrast to the first test, the slip at the first-floor joint was of measurable magnitude. Ignoring the data from DCDTs labeled S4 and S6 (due to malfunction) an average value of slip was calculated from DCDTs labelled S3 and S5, and those labelled S2 and S1. The resulting shear slip has been plotted in Figure 7.25.

The average slip at the first-floor joint reached a maximum value of 0.04 in. at 1.82 sec. It is of interest to observe that at this instant the wall experienced its maximum lateral displacement to the south (0.88 in., which is 22 times greater than the value of slip) and the north end of the wall at the first floor was lifted to a peak value of 0.34 in. Simultaneously, the base shear force was -13.7 kips.

Because of the small magnitude of the shear-slip displacement, it can be assumed that a shear friction mechanism was not fully active and Coulomb friction was providing the major resistance. The level at which shear slip occurs varies depending on the magnitude and sign of the axial load. This fact can be verified by tracing the values of wall uplift, the magnitude of base shear, and the degree of shear slip.

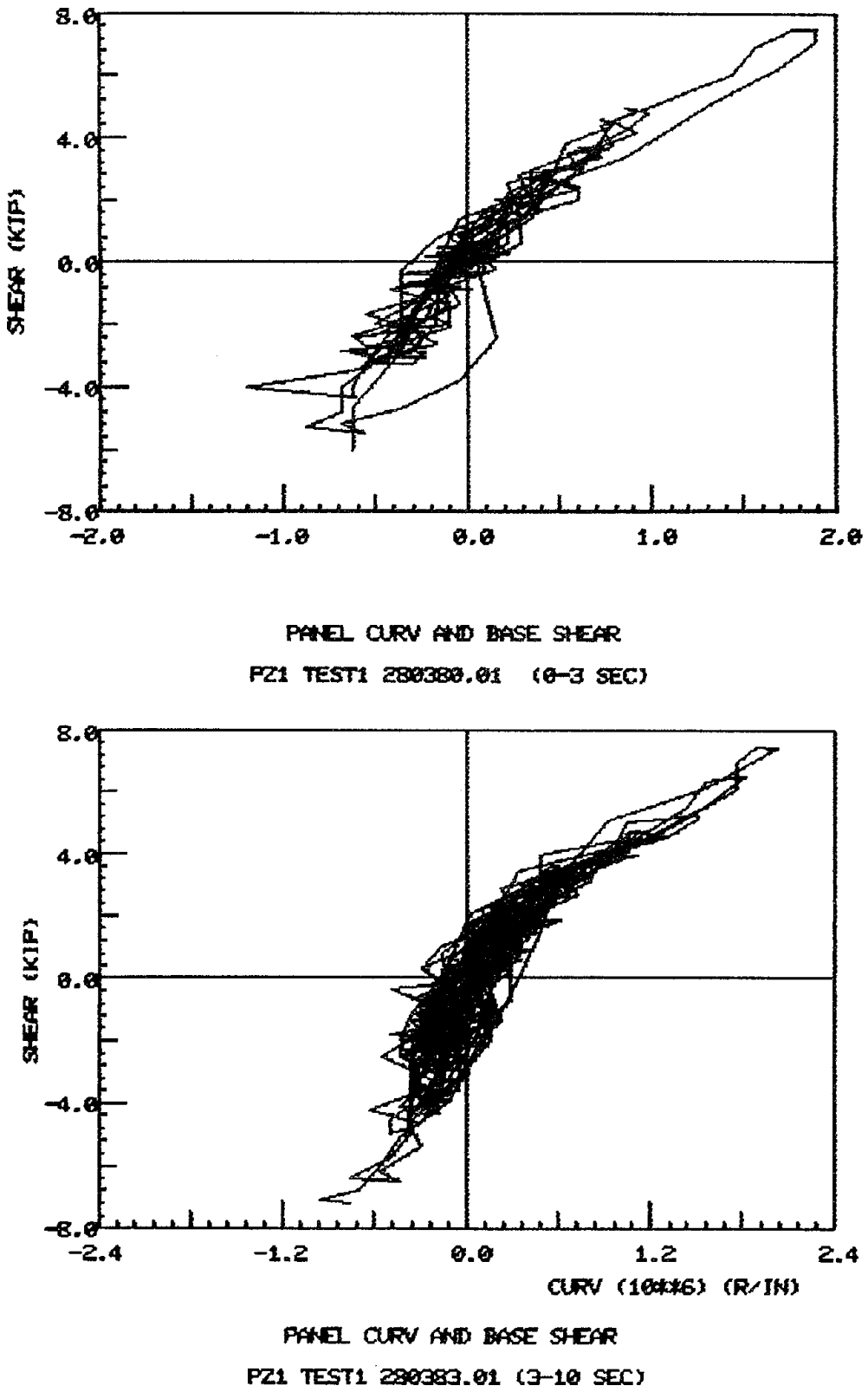

Figure 7.15 Behavior in the lower panel, curvature and shear, simple wall, EC-150, 0.18g.

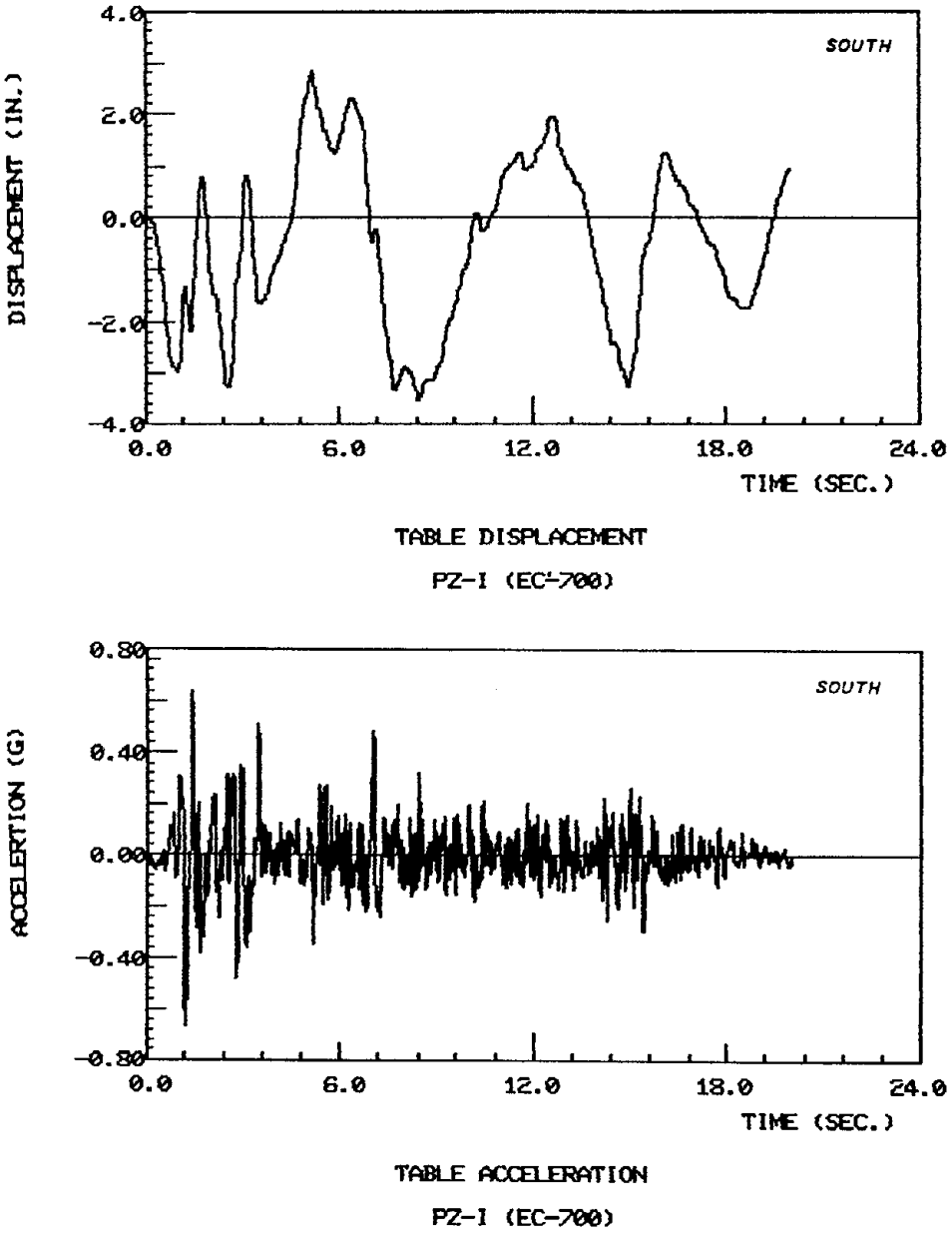

Figure 7.16 Horizontal displacement and acceleration of the shaking table, simple wall, EC-700, 0.67g.

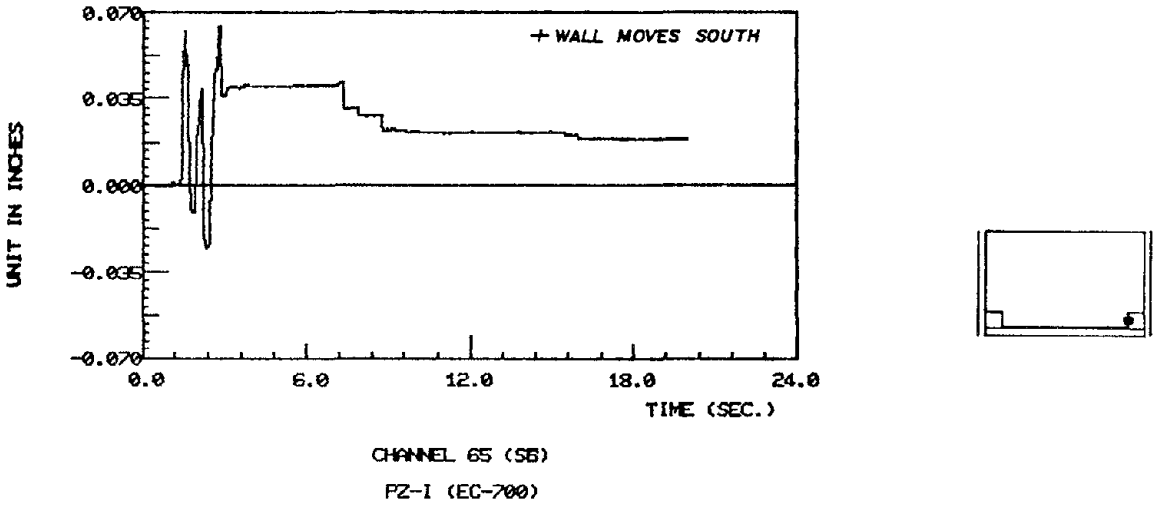

Figure 7.17 Time history of channel 65, slip, simple wall, EC-700, 0.67g.

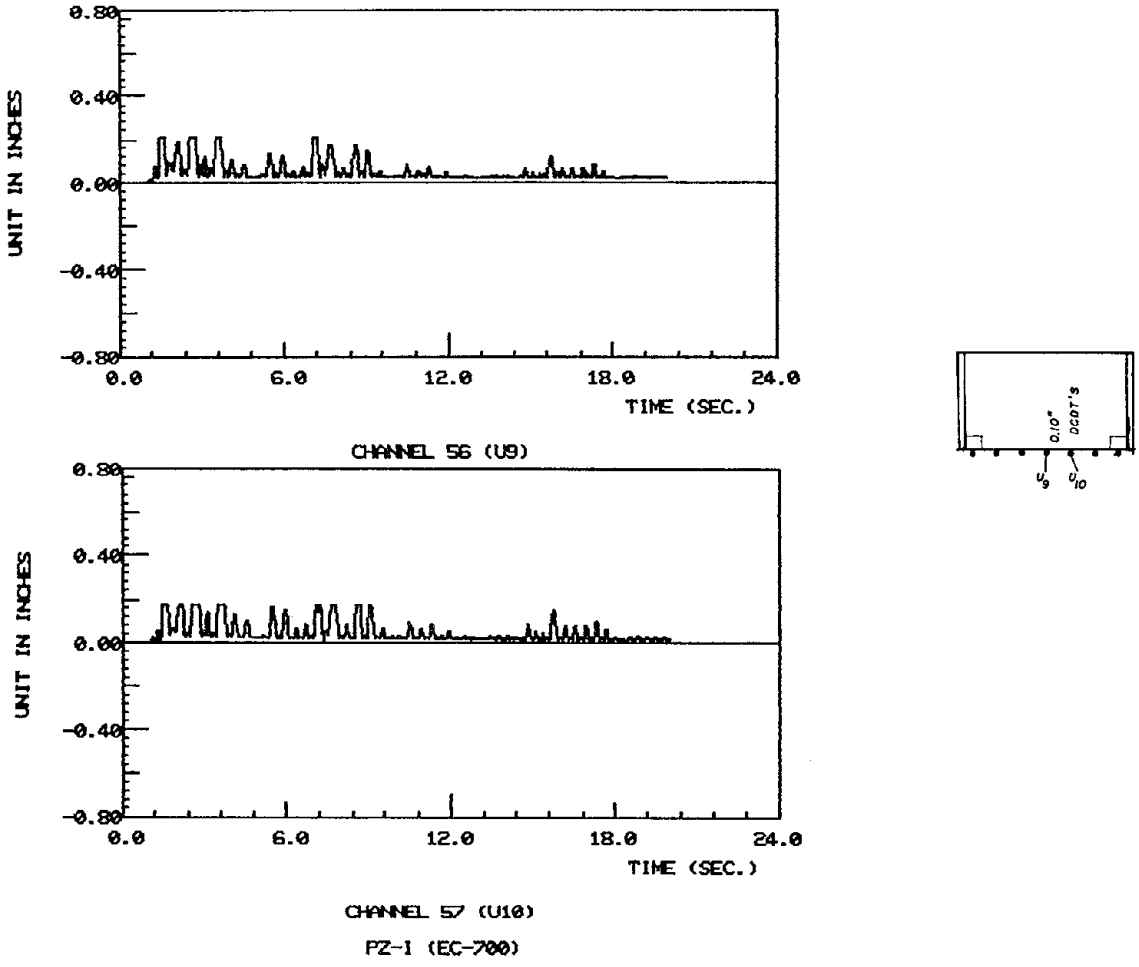

Figure 7.18 Time history of channels 56 and 57, uplifts, simple wall, EC-700, 0.67g.

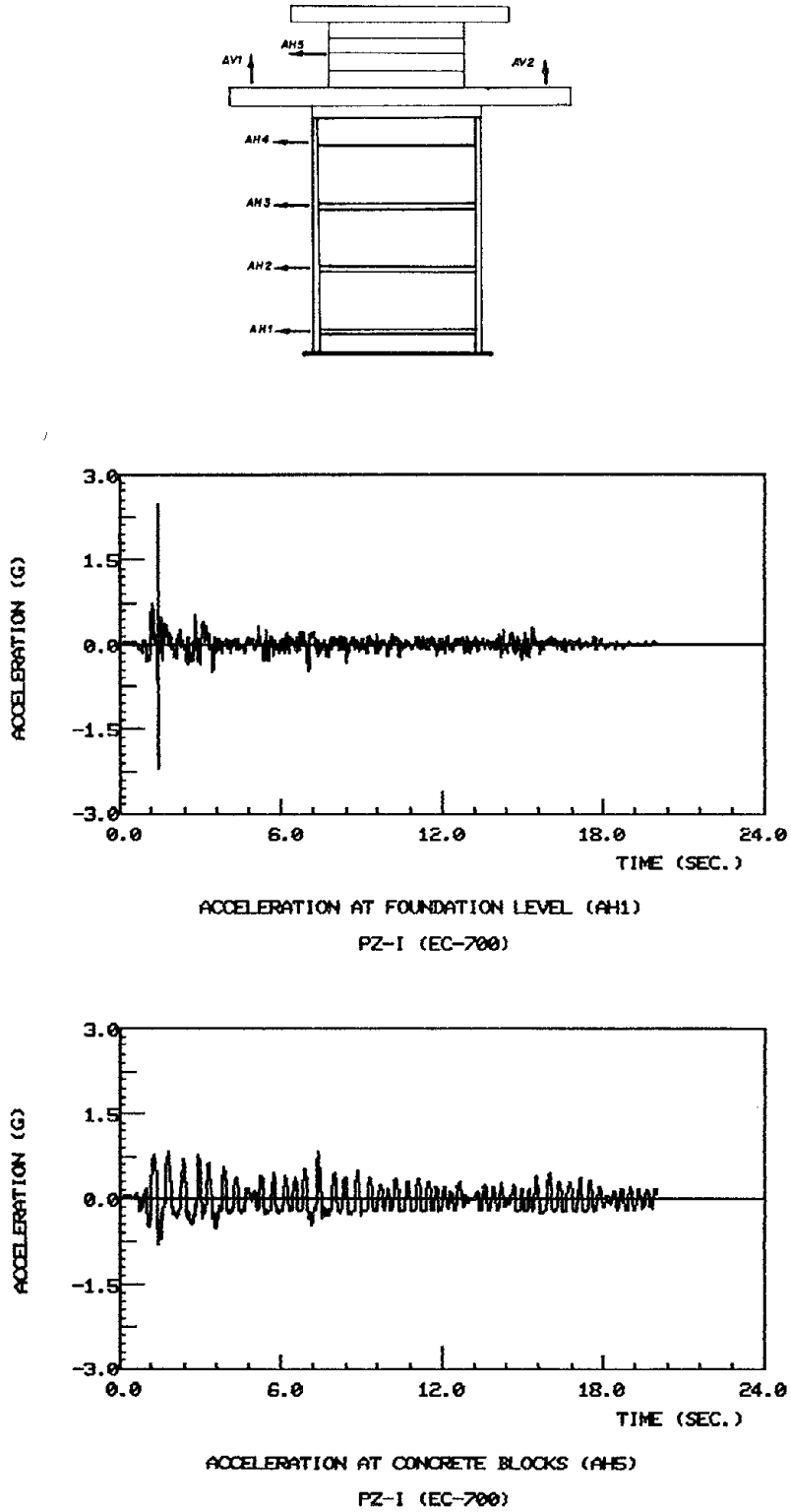

Figure 7.19 Accelerations developed within the structure, simple wall, EC-700, 0.67g.

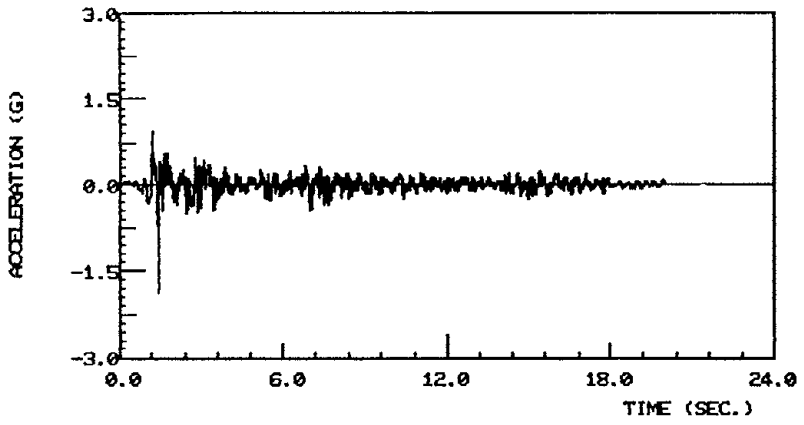

ACCELERATION AT SECOND FLOOR (AH2)

PZ-I (EC-700)

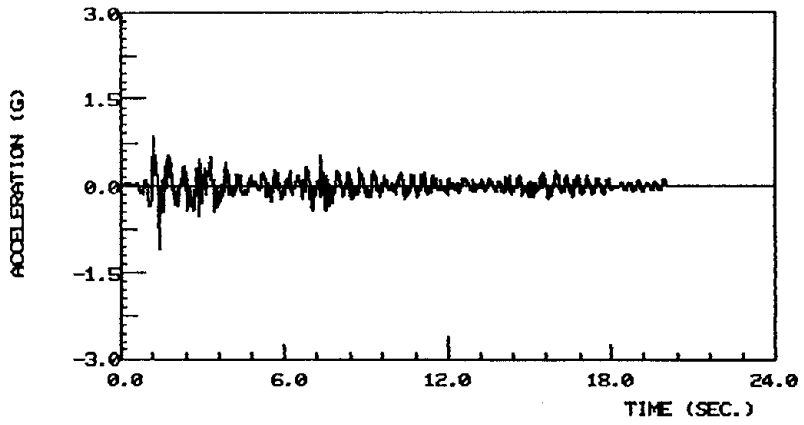

ACCELERATION AT THIRD FLOOR (AH3)

PZ-I (EC-700)

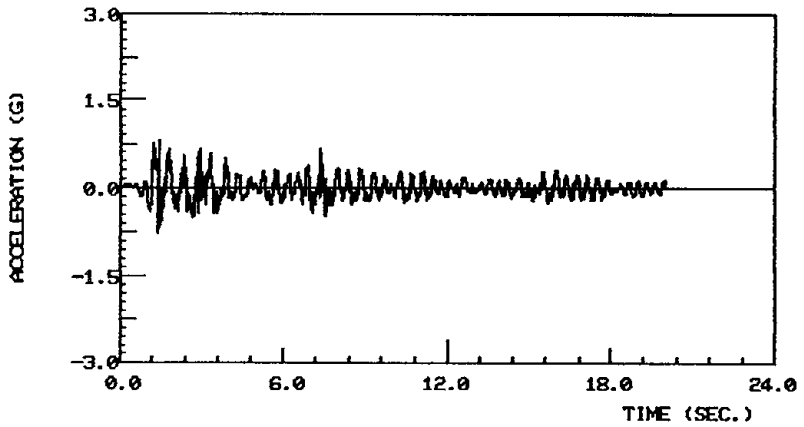

ACCELERATION AT TOP OF WALL (AH4)

PZ-I (EC-700)

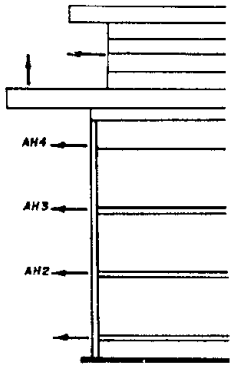

Figure 7.19 Continued.

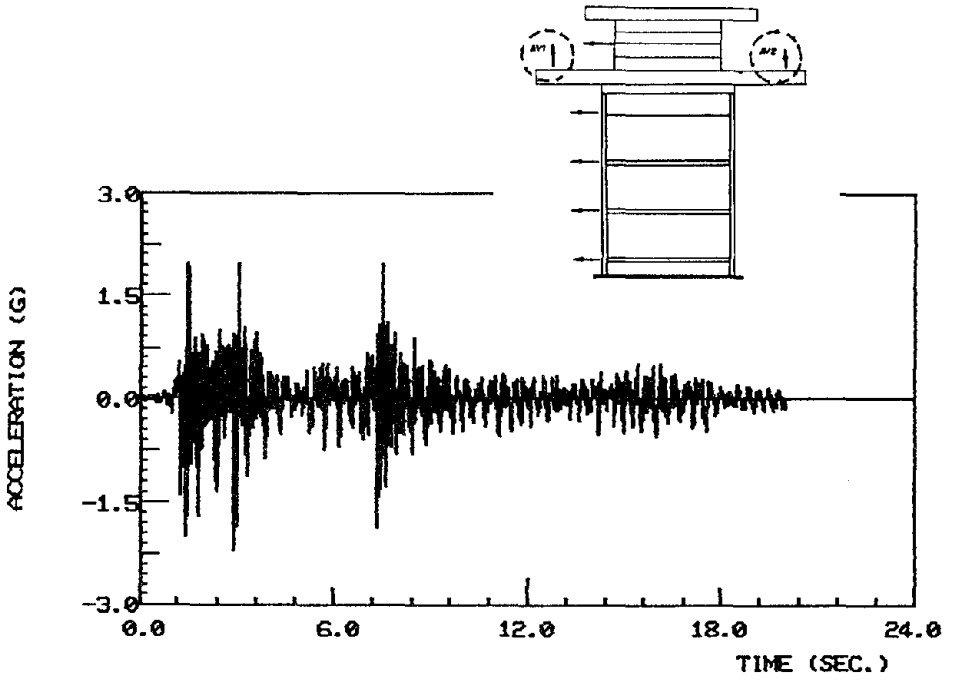

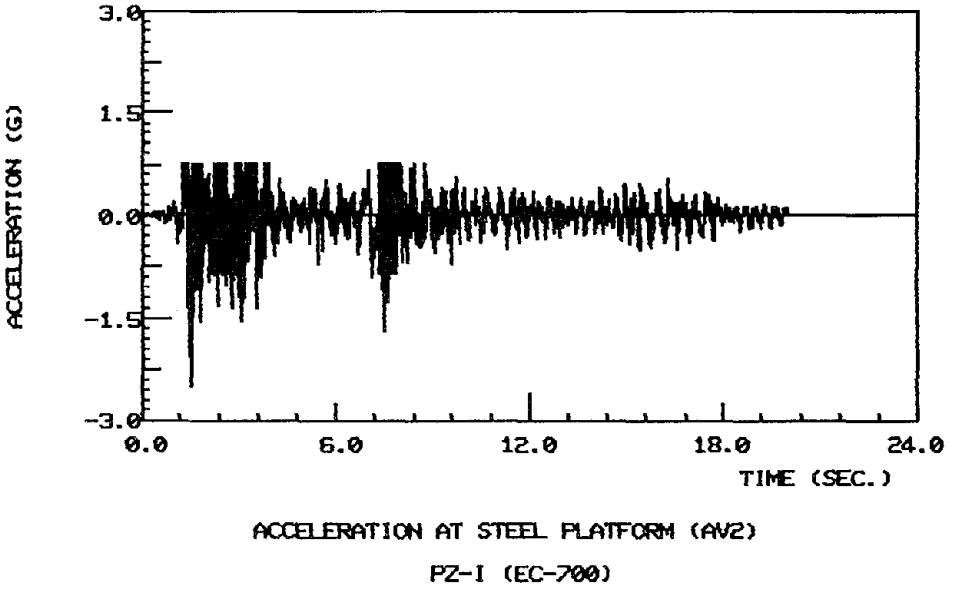

Figure 7.19 Continued.

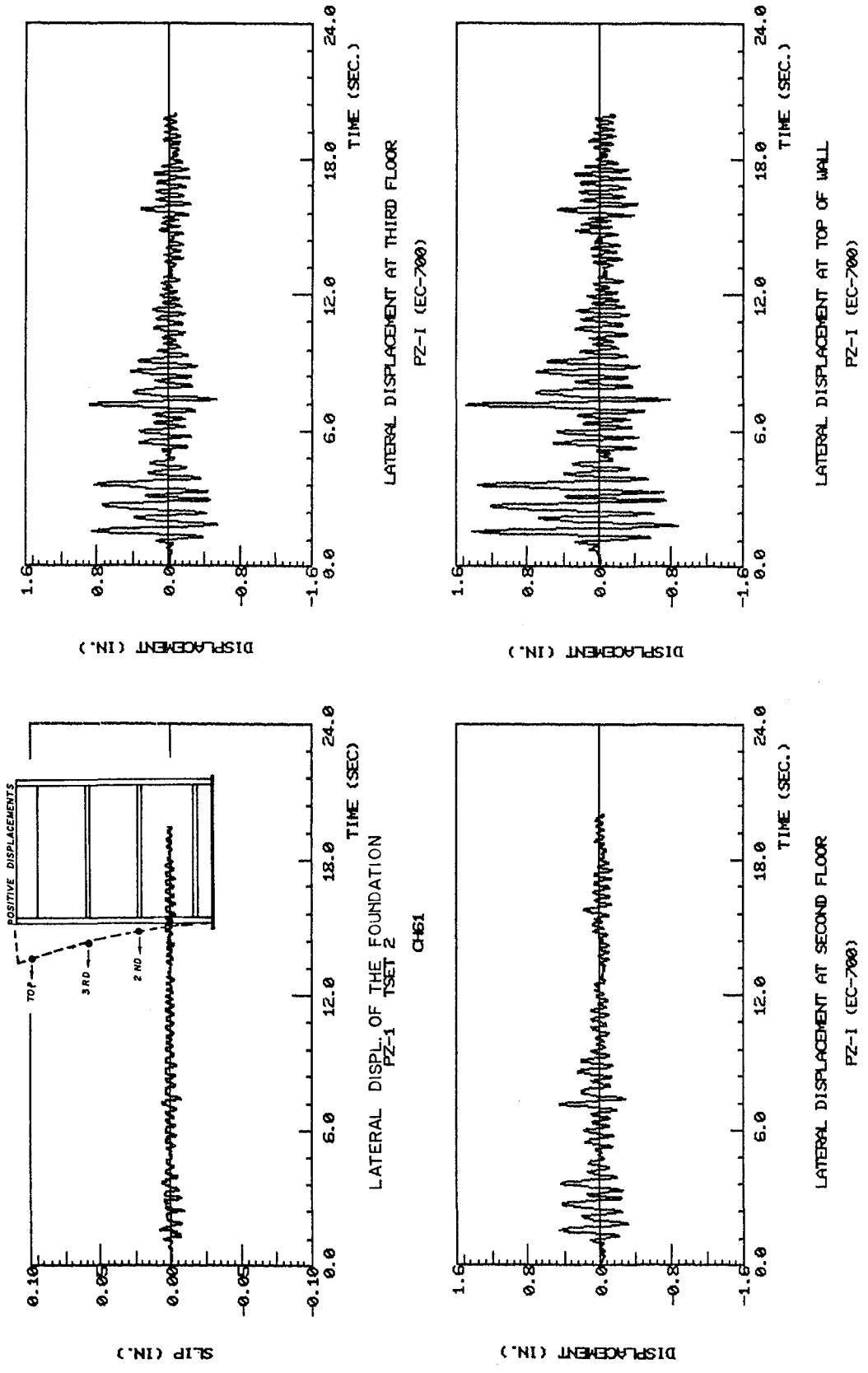

Figure 7.20 Relative lateral displacements, simple wall, EC-700, 0.67g.

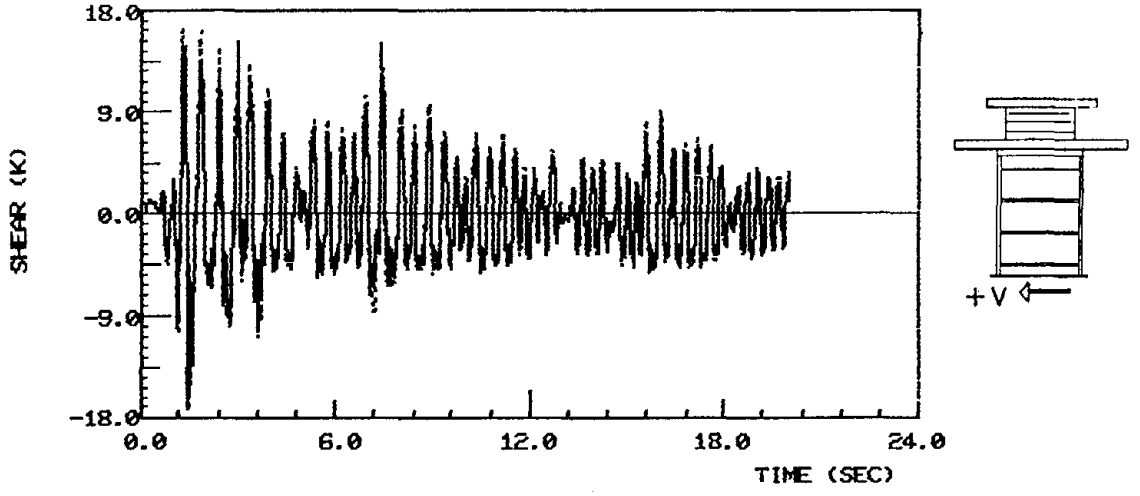

PZ-1 TEST 2

SOLID= TRANSDUCER SHEARS, DASH= INERTIAL SHEARS

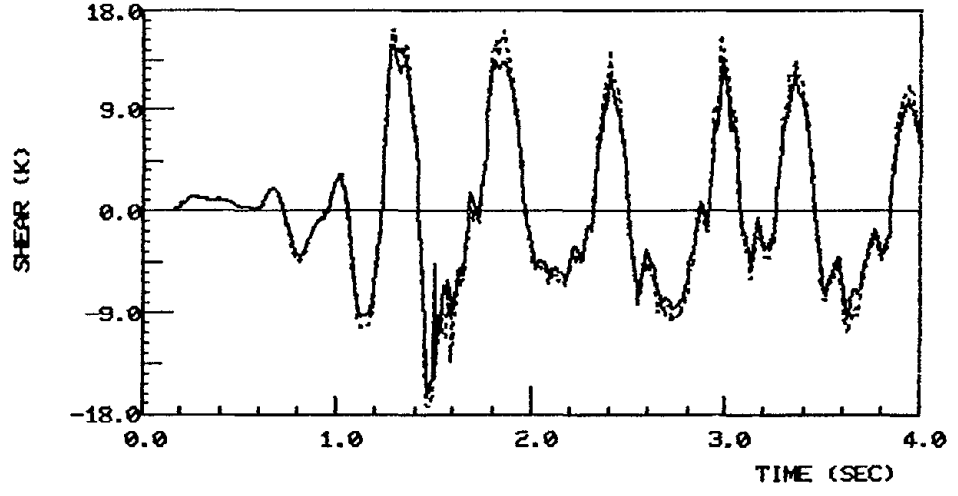

PZ-1 TEST 2

SOLID= TRANDUCER SHEARS, DASH= INERTIAL SHEARS

———— = experimental results

- - - - = computed, from Eq. 2 of Figure 7.6

Figure 7.21 Comparison between computed inertial and experimentally measured base shear, simple wall, EC-700, 0.67g.

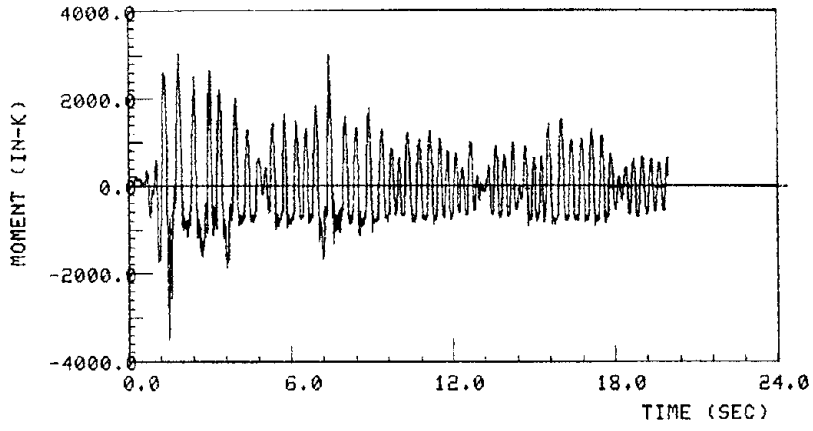

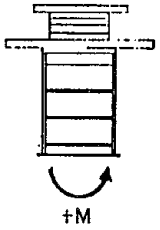

PZ-1 TEST2

OVERTURNING MOMENT AT BASE OF LOWER WALL

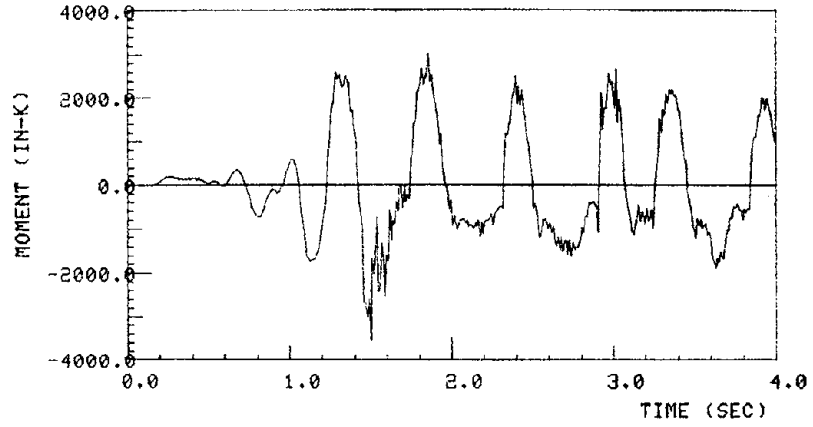

PZ-1 TEST 2

OVERTURNING MOMENT, 1ST FOUR SECONDS

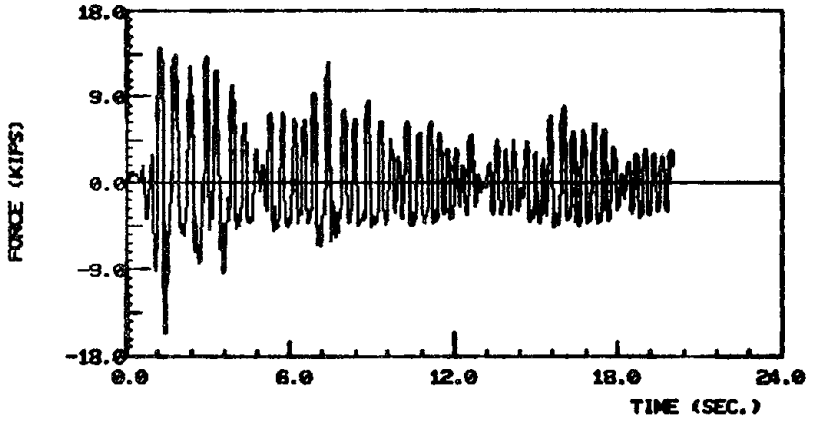

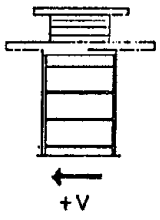

BASE SHEAR

PZ-1 (EC-700)

Figure 7.22 Base shear force and bending moment, simple wall, EC-700, 0.67g.

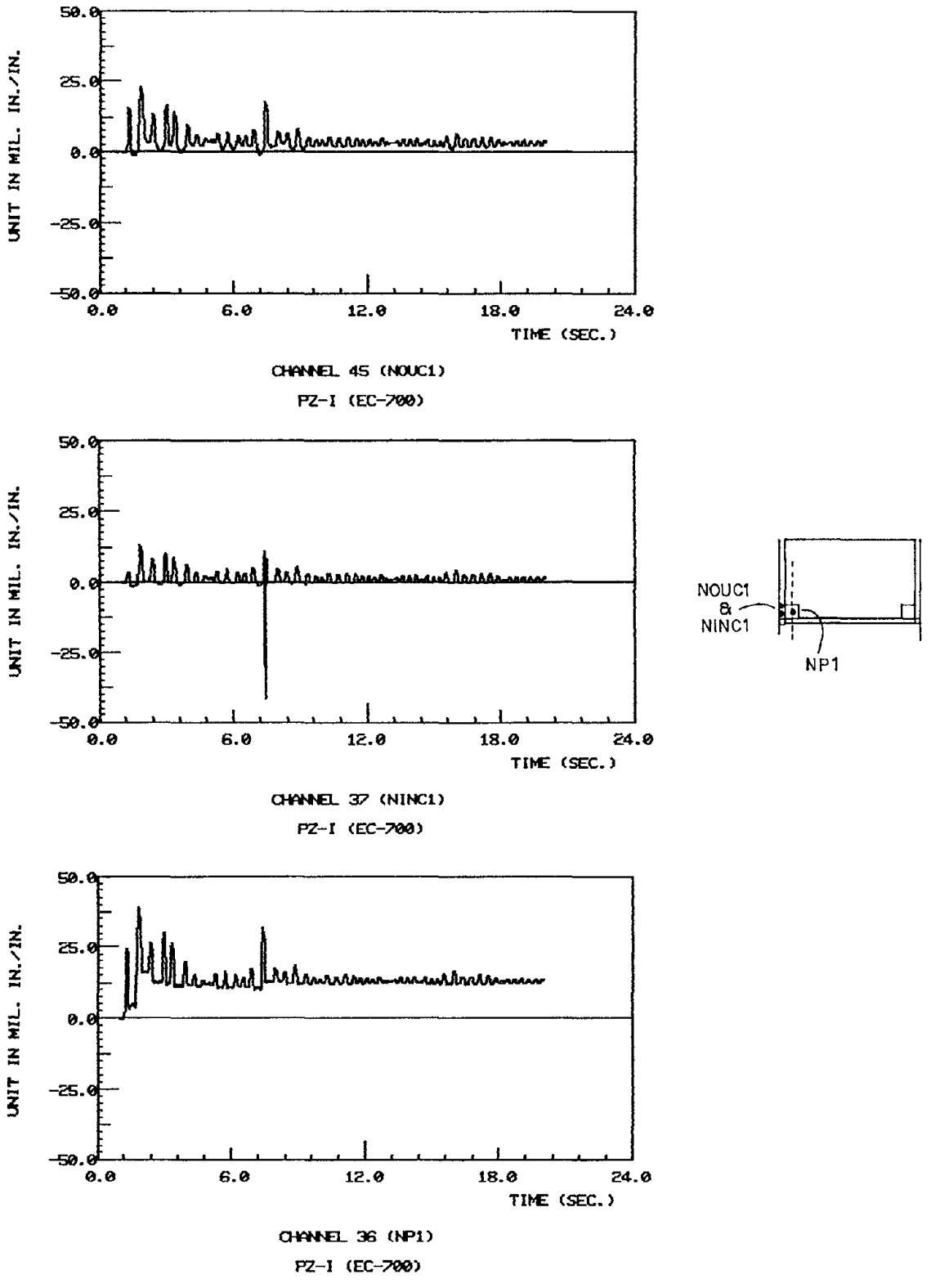

Figure 7.23 Strains in lower joint reinforcing bars, simple wall, EC-700, 0.67g.

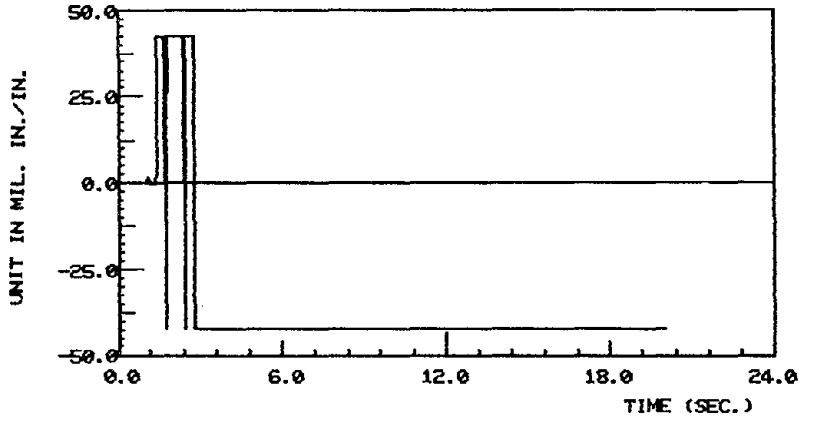

CHANNEL 33 (SP1)

PZ-I (EC-700)

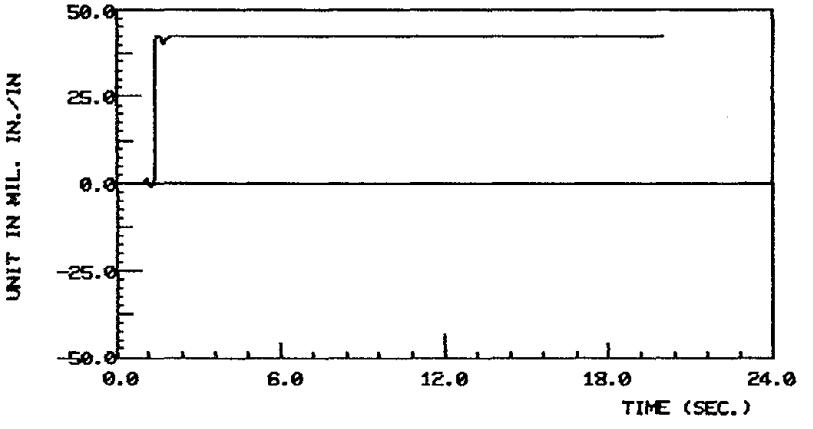

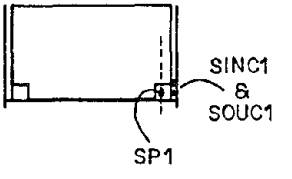

CHANNEL 34 (SINC1)

PZ-I (EC-700)

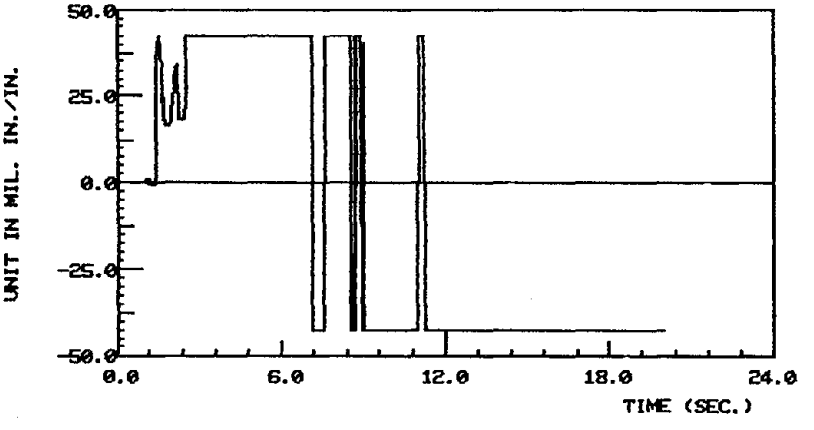

CHANNEL 35 (SOUC1)

PZ-I (EC-700)

Figure 7.23 Continued.

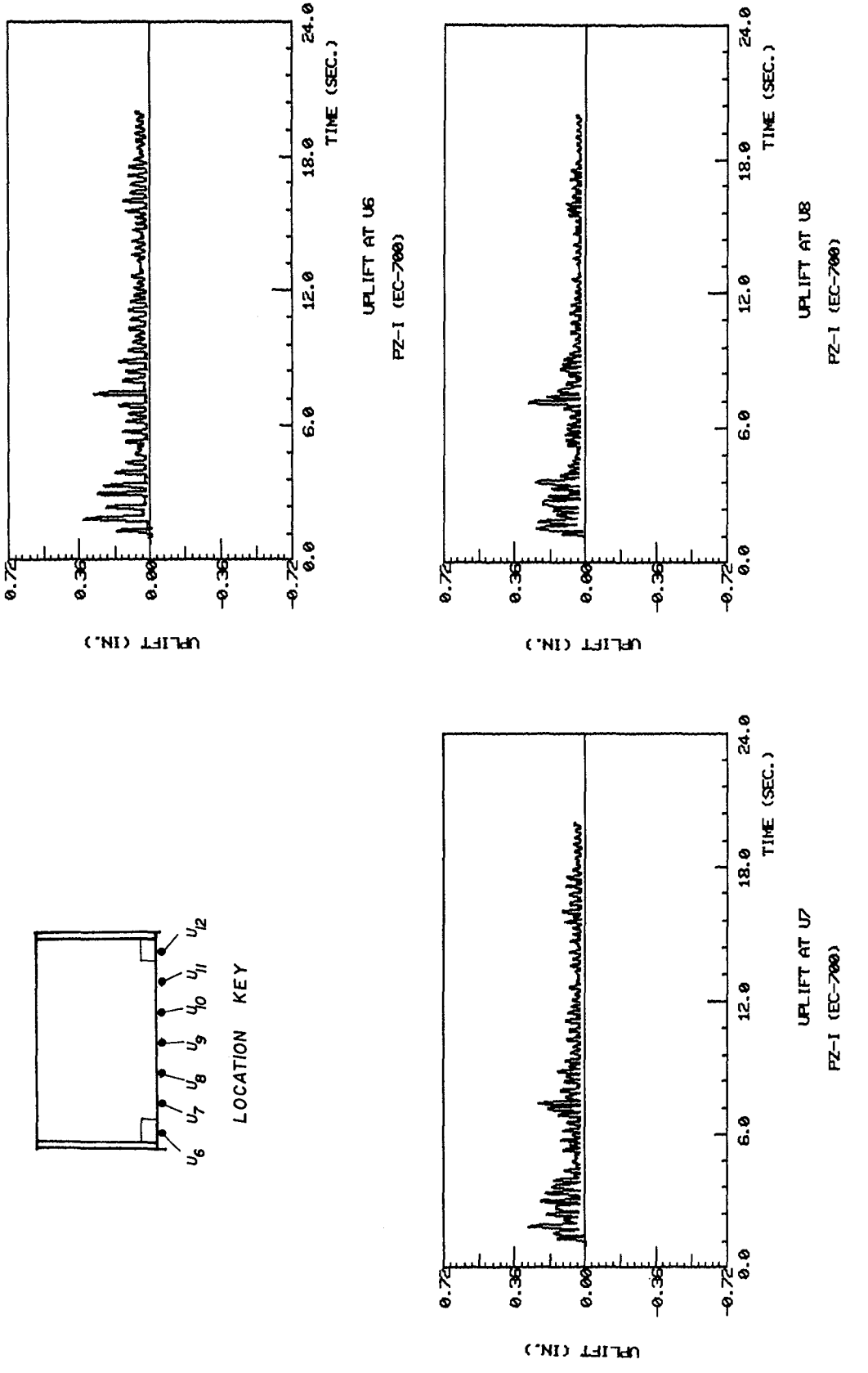

Figure 7.24 Lower panel uplift, simple wall, EC-700, 0.67g.

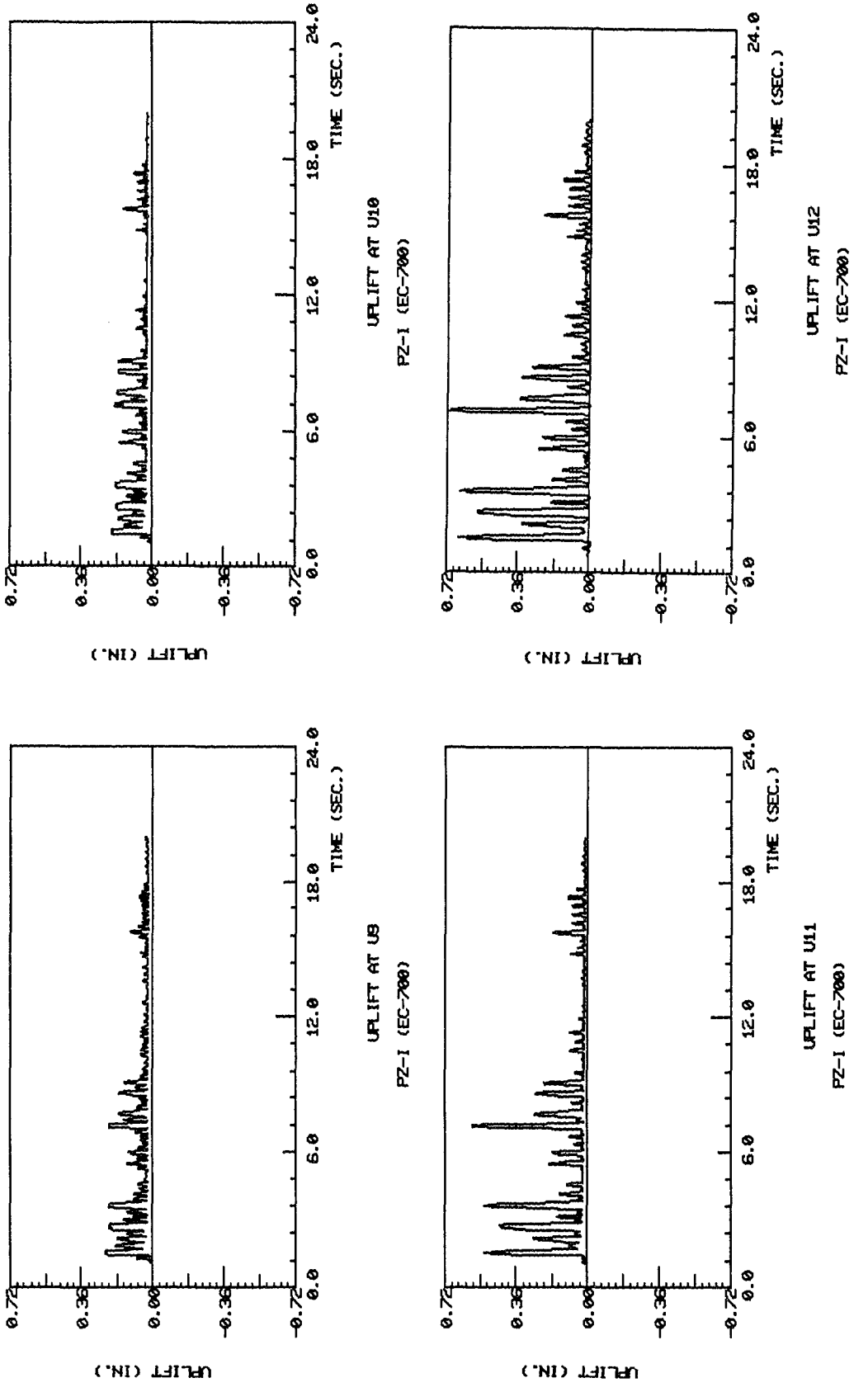

Figure 7.24 Continued.

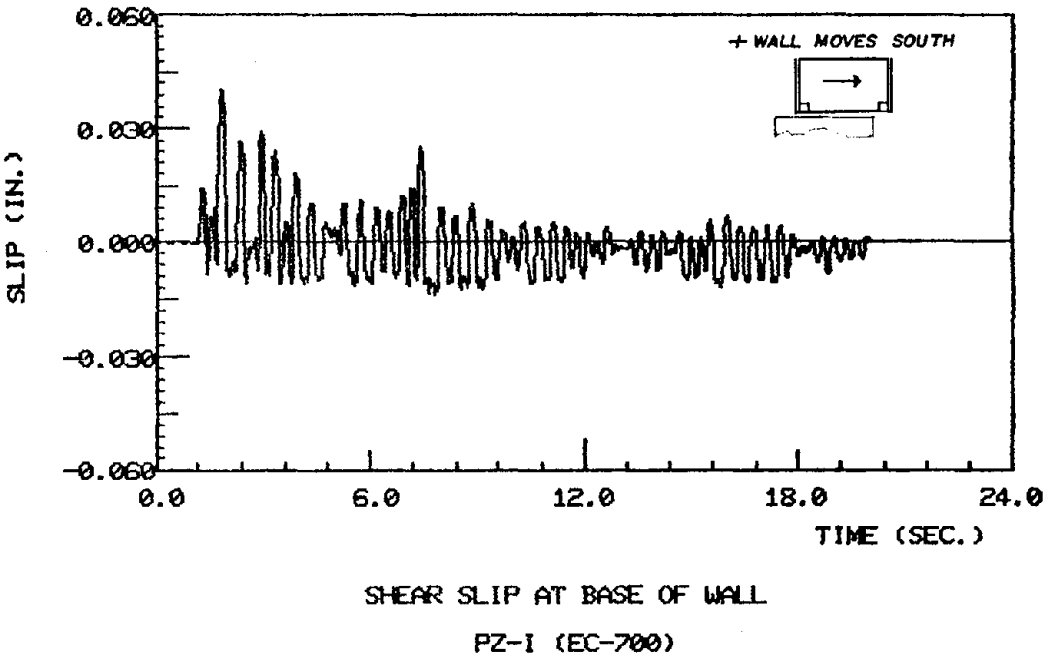

Figure 7.25 Shear-slip at base of the precast wall, simple wall, EC-700, 0.67g.

Dependence of shear slip on axial load can be illustrated by noting that the maximum slip occurred at 1.82 sec when the shear force was not at its peak value. Significant uplift values at this time indicate less resistance against shear displacement, and hence slip occurred at a lower force level.

As can be expected, a compressive axial force increases the joint capacity against shear-slip motion. For example, there was no major slip when the first-floor joint experienced its highest shear force value. This is because at this time, there was no significant gap opening, and even at the north end the joint was under compression.

The abovementioned comparison between the values of wall uplift, the magnitude of base shear, and the degree of shear slip clearly illustrates the interaction between rocking mechanism and shear-slip motion. Each major gap opening corresponded to a rather pronounced shear slip.

7.3.8 Overall Behavior of the Wall System

An average curvature for the entire wall was calculated. The resulting moment-curvature and base shear-top deflection plots are presented in Figure 7.26. These quantities have also been plotted for the first two seconds in order to show the initial stiffness and the initial hysteresis loops which are more critical in this interval because of greater load levels and deterioration.

From the base shear-top deflection plot, an initial stiffness equal to 50 kips/in. can be determined. From the first test, the average stiffness of the wall was computed to be 54 kips/in. which is very close to this initial stiffness. This was expected since the first experiment did not induce any damage that could degrade the stiffness. No attempt was made to define an initial flexural stiffness since on the moment-curvature plot a distinctive straight line could not be located in order to quantify this value.

Points identified by A, B, C on the shear force-deflection plot depict a very peculiar behavior. At point A, which corresponds to 1.44 sec, the wall suddenly lost load and stiffness. The wall base shear force was reduced by a factor of nearly 3. From point A to point B the wall deflected 0.13 in. more even though the base shear force dropped. It is interesting to note that the stiffness is regained from point B to point C. The sudden loss of load and stiffness might be attributed to loss of resisting mechanism. The data from the south panel strain gauge indicates that rupture probably occurred at that time. At present the reason for this sudden drop and increase in wall load and stiffness is not known. It is interesting to note that similar behavior can be observed after point C but to a lesser degree. This abrupt loss and gain in stiffness is also seen in the moment-curvature plot.

7.3.9 Wall Panel Behavior

As explained earlier, the data from channel 68, the diagonal deformation of the 1st panel, was ignored. Thus, it was not possible to determine shear deformation in the wall panel. Curvature of the panel was estimated by using the deformations at the panel ends to calculate an average bending.

It was important to detect any bending nonlinearity occurring within the wall panel. For this purpose the overturning moment was plotted against panel curvature. From Figure 7.27 and the magnitude of the panel curvature, it can be concluded that there was little bending nonlinearity in the precast wall panel. Although it was not possible to quantify shear deformation in the precast wall panel, it is believed that it was very small in magnitude. This is because of the small value of the deformation measured by the diagonal DCDT - D2; this deformation reached a maximum value of 0.006 in.

7.3.10 First-Floor Joint Behavior

In Chapter 1, it was noted that two major mechanisms control the behavior of horizontal joints in a simple precast panel wall. These two are shear-slip and rocking. The rational approach to investigate these dominating mechanisms is to consider plots of base shear force versus slip and base bending moment against curvature of the joint.

Figure 7.28 illustrates base shear force versus the shear slip at this level. This plot clearly indicates that most of the shear displacement occurred in one direction, i.e., toward the south end of the wall. The one-directional sense of slip displacement is certainly consistent with the severe key crushing at the south end. The hysteresis loop of this plot indicates some degree of energy dissipation but, because the shear slip is not of great significance, a maximum value of 0.04 in., it cannot be relied upon as a

major source of energy dissipation. In other words, shear displacement could provide a dependable mechanism for energy dissipation if it were of higher magnitude. A more effective shear-slip energy dissipation requires larger lateral displacements which might be threatening to the integrity of the structure.

The sequence of initial damage and deformation within the joint may be examined in detail in the response during the first four seconds of the test (see Figure 7.29).

The rocking motion associated with rotation of the joint dominated the behavior. The panel deformation was negligible; the value of shear slip was small (maximum displacement was 0.04 in.); the lateral displacement of the foundation detected by the DCDT labelled SFND can almost be omitted (maximum value was equal to 0.007 in.); the wall system did not show any significant deformation (maximum curvature was 7×10^{-5} rad/in.); and the bending in the foundation was extremely slight (the DCDTs measuring vertical motion at ends of the footing named U17 and U18 registered maximum values of 0.017 in. and 0.012 in., respectively). Exhausing the obvious sources, it can be concluded that the lateral displacements were greatly dominated by the rigid body rotation of the wall at an angle equal to joint rotation. A series of expanded time history plots are included in Figure 7.29 to provide detailed information about the load and response parameters in the period when first yield occurs.

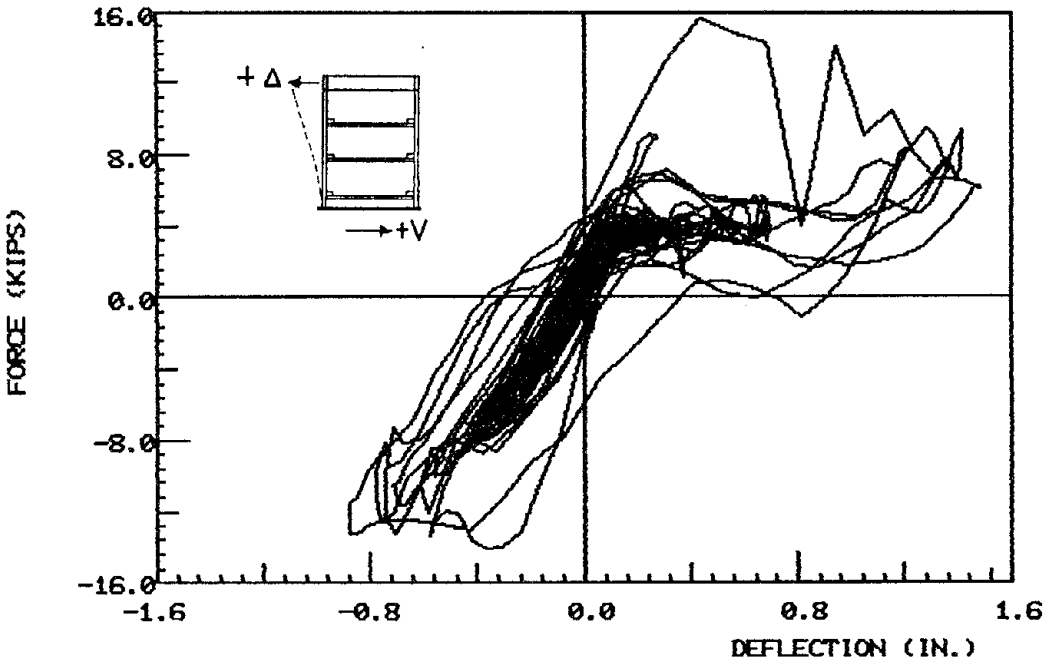

BASE SHEAR - TOP DEFLECTION

PZ-I (EC-700)

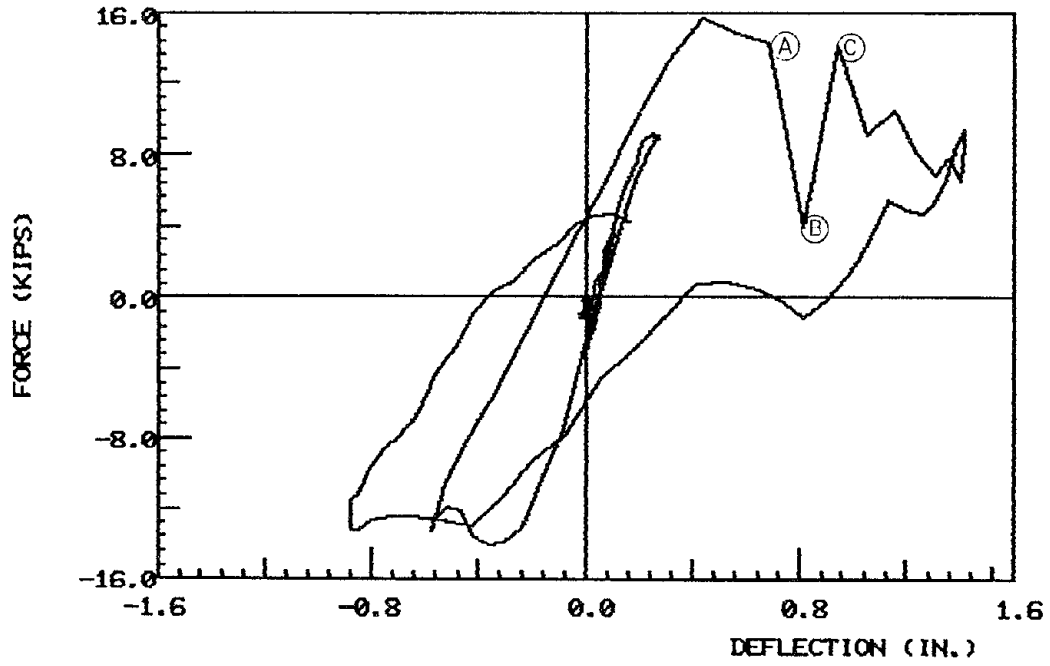

BASE SHEAR - TOP DEFLECTION (1ST 2 SECONDS)

PZ-I (EC-700)

Figure 7.26 Overall behavior of the wall, simple wall, EC-700, 0.67g.

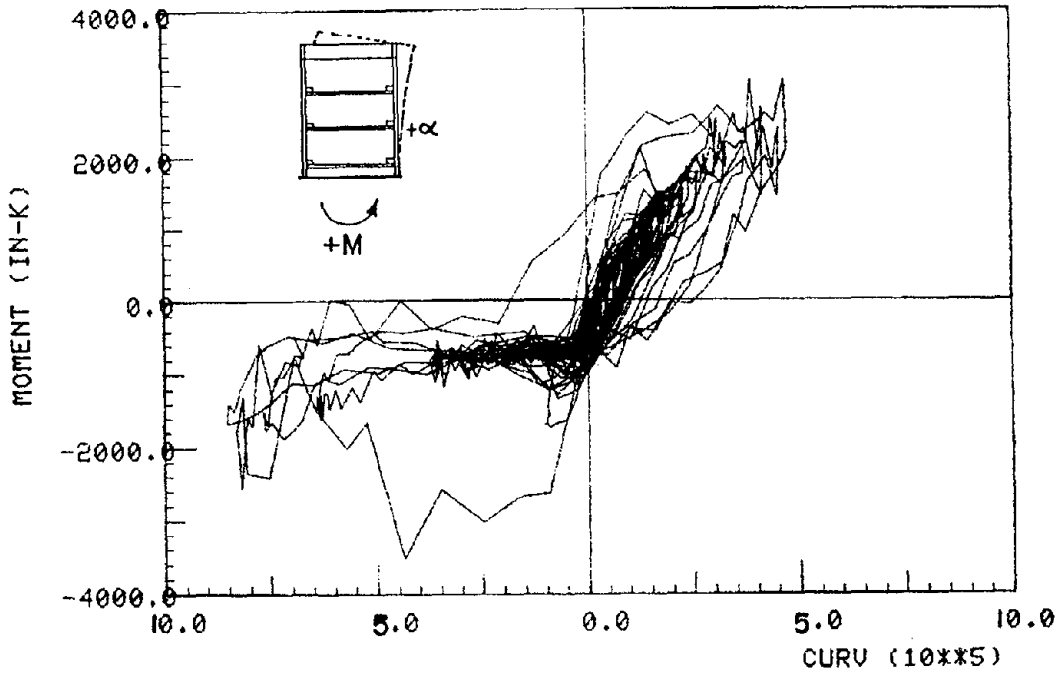

PZ-1 TEST 2

BASE MOMENT AND WALL CURVATURE

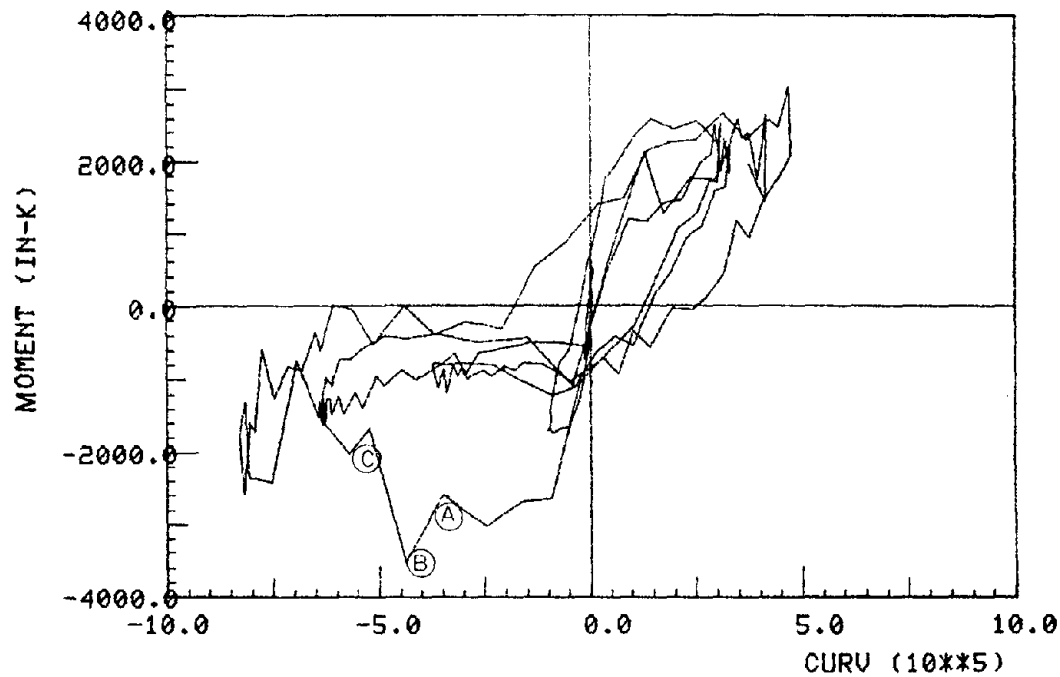

PZ-1 TEST 2

BASE MOMENT AND AVG WALL CURV.

Figure 7.26 Continued.

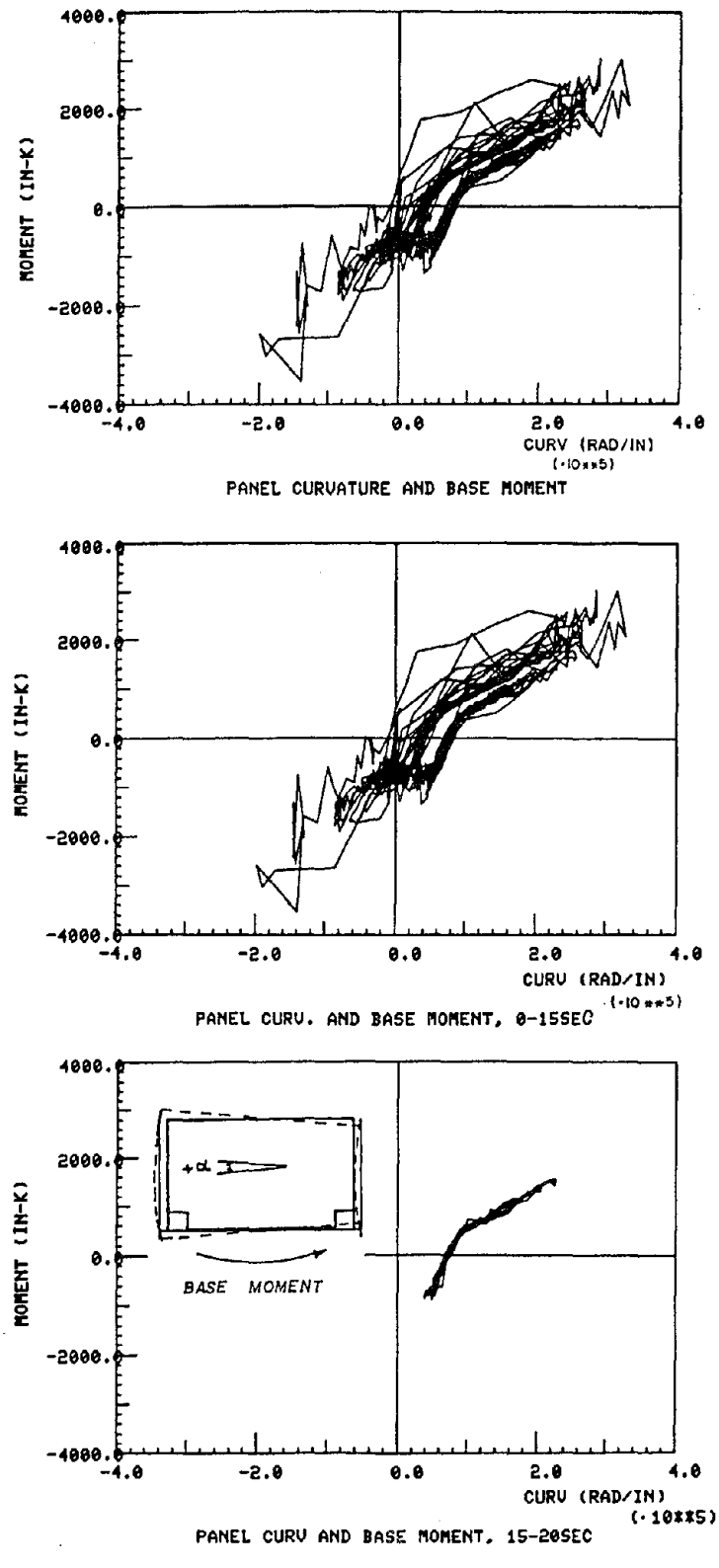

Figure 7.27 Bending in the lower wall panel, simple wall, EC-700, 0.67g.

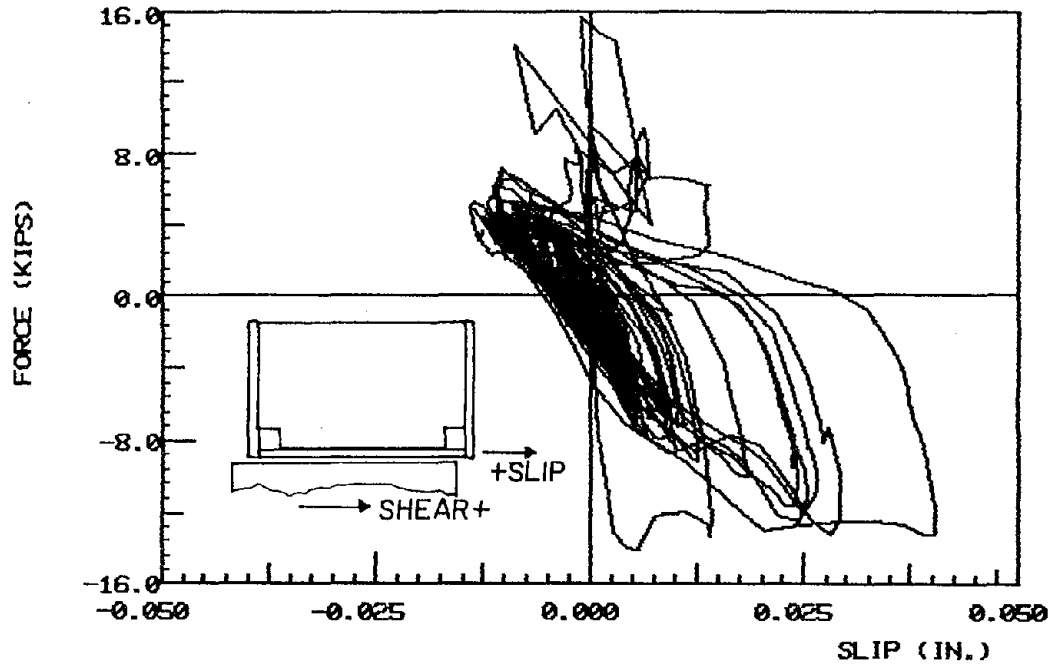

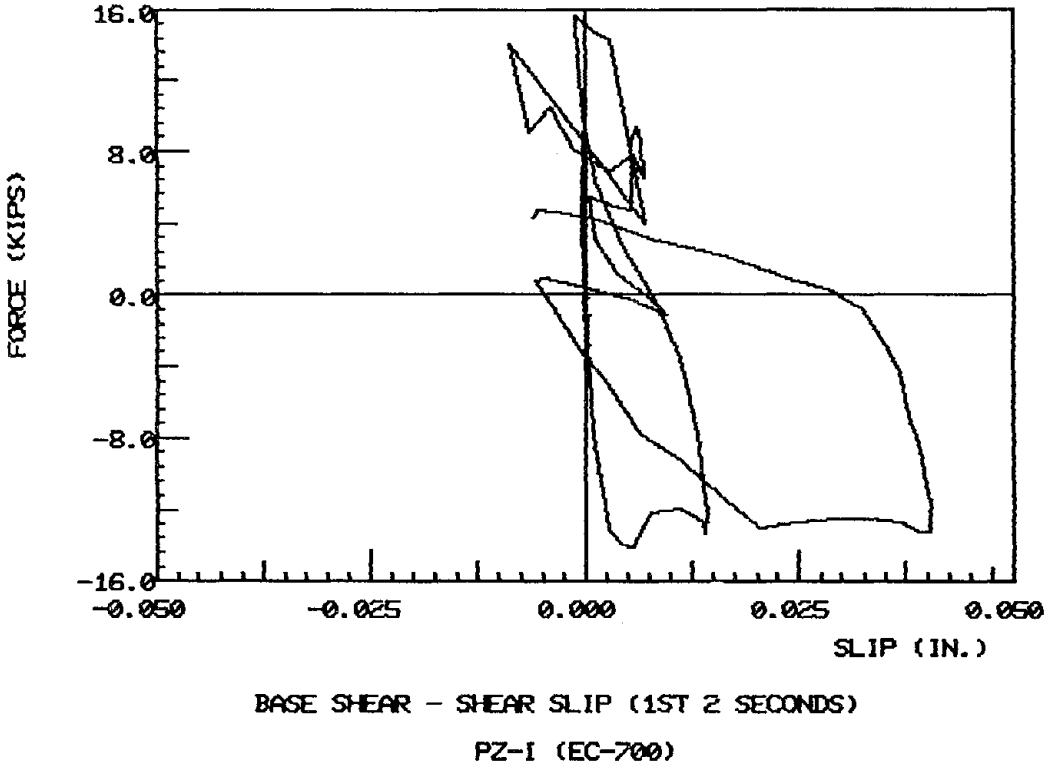

Figure 7.28 Horizontal joint shear-slip behavior, simple wall, EC-700, 0.67g.

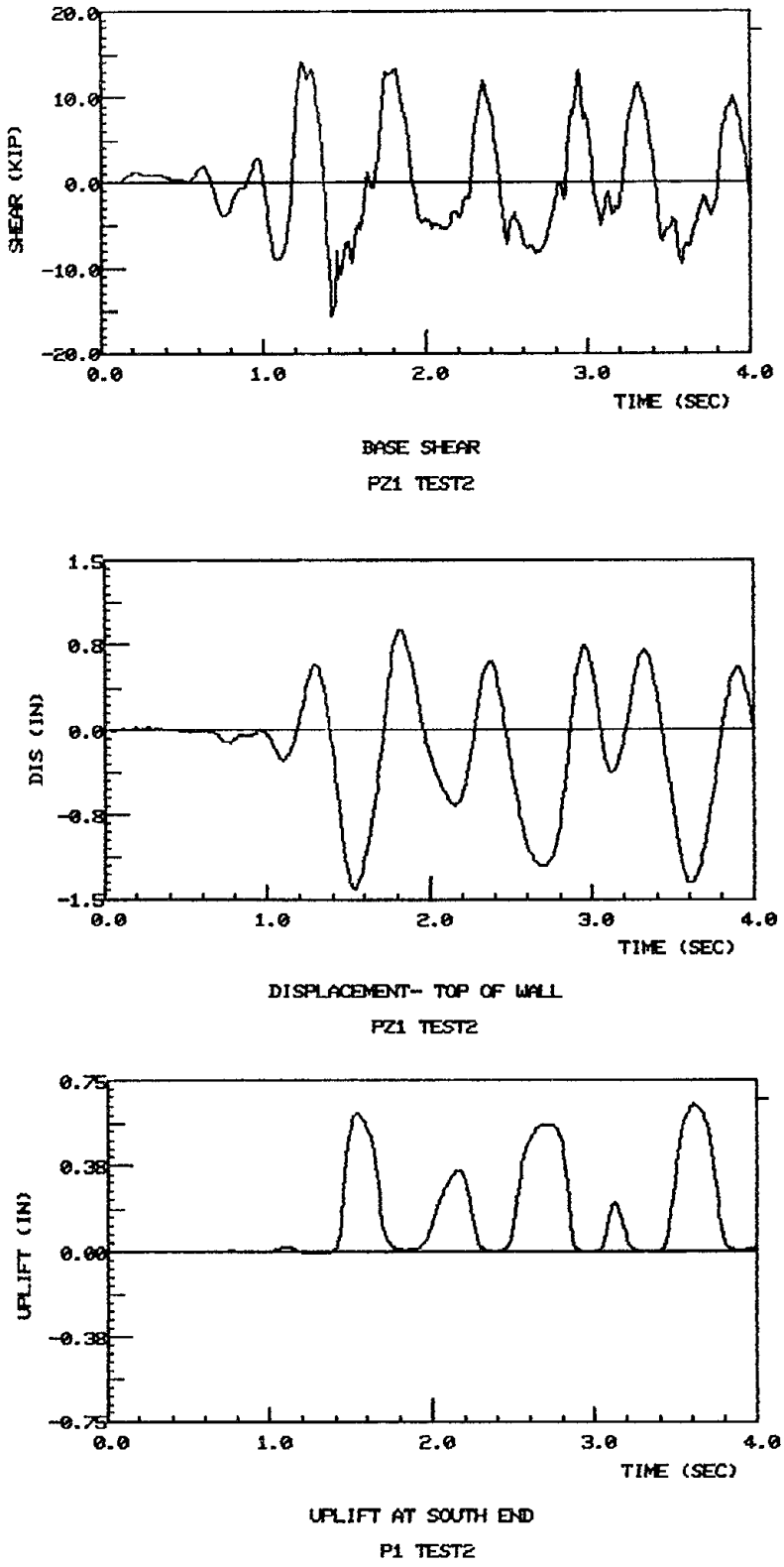

Figure 7.29 Response during initial four seconds.

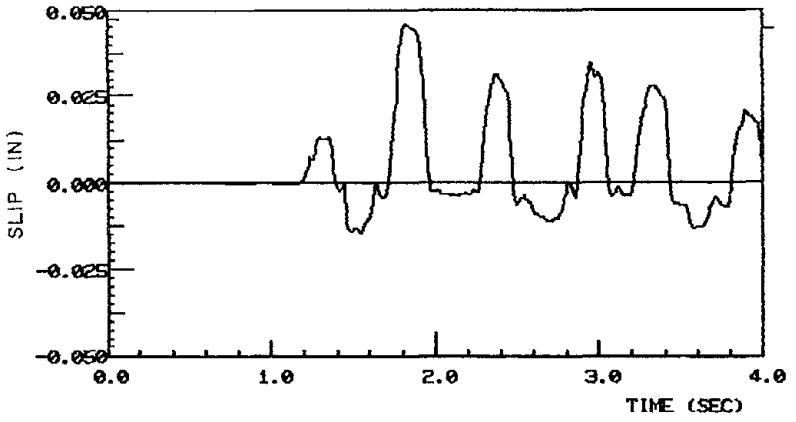

BASE SLIP

PZ1 TEST2

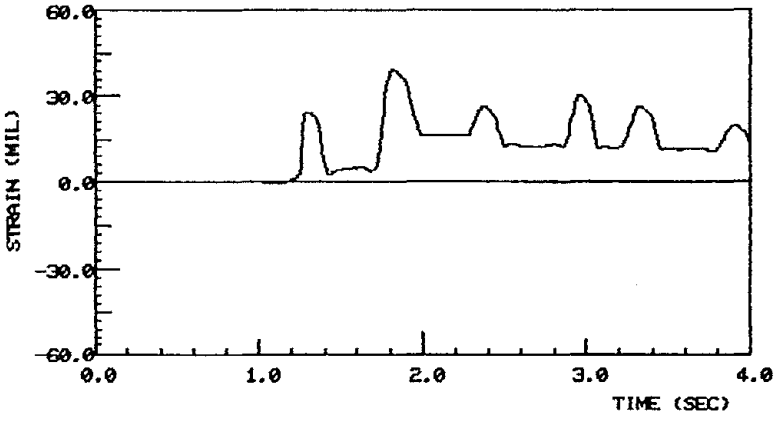

STRAIN IN NORTH PANEL BAR

PZ1 TEST2 NP1

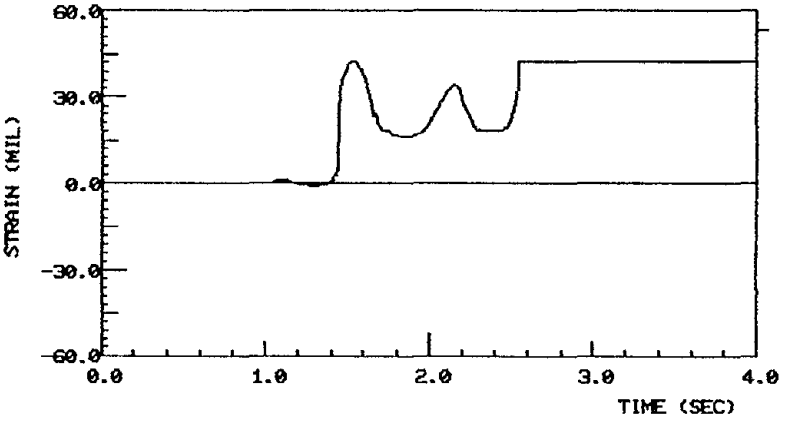

STRAIN IN SOUTH COLUMN BAR

PZ1 TEST2 SOUC1

Figure 7.29 Continued.

8. TEST RESULTS FOR FLANGED WALL

Quantitative test results of the flanged wall (PZ-III) are presented in this chapter in graphical form. The flanged wall, the first wall tested, was subjected to a series of very low amplitude motions before the main test sequence of three primary motions, EC-200, EC-750, and EC-1000 (0.22g, 0.69g and 1.08g) was applied. The last test, EC-1000, was applied to simulate a very strong aftershock. This chapter examines the results of the EC-200 and EC-750 tests which induced the first inelastic behavior and damage within the wall system.

The preliminary steps in the data reduction and analysis process included base line correction for initial instrument offsets, separation of the 87 data channels and inspections for validity of the data, as described in the previous chapter. The data presented here is in an unfiltered form.

8.1 Results from El Centro at 0.22g (EC-200) - PZ-III Wall

8.1.1 Introduction

The first test on this wall was intended to measure the behavior of the system while maintaining elastic load and deformation behavior. The input ground displacement reached 1.00 in. with a peak horizontal acceleration of 0.223g. Under this low amplitude ground motion the flanged wall maintained an elastic load deformation response. Many of the deformations measured by the attached instrumentation were too small to be considered significant or accurate relative to the capacity of the instruments. Only the basic response data characterizing the overall motion and stiffness of the wall will be presented in the following sections.

TABLE 8.1

Extreme Values from EC-200 Test, PZ-III
(table motion 0.22g)

Quantity	Extreme Value
Ground (table) displacement	2.54 cm (1.00 in.)
Ground (table) acceleration	0.223g
Acceleration at foundation	0.222g
Acceleration at second floor	0.286g
Acceleration at third floor	0.352g
Acceleration at top of wall	0.415g
Acceleration at concrete blocks	0.463g
Top of wall relative displacement	0.24 cm (0.094 in.)
Base shear force	40.5 kN (9.10k)
Base overturning moment	190.7 kN-m (1688 in.-k)
Strain-north column bar	0.012%
Strain-north panel bar	0.026%
Strain-south column bar	0.010%
Strain-south panel bar	0.007%
Curvature (average) lower panel	0.59×10^{-6} rad/cm

8.1.2 Peak Response Values

Extreme values for the primary response quantities during the elastic test of PZ-III are listed in Table 8.1. Relative displacements at the top of the wall are shown in Figure 8.1. The wall developed significant displacements between 1 and 4 sec and 5 to 6.5 sec during the 20 sec shaking period. The simultaneous base shear induced in the wall is plotted in Figure 8.2. Lateral displacement in the lowest horizontal joint (termed "slip"), as measured between the lower panel and the foundation wall, amounts to just over 1 percent of the total top-of-wall displacement. The relation between joint slip and top displacement is obvious when Figures 8.1 and 8.3 are compared.

8.1.3 Stiffness Characteristics

Overall structural system stiffnesses are frequently characterized by a top displacement versus shear force relation. Displacement and base shear, shown previously in time history form, are plotted in Figure 8.4. The average system stiffness is approximately 105.5 k/in. (184.7 kN/cm). A relation between base moment and top displacement is shown in Figure 8.5 since most of the displacement may be attributed to bending effects. The moment-displacement stiffness is 19,874 in-k/in. (884 kN-m/cm). Elastic bending stiffness of the wall panel segments is defined by the relation in Figures 8.6 and 8.7 where the average curvature, measured within the lower wall panel, is shown with the base moment. The average lower wall system bending stiffness is 1.28×10^9 in-k/rad (5.7×10^7 kN-m/rad).

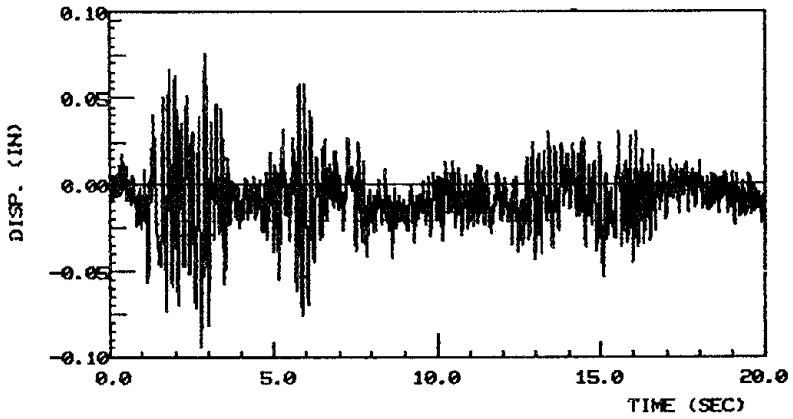

Figure 8.1 Lateral displacement at top of wall.

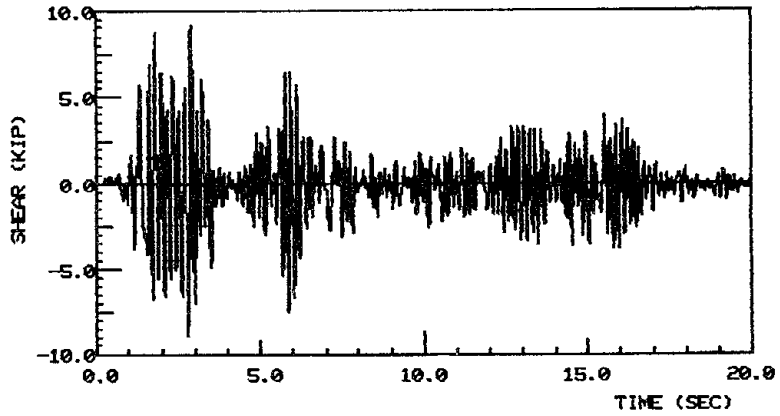

Figure 8.2 Base shear time history.

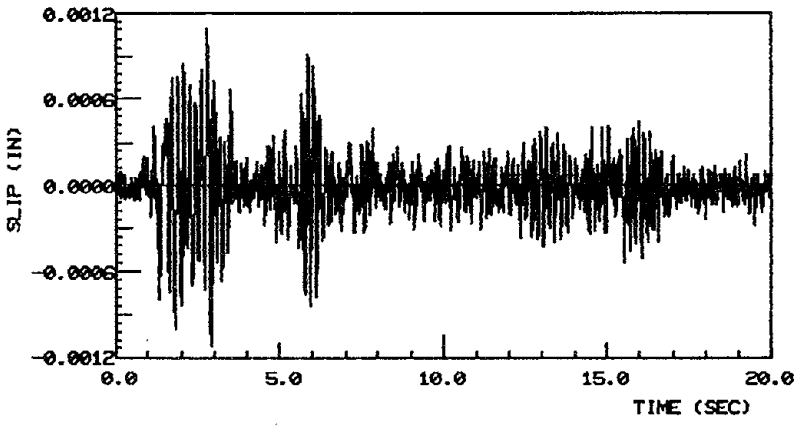

Figure 8.3 Slip at base of wall, lower joint, flanged wall, EC-200, 0.22g.

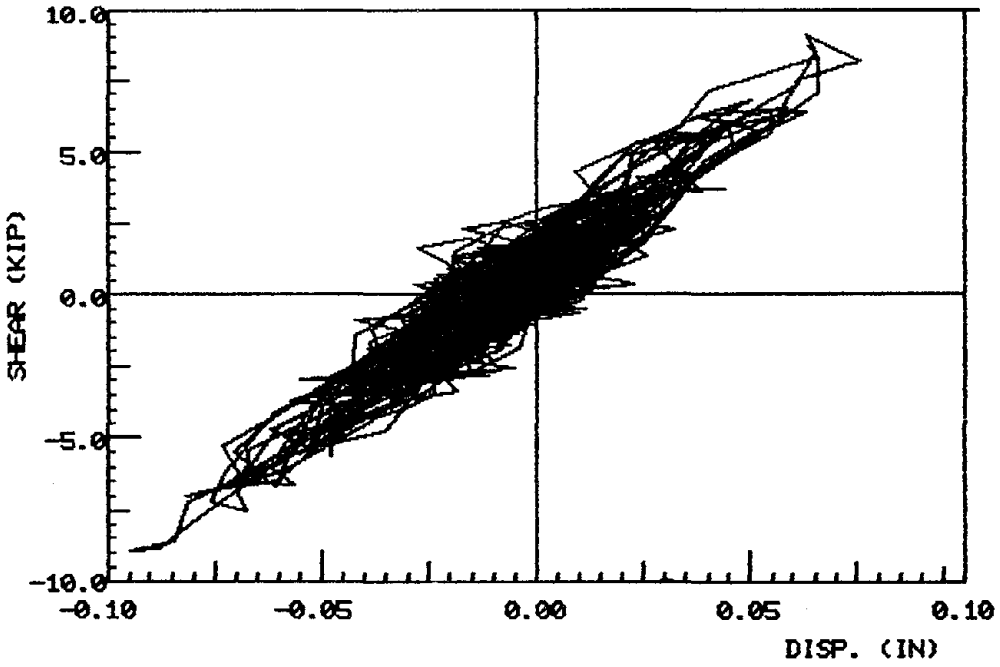

Figure 8.4 Base shear and top displacement, flanged wall, EC-200, 0.22g.

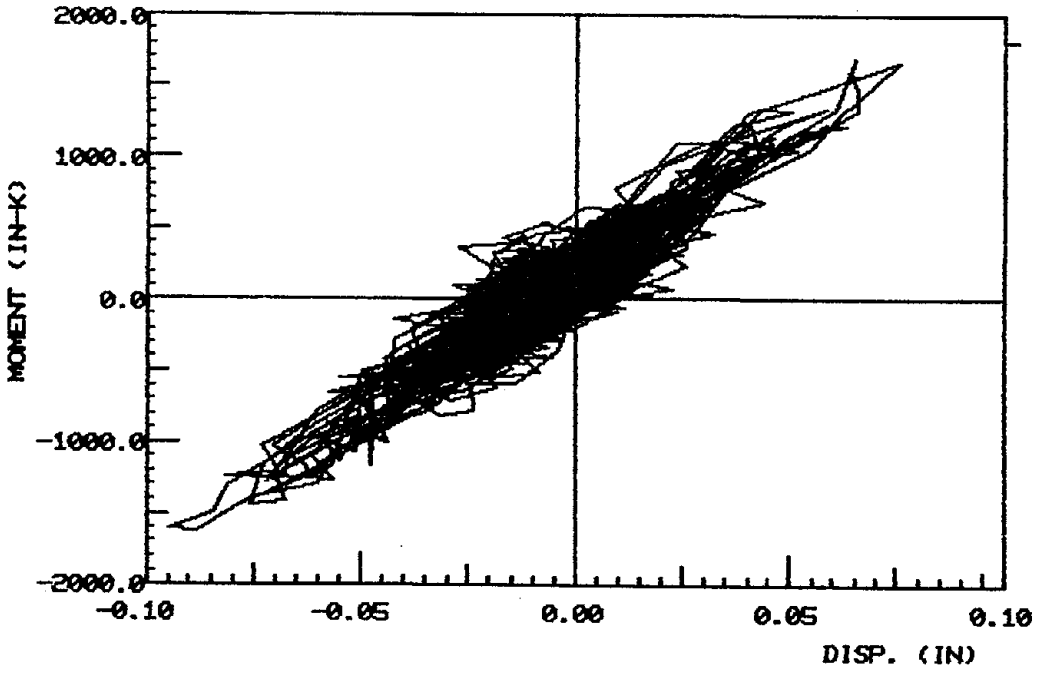

Figure 8.5 Base moment and top displacement, flanged wall, EC-200, 0.22g.

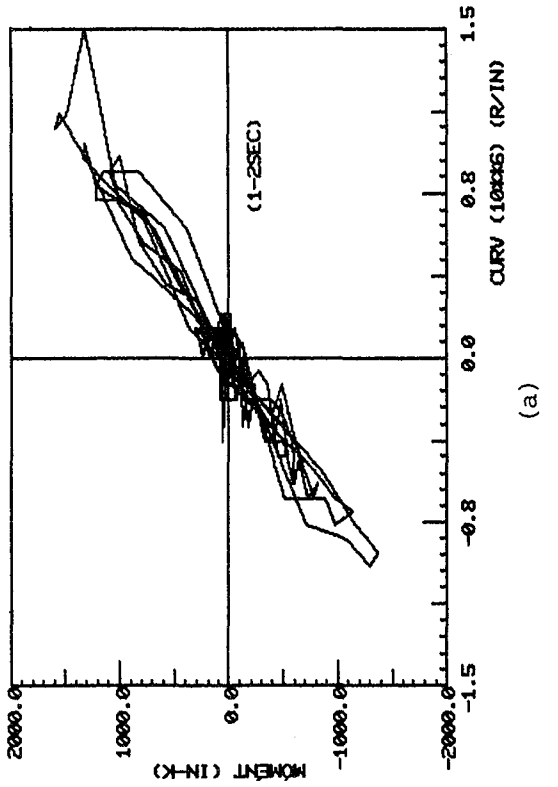

(a)

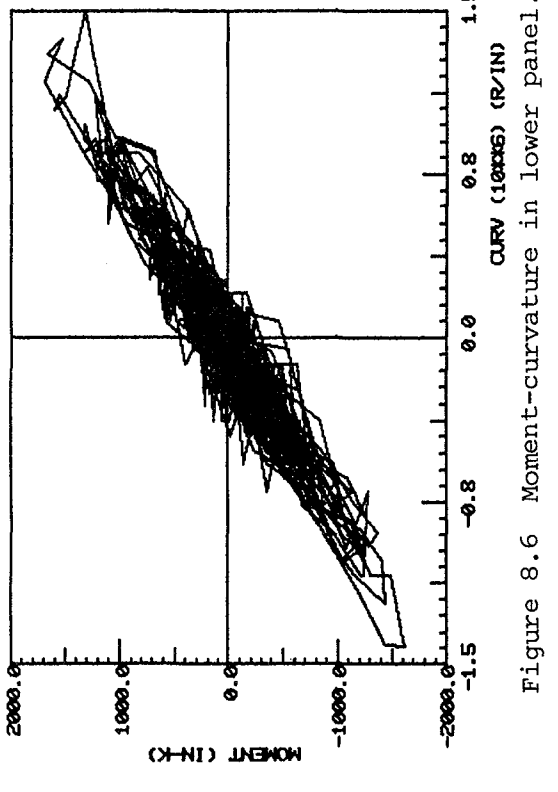

Figure 8.6 Moment-curvature in lower panel.

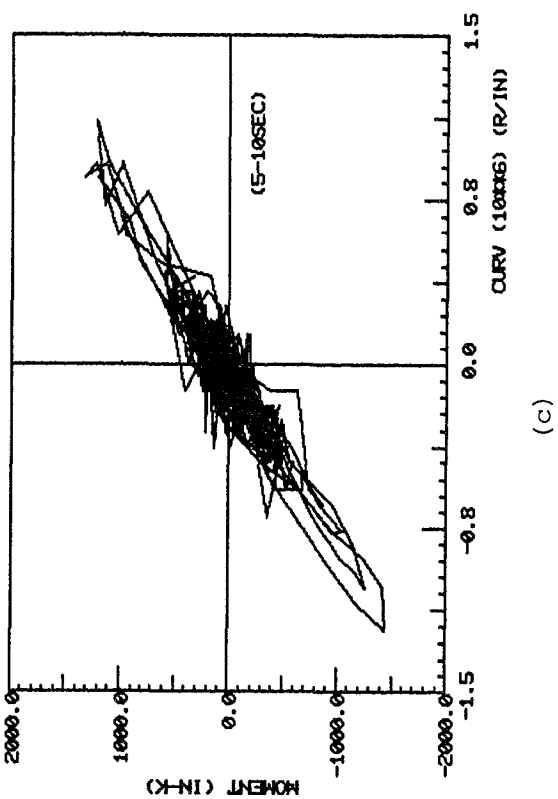

(c)

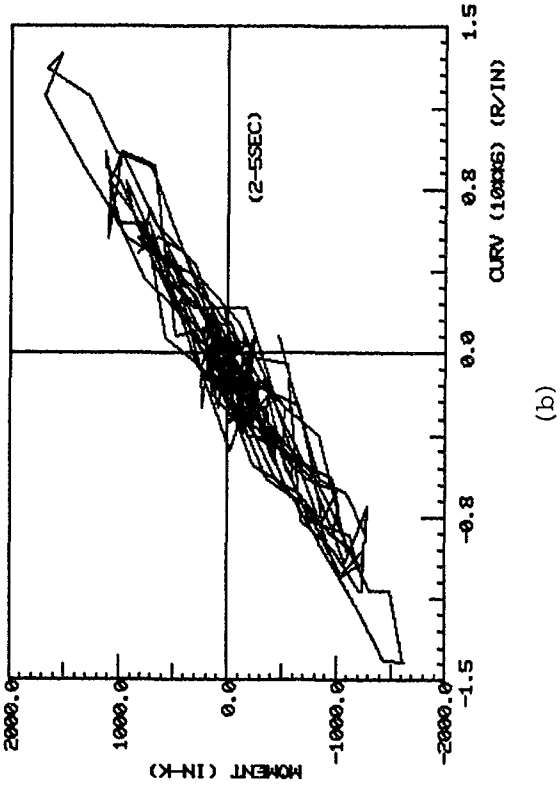

(b)

Figure 8.7 Panel moment-curvature in time interval segments, flanged wall, EC-200, 0.22g.

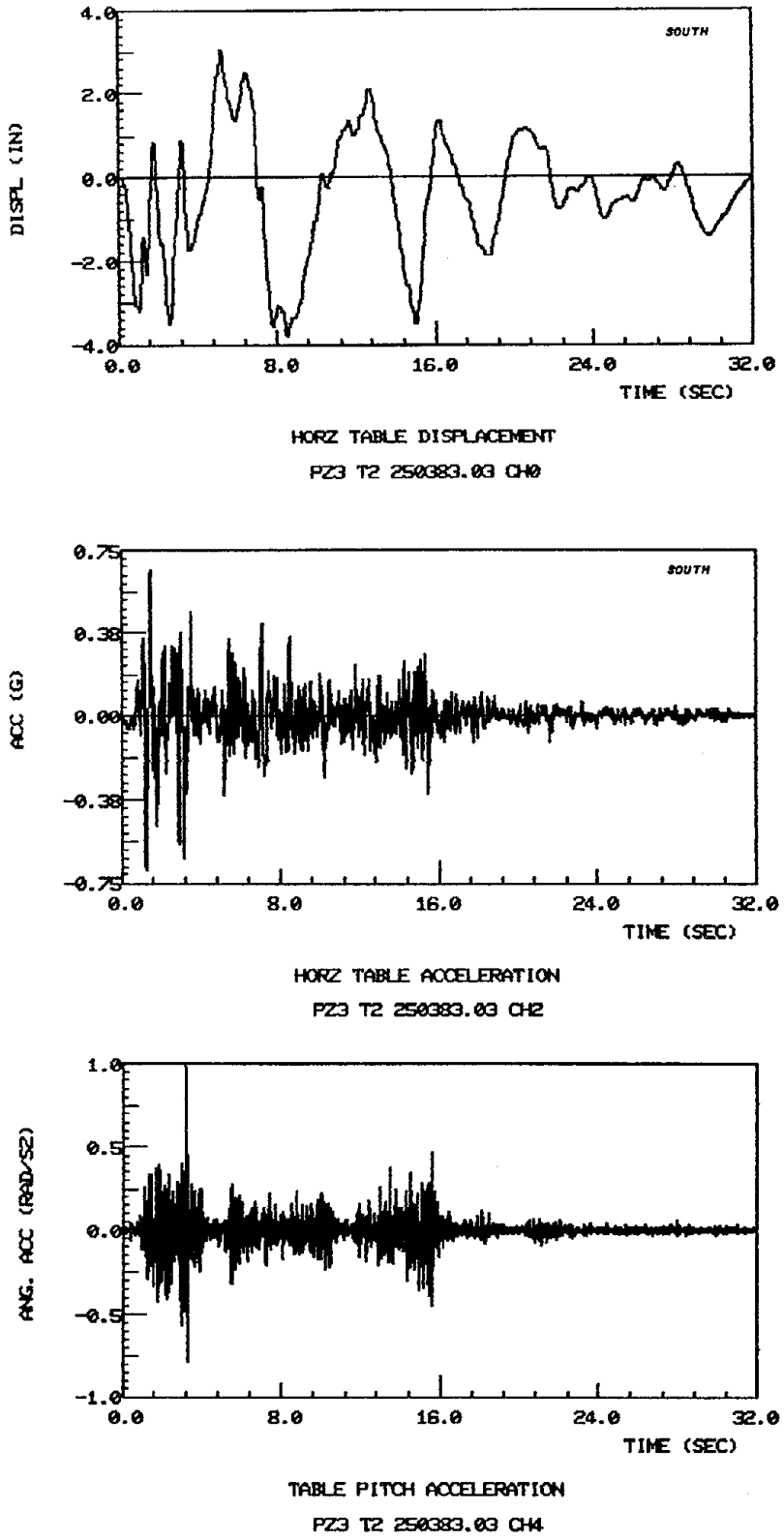

Figure 8.8 Table motion, flanged wall, EC-750, 0.69g.

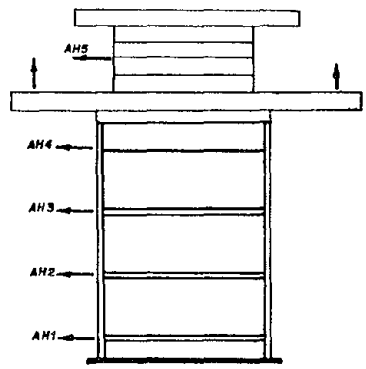

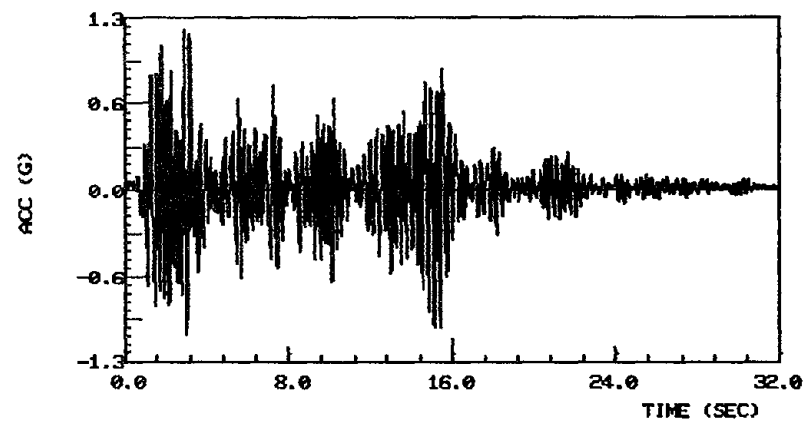

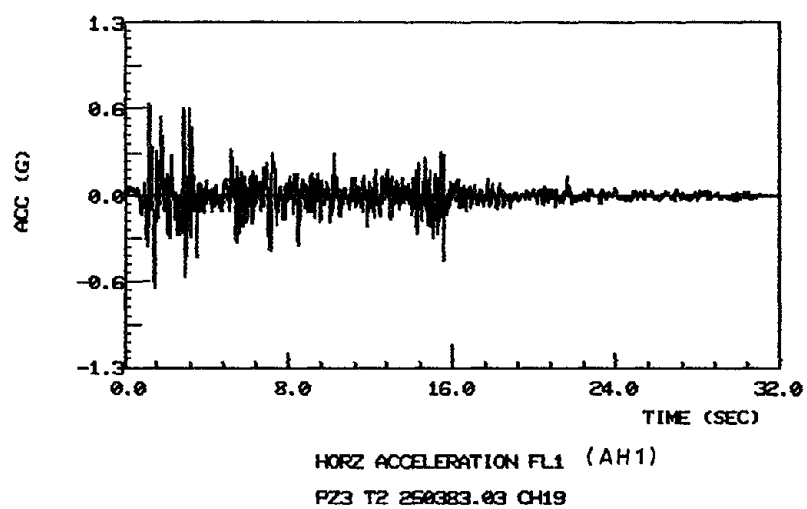

Figure 8.9 Story accelerations, time histories, flanged wall, EC-750, 0.69g.

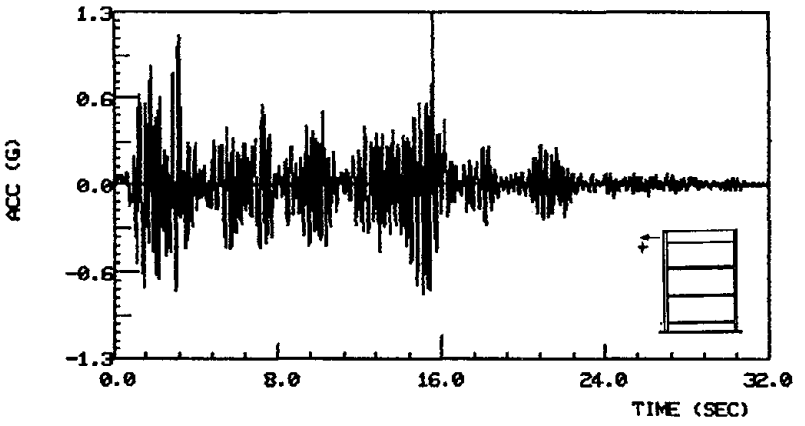

HORZ ACCELERATION FL4

PZ3 T2 250383.03 CH18

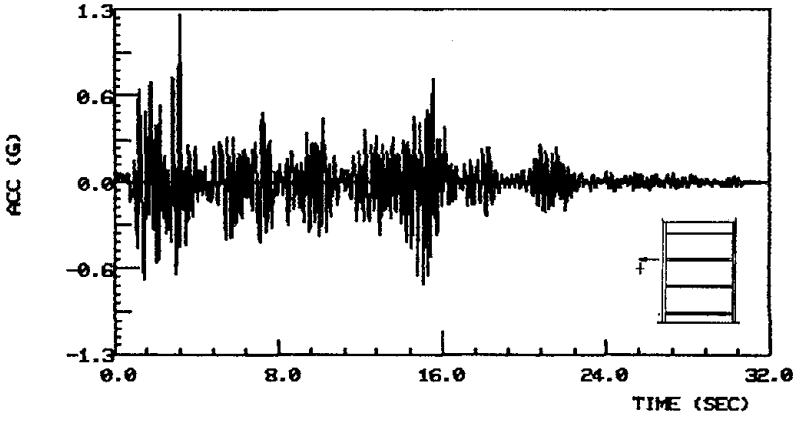

HORZ ACCELERATION FL3

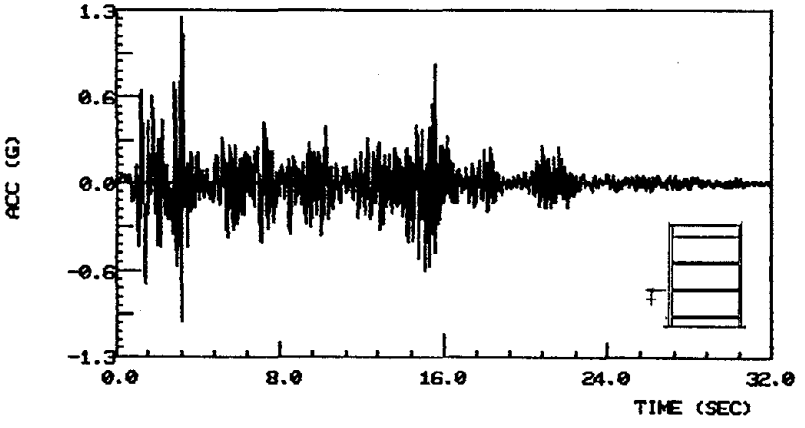

HORZ ACCELERATION FL2

PZ3 T2 250383.03 CH16

Figure 8.9 Continued.

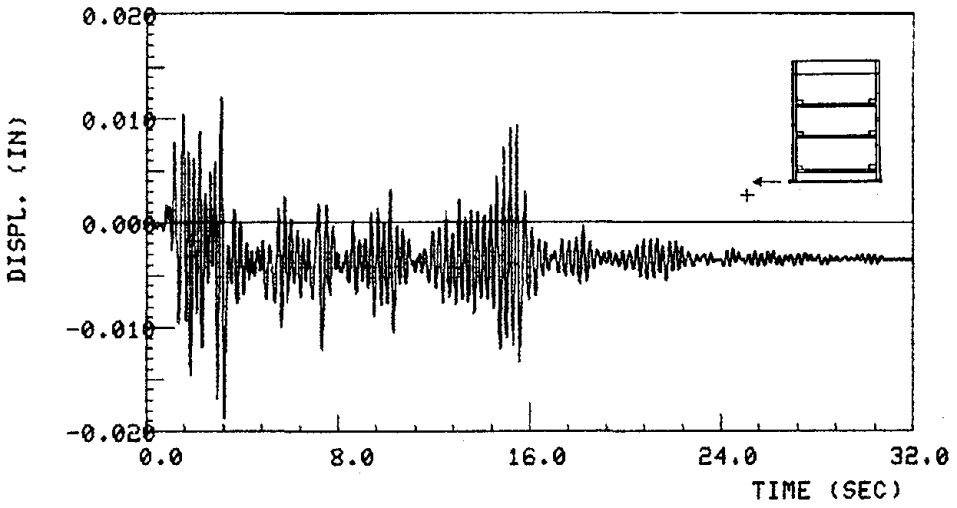

PZ-3 TEST 2

HORZ. FOUNDATION DISPLACEMENT

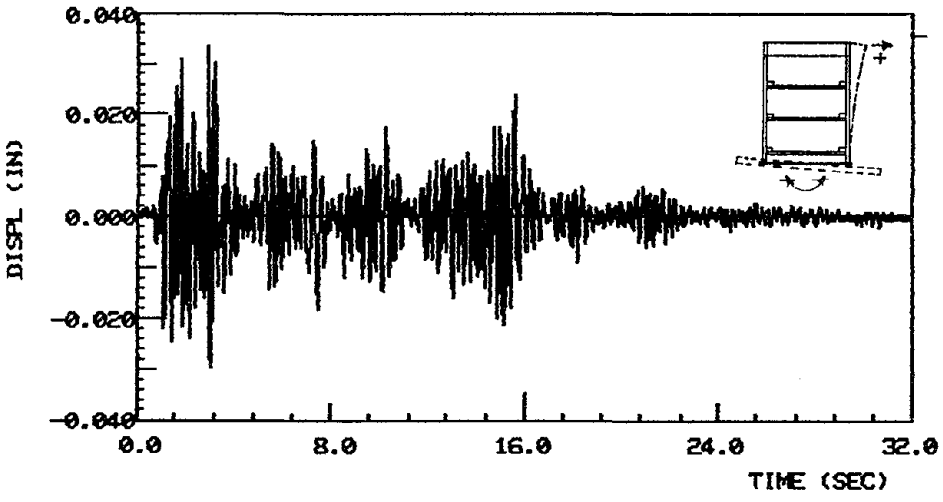

PZ-3 TEST 2

TOP OF WALL DISPL. DUE TABLE PITCH

Figure 8.10 Lateral wall displacements, flanged wall, EC-750, 0.69g.

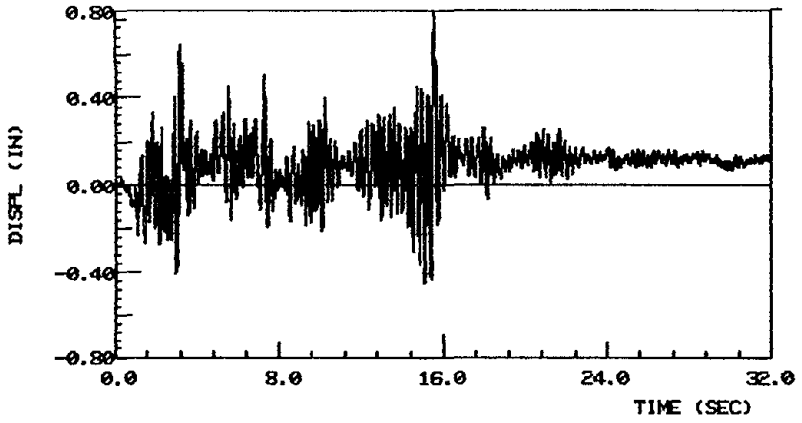

REL DISPLACEMENT LEVEL 4

PZ3 T2 25038303 RELDI4

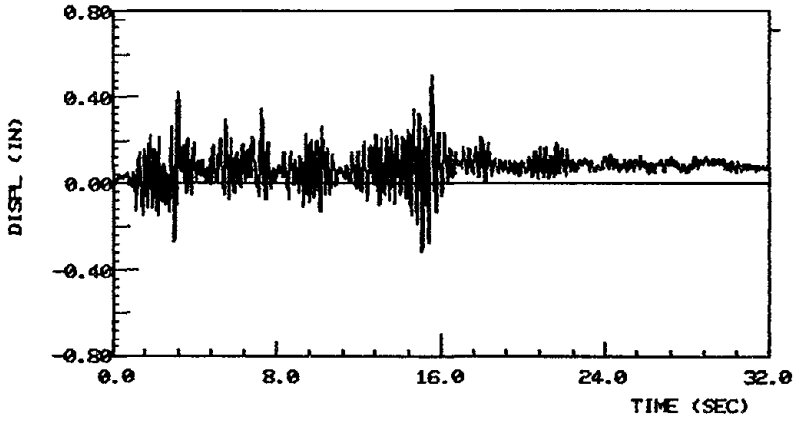

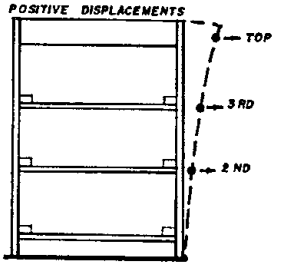

REL DISPLACEMENT FLOOR 3

PZ3 T2 25038303 RELDI3

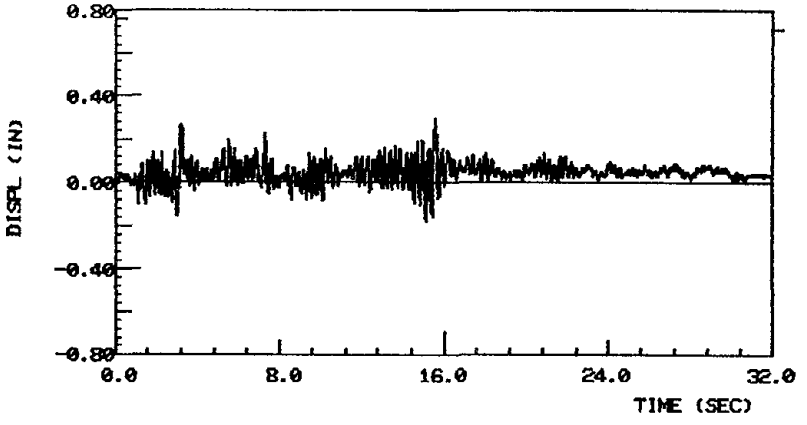

REL DISPLACEMENT FLOOR 2

PZ3 T2 25038303 RELDI2

Figure 8.10 Continued.

8.2 Results from El Centro at 0.69g, (EC-750), PZ-III Wall

8.2.1 Introduction

This strong motion induced significant damage along the base of the lower wall at the wall to floor joint. The horizontal table motion is illustrated in Figure 8.8 with time history records of the displacement and acceleration. The table reached its maximum displacement at approximately 9 sec, however, the peak accelerations occurred within the first 3.2 sec of the test.

The table pitch acceleration is a result of table-structure interaction. Timing of peak rotations and the frequencies in the pitch record were found to match the structural overturning moment record very closely. The non-stiff character of the table in pitching motion results in an apparent natural frequency for the structure on the table which is slightly lower than the real frequency of the structure on a rigid foundation.

The high amplitude motion and the high frequency local vibration of the lower steel platform resulted in accelerations in the vertical steel platform which were occasionally above the linear range of the instruments. As in PZ-I, the data from those instruments was not used in the response analysis. One of the DCDTs, at location S3, became inoperative after 16 sec because of cracking of the concrete below the instrument mounting. A second DCDT, at location FB2 (see Fig. 4.5) apparently became unplugged since no detectable signal was recorded from that channel. The potentiometer measuring the vertical displacement at the north end became inoperative just after the start of the test.

8.2.2 Structural Accelerations

Time-history records of acceleration at different locations over the height of the wall are given in Figure 8.9. The peak acceleration at the

top of the wall was 1.08g and the peak acceleration at the added mass blocks was 1.16g. Measured accelerations, along with the known structural mass, were particularly important in determining the actual internal inertial shear forces and moments. (Note - level 5 is at the concrete blocks.)

8.2.3 Lateral Displacements

The relative lateral displacements of the structure were calculated from the differences between the absolute wall displacements and the ground or shaking table motion. Figure 8.10 includes the relative lateral displacements measured over the height of the test specimen. The first record shows the lateral displacement at the foundation of the wall system itself. The displacements at this level resulted from shear deformation within the force transducers and slip in the bolted connections between table and transducer and transducer and foundation beam. At 3.25 sec a permanent slip, probably in the upper bolted joint, occurred showing as a residual displacement 0.0033 in. While the magnitude of the foundation displacement is negligible, the lateral flexibility should be included in analytical correlation studies.

Peak values of relative displacements are listed in Table 8.2 along with other response quantities. Relative displacement records at levels 2, 3, and 4 exhibit a considerable degree of similarity with increasing displacement and residual set from bottom to top. The relation seen between floor displacements and the visual detection of nearly all the damage at the wall base indicates the wall displacements are primarily a function of rotation. The amount of displacement created at level 4 (= top of the wall) by the table's pitching motion is plotted in the second frame of Figure 8.10, assuming the test wall is a rigid body pitching with the table and

TABLE 8.2

Extreme Values from EC-750 Test, PZ-III

Quantity	Extreme Value
Ground (table) displacement	9.68 cm (3.81 in.)
Ground (table) acceleration	0.69 g
Acceleration at foundation	0.68 g
Acceleration at 2nd floor	1.20 g
Acceleration at 3rd floor	1.20 g
Acceleration at top of wall	1.08 g
Acceleration at concrete blocks	1.16 g
Second floor relative displacement	0.75 cm (0.295 in.)
Third floor relative displacement	1.28 cm (0.503 in.)
Top of wall relative displacement	2.03 cm (0.799 in.)
Base shear force	97.4 kN (21.9 kip)
Base overturning moment	458 kN-m (4056 in.-k)
Strain - north column bar	4.17%
Strain - north panel bar	1.63%
Strain - south panel bar	0.17%
Strain - south column bar	0.49%
North end lower panel uplift	0.91 cm (0.36 in.)
South end lower panel uplift	0.81 cm (0.07 in.)
Slip in lower horizontal joint	0.016 cm (0.0064 in.)
Curvature (avg) in lower wall panel	0.000093 rad/cm

ignoring additional bending within the wall which might be induced by base pitching. The rigid body displacements are relatively small when compared to the total level 4 displacement.

8.2.4 Inertial Shear, Base Shear and Bending Moment

As in Chapter 7, since the force transducers only measured the shear force at the table connection, it was necessary to use calculated structural inertial forces to determine the bending moment and shear within the lower panel. Equation (2) from Figure 7.6 was again used to determine the rotational acceleration of the added mass system above the wall, then equation (1) was used to estimate individual accelerations of each steel platform. A total inertial base shear, from the accelerations and a new lumped mass, was calculated and the accuracy of the mass lumping was verified by comparing the calculated base shear and measured base shear. The total base shear measured by the transducers is plotted in Figure 8.11. The measured base shear (solid line) and the calculated inertial shear (dashed line) are compared in Figure 8.12. The agreement is satisfactory though the inertial shear tends to be slightly overestimated. Accepting the inertial force calculation, the base moment could be determined from individual lumped inertial forces and their moment arms. The resulting base moments are shown in Figure 8.13. The maximum base moment in this wall reached 4056 in-k (458 kN-m).

8.2.5 Strains in Reinforcing Bars

The high intensity of this test caused an extremely large ductility demand within the lower wall joint resulting in large strains in the reinforcement. Since there was not sufficient crushing of concrete the reinforcing bars were not exposed and visual detection of rupture was not

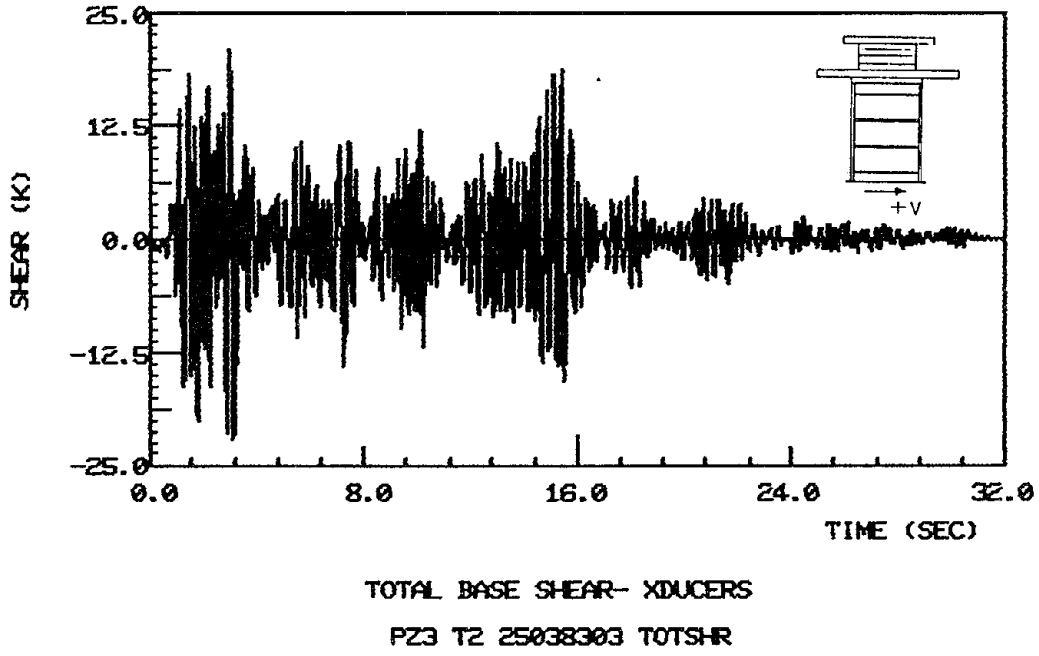

Figure 8.11 Total base shear measured by transducers, flanged wall, EC-750, 0.69g.

possible. However, after the second strong shake (1.081g, EC-1000) crushing or spalling around the bars led to inspections that found the panel bars from the north flanges ruptured and the column and web panel bars stretched and buckled. All of the bars at the south end, except the column bars, had ruptured.

Strains at the gauge locations of most of the bars that were continuous through the horizontal joint at the north end of the wall are shown in Figure 8.14a. All of the north panel bars at the first floor level were strained beyond their yield capacity at 3.2 sec. The two column bars were strained beyond the rated capacity of the gauge and the web panel bar reached a strain of 16.3 mil/in., very near to the gauge rating of 20 mil/in. From that time onward the measured strains cannot be assumed to be accurate, in fact the north outer column gauge developed enough residual strain by 16 sec to peak out the signal amplifier. Strains at the second floor horizontal

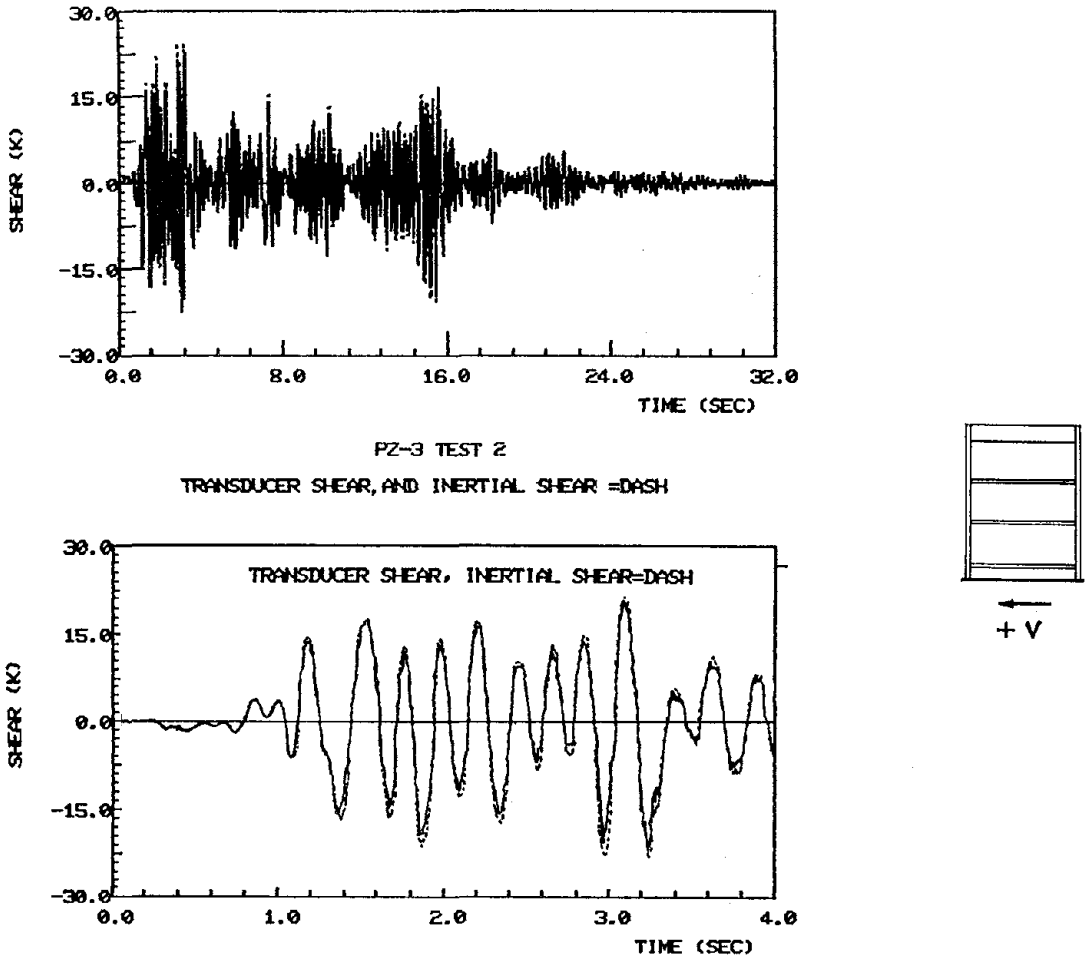

Figure 8.12 Comparison between computed inertial and measured base shear.

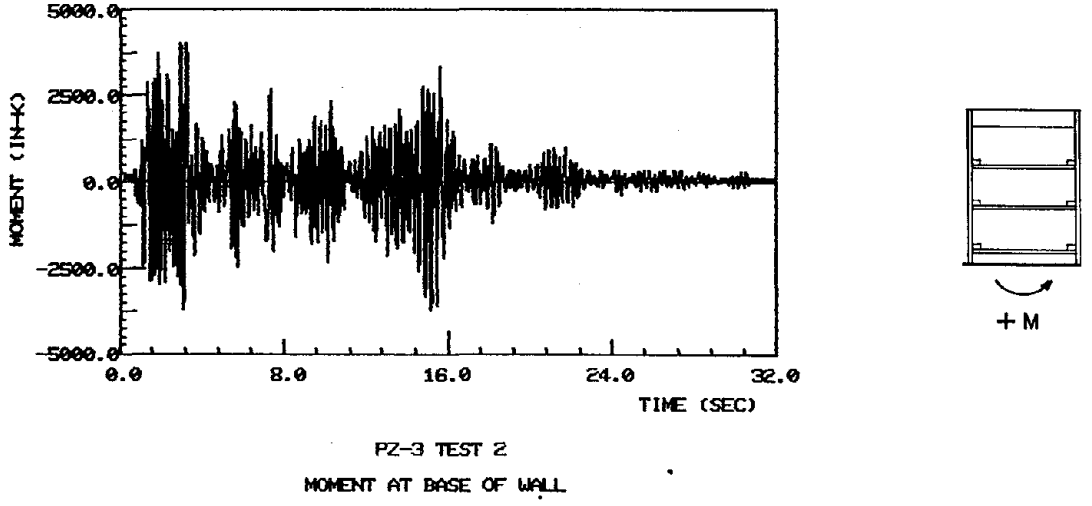

Figure 8.13 Calculated base bending moment, flanged wall, EC-750, 0.69g.

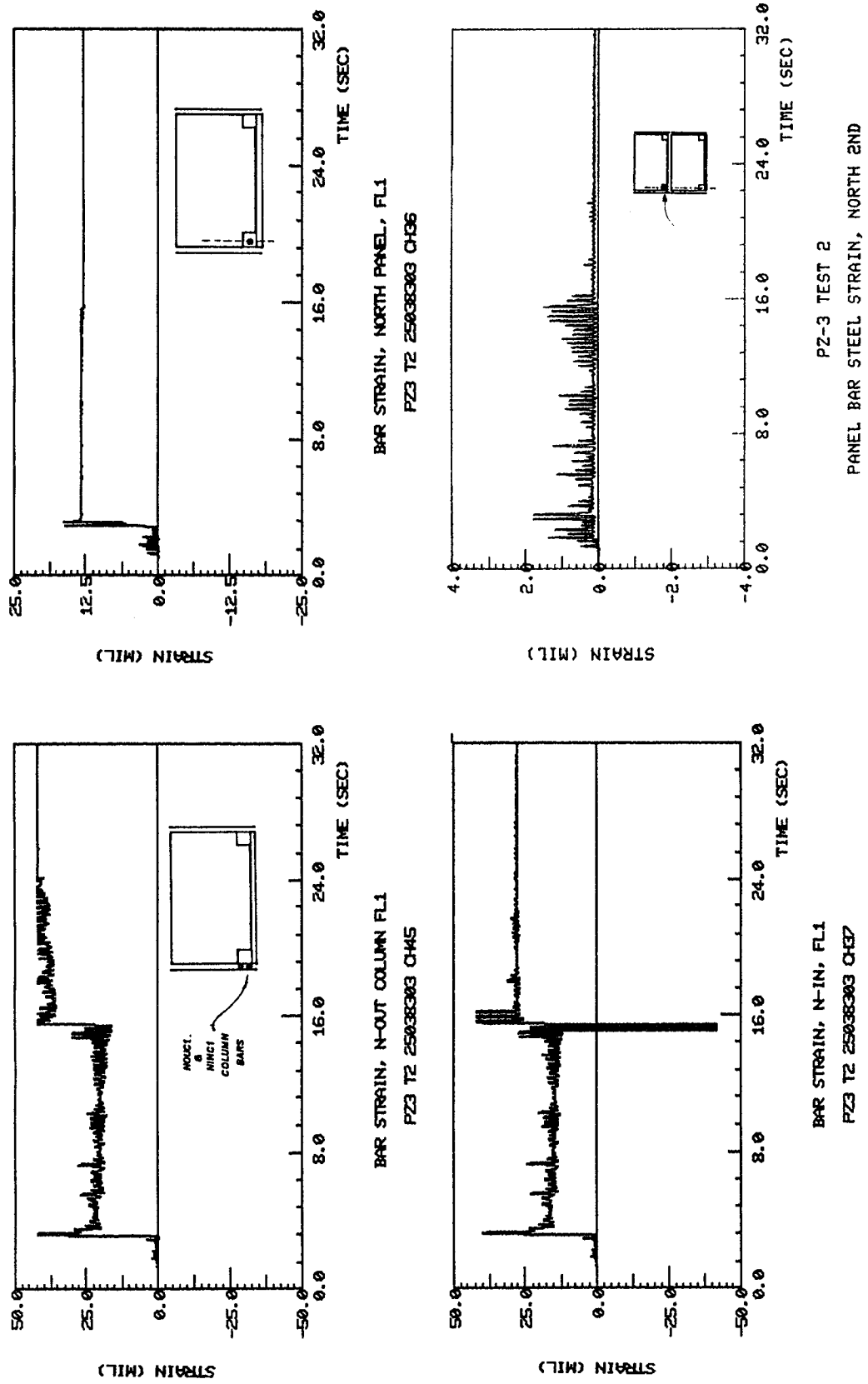

Figure 8.14a Reinforcing bar strains at north end of the wall, flanged wall, EC-750, 0.69g.

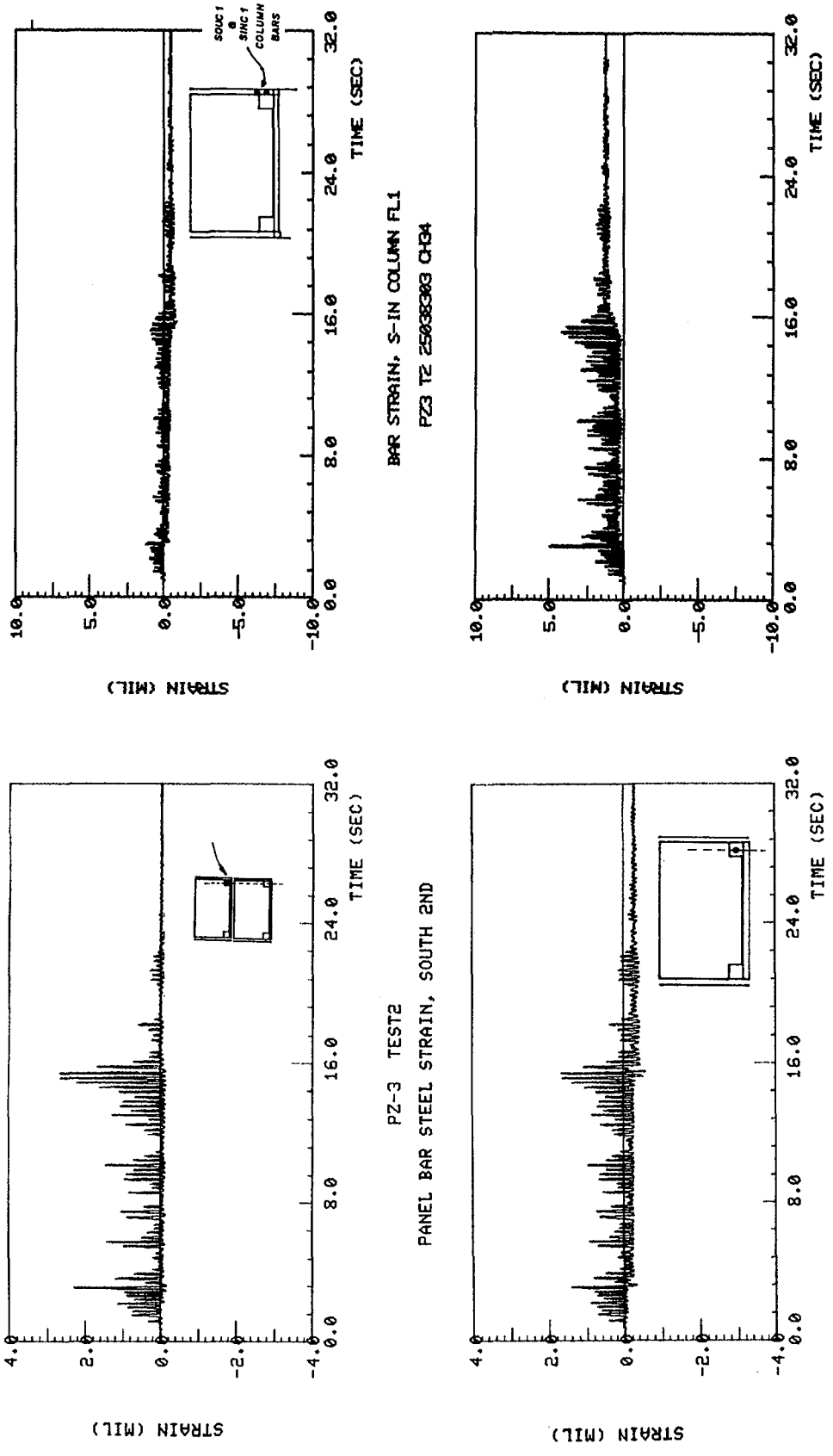

Figure 8.14b Reinforcing bar strains at south end of the wall, flanged wall, EC-750, 0.69g.

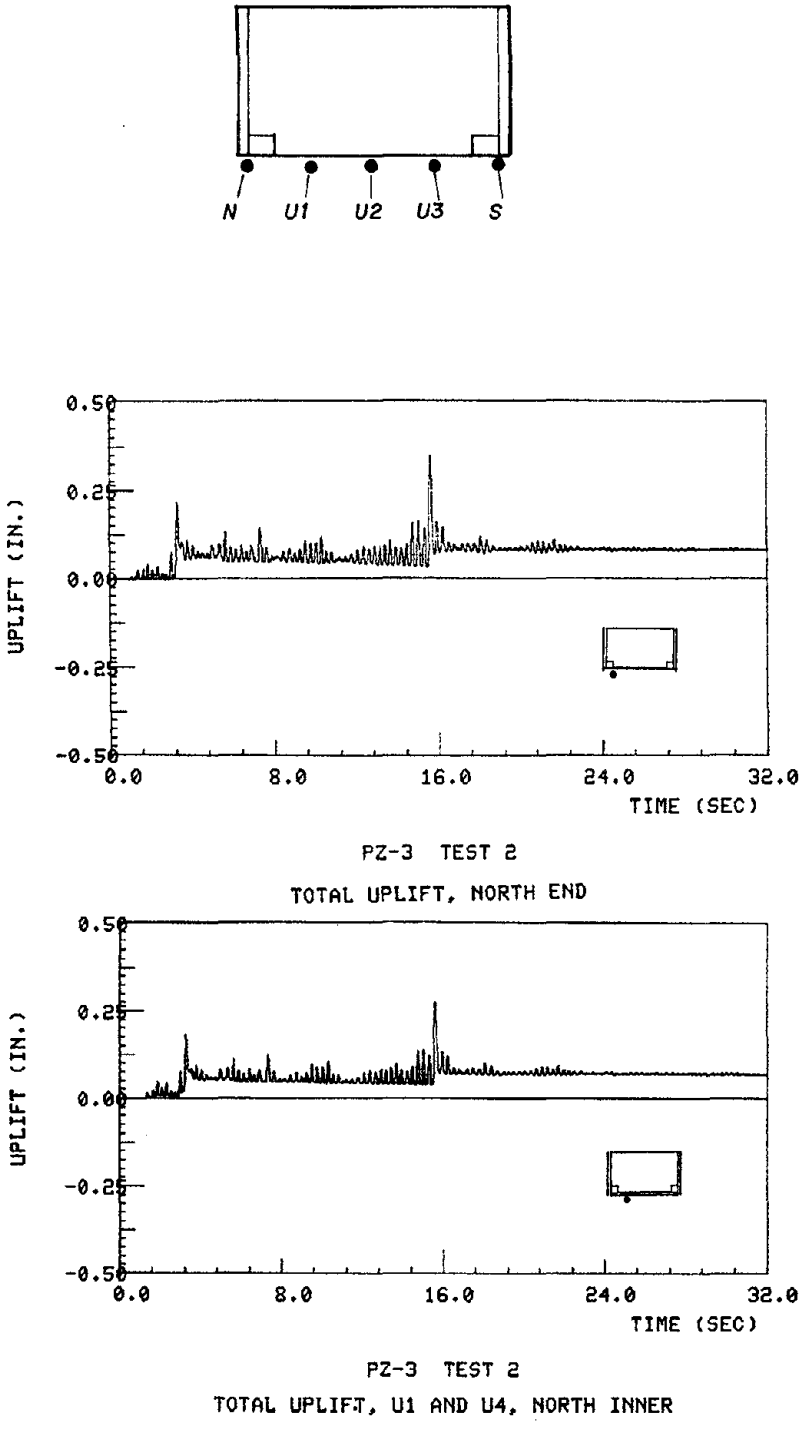

Figure 8.15 Uplift of the lower web wall, flanged wall, EC-750, 0.69g.

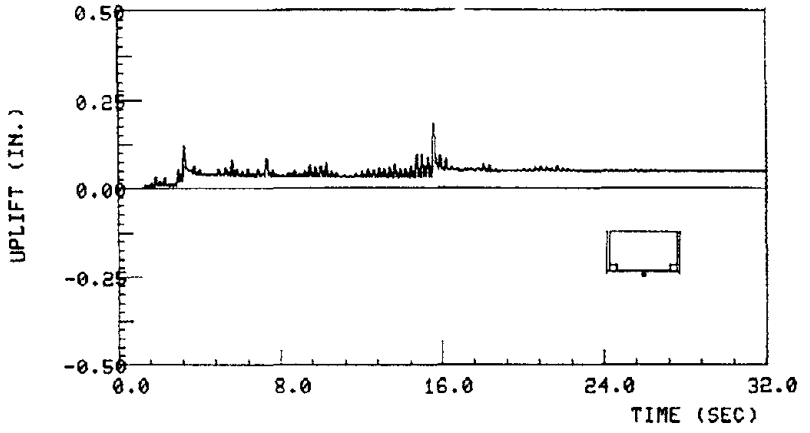

PZ-3 TEST 2
TOTAL UPLIFT, MID WALL, U5 AND U2

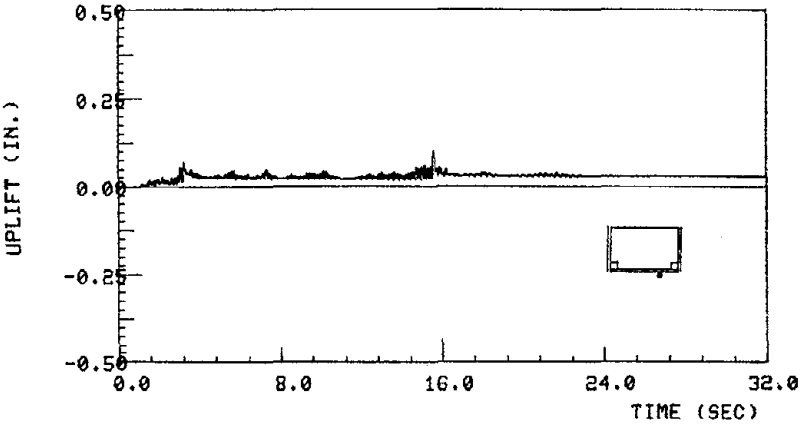

PZ-3 TEST 2
TOTAL UPLIFT, SOUTH INNER, U6 AND U3

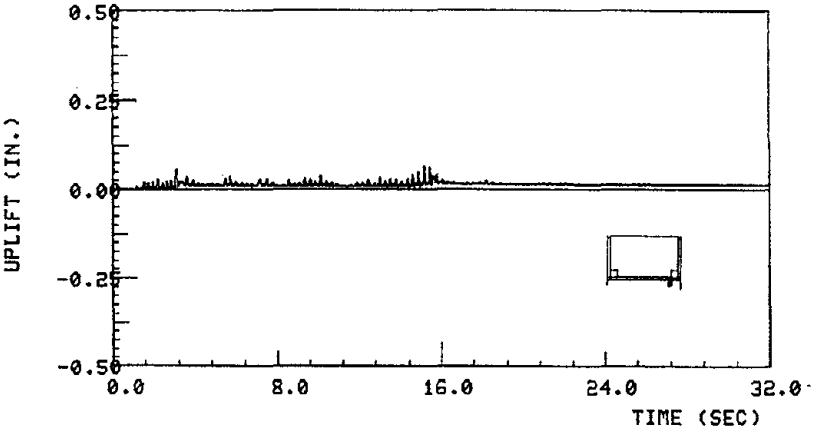

PZ-3 TEST 2
TOTAL UPLIFT SOUTH END

Figure 8.15 Continued.

joint were more moderate though a small degree of yielding did occur.

The extent of the inelastic motion at the south end, based on bar strain, was considerably lower. Records from the instrumented bars are shown in Figure 8.14b. Again, all of the bars yielded but the indicated strains are approximately 1/10 the size of the north end strains. It is apparent that the magnitude of the wall uplift was much higher at the north end.

8.2.6 Uplift along the First Floor Joint

Uplift between the first floor wall panel and the foundation wall was measured at five locations along the wall base. The uplifts are illustrated in Figure 8.15. It is obvious from a comparison of the records that the wall was uplifting predominantly at the north end.

The first large north end uplift of 0.22 in. at 3.2 sec coincides with the excessive strain in the north bars noted above. The second large peak, 0.36 in., at 16 sec also coincides with a jump and offset in north bar strains. The residual uplift of 0.09 in. is probably the result of crushed concrete fragments holding the joint open. Eighty percent of the measured uplift developed between the wall and the floor slab, the remaining twenty percent was measured between the floor and the foundation.

At the three interior locations the uplifts all mirrored the north end uplift, as would be expected under rocking motion of the wall. It was only the south-inner location that exhibited some peaks which could be correlated with the south end record, though even here the large predominant peaks result from north end uplifts.

South end uplift is considerably smaller than that seen at the north end. While the peaks are out-of-phase with the north peaks, indicating a small amount of rocking when south uplift occurred, the offsets are coincident with and due to north end uplift. The peak measured south uplift was

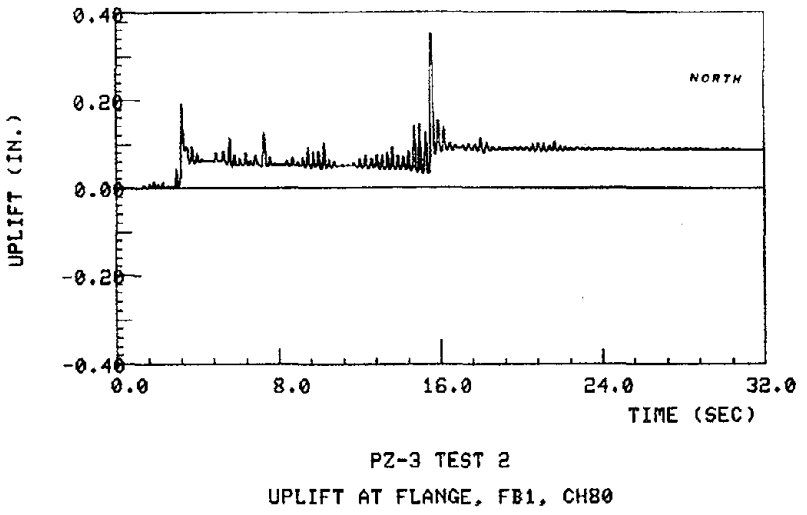

Figure 8.16 Uplift of north flange at lower joint, flanged wall, EC-750, 0.69g.

0.07 in., or only 20 percent of the amount seen at the north end.

A separate uplift measurement taken on the flange panel at the north end of the wall system recorded the total displacement occurring between the flange panel and the foundation wall - across the horizontal floor joint. The resulting flange uplift is plotted in Figure 8.16. The measurements are nearly the same as shown previously for the north end of the web wall panel with peaks of 0.19 in. and 0.35 in.

8.2.7 Shear-Slip at First Floor Joint

Horizontal slip between the first floor and the foundation is shown in Figure 8.17. The predominant peaks in slip, which is primarily toward the south, occur simultaneously with north uplift and wall rocking to the south. In terms of damage, the magnitude of the slip is almost negligible.

Horizontal slippage measured between the lower wall and floor and between the lower wall and the cast-in-place end "key" at the south end of the wall system are plotted in Figure 8.18; these were combined to define an

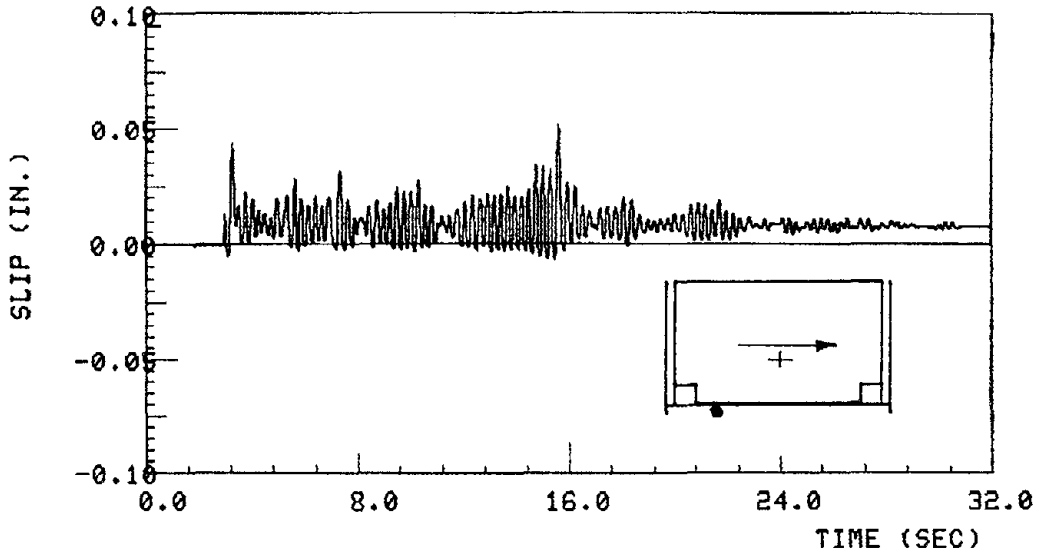

Figure 8.17 Slip between floor and foundation wall.

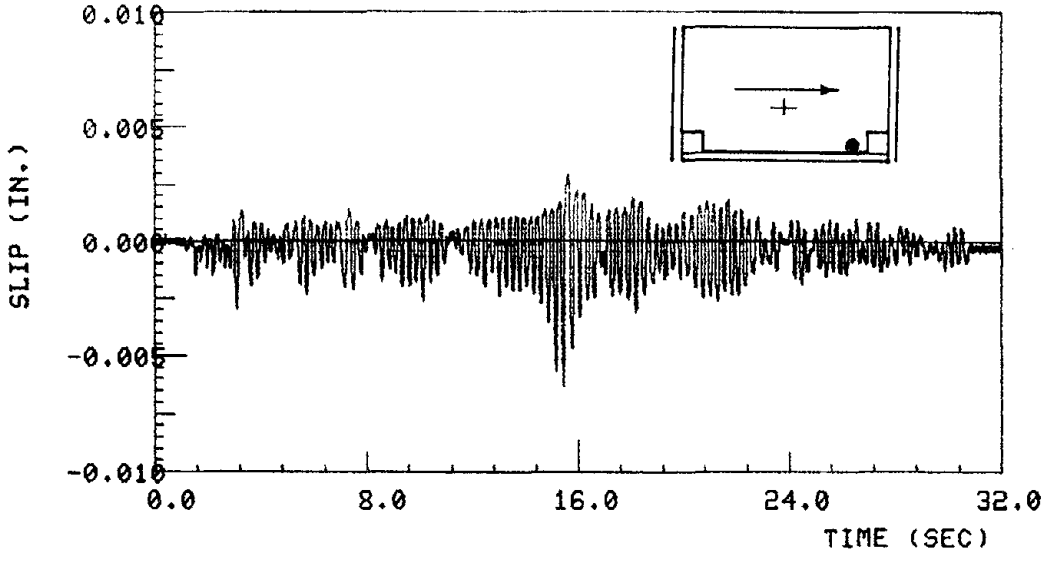

Figure 8.18 Slip below lower precast panel, flanged wall, EC-750, 0.69g.

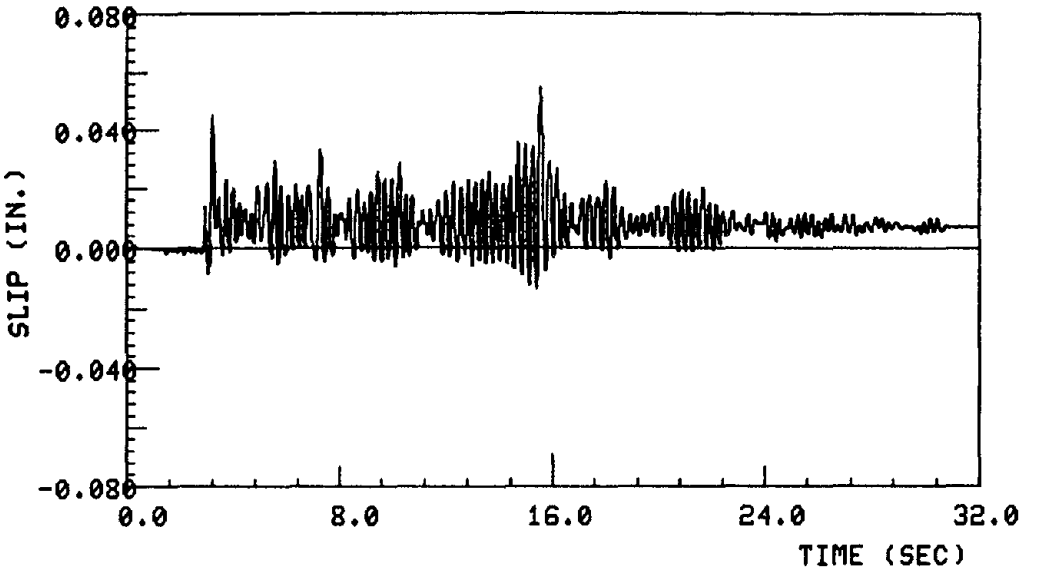

Figure 8.19 Total slip in lower joint at base of precast walls, flanged wall, EC-750, 0.69g.

average wall slip as shown. The average slip indicates that the wall is sliding in both directions, slightly favoring the north. Again, the maximum slip developed, 0.006 in., is a minor amount. The total slip occurring at the lower level is shown in Figure 8.19.

8.2.8 Behavior of Flange Walls

Deformation in the flange panels was measured to determine how effective the cast-in-place joint between wall and flange panels was in providing the necessary shear transfer to couple the elements into a single flexure-resisting cross section. The vertical north end extension of the first story panel wall, measured over a 25.1 in. gauge, is illustrated in Figure 8.20a. The vertical extension of the northern flange wall, with a 25.8 in. gauge, is shown in Figure 8.20b. The flange deformations are consistently slightly lower than the deformation of the adjacent wall, with

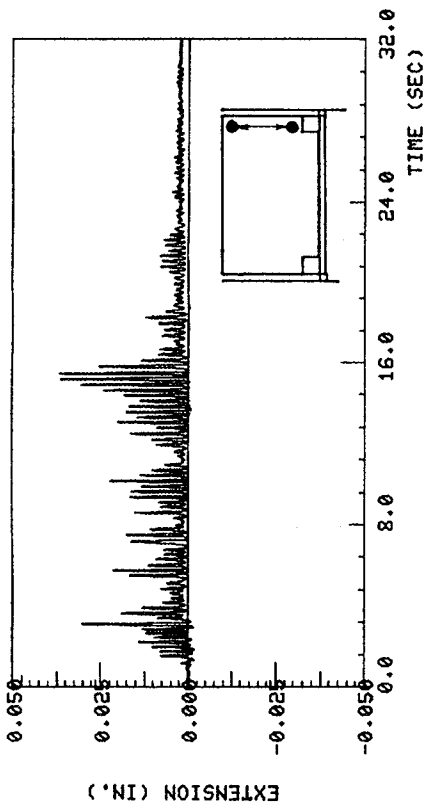

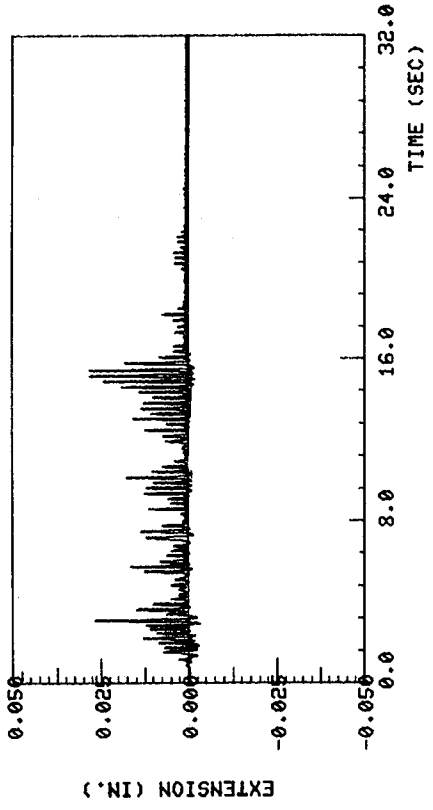

Figure 8.21 Wall and flange extensions, south end, EC-750, 0.69g.

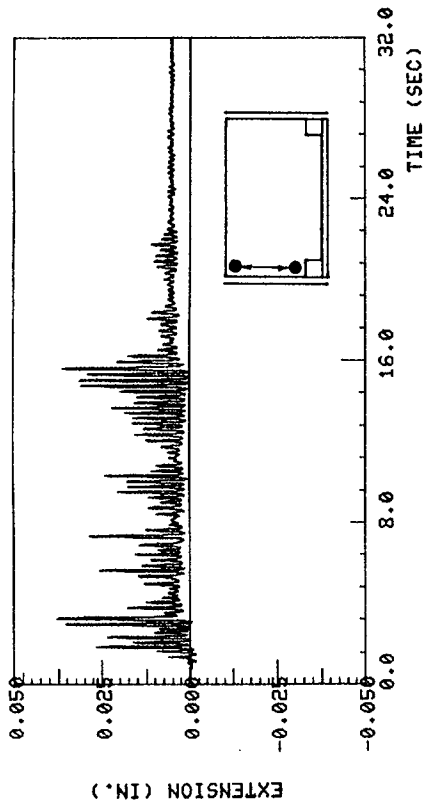

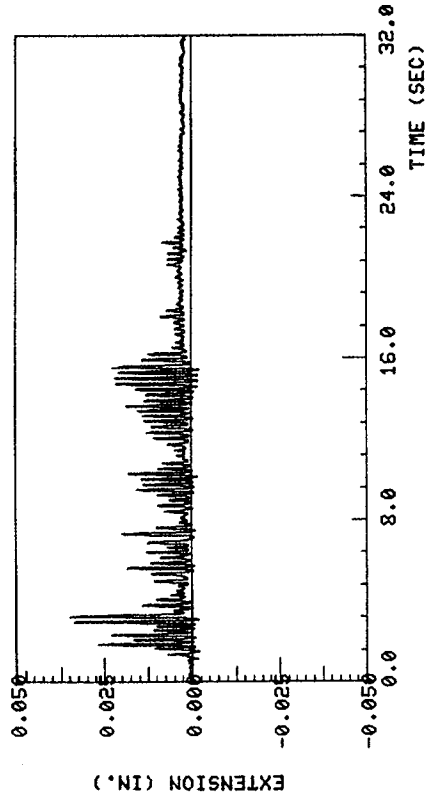

Figure 8.20 Wall and flange extensions, north end, EC-750, 0.69g.

maximum flange extension of 0.035 in. and wall extension of 0.039 in. Similar behavior is evident in Figure 8.21 for the south end deformations.

Further proof of less than perfect coupling between wall and flange is exhibited in Figure 8.22 with a direct measurement of vertical slip occurring between the web wall and the flange wall. Positive slip indicates that the web wall is uplifting with respect to the adjacent flange wall. As would be expected there is no slip when that end of the wall system is in compression. Although significant cracking between the web wall and flange walls was not visually evident, it is apparent that limited slip occurred, yet the flange walls remained effective in resisting the overturning moments.

8.2.9 Overall Behavior of the Wall System

The lower wall panel exhibited flexural cracking distributed at 3-4 in. intervals over its height at the wall extremities. Figure 8.23 includes a simultaneous plot of the overturning moment existing at the base of the wall and the average wall panel curvature. It is evident that inelastic flexural deformation was able to develop in the panel walls of this system. The wall's initial stiffness of 1.71×10^9 in-k/rad was reduced to 1.58×10^8 in-k/rad (1.9×10^8 kN-m/rad to 1.78×10^7 kN-m/rad).

The overall structural behavior of the system is indicated by the base shear and top of wall displacement plot included in Figure 8.24. The first frame includes response from the first fourteen seconds during the test and the second frame includes the complete record. All of the large deformation cycles occur in the southerly direction, a result of wall rocking and uplift at the north end. The average initial cracked section wall stiffness is 70.3 k/in and decreases to an average value of 33.1 k/in after the major cycles of north uplift with bar yielding occur (123 kN/cm to 58.0 kN/cm).

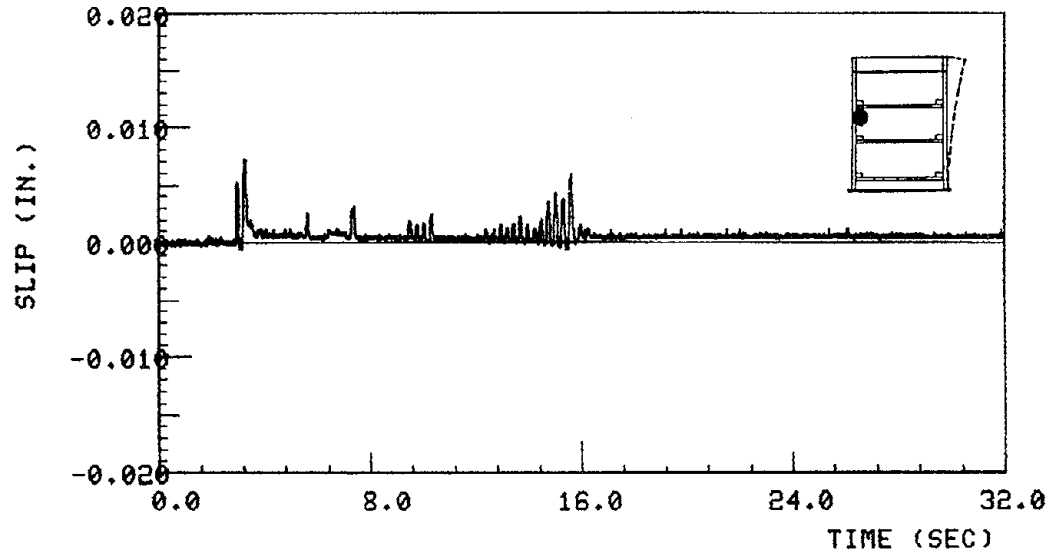

PZ-3 TEST 2

WALL-FLANGE SLIP, WF3, CH78

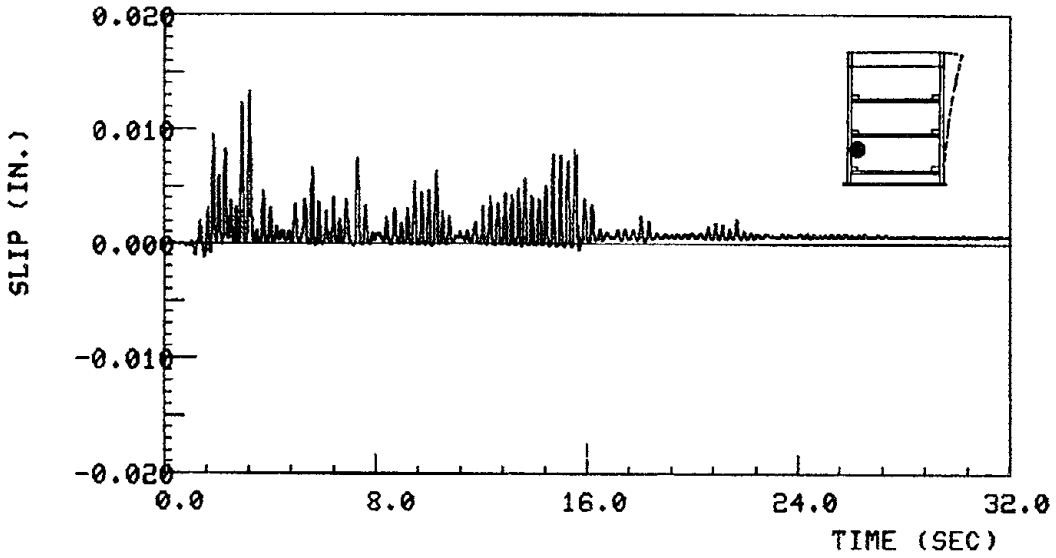

PZ-3 TEST 2

WALL-FLANGE SLIP, WF1, CH76

Figure 8.22 Slip between web and flange panels, north end, EC-750, 0.69g.

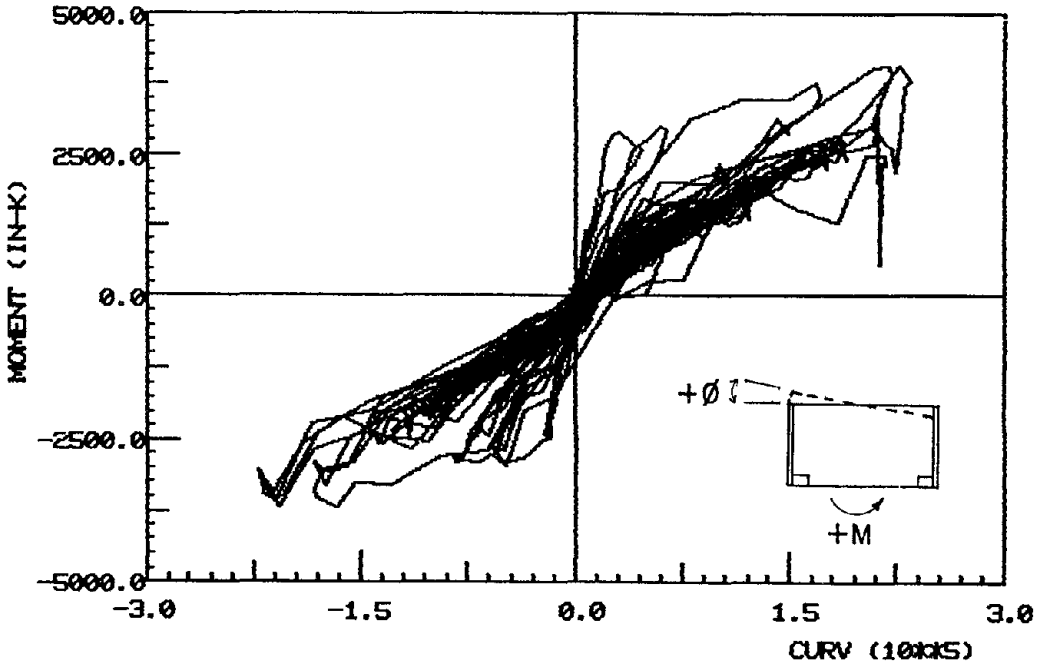

Figure 8.23 Moment-curvature relation developed in the lower web panel, flanged wall, EC-750, 0.69g.

The relatively small amount of horizontal slip at the panel-wall joint was unable to supply any significant amount of energy dissipation through friction-slip. Figure 8.25 illustrates the shear versus slip behavior in this wall system. Detailed inspection of the initial response may be accomplished using the plots of Figure 8.26 which show the first 4 seconds of the response history.

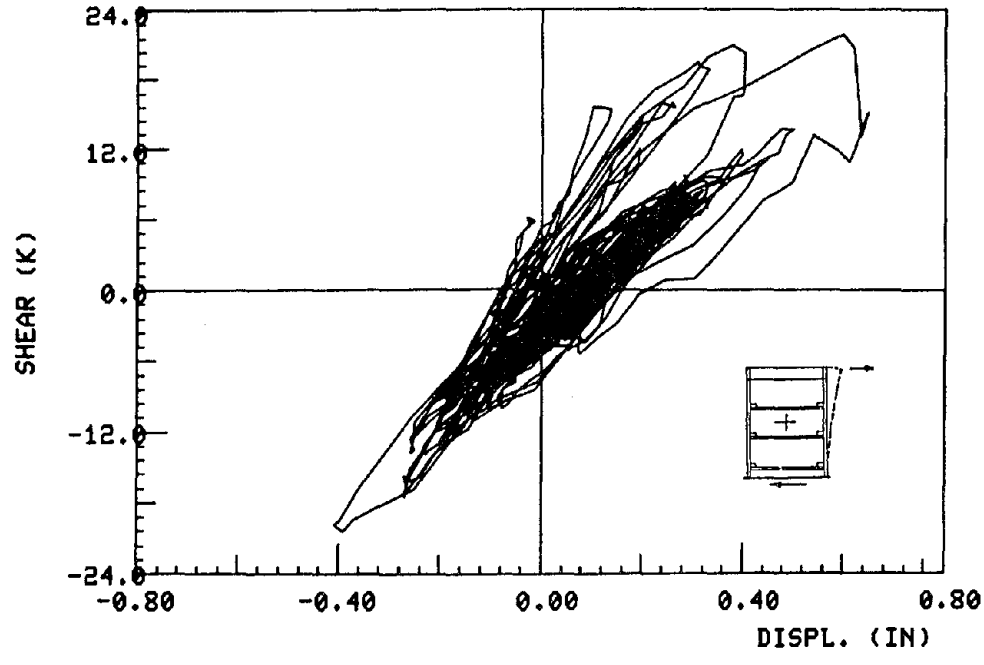

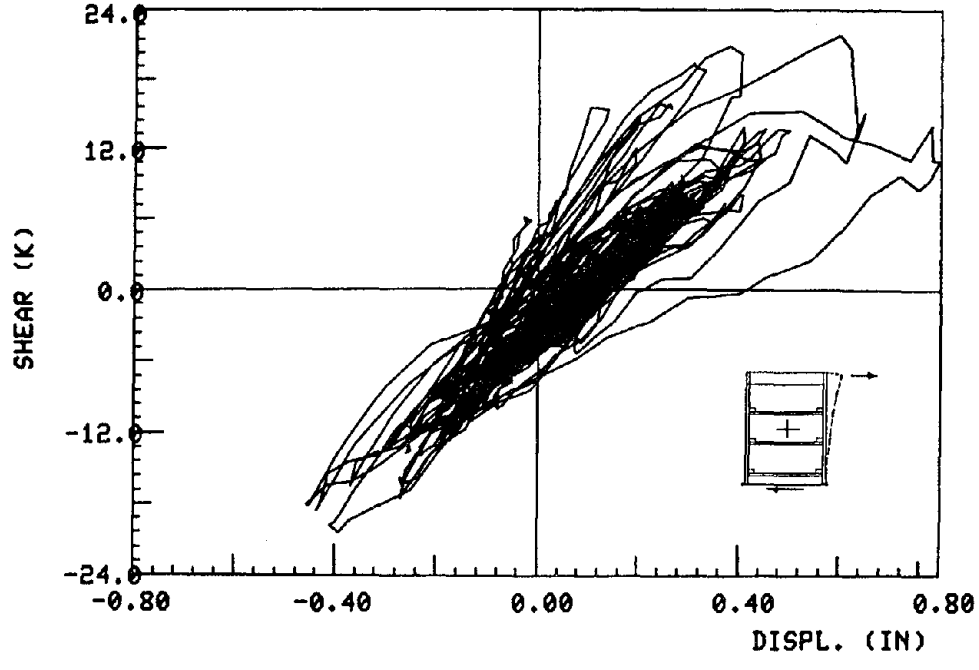

Figure 8.24 Base shear and top displacement, flanged wall, EC-750, 0.69g.

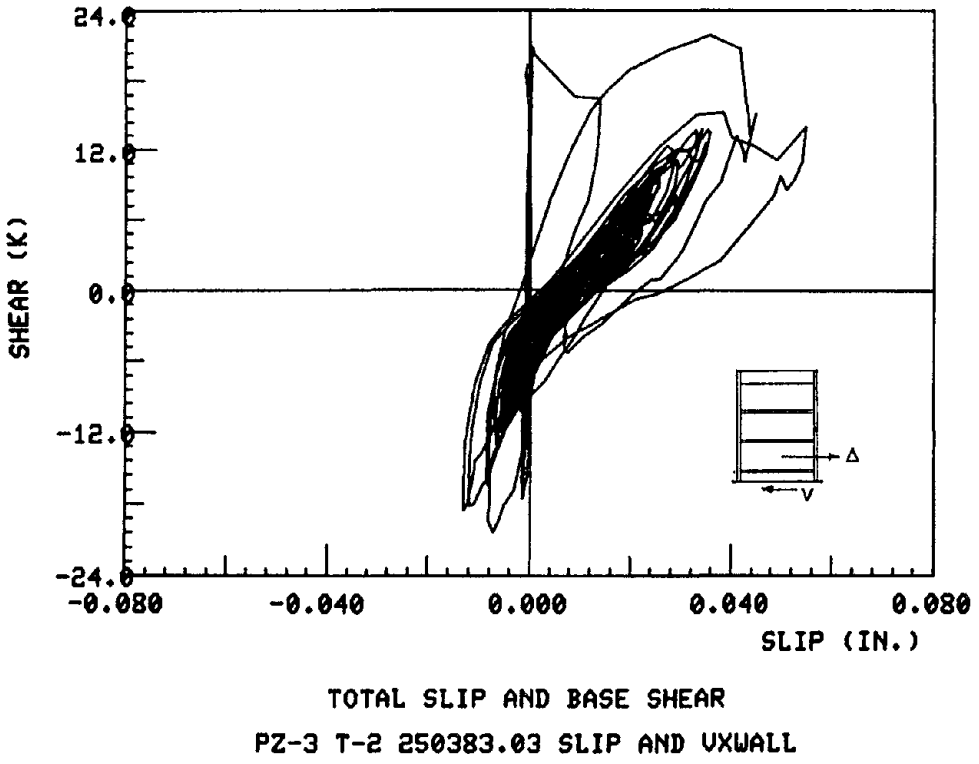

Figure 8.25 Relation between base shear and base slip at lower joint, flanged wall, EC-750, 0.69g.

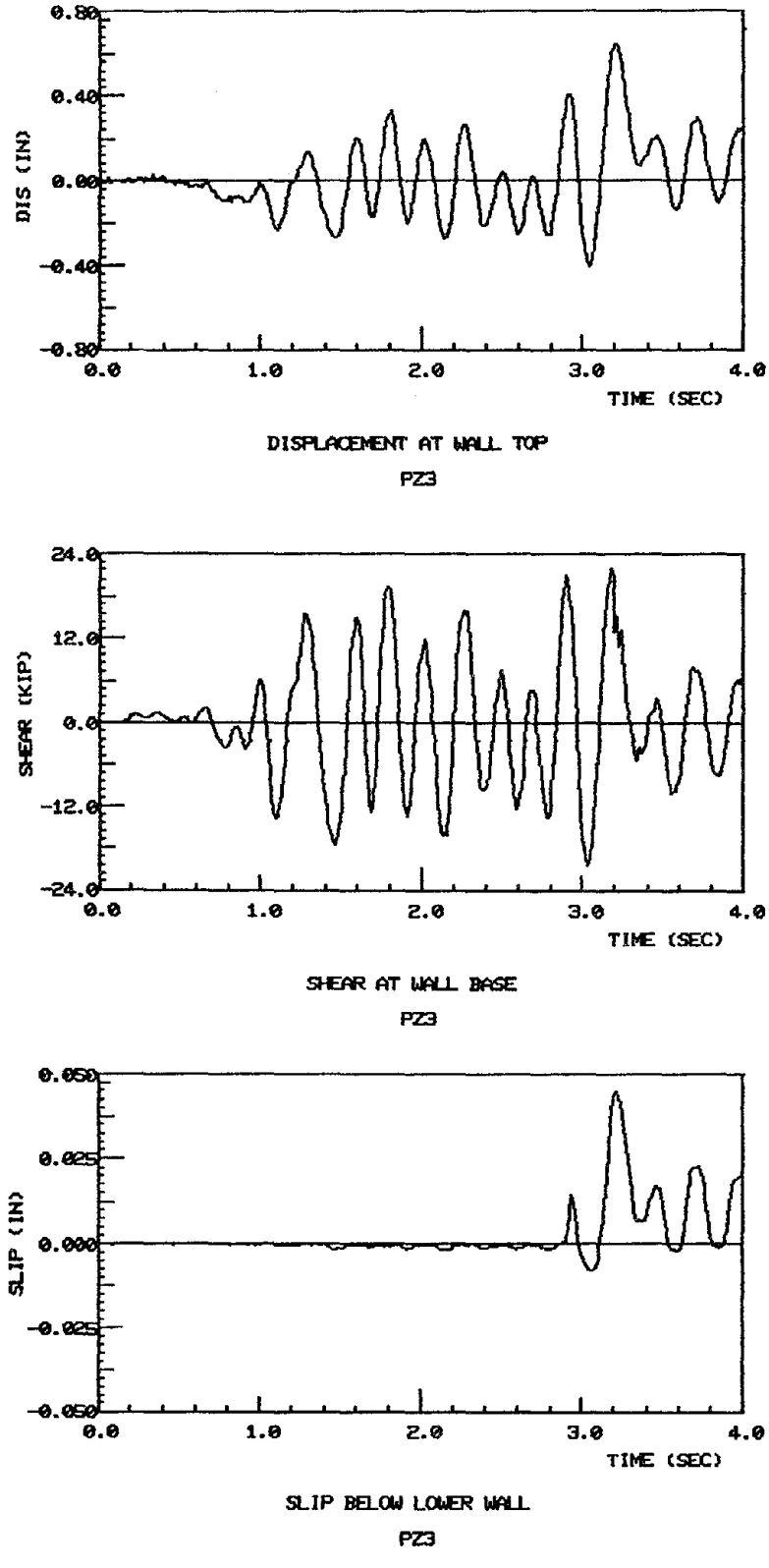

Figure 8.26 Initial response data (first 4 seconds), flanged wall, EC-750, 0.69g.

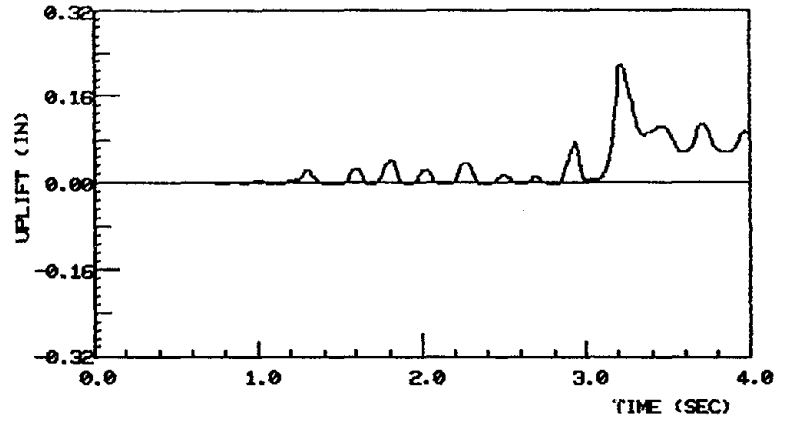

UPLIFT AT NORTH END

PZ3

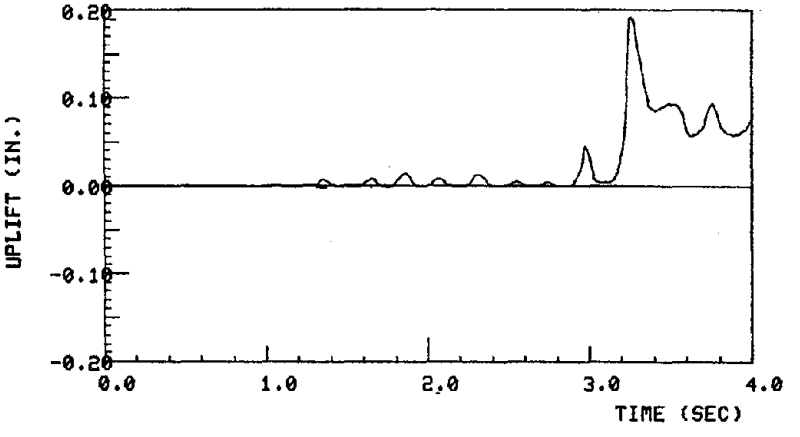

PZ-3 TEST 2

UPLIFT AT FLANGE, FB1, CH80, FIRST 4 SEC

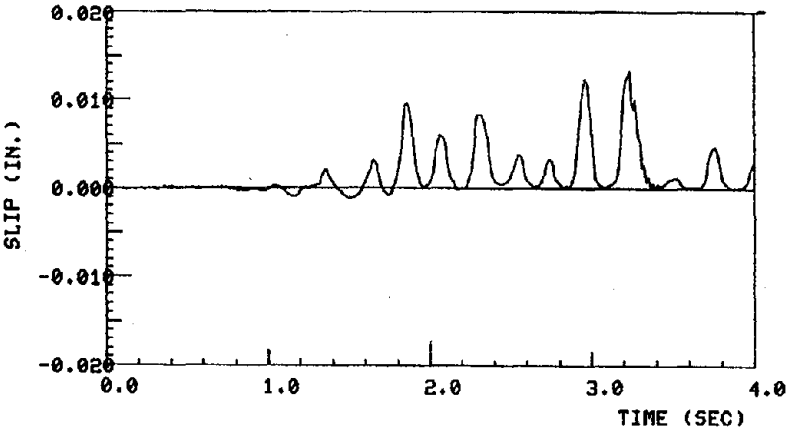

PZ-3 TEST 2

WALL-FLANGE SLIP AT WF1, FIRST 4 SEC, CH76

Figure 8.26 Continued.

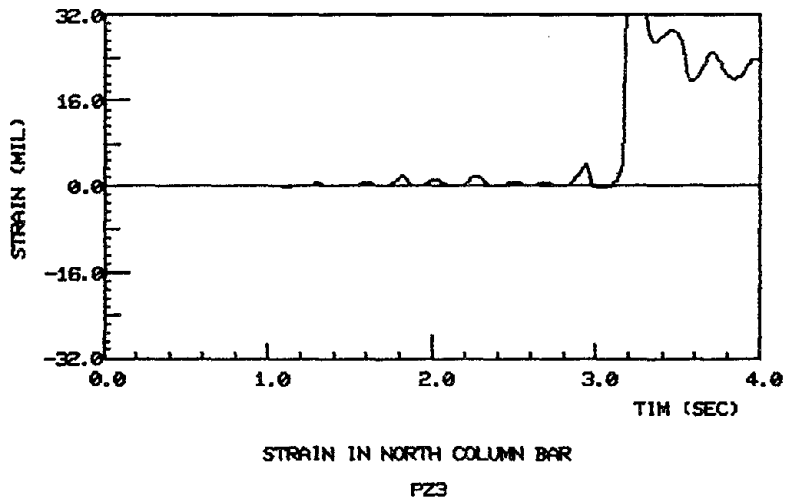

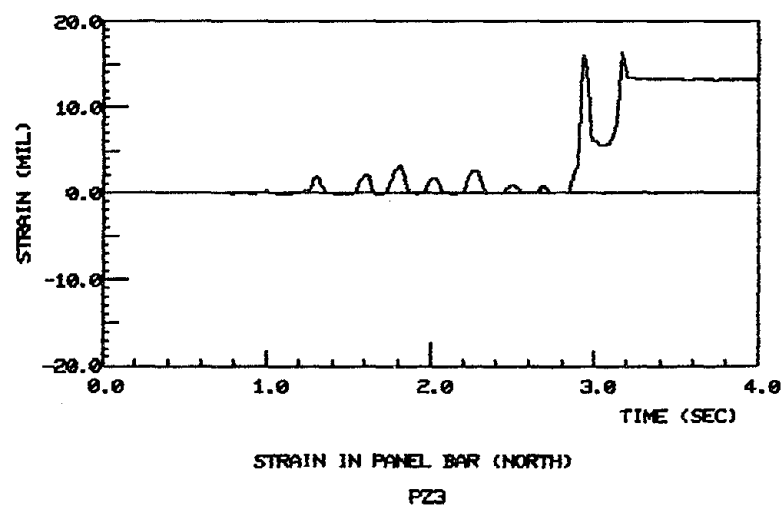

Figure 8.26 Continued.

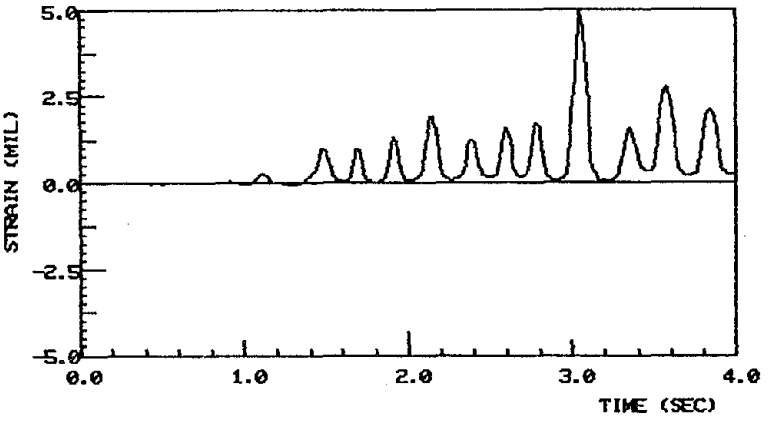

STRAIN IN SOUTH COLUMN BAR

PZ3

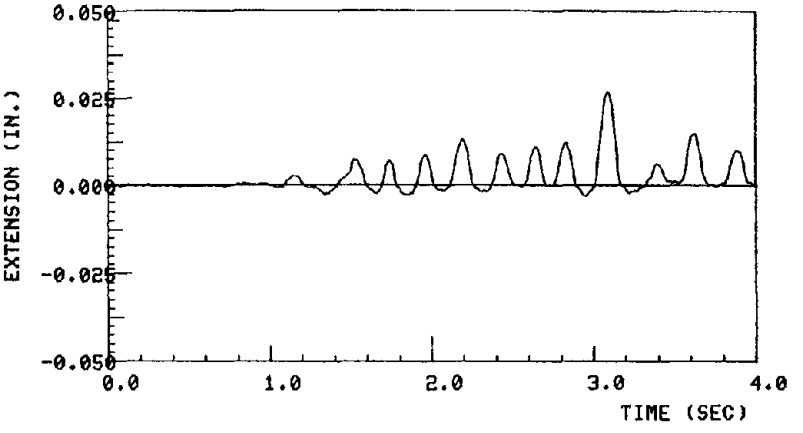

PZ-3 TEST 2

FLANGE PANEL EXTENSION, SOUTH, FB6

Figure 8.26 Continued.

9. SUMMARY AND CONCLUSIONS

The investigation described in this report included simulated earthquake shaking and response evaluation of precast large panel wall structures. The raw measured response data and visual observations have been presented in the previous chapters together with a full description of the test structures, instrumentation and test sequence. In this chapter the characteristics of large panel systems and particularly the systems tested, the test results and their implications are briefly discussed and conclusions drawn.

Large Panel Wall Systems

The vertical wall panels, in panel buildings, are individual precast elements connected in the field and act as vertical load bearing shear walls. A lack of redundancy or secondary mechanisms to carry loads if a panel fails, and the existence of joints between elements are of particular importance in considering their use in regions of seismic risk. Lack of redundancy exists in most shear wall systems and must be addressed at the conceptual level. The behavior of any shear wall composed of connected precast elements depends strongly on the strength and stiffness characteristics of the joint regions. Economically feasible systems tend to have strong precast elements with relatively weak and often brittle joints.

Model Configuration

The three large scale models tested in this program included a plain solid wall, a wall whose panels contain door openings, and a wall with adjoining end flange walls. Each model was a three story wall segment. Small cast-in-place horizontal connections, with precast panels providing forming, were used with a limited amount of continuous reinforcing between vertical panels. The joint detailing was developed in Yugoslavia and behaves

similarly to U.S. type platform systems for which the compressive capacity of the platform joint is adequate to resist crushing. In such connections the moment capacity is controlled by the yield capacity of the vertical continuous reinforcing and the shear capacity is primarily controlled by friction existing between the panel and joint filling material.

Common United States building codes classify large panel wall structures as "box-type" systems and specify a relatively high design lateral loading because of a presumed lack of ductility and the lack of redundancy in the system as a whole. Additional restrictions, not specifically addressed toward precast systems, limit the height of box-type systems to 160 ft within regions of moderate or strong seismic risk. The Uniform Building Code [19] also specifies vertical reinforcing requirements to insure a minimal ductility; these include a minimum reinforcing content of 0.15 percent and maximum spacing of reinforcement at 16 inches (46 cm).

The wall elements in this program were intended to represent components near mid-height of a 15 story large panel building located in a seismically active region. The precast panel elements contained well-distributed horizontal and vertical reinforcement. The horizontal connections between adjacent vertical panels in a stack had a limited amount of continuous vertical reinforcement concentrated only at the ends of the joint. The reinforcement ratio across the horizontal joint was 0.4 percent in the simple wall and 0.7 percent in the wall system with attached end flange walls. The spacing of the vertical reinforcement, which was concentrated at the joint extremities, was 68.7 in. (1.74m) and corresponded to a spacing of 206 in. (5.23m) in the prototype building. This configuration of reinforcing does not meet present U.S. code requirements.

Dynamic Characteristics

The first mode natural vibration periods of the simple and flanged walls were 0.19 sec and 0.16 sec, respectively, before testing. The corresponding periods for an actual prototype structure are 0.33 sec and 0.28 sec. Actual periods in 8 to 15 story large panel buildings have been reported as between 0.30 and 0.45 sec [17,18]. The 1940 Imperial Valley - El Centro SOOE earthquake record, correctly time-scaled, was used for the simulated earthquake motion in the shaking table tests because of its substantial energy content near the periods of the models.

Large panel wall systems have vibrational characteristics in the very short period range. In such short period systems inelastic energy dissipation is of less benefit in controlling response and ductility requirements are considerably higher than in longer period systems [20]. Unfortunately the strong panel-weak joint characteristic of precast panel systems tends to concentrate this high ductility demand within the weaker joint region during inelastic response caused by a strong motion excitation.

Test Results

Each of the structural models was subjected to a shaking sequence which could be classified as a moderate shake, followed by a severe motion. The initial moderate shake used a ground motion with a peak acceleration near 0.2g and the severe shakes had a peak of near 0.7g. The test configuration resulted in a base moment versus shear ratio equal to 2.7 times the base length of the wall. Moment and shear forces existed simultaneously with an axial force intended to simulate axial compression stress expected near the mid-height of a 15 story structure, 146 psi (0.96MPa) or 0.02 f'_c in the simple wall and 96 psi (0.66MPa) or 0.016 f'_c in the flanged wall.

Moderate Shaking

The initial moderate shaking tests involved ground motions with peak accelerations of 0.18g and 0.22g in the simple and flanged walls, respectively. This represented a shaking amplitude which was approximately two-thirds of the actual El Centro 1940 motion. The relatively rigid wall systems responded elastically and developed peak top story accelerations of 0.3g and 0.4g, respectively. Measured relative displacements indicated that the maximum interstory drift was less than 0.04 in. (0.10 cm) or 0.1%. The stiffness of the systems appeared to be sufficient to prohibit structural or non-structural damage in the building components. No cracking or similar visible damage was apparent. The strength of this test relative to the commonly used 'equivalent-static-design-load' may be judged by the true base shear coefficient, as measured, which was 0.32 of the weight in the simple wall and 0.38 in the flanged wall. The UBC design shear coefficient would be approximately 0.20 for region 4 (strong seismicity) construction.

Strong Shaking

The severe shaking occurred with ground motion of approximately 0.68g peak acceleration applied to both of the wall models. The wall top accelerations were magnified by the structural motion and reached 0.8g in the simple wall and 1.08g in the flanged system. Yielding and subsequent inelastic behavior was initiated very early in these tests. Maximum intensity drifts in the simple and flanged walls increased to 0.46 in. (1.2 cm) and 0.3 in. (0.8 cm) or 1.2 percent and 0.8 percent, respectively. Again the measured base shear coefficients were considerably higher than the 0.20 value derived from UBC recommendations for equivalent lateral force. The strong motion coefficient was 0.68 of the weight in the simple wall and 0.92 measured in the flanged wall - three hundred to four hundred percent larger than the code design value.

Rocking Motion

One of the basic modes of deformation in stacked precast large panel wall systems is opening of the horizontal joints and rocking of individual panels while resisting overturning moments. The dominant mechanism in both the strong motion tests was rocking of the entire wall system about the lower horizontal joint. After opening, caused by rocking, the horizontal joint does not completely close since grinding takes place within the joint and the residual crack opening grows wider with successive cycles. Crack openings were apparent at the top and bottom of the lower horozintal joints after the strong motion tests. The opening at the wall ends reached a maximum of 0.7 in. (1.78 cm) during high overturning conditions.

Slip

The second basic motion in stacked precast systems consists of relative lateral slip, at horizontal joints, between adjacent vertical elements. Though slip would naturally tend to occur once the resisting effect of friction is overcome, particularly in joints which have been opened by overturning moment-bending effects, only limited slip developed in the current tests. The slip was controlled by a joint detail which included a large block key, filled with cast concrete, at each panel lower corner used primarily as a space to connect, in the field, the continuous panel reinforcing bars. As a result of this large shear key the maximum slip was limited to 0.04 in. (0.1 cm).

Implications of Test Results

Three distinct seismic resistant design techniques may be employed in large panel precast concrete construction. (i) Monolithic design attempts to join individual panel elements with connections which are at least as

strong as the panels themselves and are capable of developing the full panel strengths. (ii) Weak vertical/strong horizontal connection systems have been proposed where two or more vertical stacks of panels exist adjacent to one another and initial inelasticity and energy dissipation are intentionally directed into the vertical joints between adjacent stacks. (iii) Weak horizontal connection systems depend on inelasticity and yielding within horizontal joints to limit the forces transferred to the structure by the ground motion and to dissipate internal energy absorbed by the system.

For reasons of economy and configuration/layout constraints, weak horizontal connection systems, as in the models tested, are the most common large panel systems presently used. Unfortunately, these same systems have been viewed as presenting the greatest difficulty in obtaining satisfactory aseismic design and performance. The following specific problems will be discussed in relation to the test program carried out in this project:

1. Force isolation effects of inelasticity in a single joint may prevent the spread of yielding to other locations in the system.
2. Inelasticity tends to become highly concentrated within one or two horizontal joints.
3. Concentration of inelasticity causes exceptional local ductility demands.
4. Once yielding is initiated within a joint, there is no remaining elastic constraint on the system deformation.
5. The energy dissipation capacity of small horizontal joints is limited.

Joint Behavior-Rocking Mechanism

A rocking mechanism in the lowest horizontal joint was the dominant source of nonlinear inelastic response for the wall systems tested as part of this project. Increasing overturning moment initiated yielding in the vertical

reinforcement at the horizontal joint and the subsequent rocking with continued yield effectively limited the amount of shear and moment which could be induced in the wall by the ground motion. Once the reinforcement became appreciably stretched and buckled under compression on reversed cycles, the moment transferred through the joint was limited to an amount provided by the gravity restoring force. This effect was clearly apparent in Figure 7.22 where the normal cycles of moment appeared to be truncated when the moment is negative.

The isolating effect of the base rocking, which developed within the initial four seconds of the strong motion tests, prevented the spread of inelastic behavior to horizontal joints above because the maximum base moment could only reach a limited magnitude and moments in upper joints could not reach yield levels. This effect was accentuated by the concentration of continuous vertical reinforcing at the ends of the horizontal joint. All of the tension reinforcing across the joint yielded nearly simultaneously and the overall moment-rotation behavior resembled a bilinear mechanism with subsequent stiffness degradation. During large amplitude cycles the base moment was limited by the plastic deformation of reinforcing bars which had not already ruptured; during small cycles the buckled steel was ineffective and the effective stiffness was defined by the gravity restoring force.

The ductility demand in the lower joint, with nearly all the deformation occurring in that region, became very high. The overall structural displacement ductilities of 4.6 in the simple wall and 4.0 in the flanged wall were primarily a result of concentrated deformation, and therefore ductility demand, in the relatively small joint region; in fact, within the two cracks occurring above and below the joint itself. This excessive demand for deformation resulted in reinforcing bar fractures near the crack location.

Though the welded connection between continuous panel bars exacerbated the rupturing, non-welded continuous bars ruptured as well.

There was no typical elastic constraint on system deformation or response once the vertical reinforcing bars yielded and the wall was rocking. Some degree of elastic constraint is usually available in shear walls whose ductile monolithic design uses distributed vertical reinforcing across the wall. In the test models, with reinforcing well distributed within the precast panels but concentrated at wall ends in the horizontal joints, all of the reinforcing in the joint yielded simultaneously. The only "effective" constraint, in the limit, was provided by the gravity restoring force which decreased with increased displacement as $P - \Delta$ effects grew.

Energy dissipation in the complete system is relatively small since nearly all such energy use must occur in a single inelastic region. The rocking type of mechanism has been traditionally considered to be a relatively poor source of energy dissipation because of the resultant tremendous concentration of load and deformation within the few continuous vertical bars and the small compression zone of the horizontal joint. The ability of platform type systems, particularly with floors comprised of hollow core panels, to sustain a high compression block force at the extreme end of the joint has been frequently questioned. In the present tests the cast-in-place joint material, with higher compression strength than the panel material, was able to meet bending compression block demands successfully. The energy dissipation capacity of the joint was actually limited by the small dissipation capacity of the few continuous reinforcing bars and by the destruction of compression concrete at the wall extremes due to lack of confinement, spalling and buckling of the previously stretched reinforcing steel.

Fortunately, behavior of short period systems is not as dependent as longer period systems on energy dissipation [20,21]. In the tests described in this report it appears that the overall response of the wall system, a function of rocking motion, was primarily affected by the isolating mechanism and by the stiffness softening effect of that motion. Inspection of the test data indicates that more extensive damage always occurred at one end of the wall relative to the other. This was a logical result of the isolating effect of rocking, as already discussed. However the result of such unsymmetric damage was effectively to create a direction dependent stiffness. Throughout the subsequent response the system stiffness and natural period varied, as the average period lengthened. The combination of force isolation, varying stiffness and lack of buildup of harmonic response, and ability of the joint to maintain compressive force capacity during rocking allowed this system to survive a major earthquake motion without collapse or loss of vertical load carrying ability.

Overall Response Evaluation

The large panel precast wall system described in this report appears to have met two basic limit state performance criteria; namely, (i) the ability to withstand a moderate amplitude earthquake (0.2g ground acceleration) which contains significant energy in the range of the period of the structure, while responding primarily in a linear elastic manner without visible damage, and (ii) the ability to survive a major ground motion (0.7g acceleration) while maintaining vertical load carrying capacity and avoiding collapse. The strong motion was withstood with inelastic deformation and damage due to wall rocking while relative lateral slip was contained by special keys. Detailing within the joint region maintained the stability of the system while allowing large deformation.

The actual base shear coefficients for the moderate shaking and the major shaking were approximately 0.35 and 0.68 to 0.92, respectively. An equivalent lateral load base design shear coefficient for a 'box-system' as suggested by the Uniform Building Code would be approximately 0.20. The wall system tested had an elastic capcity which was higher than required by code but successfully withstood lateral forces as high as four hundred percent of the code design force.

Conclusions

The design and detailing of the particular precast large panel building system examined in this project successfully met two critical performance limit states including withstanding a major earthquake motion without collapse. Opening and rocking which developed in the lower horizontal joint resulted in a force isolating effect and limited the amplitude of inertial shear which could be transferred into the system. Forces and damage within the remainder of the structure were not great enough to spread the inelastic behavior. The amplitude of the rocking itself, a function of a particular earthquake, was controlled or limited by the continuous variation of the natural period of the system. This variation in natural period and the isolating effect of the rocking mechanism combined to limit the amount of energy, from the earthquake motion, that had to be absorbed by the system.

The detailing allowed stable rocking to occur without extensive degradation of the joint particularly in the form of concrete crushing. Joint damage and its effect on performance of the system may be more significant as axial force, due to vertical loading, increases. Energy dissipation qualities need not be the prime design objectives for precast panel wall structures if stability and protection against strength degradation are provided.

Initial inspection of the data presented in this report suggests that some minor improvements might be used to enhance the performance of the system. Energy dissipation capacity, though not as critical for short period structures, could be improved for systems in regions of moderate seismicity by designing joint strength closer to panel strength thus allowing a spread of inelasticity over a greater hinge region. Under strong motion, however, the spread of inelasticity into panels may have an undesirable impact on the system's ultimate stability. Distributed continuous vertical reinforcement along the length of the joint would provide some elastic constraint on overall displacement but would not be economically feasible due to increased field joining operations. Ductility could be increased by providing additional confinement around vertical bars to prevent buckling in the joint regions near the ends of the wall where high compressive stresses, due to bending, develop. Additional confinement would be particularly desirable within the block keys at the ends of each wall where spalling occurred accompanied by bar buckling. A final increase in ductility might be obtained by preventing bonding of the vertical reinforcing for a measured distance above, below and through the horizontal joint - allowing yield to develop over a greater portion of the bar than occurred near the crack in the models tested.

Considerable detailed study of the data from these tests is necessary before any definite conclusions or detailed implications or recommendations for design may be made. The rocking motion detected here may be an acceptable limit state behavior depending on the magnitude of ground motion expected at a particular site. Under extreme motion the rocking provides an isolating effect similar to results found in steel frame response [10] where uplift was allowed and internal force levels were decreased by the isolation. Additional testing and analysis of this type of motion in precast systems, particularly

with complete three dimensional response, is desirable before it is considered to be an acceptable limit state. A subsequent report will include detailed study of deformation mechanisms in the test specimens and analytical correlation studies.

REFERENCES

1. ACI Committee 318, Building Code Requirements for Reinforced Concrete, (ACI 318-77), Detroit, American Concrete Institute, 1977.

2. Ahlberg, H. J., Nilson, E. N. and Walsh, J. L., 'The Theory of Splines and Their Application', Academic Press, New York 1967.

3. Becker, J. M. and Llorente, C., 'Seismic Design of Precast Concrete Panel Buildings', Proceedings on Earthquake Resistant Reinforced Concrete Building Construction, V3, University of California, Berkeley, 1977.

4. Becker, J. M., Llorente, C. and Mueller, P., "Seismic Response of Concrete Precast Walls", Earthquake Engineering and Structural Dynamics, V8, J. Wiley and Sons, 1980.

5. Borges, J., Ravara, A., Pereira, J. and Monteiro, V., "Methodology for Seismic Studies of Prefabricated Panel Buildings", 4th European Symposium on Earthquake Engineering, London, 1972.

6. Gavrilovic, P. and Velkov, M., "Experimental Testing of Three Storey Models and Connection Systems of Modified Rad-Balency System", Institute of Earthquake Engineering and Engineering Seismology, University Kiril and Metodij, Skopje, 1981.

7. Ghanaat, Y. and Clough, R., "Shaking Table Tests of a Tubular Steel Frame Model", Earthquake Engineering Research Center Report No. UCB/EERC-82/02, University of California, Berkeley, 1982.

8. Ghanaat, Y., "Study of X-Braced Steel Frame Structures Under Earthquake Simulation", Earthquake Engineering Research Center Report No. UCB/EERC-80/08, University of California, Berkeley, 1980.

9. Hanson, N., "Seismic Tests of Horizontal Joints", Portland Cement Association, Skokie, Ill., 1979.

10. Huckelbridge, A. A., "Earthquake Simulator Tests of a Nine-story Steel Frame with Columns Allowed to Uplift", Earthquake Engineering Research Center Report No. UCB/EERC-77/23, University of California, Berkeley, 1977.

11. Llorente, C., "Inelastic Behavior of Precast Concrete Shear Walls", PhD Thesis, MIT, Cambridge, Mass., 1981.

12. Mueller, P. and Becker, J. M., "Seismic Response of Large Panel Precast Buildings", Advanced Design Concepts Seminar, ACI, Dallas, Texas, 1979.

13. Polyakov, S., "Design of Earthquake Resistant Structures", MIR Publishers, Moscow, 1974.

14. Rea, D. and Penzien, J., "Dynamic Response of a 20ft. by 20ft. Shaking Table", Proceedings of the 5th World Conference on Earthquake Engineering, Rome, 1973.

15. Verbic, B., "Nonlinear Behavior of Large Panel Connections", Research Conference on Earthquake Engineering, Skopje, 1980.

16. Zeck, U. I., "Joints in Large Panel Precast Concrete Structures", MIT, Cambridge, Mass., 1976.

17. Bouwkamp, J. G., Kolleger, J. P. and Stephen, R. M., "Dynamic Properties of an 8-Story Prefabricated Panel Building", Earthquake Engineering Research Center Report No. UCB/EERC-80/30, University of California, Berkeley, 1980.

18. Aoyama, H., Ikeda, A., Nagai, T. and Kawamura, S., "Development of 15 Story Precast Concrete Apartment House, Planning and Earthquake Resistant Design with Dynamic Elastic-Plastic Analysis", Japan-U.S. Science Seminar, Seattle, Wash., 1971.

19. International Conference of Building Officials, "Uniform Building Code", Whittier, Calif., 1982.

20. Clough, R. W., "Effect of Stiffness Degradation on Earthquake Ductility Requirements," Structures and Materials Research, Report 66-16, University of California, Berkeley, 1966.

21. Becker, J. and Mueller, P., "The Role of Connections in the Aseismic Design of Large Panel Buildings", Research Conference on Earthquake Engineering, Skopje, 1980.

APPENDIX A

LIST OF DATA CHANNELS

TABLE A.1
Data Channels for PZ-I

Channel No.	Name	Description	Units
0	AVHTDISP	Average horizontal table displacement	in.
1	AVVTDISP	Average vertical table displacement	in.
2	AVHTACC	Average horizontal table acceleration	g
3	AVVTACC	Average vertical table acceleration	g
4	PITCH ACC	Table pitch acceleration	rad/s^2
5	ROLL ACC	Table roll acceleration	rad/s^2
6	TWIST ACC	Table twist acceleration	rad/s^2
7	BLANK	--	--
8	H1DISP	Horizontal table displacement at actuator H1	in.
9	H2DISP	Horizontal table displacement at actuator H2	in.
10	H3DISP	Horizontal table displacement at actuator H3	in.
11	H1FORCE	Force in horizontal actuator H1	Kips
12	V1DISP	Vertical displacement at actuator V1	in.
13	V2DISP	Vertical displacement at actuator V2	in.
14	V3DISP	Vertical displacement at actuator V3	in.
15	V4DISP	Vertical displacement at actuator V4	in.
16	AH2	Horizontal acceleration at second floor	g
17	AH3	Horizontal acceleration at third floor	g

TABLE A.1 (Continued).

Channel No.	Name	Description	Units
18	AH4	Horizontal acceleration at top of wall	g
19	AH1	Horizontal acceleration at foundation level	g
20	AH5	Horizontal acceleration at mass blocks	g
21	AV1	Vertical acceleration at north end of supporting platform	g
22	AV2	Vertical acceleration at south end of supporting platform	g
23	POTN	Vertical displacement between top and bottom of wall at north side	in.
24	POTS	Vertical displacement between top and bottom of wall at south side	in.
25	DIS2	Horizontal displacement at second floor	in.
26	DIS3	Horizontal displacement at third floor	in.
27	DIS4	Horizontal displacement at top cast-in-place wall	in.
28	SHFTNE	Force in north-east shear force transducer	Kips
29	SHFTSE	Force in south-east shear force transducer	Kips
30	SHFTSW	Force in south-west shear force transducer	Kips
31	SHFTNW	Force in north-west shear force transducer	Kips
32	TM1	Axial strain in top middle bar of horizontal joint (first floor)	milli in./in.
33	SP1	Axial strain in panel bar at south end (first floor)	milli in./in.
34	SINC1	Axial strain in inside column bar at south end (first floor)	milli in./in.
35	SOUC1	Axial strain in outside column bar at south end (first floor)	milli in./in.

TABLE A.1 (Continued).

Channel No.	Name	Description	Units
36	NP1	Axial strain in panel bar at north end (first floor)	milli in./in.
37	NINC1	Axial strain in inside column bar at north end (first floor)	milli in./in.
38	TM2	Axial strain in top middle bar of horizontal joint (second floor)	milli in./in.
39	SP2	Axial strain in panel bar at south end (second floor)	milli in./in.
40	SINC2	Axial strain in inside column bar at south end (second floor)	milli in./in.
41	SOUC2	Axial strain in outside column bar at south end (second floor)	milli in./in.
42	NP2	Axial strain in panel bar at north end (second floor)	milli in./in.
43	NINC2	Axial strain in inside column bar at north end (second floor)	milli in./in.
44	NOUC2	Axial strain in outside column bar at north end (second floor)	milli in./in.
45	NOUC1	Axial strain in outside column bar at north end (first floor)	milli in./in.
46	BLANK	--	--
47	BLANK	--	--
48	U1	First-floor slab panel uplift with respect to foundation at U1	in.
49	U2	First-floor slab panel uplift with respect to foundation at U2	in.
50	U3	First-floor slab panel uplift with respect to foundation at U3	in.
51	U4	First-floor slab panel uplift with respect to foundation at U4	in.

TABLE A.1 (Continued).

Channel No.	Name	Description	Units
52	U5	First-floor slab panel uplift with respect to foundation at U5	in.
53	S3	Slip between first-floor wall panel and north-end key of first floor	in.
54	U7	First-floor wall panel uplift with respect to first-floor slab panel at U7	in.
55	U8	First-floor wall panel uplift with respect to first-floor slab panel at U8	in.
56	U9	First-floor wall panel uplift with respect to first-floor slab panel at U9	in.
57	U10	First-floor wall panel uplift with respect to first-floor slab panel at U10	in.
58	U11	First-floor wall panel uplift with respect to first-floor slab panel at U11	in.
59	U12	First-floor wall panel uplift with respect to first-floor slab panel at U12	in.
60	S1	Slip between first-floor slab panel and bottom cast-in-place wall at north	in.
61	SFND	Horzontal displacement of foundation	in.
62	U6	First-floor wall panel uplift with respect to first-floor slab at U6	in.
63	S4	Slip between first-floor wall panel and first-floor slab panel at north end	in.
64	S5	Slip between first-floor wall panel and first-floor slab panel at south end	in.
65	S6	Slip between first-floor wall panel and south-end key of first floor	in.

TABLE A.1 (Continued).

Channel No.	Name	Description	Units
66	S7	Slip between first-floor wall panel and second-floor slab panel	in.
67	S8	Slip between second-floor wall panel and north-end key of second floor	in.
68	D1	Diagonal deformation in first-floor wall panel	in.
69	D2	Diagonal deformation in first-floor wall panel	in.
70	D3	Diagonal deformation in second-floor wall panel	in.
71	D4	Diagonal deformation in second-floor wall panel	in.
72	B1	First-floor slab panel uplift with respect to foundation at B1	in.
73	B2	First-floor slab panel uplift with respect to foundation at B2	in.
74	B3	Vertical deformation in first-floor wall panel at north end	in.
75	B4	Vertical deformation in first-floor wall panel at south end	in.
76	U13	Second-floor slab panel uplift with respect to first-floor wall panel at U13	in.
77	U14	Second-floor slab panel uplift with respect to first-floor wall panel at U14	in.
78	U15	Second-floor wall panel uplift with respect to second-floor slab panel at U15	in.
79	U16	Second-floor wall panel uplift with respect to second-floor slab panel at U16	in.
80	U17	Foundation uplift at north end	in.
81	U18	Foundation uplift at south end	in.
82	S2	Slip between first-floor slab panel and bottom cast-in-place wall at south end	in.

TABLE A.2

Data Channels for PZ-II

Channel No.	Name	Description	Units
0	AVHTDISP	Average horizontal table displacement	in.
1	AVVTDISP	Average vertical table displacement	in.
2	AVHTACC	Average horizontal table acceleration	g
3	AVVTACC	Average vertical table acceleration	g
4	PITCH ACC	Table pitch acceleration	rad/s^2
5	ROLL ACC	Table roll acceleration	rad/s^2
6	TWIST ACC	Table twist acceleration	rad/s^2
7	BLANK	--	--
8	H1DISP	Horizontal table displacement at actuator H1	in.
9	H2DISP	Horizontal table displacement at actuator H2	in.
10	H3DISP	Horizontal table displacement at actuator H3	in.
11	H1FORCE	Force in horizontal actuator H1	Kips
12	V1DISP	Vertical displacement at actuator V1	in.
13	V2DISP	Vertical displacement at actuator V2	in.
14	V3DISP	Vertical displacement at actuator V3	in.
15	V4DISP	Vertical displacement at actuator V4	in.
16	AH2	Horizontal acceleration at second floor	g
17	AH3	Horizontal acceleration at third floor	g

TABLE A.2 (Continued).

Channel No.	Name	Description	Units
18	AH4	Horizontal acceleration at top of wall	g
19	AH1	Horizontal acceleration at foundation level	g
20	AH5	Horizontal acceleration at mass blocks	g
21	AV1	Vertical acceleration at north end of supporting platform	g
22	AV2	Vertical acceleration at south end of supporting platform	g
23	POTN	Vertical displacement between top and bottom of wall at north side	in.
24	POTS	Vertical displacement between top and bottom of wall at south side	in.
25	DIS2	Horizontal displacement at second floor	in.
26	DIS3	Horizontal displacement at third floor	in.
27	DIS4	Horizontal displacement at top cast-in-place wall	in.
28	SHFTNE	Force in north-east shear force transducer	Kips
29	SHFTSE	Force in south-east shear force transducer	Kips
30	SHFTSW	Force in south-west shear force transducer	Kips
31	SHFTNW	Force in north-west shear force transducer	Kips
32	TM1	Axial strain in top middle bar of horizontal joint (first floor	milli in./in.
33	SP1	Axial strain in panel bar at south end (first floor)	milli in./in.
34	SINC1	Axial strain in inside column bar at south end (first floor)	milli in./in.
35	SOUC1	Axial strain in outside column bar at south end (first floor)	milli in./in.

TABLE A.2 (Continued).

Channel No.	Name	Description	Units
36	NP1	Axial strain in panel bar at north end (first floor)	milli in./in.
37	NINC1	Axial strain in inside column bar at north end (first floor)	milli in./in.
38	TM2	Axial strain in top middle bar of horizontal joint (second floor)	milli in./in.
39	SP2	Axial strain in panel bar at south end (second floor)	milli in./in.
40	PB1	Axial strain in bottom panel bar above door opening (first floor)	milli in./in.
41	SOUC2	Axial strain in outside column at south end (second floor)	milli in./in.
42	NP2	Axial strain in panel bar at north end (second floor)	milli in./in.
43	PT1	Axial strain in top panel bar above door opening (first floor)	milli in./in.
44	NOUC2	Axial strain in outside column at north end (second floor)	milli in./in.
45	NOUC1	Axial strain in outside column at north end (first floor)	milli in./in.
46	BFE2	Axial strain in top middle bar of horizontal joint near door opening (second floor)	milli in./in.
47	BFE3	Axial strain in top middle bar of horizontal joint near door opening (third floor)	milli in./in.
48	U1	First-floor slab panel uplift with respect to foundation at U1	in.
49	U2	First-floor slab panel uplift with respect to foundation at U2	in.
50	U14	Second-floor wall panel uplift with respect to second-floor slab panel at U14	in.

TABLE A.2 (Continued).

Channel No.	Name	Description	Units
51	U12	Second-floor slab panel uplift with respect to first-floor wall panel at U12	in.
52	S1	Slip between first-floor slab panel and bottom cast-in-place wall	in.
53	B1	First-floor slab panel uplift with respect to foundation at B1	in.
54	U7	First-floor wall panel uplift with respect to first-floor slab panel at U7	in.
55	U8	First-floor wall panel uplift with respect to first-floor slab panel at U8	in.
56	U9	Second-floor slab panel uplift with respect to first-floor wall panel at U9	in.
57	U10	Second-floor slab panel uplift with respect to first-floor wall panel at U10	in.
58	U3	First-floor wall panel uplift with respect to first-floor slab panel at U3	in.
59	U4	First-floor wall panel uplift with respect to first-floor slab panel at U4	in
60	B2	First-floor slab panel uplift with respect to foundation at B2	in.
61	SFND	Horizontal displacement of foundation	in.
62	U6	First-floor wall panel uplift with respect to first-floor slab panel at U6	in.
63	S4	Slip between first-floor wall panel and first-floor slab panel at north end	in.
64	S5	Slip between first-floor wall panel and first-floor slab panel at south end	in.
65	S6	Slip between first-floor wall panel and south-end key of first floor	in.

TABLE A.2 (Continued).

Channel No.	Name	Description	Units
66	S7	Slip between first-floor wall panel and second-floor slab panel at north end	in.
67	S8	Slip between first-floor wall panel and second-floor slab panel at south end	in.
68	D1	Diagonal deformation in north half of first-floor wall panel	in.
69	D2	Diagonal deformation in north half of first-floor wall panel	in.
70	D3	Diagonal deformation above door opening of first-floor wall panel	in.
71	D4	Diagonal deformation above door opening of first-floor wall panel	in.
72	U5	First-floor wall panel uplift with respect to first-floor slab panel at U5	in.
73	U6	First-floor wall panel uplift with respect to first-floor slab panel at U6	in.
74	B3	Vertical deformation in first-floor wall panel at north end	in.
75	B4	Vertical deformation in first-floor wall panel at south end	in.
76	U13	Second-floor wall panel uplift with respect to second-floor slab panel at U13	in.
77	U11	Second-floor slab panel uplift with respect to first-floor wall panel at U11	in.
78	D5	Diagonal deformation in south half of first-floor wall panel	in.
79	D6	Diagonal deformation in south half of first-floor wall panel	in.

TABLE A.2 (Continued).

Channel No.	Name	Description	Units
80	D7	Diagonal deformation in north half of second-floor wall panel	in.
81	D8	Diagonal deformation in north half of second-floor wall panel	in.
82	D9	Diagonal deformation above door opening of second-floor wall panel	in.
83	D10	Diagonal deformation above door opening of second-floor wall panel	in.
84	D11	Diagonal deformation in south half of second-floor wall panel	in.
85	D12	Diagonal deformation in south half of second-floor wall panel	in.
86	S9	Slip between second-floor wall panel and north-end key of second floor	in.
87	S10	Slip between second-floor wall panel and south-end key of second floor	in.
88	PL1	Axial strain in panel bar near door opening (first floor)	in.

TABLE A.3
Data Channels for PZ-III

Channel No.	Name	Description	Units
0	AVHTDISP	Average horizontal table displacement	in.
1	AVVTDISP	Average vertical table displacement	in.
2	AVHTACC	Average horizontal table acceleration	g
3	AVVTACC	Average vertical table acceleration	g
4	PITCH ACC	Table pitch acceleration	rad/s^2
5	ROLL ACC	Table Roll acceleration	rad/s^2
6	TWIST ACC	Table Twist acceleration	rad/s^2
7	BLANK	--	--
8	H1DISP	Horizontal table displacement at actuator H1	in.
9	H2DISP	Horizontal table displacement at actuator H2	in.
10	H3DISP	Horizontal table displacement at actuator H3	in.
11	H1FORCE	Force in horizontal actuator H1	Kips
12	V1 DISP	Vertical displacement at actuator V1	in.
13	V2 DISP	Vertical displacement at actuator V2	in.
14	V3 DISP	Vertical displacement at actuator V3	in.
15	V4 DISP	Vertical displacement at actuator V4	in.
16	AH2	Horizontal acceleration at second floor	g
17	AH3	Horizontal acceleration at third floor	g
18	AH4	Horizontal acceleration at top of wall	g
19	AH1	Horizontal acceleration at foundation level	g
20	AH5	Horizontal acceleration at mass blocks	g
21	AV1	Vertical acceleration at north end of supporting platform	g
22	AV2	Vertical acceleration at south end of supporting platform	g
23	POTN	Vertical displacement between top and bottom of wall at north side	in.
24	POTS	Vertical displacement between top and bottom of wall at south side	in.

TABLE A.3 (Continued).

Channel No.	Name	Description	Units
25	DIS2	Horizontal displacement at second floor	in.
26	DIS3	Horizontal displacement at third floor	in.
27	DIS4	Horizontal displacement at top cast-in-place wall	in.
28	SHFTNE	Force in north-east shear force transducer	Kips
29	SHFTSE	Force in south-east shear force transducer	Kips
30	SHFTSW	Force in south-west shear force transducer	Kips
31	SHFTNW	Force in north-west shear force transducer	Kips
32	TM1	Axial strain in top middle bar of horizontal joint (first floor)	milli in./in.
33	SP1	Axial strain in panel bar at south end (first floor)	milli in./in.
34	SINC1	Axial strain in inside column bar at south end (first floor)	milli in./in.
35	SOUC1	Axial strain in outside column bar at south end (first floor)	milli in./in.
36	NP1	Axial strain in panel bar at north end (first floor)	milli in./in.
37	NINC1	Axial strain in inside column bar at north end (first floor)	milli in./in.
38	TM2	Axial strain in top middle bar of horizontal joint (second floor)	milli in./in.
39	SP2	Axial strain in panel bar at south end (first floor)	milli in./in.
40	SINC2	Axial strain in inside column bar at south end (second floor)	milli in./in.
41	SOUC2	Axial strain in outside column bar at south end (second floor)	milli in./in.
42	NP2	Axial strain in panel bar at north end (second floor)	milli in./in.
43	NINC2	Axial strain in inside column bar at north end (second floor)	milli in./in.

TABLE A.3 (Continued).

Channel No.	Name	Description	Units
44	NOUC2	Axial strain in outside column bar at north end (second floor)	milli in./in.
45	NOUC1	Axial strain in outside column bar at north end (first floor)	milli in./in.
46	BLANK	--	--
47	BLANK	--	--
48	U1	First-floor slab panel uplift with respect to foundation at U1	in.
49	U2	First-floor slab panel uplift with respect to foundation at U2	in.
50	U3	First-floor slab panel uplift with respect to foundation at U3	in.
51	U4	First-floor wall panel uplift with respect to first-floor slab panel at U4	in.
52	U5	First-floor wall panel uplift with respect to first-floor slab panel at U5	in.
53	U6	First-floor wall panel uplift with respect to first-floor slab panel at U6	in.
54	U7	First-floor wall panel uplift with respect to first-floor slab panel at U7	in.
55	U8	First-floor wall panel uplift with respect to first-floor slab panel at U8	in.
56	U9	Second-floor slab panel uplift with respect to first-floor wall panel at U9	in.
57	U10	Second-floor slab panel uplift with respect to first-floor wall panel at U10	in.
58	U11	Second-floor wall panel uplift with respect to second-floor slab panel at U11	in.

TABLE A.3 (Continued).

Channel No.	Name	Description	Units
59	U12	Second-floor wall panel uplift with respect to second-floor slab panel at U12	in.
60	S1	Slip between first-floor slab panel and bottom cast-in-place wall	in.
61	SFND	Horizontal displacement of foundation	in.
62	S3	Slip between first-floor wall panel and north-end key of first floor	in.
63	S4	Slip between first-floor wall panel and first-floor slab panel at north end	in.
64	S5	Slip between first-floor wall panel and first-floor slab panel at south end	in.
65	S6	Slip between first-floor wall panel and south-end key of first floor	in.
66	S7	Slip between first-floor wall panel and second-floor slab panel	in.
67	S8	Slip between second-floor wall panel and north-end key of second floor	in.
68	D1	Diagonal deformation in first-floor wall panel	in.
69	D2	Diagonal deformation in first-floor wall panel	in.
70	D3	Diagonal deformation in second-floor wall panel	in.
71	D4	Diagonal deformation in second-floor wall panel	in.
72	B1	First-floor slab panel uplift with respect to foundation at B1	in.
73	B2	First-floor slab panel uplift with respect to foundation at B2	in.
74	B3	Vertical deformation in first-floor wall panel at north end	in.
75	B4	Vertical deformation in first-floor wall panel at south end	in.

TABLE A.3 (Continued).

Channel No.	Name	Description	Units
76	WF1	Vertical displacement between first-floor wall panel and north-end flange panel	in.
77	WF2	Vertical displacement between first-floor wall panel and south-end flange panel	in.
78	WF3	Vertical displacement between second-floor wall panel and north-end flange panel	in.
79	WF4	Vertical displacement between second-floor wall panel and south-end flange panel	in.
80	FB1	Vertical displacement between first-floor slab panel and first-floor flange panel at north end close to web	in.
81	FB2	Vertical displacement between first-floor slab panel and first-floor flange panel at north end away from web	in.
82	Fb3	Vertical displacement between first-floor slab panel and first-floor flange panel at south end close to web	in.
83	FB4	Vertical displacement between first-floor slab panel and first-floor flange panel at south end away from web	in.
84	FB5	Vertical deformation in first-floor flange panel at north end	in.
85	FB6	Vertical deformation in first-floor flange panel at south end	in.
86	FB7	Vertical displacement between first-floor flange panel and second-floor flange panel at north end	in.
87	FB8	Vertical displacement between first-floor flange panel and second-floor flange panel at south end	in.

APPENDIX B

JOINT DETAILS
AND MATERIAL PROPERTIES

Note: Dimensions on all of the diagrams in this Appendix are in inches.

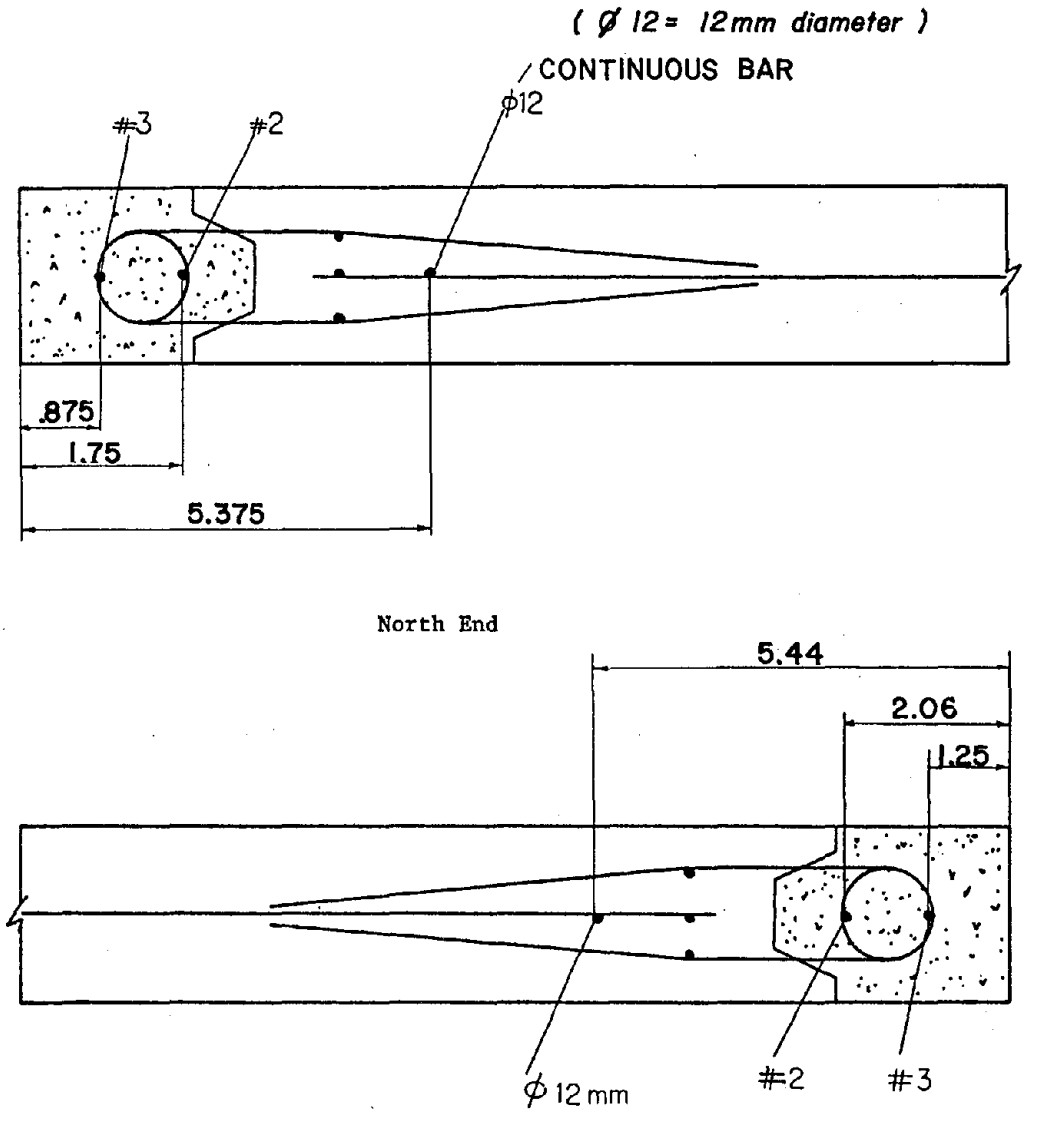

Figure B.1 Joint detail for simple wall, PZ-I, (inch units).

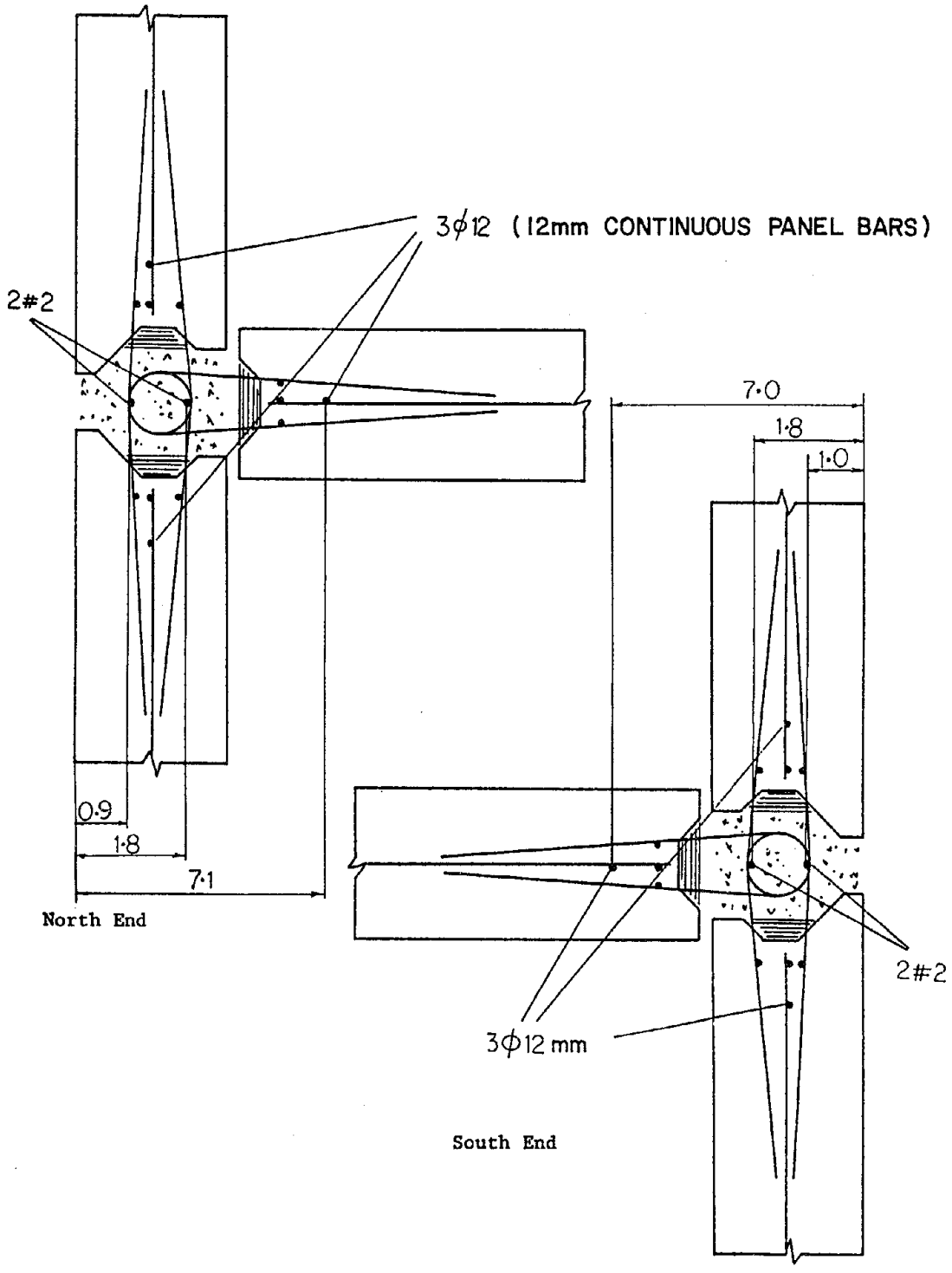

Figure B.2 Joint details for flanged wall, PZ-III, (inch units).

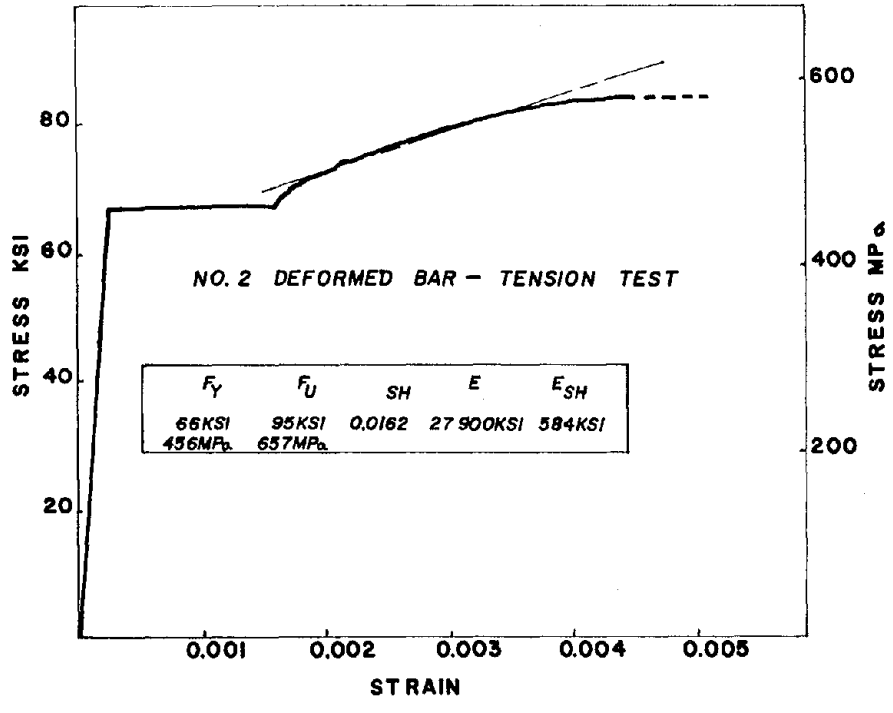

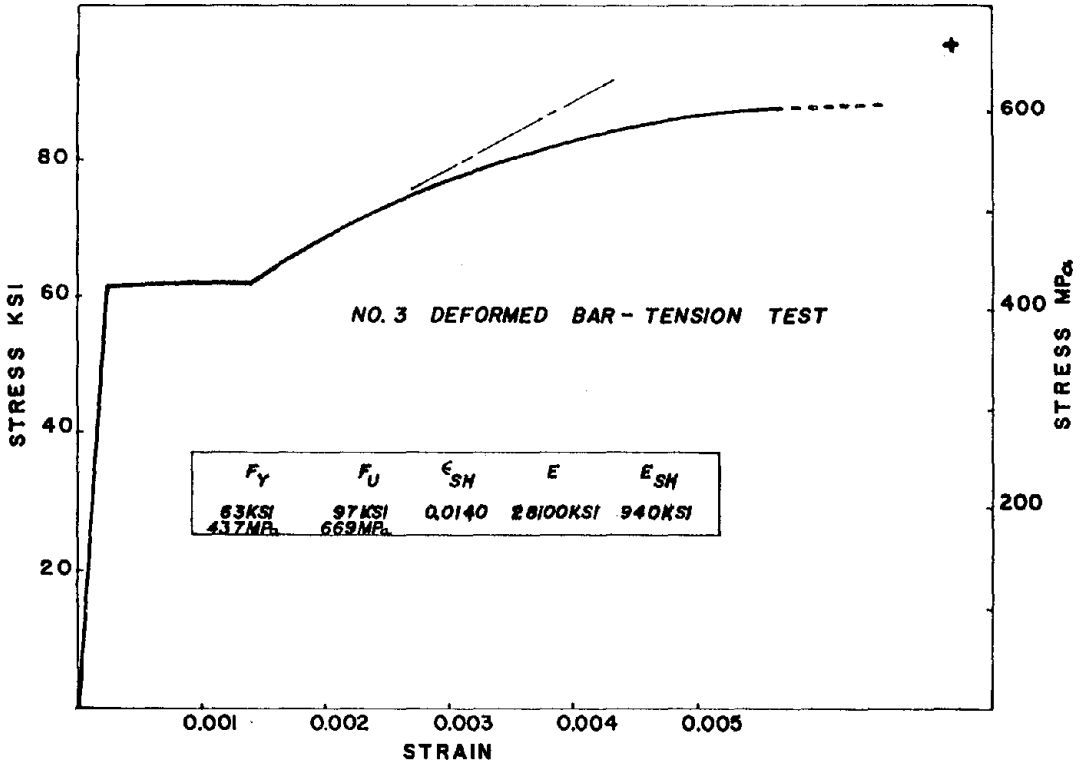

Figure B.3 Steel strength and deformation characteristics of U.S. size bars used in some cast-in-place connections. (Yugoslav bar characteristics unavailable)

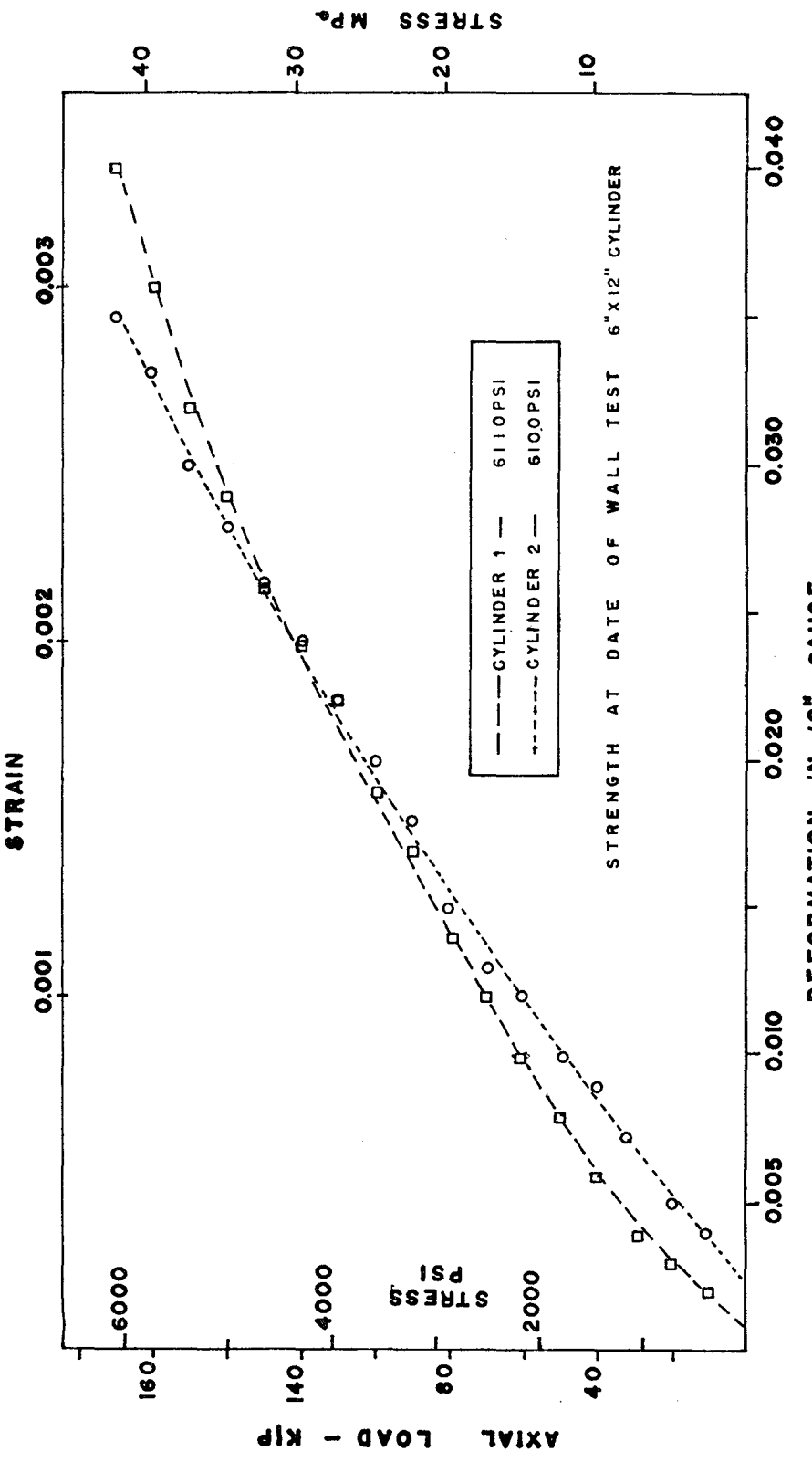

Figure B.4 Cylinder test results for the cast-in-place joint concrete.

APPENDIX C

LOCATION OF DCDT'S, ACCELEROMETERS, POTENTIOMETERS, AND STRAIN GAUGES

Note: Dimensions on all of the diagrams in this appendix are in inches.

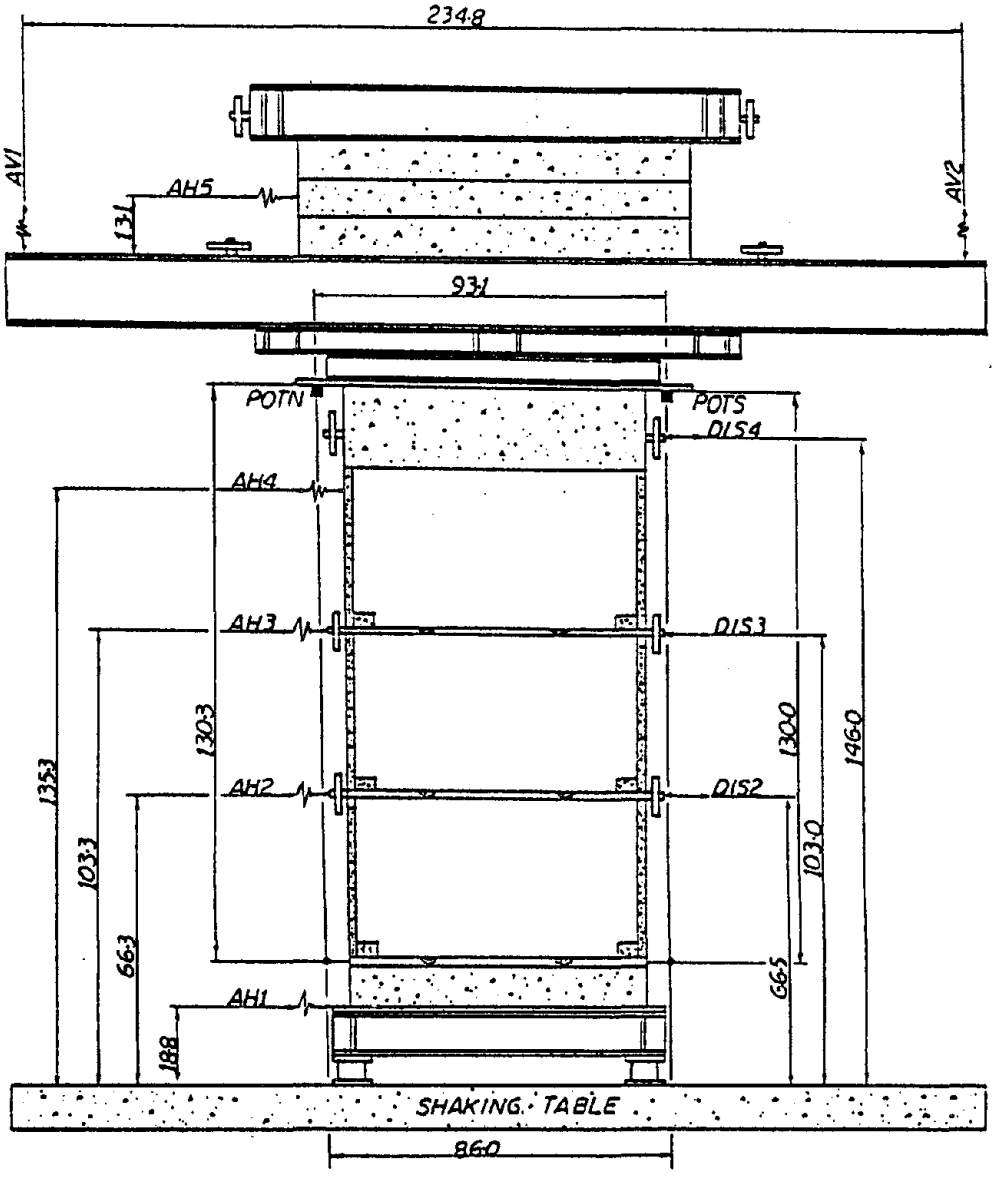

Figure C.1 Location of accelerometers and potentiometers for PZ-I.

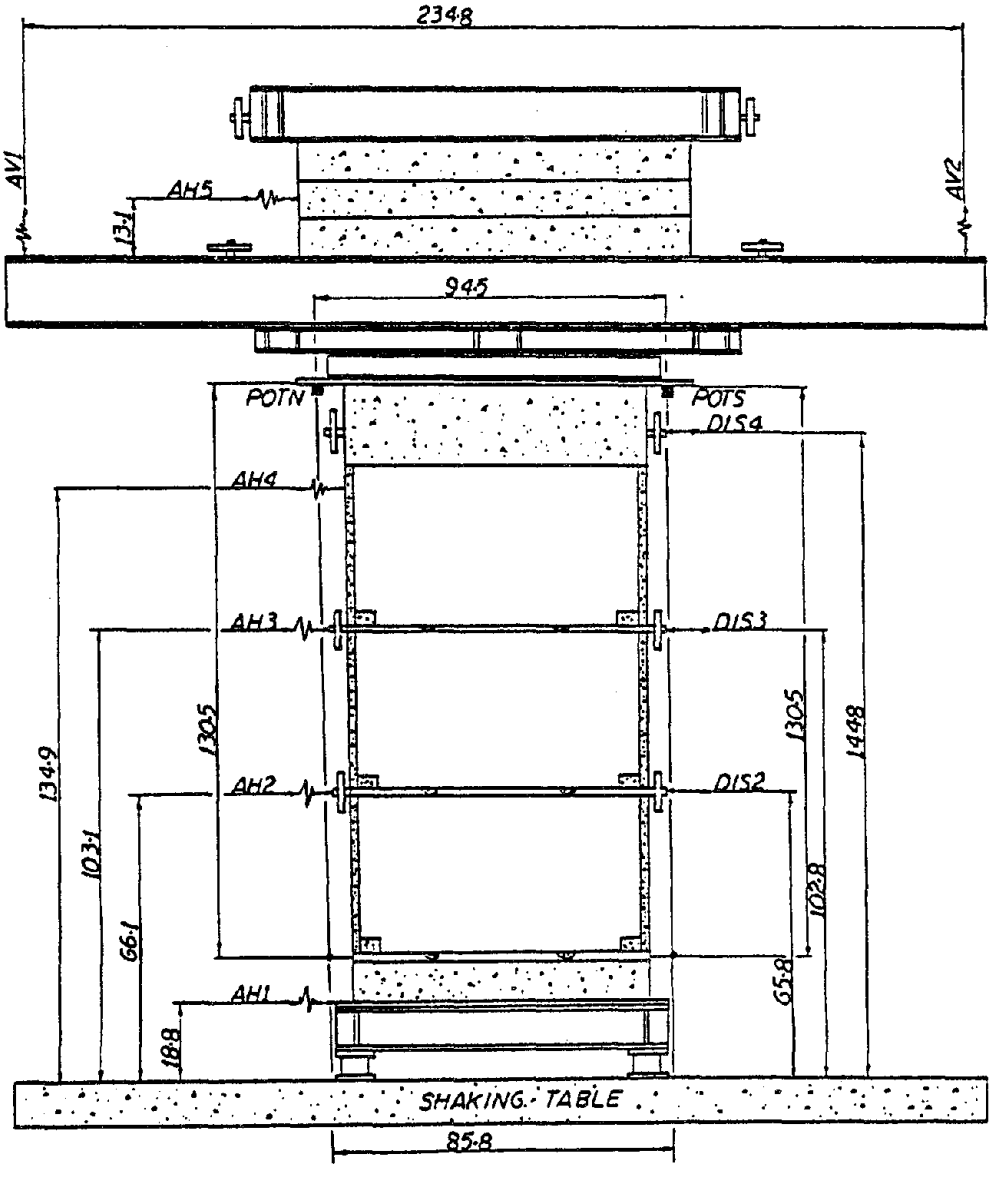

Figure C.2 Location of accelerometers and potentiometers for PZ-II.

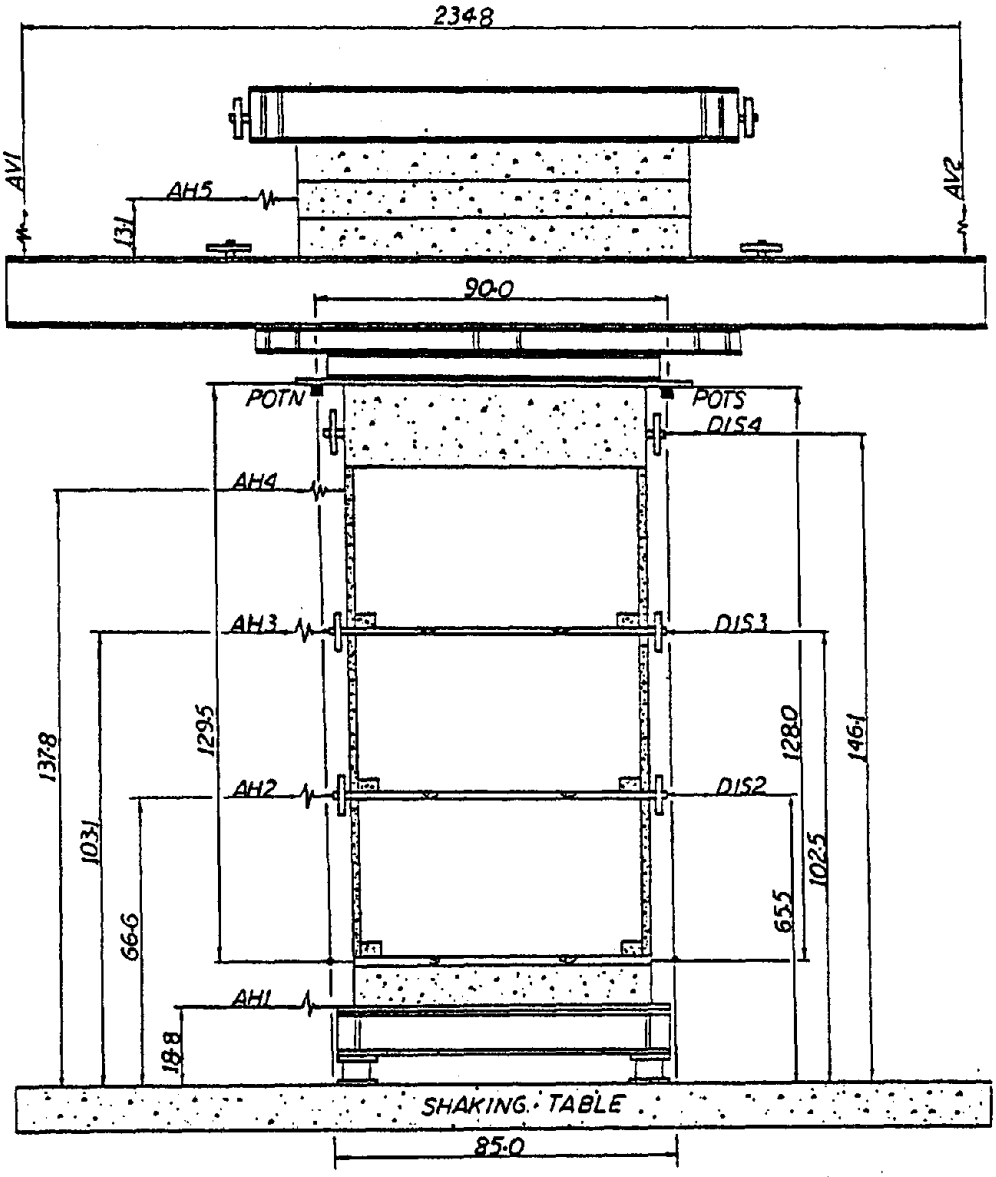

Figure C.3 Location of accelerometers and potentiometers for PZ-III.

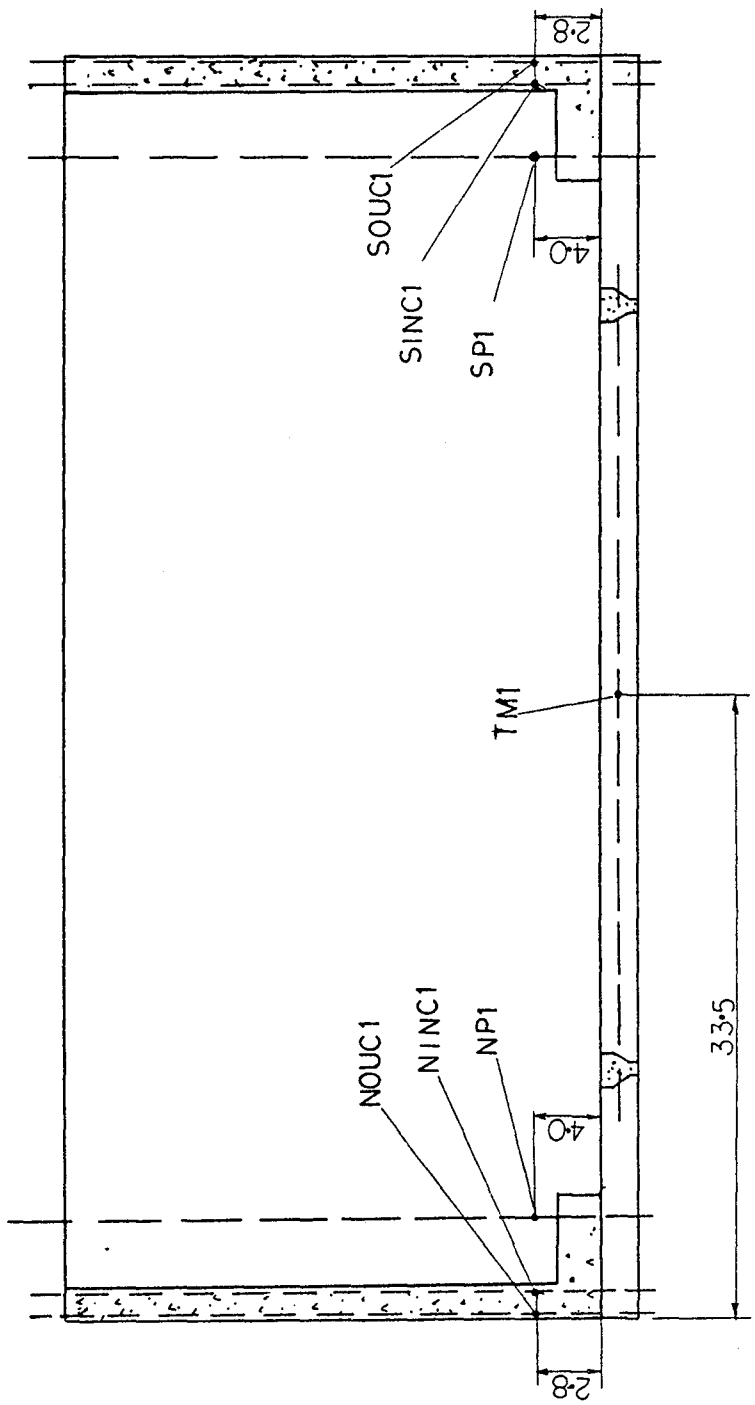

Figure C.4 First-floor strain gauges for PZ-I.

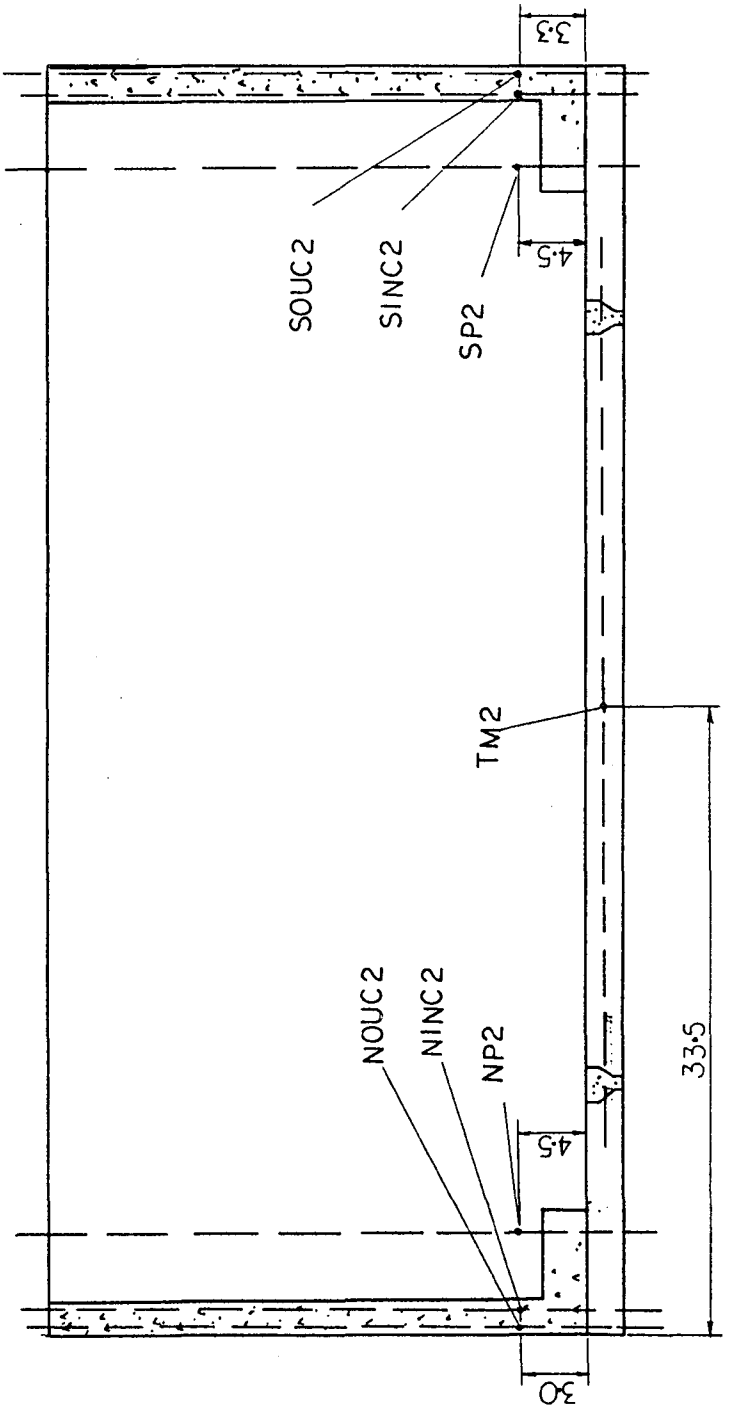

Figure C.5 Second-floor strain gauges for PZ-I.

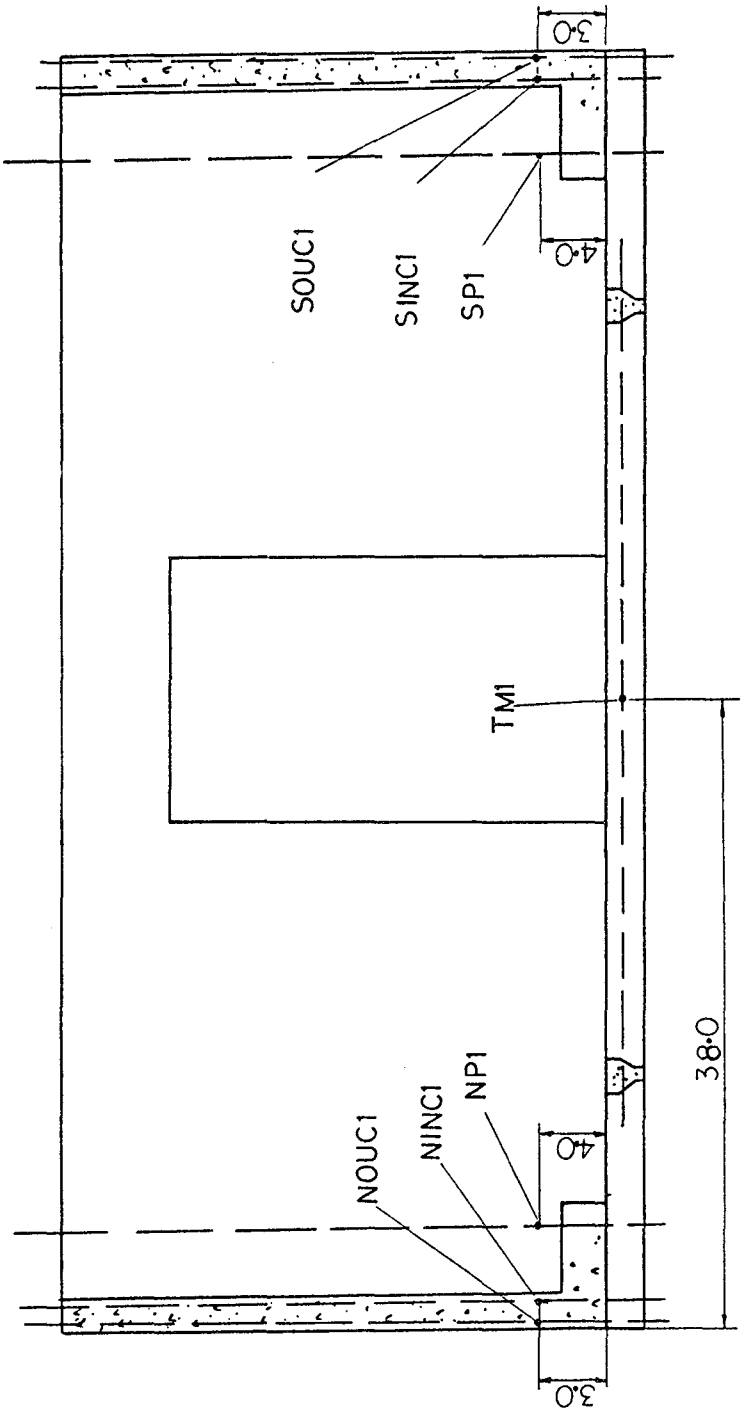

Figure C.6 First-floor strain gauges for PZ-II.

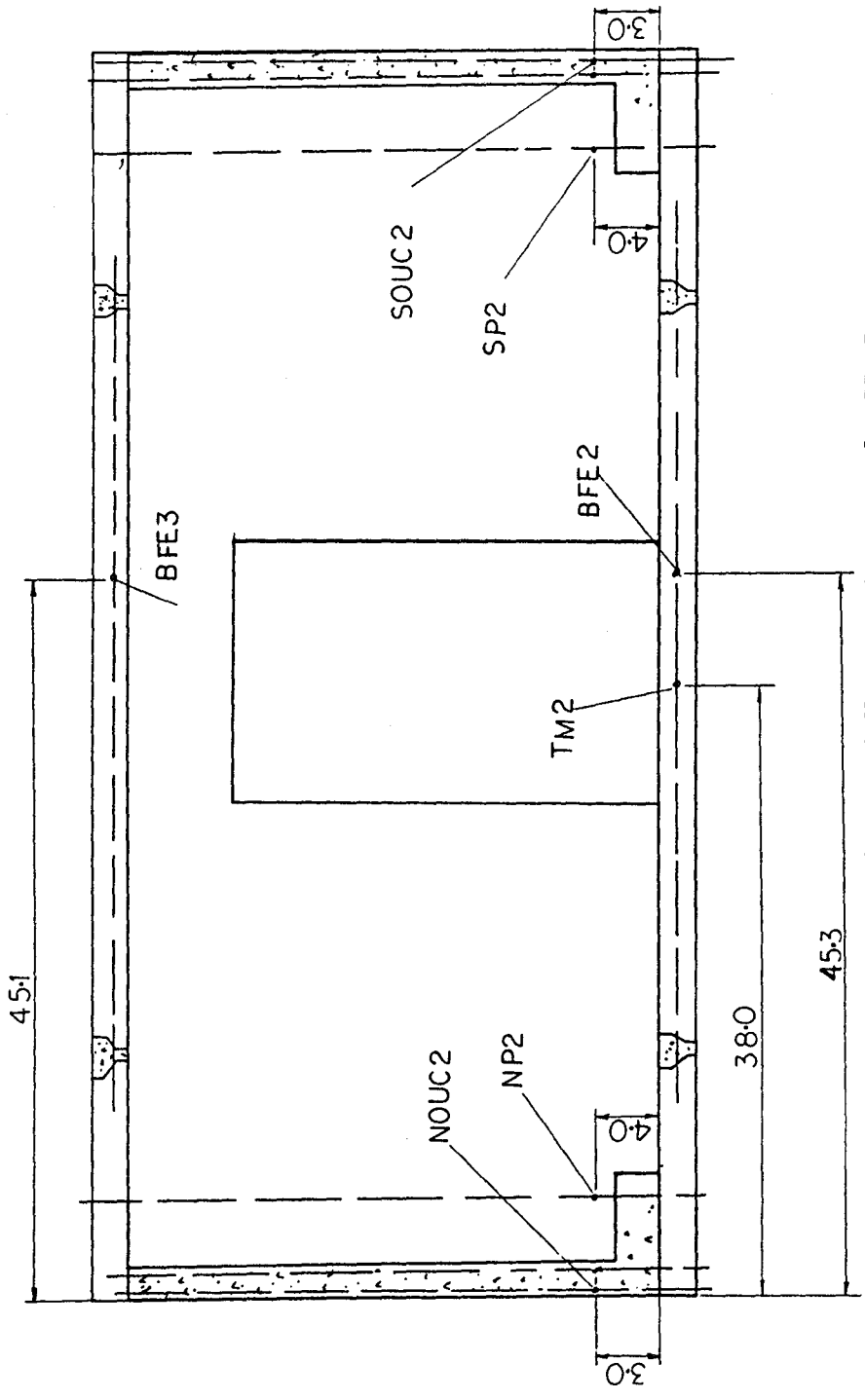

Figure C.7 Second-floor strain gauges for PZ-II.

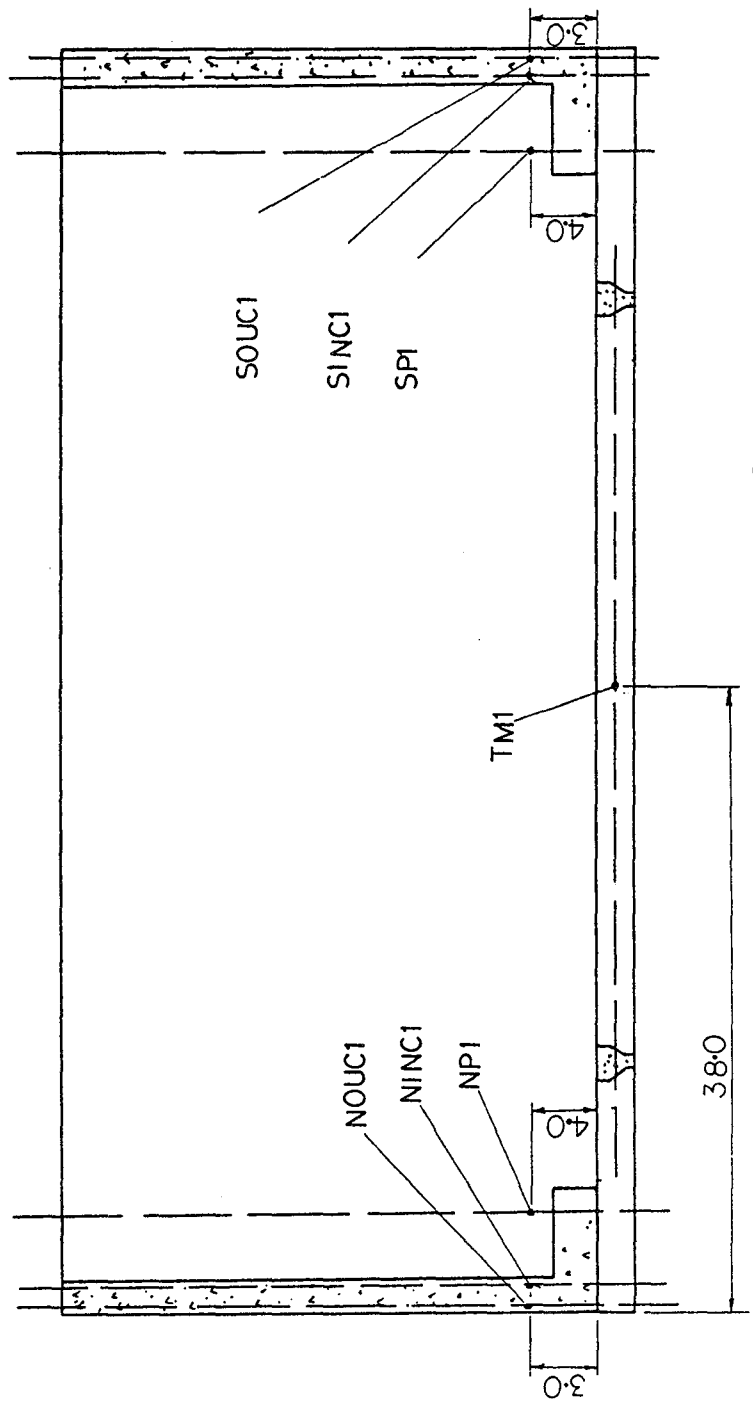

Figure C.8 First-floor strain gauges for PZ-III.

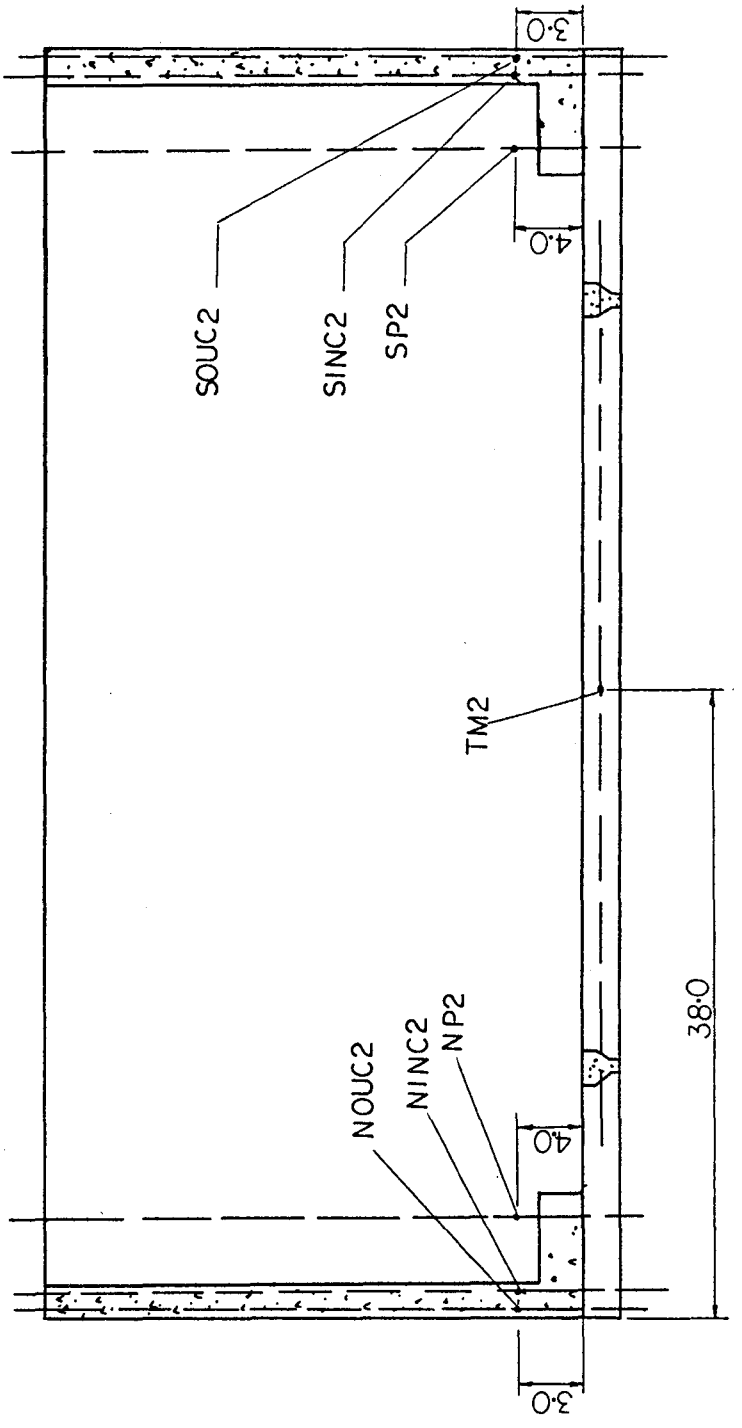

Figure C.9 Second-floor strain gauges for PZ-III.

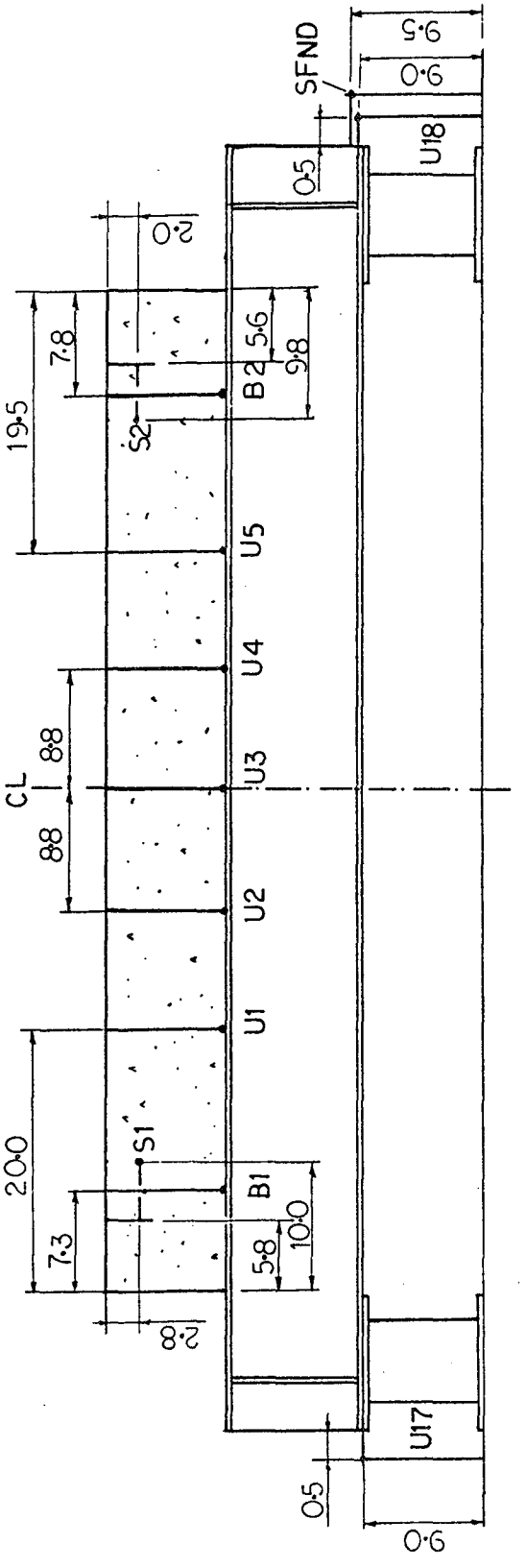

Figure C.10 Location of DCDT's for PZ-I.

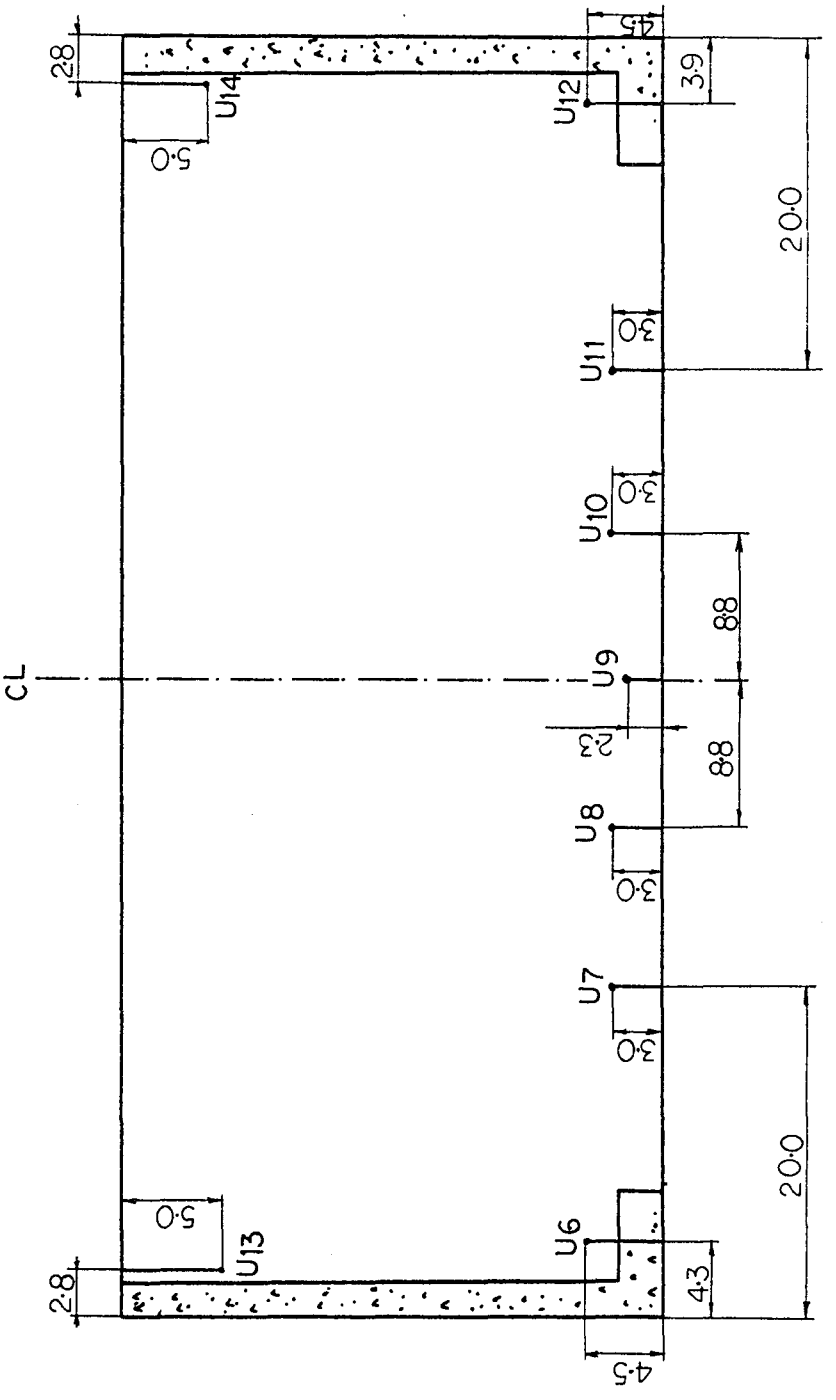

Figure C.10 Continued.

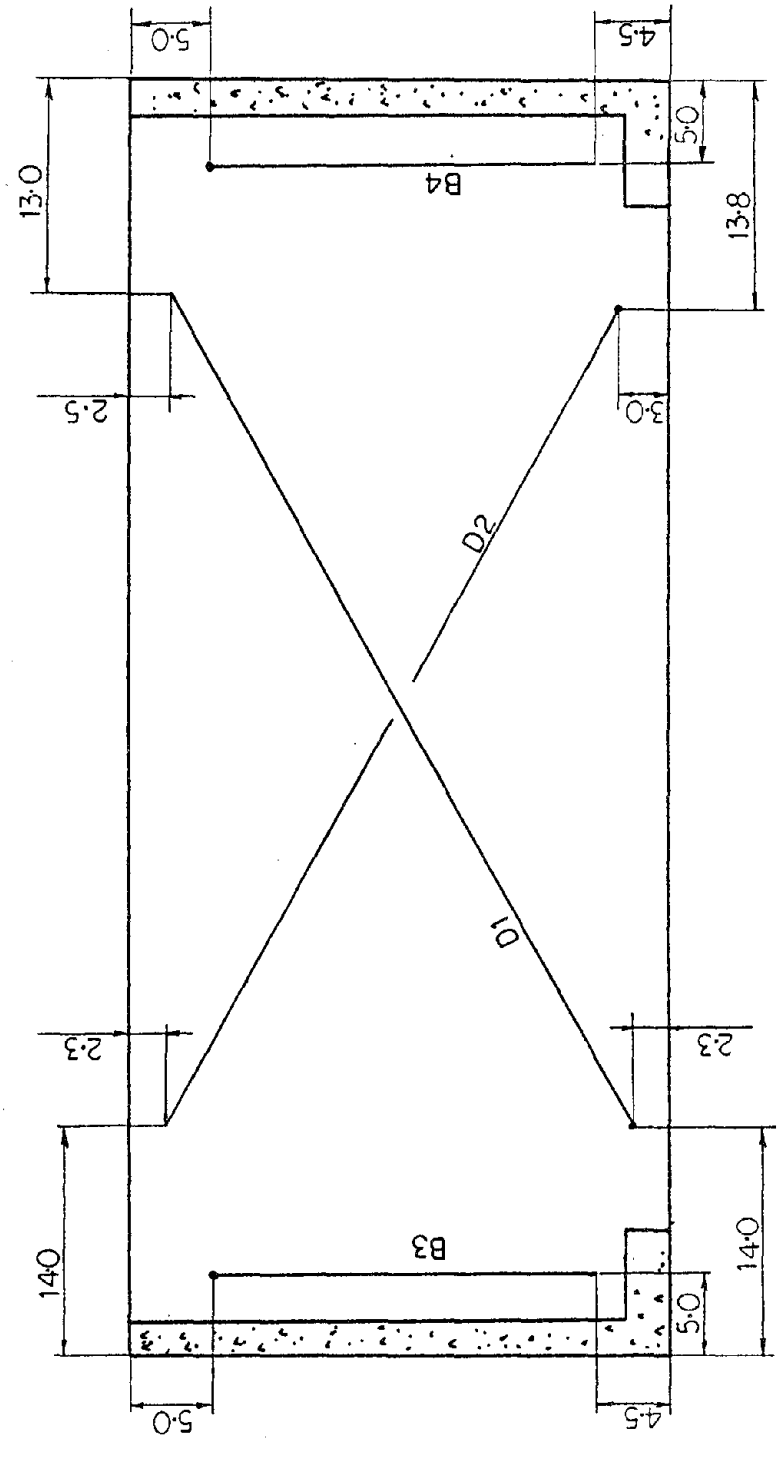

Figure C.10 Continued.

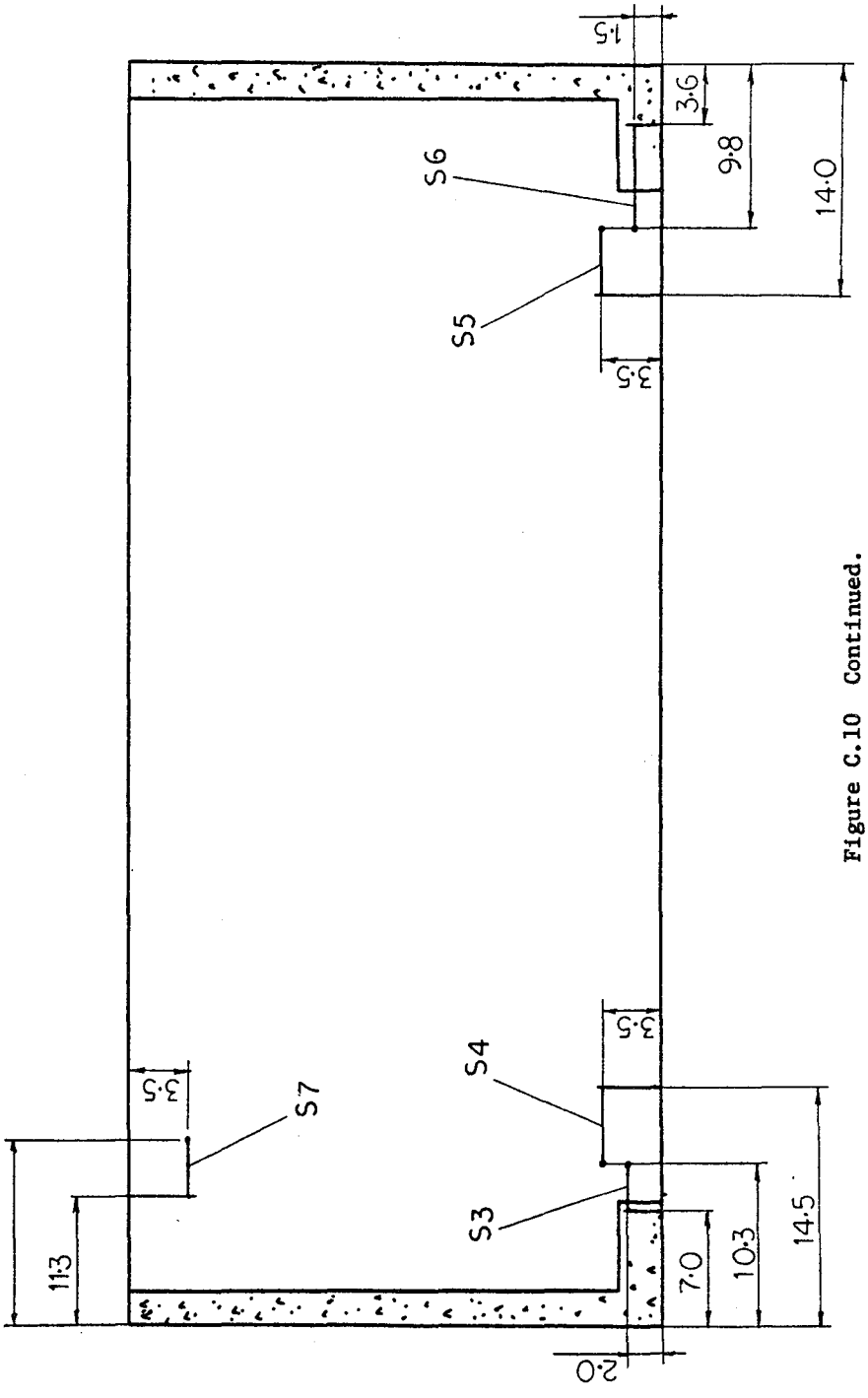

Figure C.10 Continued.

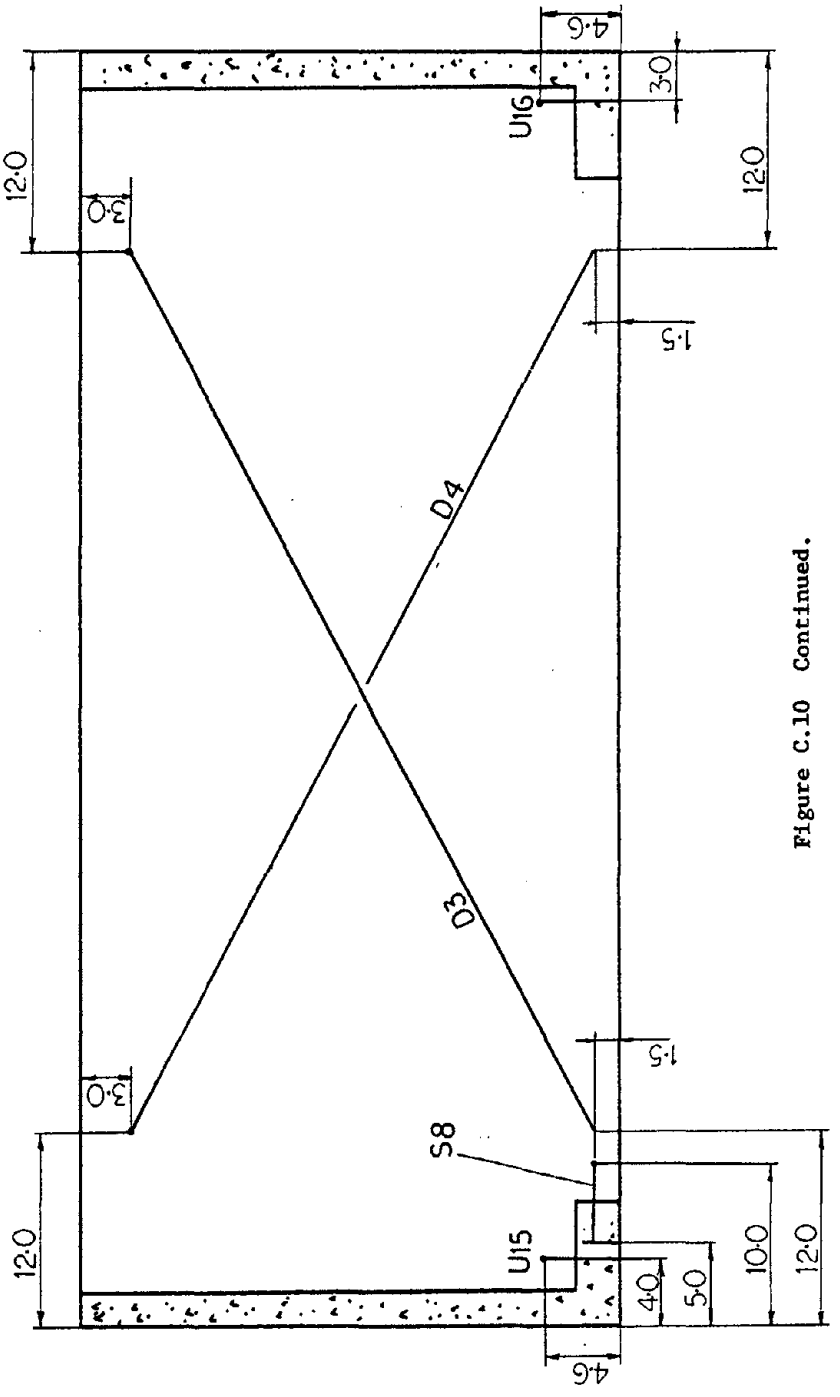

Figure C.10 Continued.

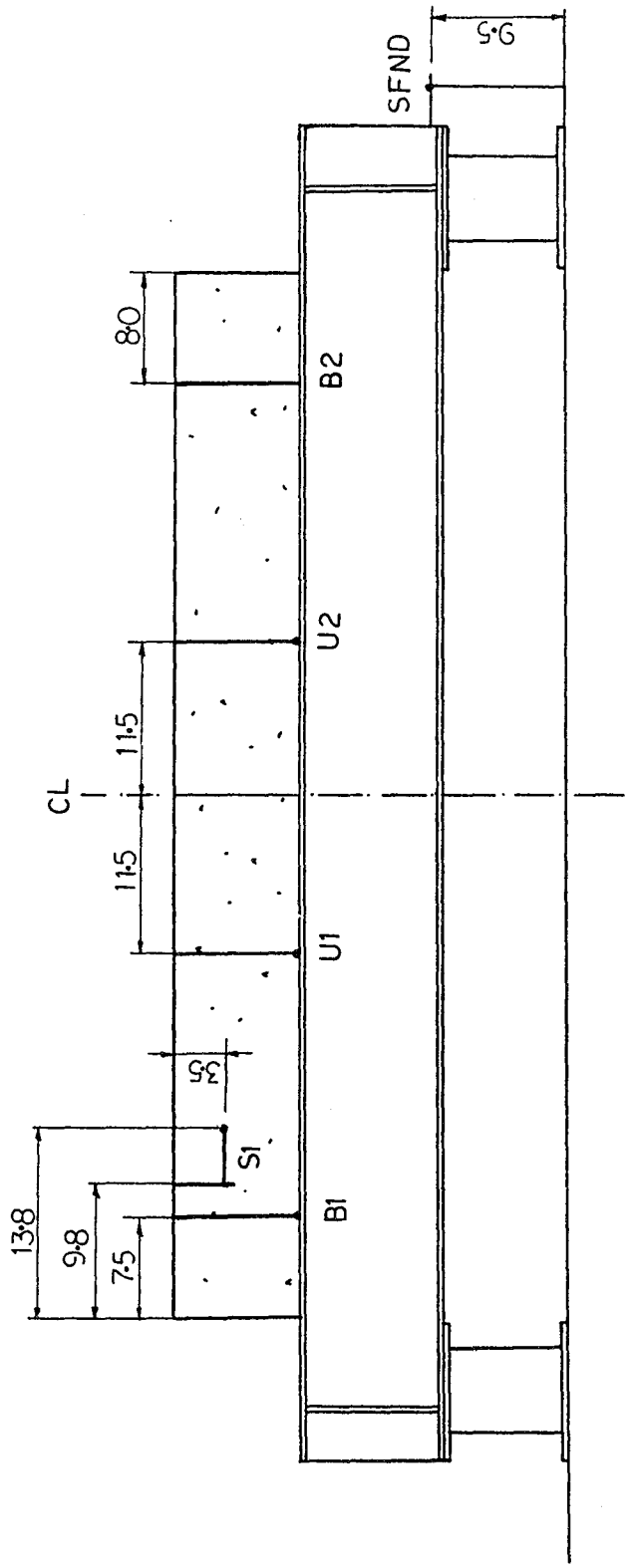

Figure C.11 Location of DCDT's for PZ-II.

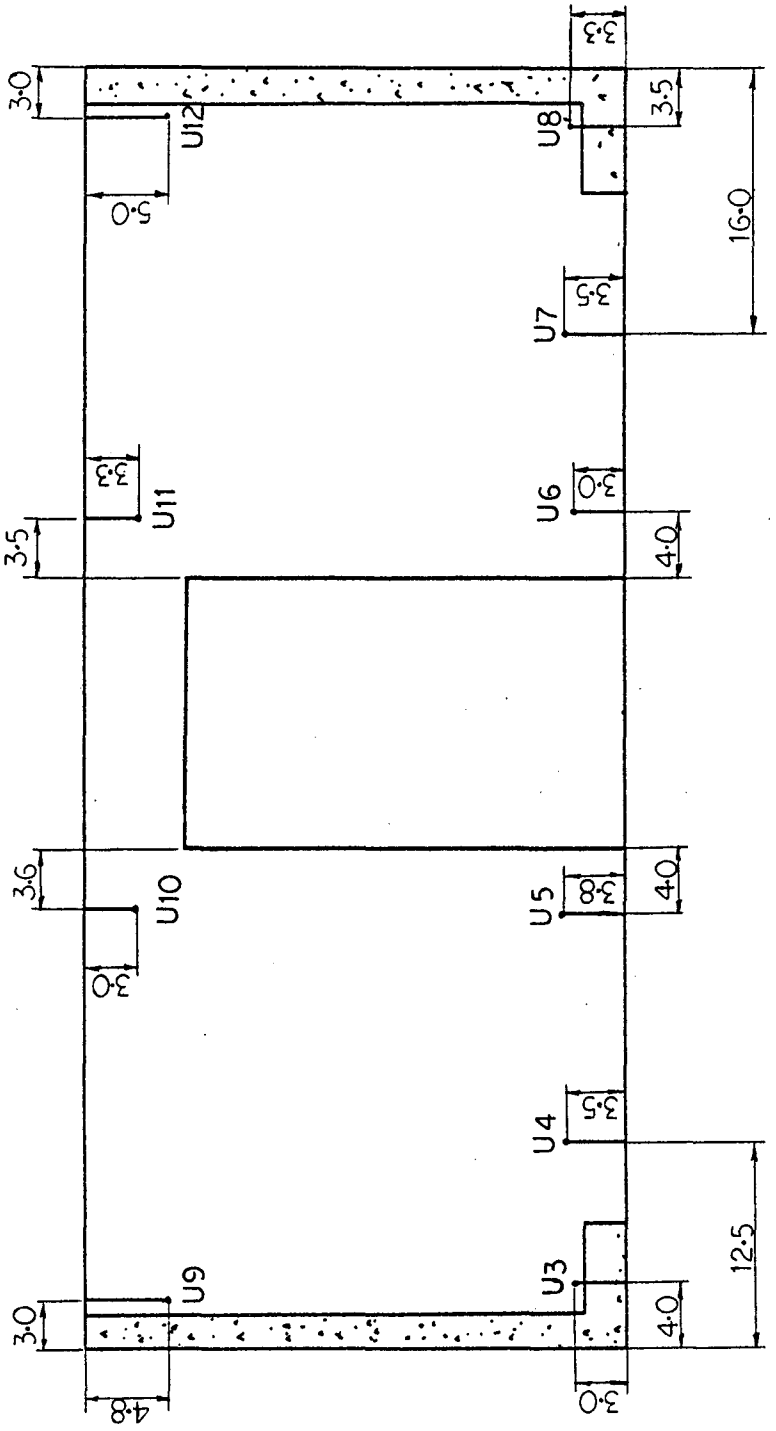

Figure C.11 Continued.

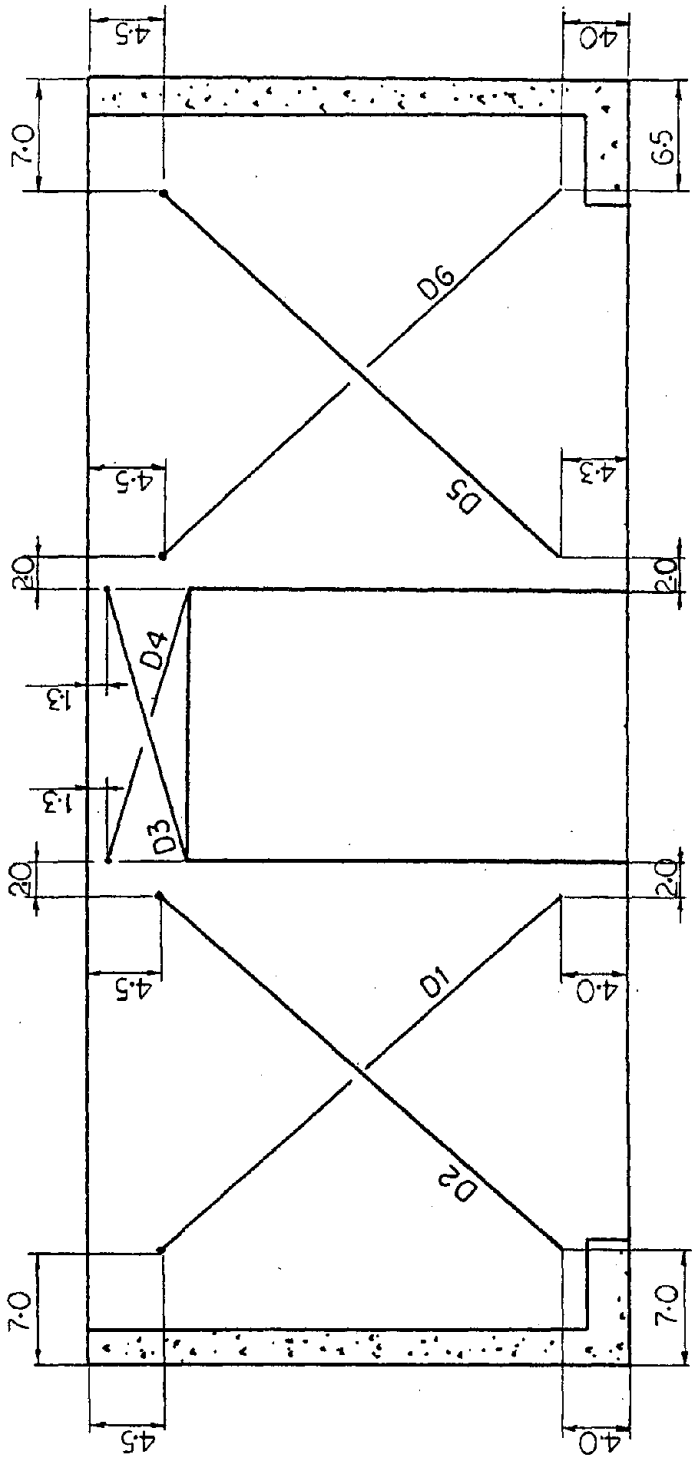

Figure C.11 Continued.

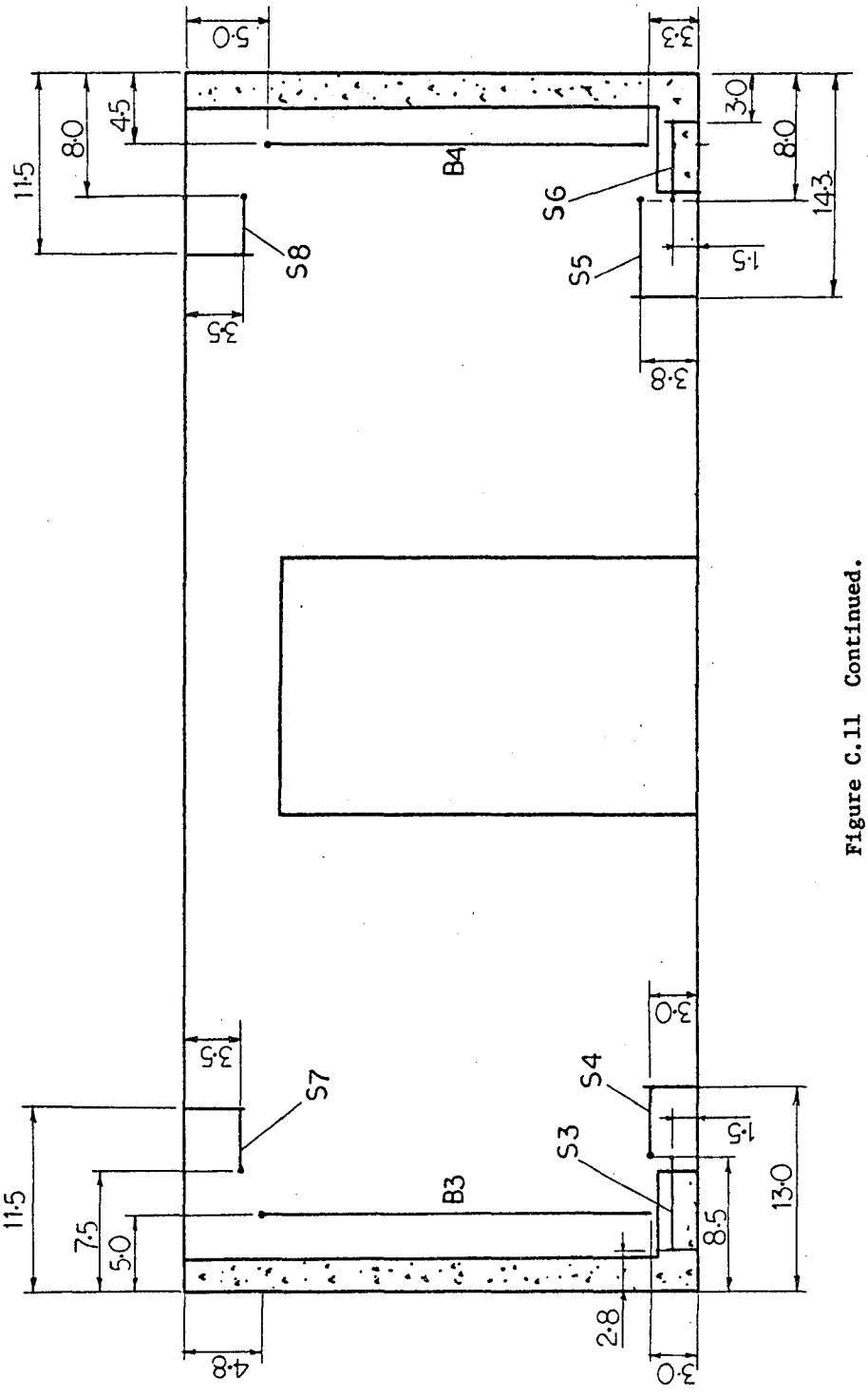

Figure C.11 Continued.

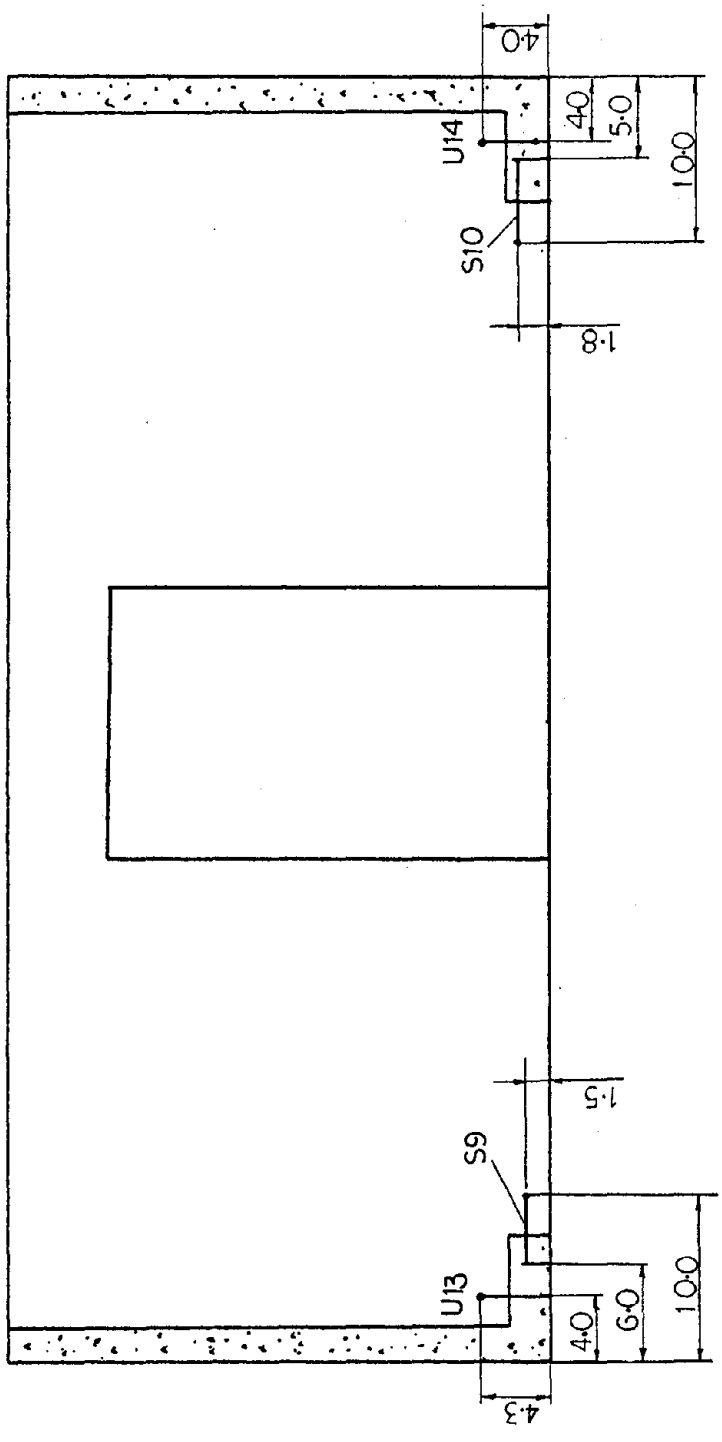

Figure C.11 Continued.

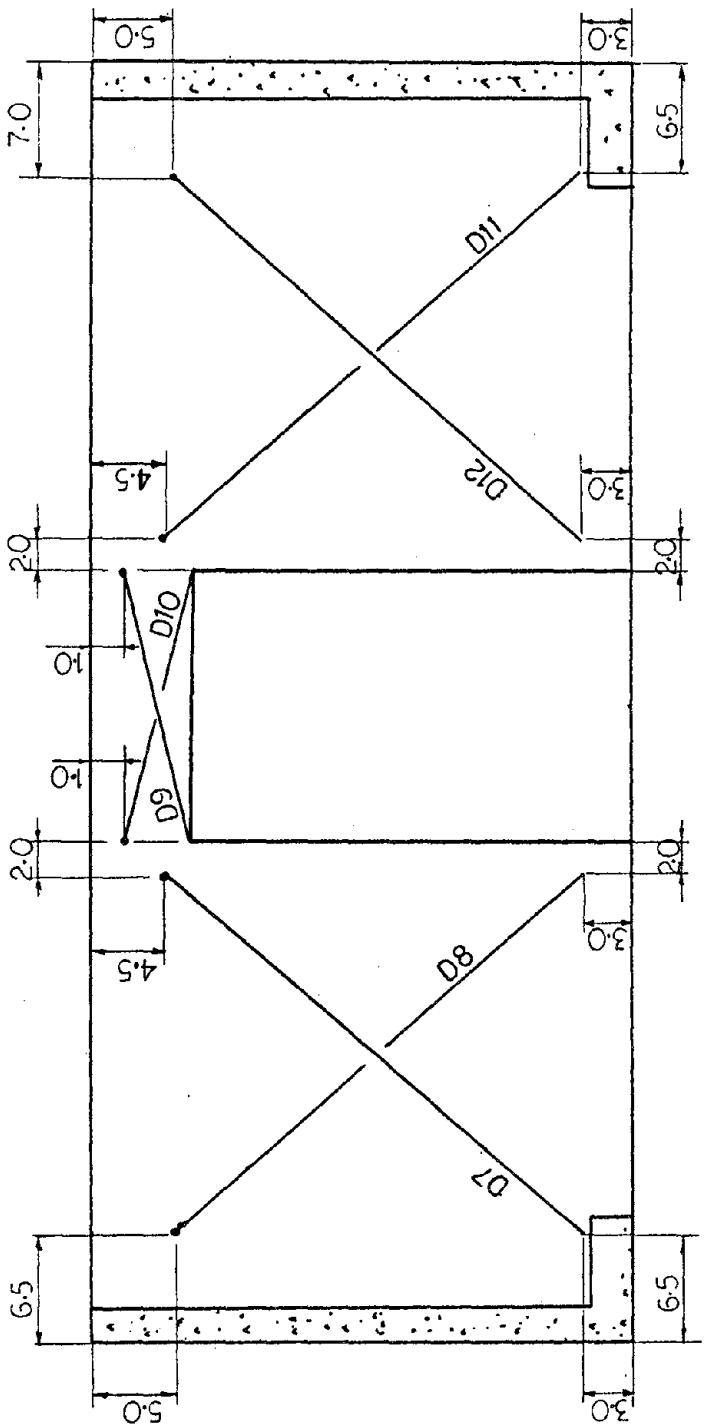

Figure C.11 Continued.

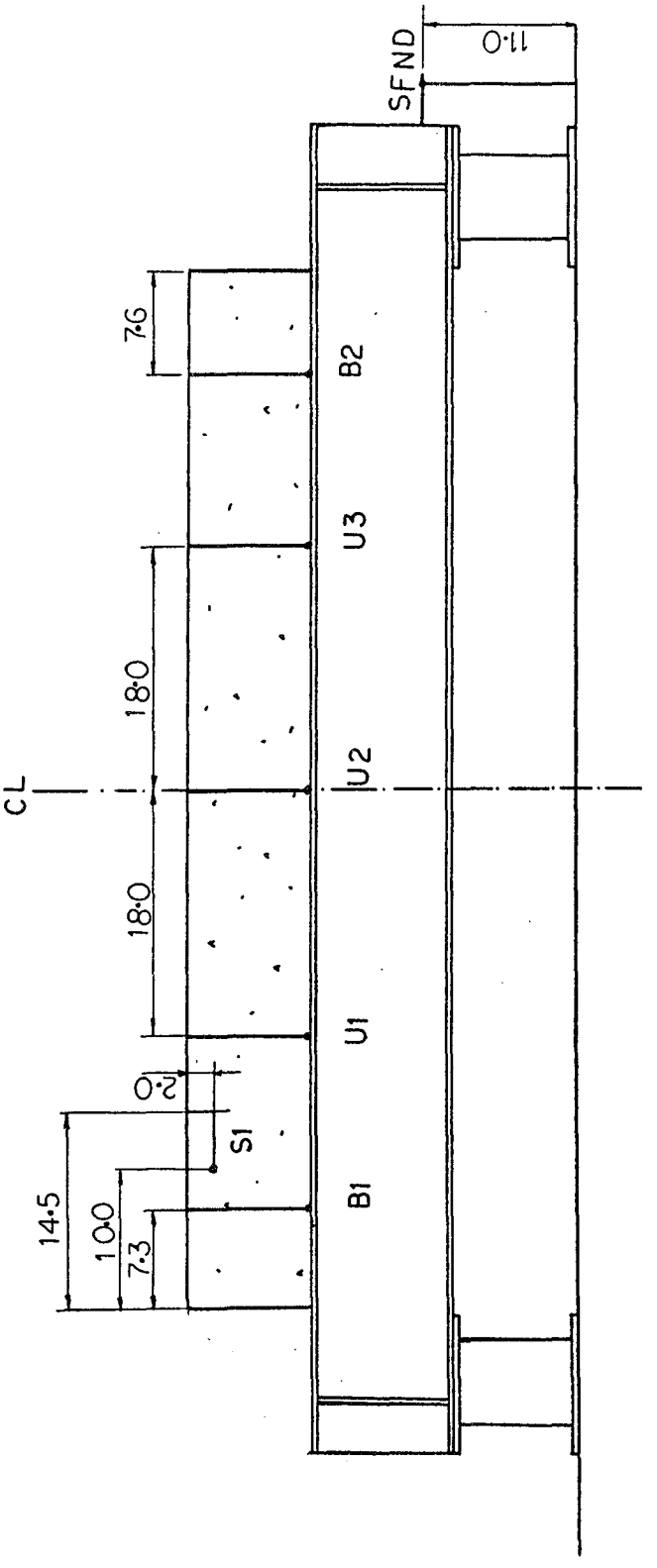

Figure C.12 Location of DCDT's for PZ-III.

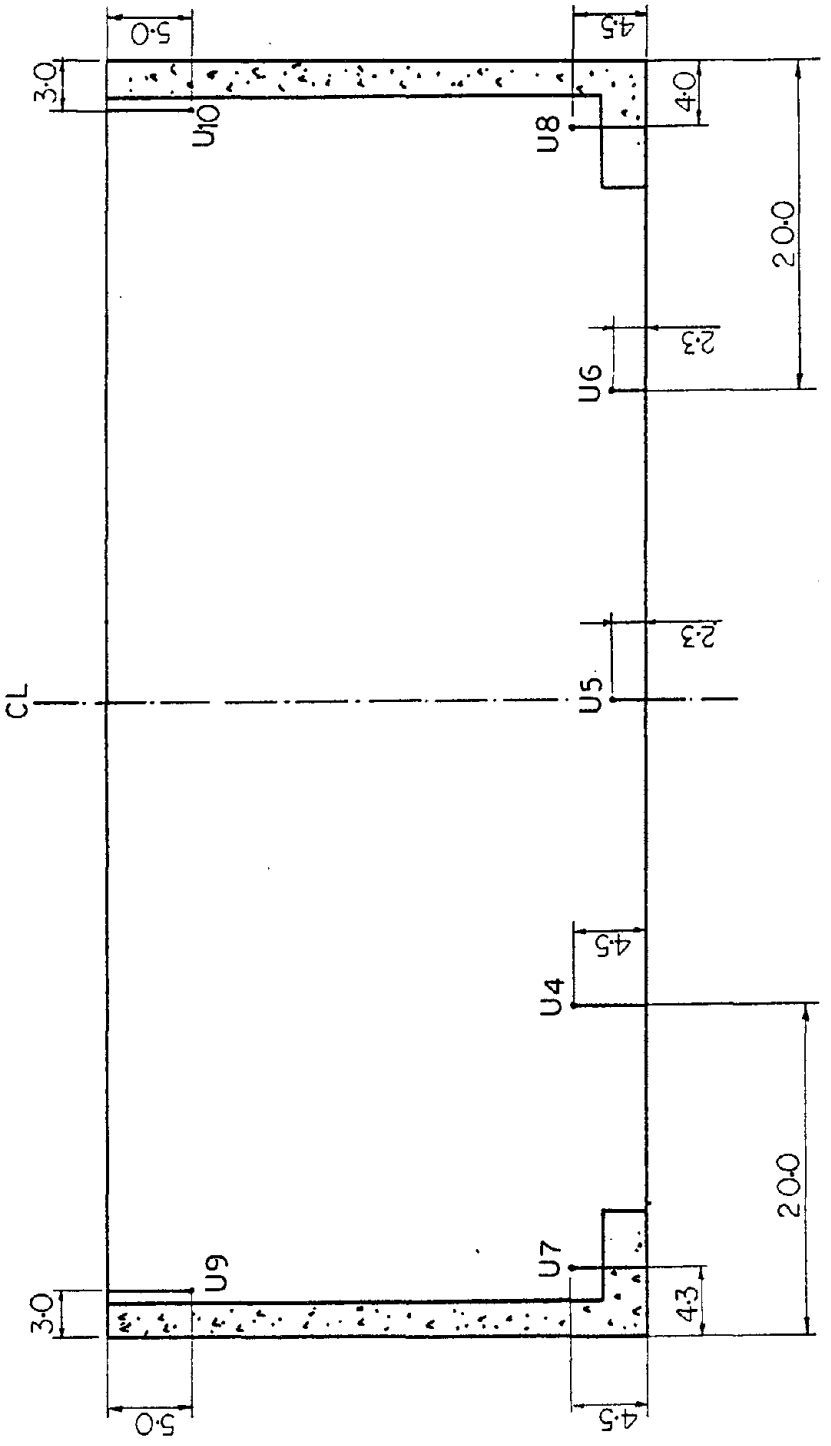

Figure C.12 Continued.

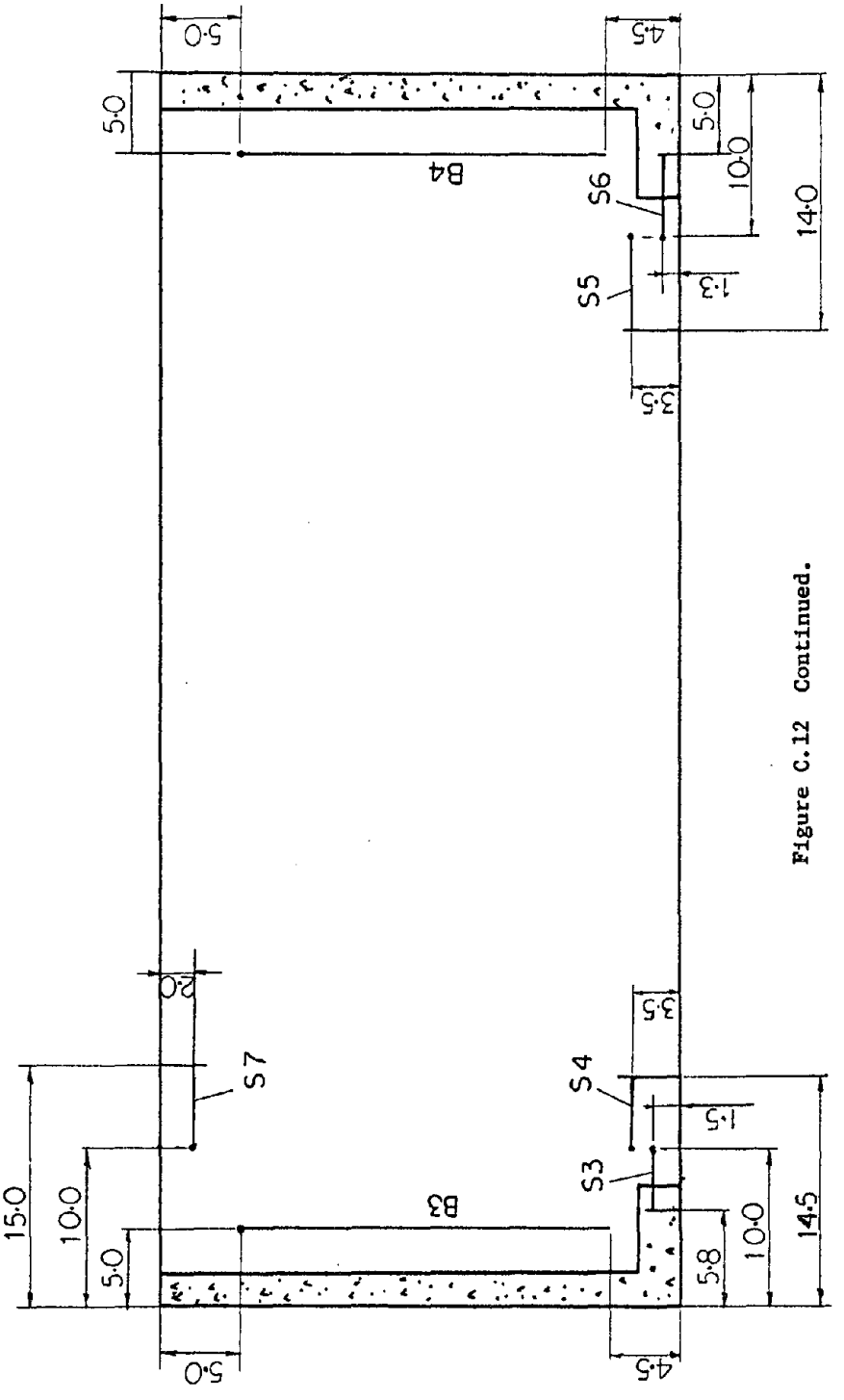

Figure C.12 Continued.

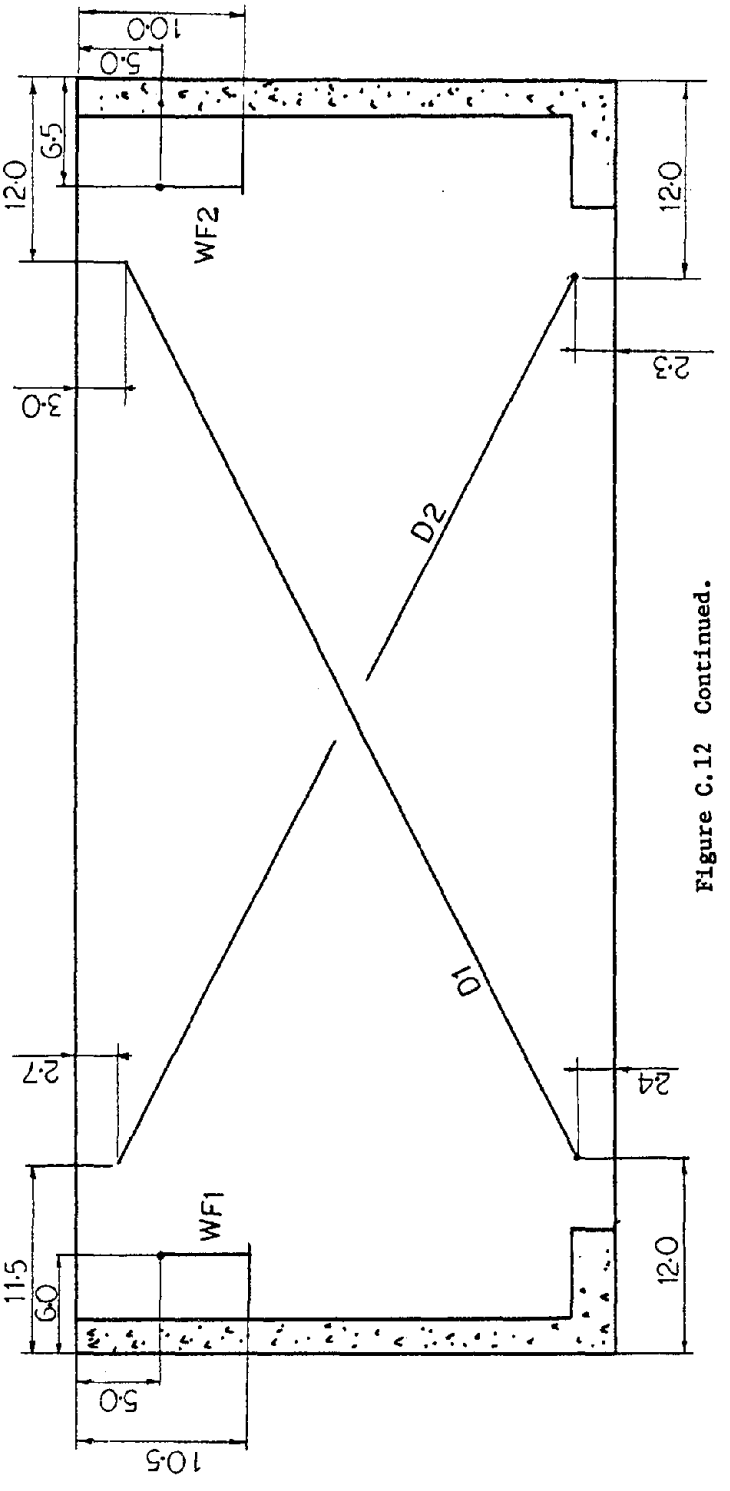

Figure C.12 Continued.

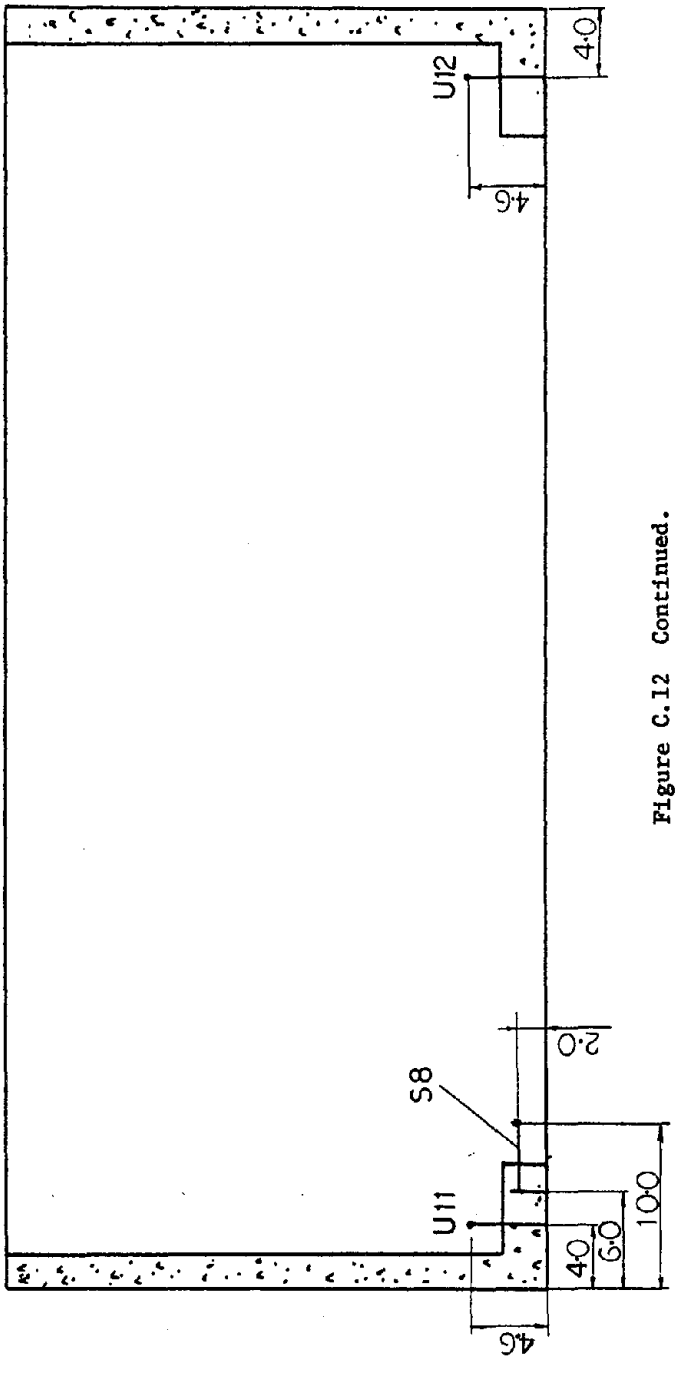

Figure C.12 Continued.

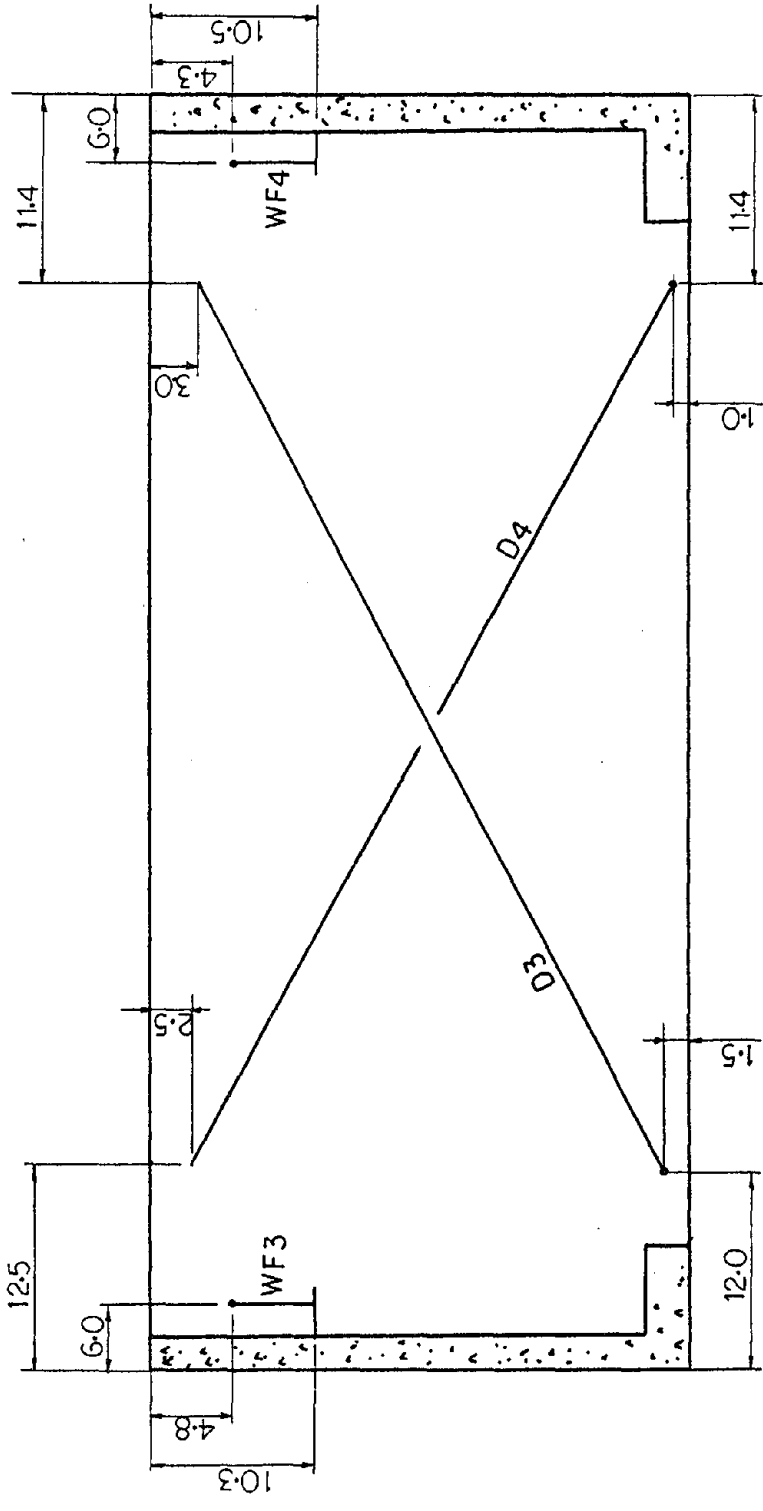

Figure C.12 Continued.

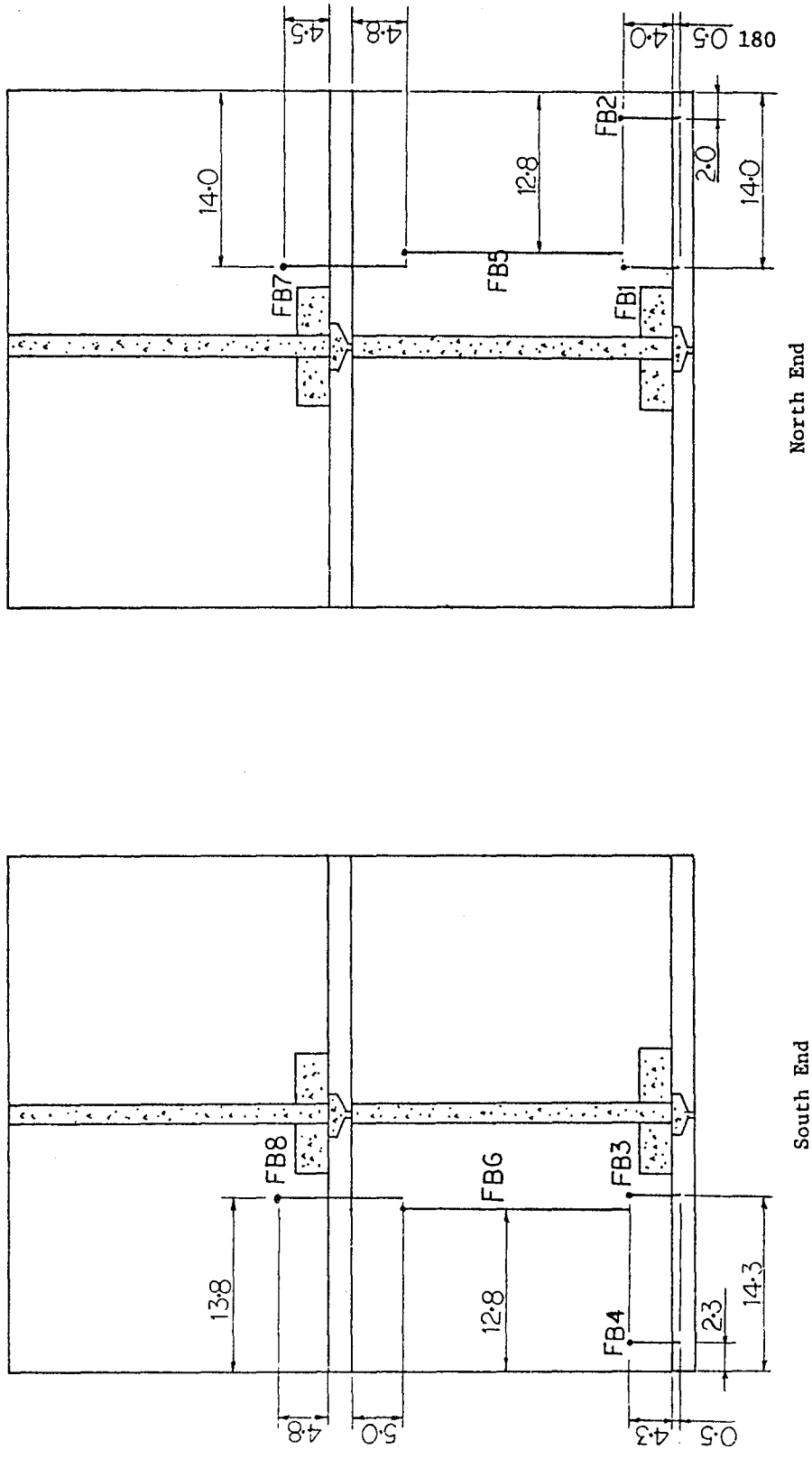

Figure C.12 Continued.

EARTHQUAKE ENGINEERING RESEARCH CENTER REPORTS

NOTE: Numbers in parentheses are Accession Numbers assigned by the National Technical Information Service; these are followed by a price code. Copies of the reports may be ordered from the National Technical Information Service, 5285 Port Royal Road, Springfield, Virginia, 22161. Accession Numbers should be quoted on orders for reports (PB --- ---) and remittance must accompany each order. Reports without this information were not available at time of printing. The complete list of EERC reports (from EERC 67-1) is available upon request from the Earthquake Engineering Research Center, University of California, Berkeley, 47th Street and Hoffman Boulevard, Richmond, California 94804.

UCB/EERC-77/01 "PLUSH - A Computer Program for Probabilistic Finite Element Analysis of Seismic Soil-Structure Interaction," by M.P. Romo Organista, J. Lysmer and H.B. Seed - 1977 (PB81 177 651)A05

UCB/EERC-77/02 "Soil-Structure Interaction Effects at the Humboldt Bay Power Plant in the Ferndale Earthquake of June 7, 1975," by J.E. Valera, H.B. Seed, C.F. Tsai and J. Lysmer - 1977 (PB 265 795)A04

UCB/EERC-77/03 "Influence of Sample Disturbance on Sand Response to Cyclic Loading," by K. Mori, H.B. Seed and C.K. Chan - 1977 (PB 267 352)A04

UCB/EERC-77/04 "Seismological Studies of Strong Motion Records," by J. Shoja-Taheri - 1977 (PB 269 655)A10

UCB/EERC-77/05 Unassigned

UCB/EERC-77/06 "Developing Methodologies for Evaluating the Earthquake Safety of Existing Buildings," by No. 1 - B. Bresler; No. 2 - B. Bresler, T. Okada and D. Zisling; No. 3 - T. Okada and B. Bresler; No. 4 - V.V. Bertero and B. Bresler - 1977 (PB 267 354)A08

UCB/EERC-77/07 "A Literature Survey - Transverse Strength of Masonry Walls," by Y. Omote, R.L. Mayes, S.W. Chen and R.W. Clough - 1977 (PB 277 933)A07

UCB/EERC-77/08 "DRAIN-TABS: A Computer Program for Inelastic Earthquake Response of Three Dimensional Buildings," by R. Guendelman-Israel and G.H. Powell - 1977 (PB 270 693)A07

UCB/EERC-77/09 "SUBWALL: A Special Purpose Finite Element Computer Program for Practical Elastic Analysis and Design of Structural Walls with Substructure Option," by D.Q. Le, H. Peterson and E.P. Popov - 1977 (PB 270 567)A05

UCB/EERC-77/10 "Experimental Evaluation of Seismic Design Methods for Broad Cylindrical Tanks," by D.P. Clough (PB 272 280)A13

UCB/EERC-77/11 "Earthquake Engineering Research at Berkeley - 1976," - 1977 (PB 273 507)A09

UCB/EERC-77/12 "Automated Design of Earthquake Resistant Multistory Steel Building Frames," by N.D. Walker, Jr. - 1977 (PB 276 526)A09

UCB/EERC-77/13 "Concrete Confined by Rectangular Hoops Subjected to Axial Loads," by J. Vallenas, V.V. Bertero and E.P. Popov - 1977 (PB 275 165)A06

UCB/EERC-77/14 "Seismic Strain Induced in the Ground During Earthquakes," by Y. Sugimura - 1977 (PB 284 201)A04

UCB/EERC-77/15 Unassigned

UCB/EERC-77/16 "Computer Aided Optimum Design of Ductile Reinforced Concrete Moment Resisting Frames," by S.W. Zagajeski and V.V. Bertero - 1977 (PB 280 137)A07

UCB/EERC-77/17 "Earthquake Simulation Testing of a Stepping Frame with Energy-Absorbing Devices," by J.M. Kelly and D.F. Tsztoo - 1977 (PB 273 506)A04

UCB/EERC-77/18 "Inelastic Behavior of Eccentrically Braced Steel Frames under Cyclic Loadings," by C.W. Roeder and E.P. Popov - 1977 (PB 275 526)A15

UCB/EERC-77/19 "A Simplified Procedure for Estimating Earthquake-Induced Deformations in Dams and Embankments," by F.I. Makdisi and H.B. Seed - 1977 (PB 276 820)A04

UCB/EERC-77/20 "The Performance of Earth Dams during Earthquakes," by H.B. Seed, F.I. Makdisi and P. de Alba - 1977 (PB 276 821)A04

UCB/EERC-77/21 "Dynamic Plastic Analysis Using Stress Resultant Finite Element Formulation," by P. Lukkunapvasit and J.M. Kelly - 1977 (PB 275 453)A04

UCB/EERC-77/22 "Preliminary Experimental Study of Seismic Uplift of a Steel Frame," by R.W. Clough and A.A. Huckelbridge 1977 (PB 278 769)A08

UCB/EERC-77/23 "Earthquake Simulator Tests of a Nine-Story Steel Frame with Columns Allowed to Uplift," by A.A. Huckelbridge - 1977 (PB 277 944)A09

UCB/EERC-77/24 "Nonlinear Soil-Structure Interaction of Skew Highway Bridges," by M.-C. Chen and J. Penzien - 1977 (PB 276 176)A07

UCB/EERC-77/25 "Seismic Analysis of an Offshore Structure Supported on Pile Foundations," by D.D.-N. Liou and J. Penzien 1977 (PB 283 180)A06

UCB/EERC-77/26 "Dynamic Stiffness Matrices for Homogeneous Viscoelastic Half-Planes," by G. Dasgupta and A.K. Chopra - 1977 (PB 279 654)A06

UCB/EERC-77/27 "A Practical Soft Story Earthquake Isolation System," by J.M. Kelly, J.M. Eidinger and C.J. Derham - 1977 (PB 276 814)A07

UCB/EERC-77/28 "Seismic Safety of Existing Buildings and Incentives for Hazard Mitigation in San Francisco: An Exploratory Study," by A.J. Meltsner - 1977 (PB 281 970)A05

UCB/EERC-77/29 "Dynamic Analysis of Electrohydraulic Shaking Tables," by D. Rea, S. Abedi-Hayati and Y. Takahashi 1977 (PB 282 569)A04

UCB/EERC-77/30 "An Approach for Improving Seismic - Resistant Behavior of Reinforced Concrete Interior Joints," by B. Galunic, V.V. Bertero and E.P. Popov - 1977 (PB 290 870)A06

UCB/EERC-78/01 "The Development of Energy-Absorbing Devices for Aseismic Base Isolation Systems," by J.M. Kelly and D.F. Tsztoo - 1978 (PB 284 978)A04

UCB/EERC-78/02 "Effect of Tensile Prestrain on the Cyclic Response of Structural Steel Connections, by J.G. Bouwkamp and A. Mukhopadhyay - 1978

UCB/EERC-78/03 "Experimental Results of an Earthquake Isolation System using Natural Rubber Bearings," by J.M. Eidinger and J.M. Kelly - 1978 (PB 281 686)A04

UCB/EERC-78/04 "Seismic Behavior of Tall Liquid Storage Tanks," by A. Niwa - 1978 (PB 284 017)A14

UCB/EERC-78/05 "Hysteretic Behavior of Reinforced Concrete Columns Subjected to High Axial and Cyclic Shear Forces," by S.W. Zagajeski, V.V. Bertero and J.G. Bouwkamp - 1978 (PB 283 858)A13

UCB/EERC-78/06 "Three Dimensional Inelastic Frame Elements for the ANSR-I Program," by A. Riahi, D.G. Row and G.H. Powell - 1978 (PB 295 755)A04

UCB/EERC-78/07 "Studies of Structural Response to Earthquake Ground Motion," by O.A. Lopez and A.K. Chopra - 1978 (PB 282 790)A05

UCB/EERC-78/08 "A Laboratory Study of the Fluid-Structure Interaction of Submerged Tanks and Caissons in Earthquakes," by R.C. Byrd - 1978 (PB 284 957)A08

UCB/EERC-78/09 Unassigned

UCB/EERC-78/10 "Seismic Performance of Nonstructural and Secondary Structural Elements," by I. Sakamoto - 1978 (PB81 154 593)A05

UCB/EERC-78/11 "Mathematical Modelling of Hysteresis Loops for Reinforced Concrete Columns," by S. Nakata, T. Sproul and J. Penzien - 1978 (PB 298 274)A05

UCB/EERC-78/12 "Damageability in Existing Buildings," by T. Blejwas and B. Bresler - 1978 (PB 80 166 978)A05

UCB/EERC-78/13 "Dynamic Behavior of a Pedestal Base Multistory Building," by R.M. Stephen, E.L. Wilson, J.G. Bouwkamp and M. Button - 1978 (PB 286 650)A08

UCB/EERC-78/14 "Seismic Response of Bridges - Case Studies," by R.A. Imbsen, V. Nutt and J. Penzien - 1978 (PB 286 503)A10

UCB/EERC-78/15 "A Substructure Technique for Nonlinear Static and Dynamic Analysis," by D.G. Row and G.H. Powell - 1978 (PB 288 077)A10

UCB/EERC-78/16 "Seismic Risk Studies for San Francisco and for the Greater San Francisco Bay Area," by C.S. Oliveira - 1978 (PB 81 120 115)A07

UCB/EERC-78/17 "Strength of Timber Roof Connections Subjected to Cyclic Loads," by P. Gülkan, R.L. Mayes and R.W. Clough - 1978 (HUD-000 1491)A07

UCB/EERC-78/18 "Response of K-Braced Steel Frame Models to Lateral Loads," by J.G. Bouwkamp, R.M. Stephen and E.P. Popov - 1978

UCB/EERC-78/19 "Rational Design Methods for Light Equipment in Structures Subjected to Ground Motion," by J.L. Sackman and J.M. Kelly - 1978 (PB 292 357)A04

UCB/EERC-78/20 "Testing of a Wind Restraint for Aseismic Base Isolation," by J.M. Kelly and D.E. Chitty - 1978 (PB 292 833)A03

UCB/EERC-78/21 "APOLLO - A Computer Program for the Analysis of Pore Pressure Generation and Dissipation in Horizontal Sand Layers During Cyclic or Earthquake Loading," by P.P. Martin and H.B. Seed - 1978 (PB 292 835)A04

UCB/EERC-78/22 "Optimal Design of an Earthquake Isolation System," by M.A. Bhatti, K.S. Pister and E. Polak - 1978 (PB 294 735)A06

UCB/EERC-78/23 "MASH - A Computer Program for the Non-Linear Analysis of Vertically Propagating Shear Waves in Horizontally Layered Deposits," by P.P. Martin and H.B. Seed - 1978 (PB 293 101)A05

UCB/EERC-78/24 "Investigation of the Elastic Characteristics of a Three Story Steel Frame Using System Identification," by I. Kaya and H.D. McNiven - 1978 (PB 296 225)A06

UCB/EERC-78/25 "Investigation of the Nonlinear Characteristics of a Three-Story Steel Frame Using System Identification," by I. Kaya and H.D. McNiven - 1978 (PB 301 363)A05

UCB/EERC-78/26 "Studies of Strong Ground Motion in Taiwan," by Y.M. Hsiung, B.A. Bolt and J. Penzien - 1978 (PB 298 436)A06

UCB/EERC-78/27 "Cyclic Loading Tests of Masonry Single Piers: Volume 1 - Height to Width Ratio of 2," by P.A. Hidalgo, R.L. Mayes, H.D. McNiven and R.W. Clough - 1978 (PB 296 211)A07

UCB/EERC-78/28 "Cyclic Loading Tests of Masonry Single Piers: Volume 2 - Height to Width Ratio of 1," by S.-W.J. Chen, P.A. Hidalgo, R.L. Mayes, R.W. Clough and H.D. McNiven - 1978 (PB 296 212)A09

UCB/EERC-78/29 "Analytical Procedures in Soil Dynamics," by J. Lysmer - 1978 (PB 298 445)A06

UCB/EERC-79/01 "Hysteretic Behavior of Lightweight Reinforced Concrete Beam-Column Subassemblages," by B. Forzani, E.P. Popov and V.V. Bertero - April 1979(PB 298 267)A06

UCB/EERC-79/02 "The Development of a Mathematical Model to Predict the Flexural Response of Reinforced Concrete Beams to Cyclic Loads, Using System Identification," by J. Stanton & H. McNiven - Jan. 1979(PB 295 875)A10

UCB/EERC-79/03 "Linear and Nonlinear Earthquake Response of Simple Torsionally Coupled Systems," by C.L. Kan and A.K. Chopra - Feb. 1979(PB 298 262)A06

UCB/EERC-79/04 "A Mathematical Model of Masonry for Predicting its Linear Seismic Response Characteristics," by Y. Mengi and H.D. McNiven - Feb. 1979(PB 298 266)A06

UCB/EERC-79/05 "Mechanical Behavior of Lightweight Concrete Confined by Different Types of Lateral Reinforcement," by M.A. Manrique, V.V. Bertero and E.P. Popov - May 1979(PB 301 114)A06

UCB/EERC-79/06 "Static Tilt Tests of a Tall Cylindrical Liquid Storage Tank," by R.W. Clough and A. Niwa - Feb. 1979 (PB 301 167)A06

UCB/EERC-79/07 "The Design of Steel Energy Absorbing Restrainers and Their Incorporation into Nuclear Power Plants for Enhanced Safety: Volume 1 - Summary Report," by P.N. Spencer, V.F. Zackay, and E.R. Parker - Feb. 1979(UCB/EERC-79/07)A09

UCB/EERC-79/08 "The Design of Steel Energy Absorbing Restrainers and Their Incorporation into Nuclear Power Plants for Enhanced Safety: Volume 2 - The Development of Analyses for Reactor System Piping,""Simple Systems" by M.C. Lee, J. Penzien, A.K. Chopra and K, Suzuki "Complex Systems" by G.H. Powell, E.L. Wilson, R.W. Clough and D.G. Row - Feb. 1979(UCB/EERC-79/08)A10

UCB/EERC-79/09 "The Design of Steel Energy Absorbing Restrainers and Their Incorporation into Nuclear Power Plants for Enhanced Safety: Volume 3 - Evaluation of Commercial Steels," by W.S. Owen, R.M.N. Pelloux, R.O. Ritchie, M. Faral, T. Ohhashi, J. Toplosky, S.J. Hartman, V.F. Zackay and E.R. Parker - Feb. 1979(UCB/EERC-79/09)A04

UCB/EERC-79/10 "The Design of Steel Energy Absorbing Restrainers and Their Incorporation into Nuclear Power Plants for Enhanced Safety: Volume 4 - A Review of Energy-Absorbing Devices," by J.M. Kelly and M.S. Skinner - Feb. 1979(UCB/EERC-79/10)A04

UCB/EERC-79/11 "Conservatism In Summation Rules for Closely Spaced Modes," by J.M. Kelly and J.L. Sackman - May 1979(PB 301 328)A03

UCB/EERC-79/12 "Cyclic Loading Tests of Masonry Single Piers; Volume 3 - Height to Width Ratio of 0.5," by P.A. Hidalgo, R.L. Mayes, H.D. McNiven and R.W. Clough - May 1979(PB 301 321)A08

UCB/EERC-79/13 "Cyclic Behavior of Dense Course-Grained Materials in Relation to the Seismic Stability of Dams," by N.G. Banerjee, H.B. Seed and C.K. Chan - June 1979(PB 301 373)A13

UCB/EERC-79/14 "Seismic Behavior of Reinforced Concrete Interior Beam-Column Subassemblages," by S. Viwathanatepa, E.P. Popov and V.V. Bertero - June 1979(PB 301 326)A10

UCB/EERC-79/15 "Optimal Design of Localized Nonlinear Systems with Dual Performance Criteria Under Earthquake Excitations," by M.A. Bhatti - July 1979(PB 80 167 109)A06

UCB/EERC-79/16 "OPTDYN - A General Purpose Optimization Program for Problems with or without Dynamic Constraints," by M.A. Bhatti, E. Polak and K.S. Pister - July 1979(PB 80 167 091)A05

UCB/EERC-79/17 "ANSR-II, Analysis of Nonlinear Structural Response, Users Manual," by D.P. Mondkar and G.H. Powell July 1979(PB 80 113 301)A05

UCB/EERC-79/18 "Soil Structure Interaction in Different Seismic Environments," A. Gomez-Masso, J. Lysmer, J.-C. Chen and H.B. Seed - August 1979(PB 80 101 520)A04

UCB/EERC-79/19 "ARMA Models for Earthquake Ground Motions," by M.K. Chang, J.W. Kwiatkowski, R.F. Nau, R.M. Oliver and K.S. Pister - July 1979(PB 301 166)A05

UCB/EERC-79/20 "Hysteretic Behavior of Reinforced Concrete Structural Walls," by J.M. Vallenas, V.V. Bertero and E.P. Popov - August 1979(PB 80 165 905)A12

UCB/EERC-79/21 "Studies on High-Frequency Vibrations of Buildings - 1: The Column Effect," by J. Lubliner - August 1979 (PB 80 158 553)A03

UCB/EERC-79/22 "Effects of Generalized Loadings on Bond Reinforcing Bars Embedded in Confined Concrete Blocks," by S. Viwathanatepa, E.P. Popov and V.V. Bertero - August 1979(PB 81 124 018)A14

UCB/EERC-79/23 "Shaking Table Study of Single-Story Masonry Houses, Volume 1: Test Structures 1 and 2," by P. Gülkan, R.L. Mayes and R.W. Clough - Sept. 1979 (HUD-000 1763)A12

UCB/EERC-79/24 "Shaking Table Study of Single-Story Masonry Houses, Volume 2: Test Structures 3 and 4," by P. Gülkan, R.L. Mayes and R.W. Clough - Sept. 1979 (HUD-000 1836)A12

UCB/EERC-79/25 "Shaking Table Study of Single-Story Masonry Houses, Volume 3: Summary, Conclusions and Recommendations," by R.W. Clough, R.L. Mayes and P. Gülkan - Sept. 1979 (HUD-000 1837)A06

UCB/EERC-79/26 "Recommendations for a U.S.-Japan Cooperative Research Program Utilizing Large-Scale Testing Facilities," by U.S.-Japan Planning Group - Sept. 1979(PB 301 407)A06

UCB/EERC-79/27 "Earthquake-Induced Liquefaction Near Lake Amatitlan, Guatemala," by H.B. Seed, I. Arango, C.K. Chan, A. Gomez-Masso and R. Grant de Ascoli - Sept. 1979(NUREG-CR1341)A03

UCB/EERC-79/28 "Infill Panels: Their Influence on Seismic Response of Buildings," by J.W. Axley and V.V. Bertero Sept. 1979(PB 80 163 371)A10

UCB/EERC-79/29 "3D Truss Bar Element (Type 1) for the ANSR-II Program," by D.P. Mondkar and G.H. Powell - Nov. 1979 (PB 80 169 709)A02

UCB/EERC-79/30 "2D Beam-Column Element (Type 5 - Parallel Element Theory) for the ANSR-II Program," by D.G. Row, G.H. Powell and D.P. Mondkar - Dec. 1979(PB 80 167 224)A03

UCB/EERC-79/31 "3D Beam-Column Element (Type 2 - Parallel Element Theory) for the ANSR-II Program," by A. Riahi, G.H. Powell and D.P. Mondkar - Dec. 1979(PB 80 167 216)A03

UCB/EERC-79/32 "On Response of Structures to Stationary Excitation," by A. Der Kiureghian - Dec. 1979(PB 80166 929)A03

UCB/EERC-79/33 "Undisturbed Sampling and Cyclic Load Testing of Sands," by S. Singh, H.B. Seed and C.K. Chan Dec. 1979(ADA 087 298)A07

UCB/EERC-79/34 "Interaction Effects of Simultaneous Torsional and Compressional Cyclic Loading of Sand," by P.M. Griffin and W.N. Houston - Dec. 1979(ADA 092 352)A15

UCB/EERC-80/01 "Earthquake Response of Concrete Gravity Dams Including Hydrodynamic and Foundation Interaction Effects," by A.K. Chopra, P. Chakrabarti and S. Gupta - Jan. 1980(AD-A087297)A10

UCB/EERC-80/02 "Rocking Response of Rigid Blocks to Earthquakes," by C.S. Yim, A.K. Chopra and J. Penzien - Jan. 1980 (PB80 166 002)A04

UCB/EERC-80/03 "Optimum Inelastic Design of Seismic-Resistant Reinforced Concrete Frame Structures," by S.W. Zagajeski and V.V. Bertero - Jan. 1980(PB80 164 635)A06

UCB/EERC-80/04 "Effects of Amount and Arrangement of Wall-Panel Reinforcement on Hysteretic Behavior of Reinforced Concrete Walls," by R. Iliya and V.V. Bertero - Feb. 1980(PB81 122 525)A09

UCB/EERC-80/05 "Shaking Table Research on Concrete Dam Models," by A. Niwa and R.W. Clough - Sept. 1980(PB81 122 368)A06

UCB/EERC-80/06 "The Design of Steel Energy-Absorbing Restrainers and their Incorporation into Nuclear Power Plants for Enhanced Safety (Vol 1A): Piping with Energy Absorbing Restrainers: Parameter Study on Small Systems," by G.H. Powell, C. Oughourlian and J. Simons - June 1980

UCB/EERC-80/07 "Inelastic Torsional Response of Structures Subjected to Earthquake Ground Motions," by Y. Yamazaki April 1980(PB81 122 327)A08

UCB/EERC-80/08 "Study of X-Braced Steel Frame Structures Under Earthquake Simulation," by Y. Ghanaat - April 1980 (PB81 122 335)A11

UCB/EERC-80/09 "Hybrid Modelling of Soil-Structure Interaction," by S. Gupta, T.W. Lin, J. Penzien and C.S. Yeh May 1980(PB81 122 319)A07

UCB/EERC-80/10 "General Applicability of a Nonlinear Model of a One Story Steel Frame," by B.I. Sveinsson and H.D. McNiven - May 1980(PB81 124 877)A06

UCB/EERC-80/11 "A Green-Function Method for Wave Interaction with a Submerged Body," by W. Kioka - April 1980 (PB81 122 269)A07

UCB/EERC-80/12 "Hydrodynamic Pressure and Added Mass for Axisymmetric Bodies," by F. Nilrat - May 1980(PB81 122 343)A08

UCB/EERC-80/13 "Treatment of Non-Linear Drag Forces Acting on Offshore Platforms," by B.V. Dao and J. Penzien May 1980(PB81 153 413)A07

UCB/EERC-80/14 "2D Plane/Axisymmetric Solid Element (Type 3 - Elastic or Elastic-Perfectly Plastic) for the ANSR-II Program," by D.P. Mondkar and G.H. Powell - July 1980(PB81 122 350)A03

UCB/EERC-80/15 "A Response Spectrum Method for Random Vibrations," by A. Der Kiureghian - June 1980(PB81 122 301)A03

UCB/EERC-80/16 "Cyclic Inelastic Buckling of Tubular Steel Braces," by V.A. Zayas, E.P. Popov and S.A. Mahin June 1980(PB81 124 885)A10

UCB/EERC-80/17 "Dynamic Response of Simple Arch Dams Including Hydrodynamic Interaction," by C.S. Porter and A.K. Chopra - July 1980(PB81 124 000)A13

UCB/EERC-80/18 "Experimental Testing of a Friction Damped Aseismic Base Isolation System with Fail-Safe Characteristics," by J.M. Kelly, K.E. Beucke and M.S. Skinner - July 1980(PB81 148 595)A04

UCB/EERC-80/19 "The Design of Steel Energy-Absorbing Restrainers and their Incorporation into Nuclear Power Plants for Enhanced Safety (Vol 1B): Stochastic Seismic Analyses of Nuclear Power Plant Structures and Piping Systems Subjected to Multiple Support Excitations," by M.C. Lee and J. Penzien - June 1980

UCB/EERC-80/20 "The Design of Steel Energy-Absorbing Restrainers and their Incorporation into Nuclear Power Plants for Enhanced Safety (Vol 1C): Numerical Method for Dynamic Substructure Analysis," by J.M. Dickens and E.L. Wilson - June 1980

UCB/EERC-80/21 "The Design of Steel Energy-Absorbing Restrainers and their Incorporation into Nuclear Power Plants for Enhanced Safety (Vol 2): Development and Testing of Restraints for Nuclear Piping Systems," by J.M. Kelly and M.S. Skinner - June 1980

UCB/EERC-80/22 "3D Solid Element (Type 4-Elastic or Elastic-Perfectly-Plastic) for the ANSR-II Program," by D.P. Mondkar and G.H. Powell - July 1980(PB81 123 242)A03

UCB/EERC-80/23 "Gap-Friction Element (Type 5) for the ANSR-II Program," by D.P. Mondkar and G.H. Powell - July 1980 (PB81 122 285)A03

UCB/EERC-80/24 "U-Bar Restraint Element (Type 11) for the ANSR-II Program," by C. Oughourlian and G.H. Powell July 1980(PB81 122 293)A03

UCB/EERC-80/25 "Testing of a Natural Rubber Base Isolation System by an Explosively Simulated Earthquake," by J.M. Kelly - August 1980(PB81 201 360)A04

UCB/EERC-80/26 "Input Identification from Structural Vibrational Response," by Y. Hu - August 1980(PB81 152 308)A05

UCB/EERC-80/27 "Cyclic Inelastic Behavior of Steel Offshore Structures," by V.A. Zayas, S.A. Mahin and E.P. Popov August 1980(PB81 196 180)A15

UCB/EERC-80/28 "Shaking Table Testing of a Reinforced Concrete Frame with Biaxial Response," by M.G. Oliva October 1980(PB81 154 304)A10

UCB/EERC-80/29 "Dynamic Properties of a Twelve-Story Prefabricated Panel Building," by J.G. Bouwkamp, J.P. Kollegger and R.M. Stephen - October 1980(PB82 117 128)A06

UCB/EERC-80/30 "Dynamic Properties of an Eight-Story Prefabricated Panel Building," by J.G. Bouwkamp, J.P. Kollegger and R.M. Stephen - October 1980(PB81 200 313)A05

UCB/EERC-80/31 "Predictive Dynamic Response of Panel Type Structures Under Earthquakes," by J.P. Kollegger and J.G. Bouwkamp - October 1980(PB81 152 316)A04

UCB/EERC-80/32 "The Design of Steel Energy-Absorbing Restrainers and their Incorporation into Nuclear Power Plants for Enhanced Safety (Vol 3): Testing of Commercial Steels in Low-Cycle Torsional Fatigue," by P. Spencer, E.R. Parker, E. Jongewaard and M. Drory

UCB/EERC-80/33 "The Design of Steel Energy-Absorbing Restrainers and their Incorporation into Nuclear Power Plants for Enhanced Safety (Vol 4): Shaking Table Tests of Piping Systems with Energy-Absorbing Restrainers," by S.F. Stiemer and W.G. Godden - Sept. 1980

UCB/EERC-80/34 "The Design of Steel Energy-Absorbing Restrainers and their Incorporation into Nuclear Power Plants for Enhanced Safety (Vol 5): Summary Report," by P. Spencer

UCB/EERC-80/35 "Experimental Testing of an Energy-Absorbing Base Isolation System," by J.M. Kelly, M.S. Skinner and K.E. Beucke - October 1980(PB81 154 072)A04

UCB/EERC-80/36 "Simulating and Analyzing Artificial Non-Stationary Earthquake Ground Motions," by R.F. Nau, R.M. Oliver and K.S. Pister - October 1980(PB81 153 397)A04

UCB/EERC-80/37 "Earthquake Engineering at Berkeley - 1980," - Sept. 1980(PB81 205 874)A09

UCB/EERC-80/38 "Inelastic Seismic Analysis of Large Panel Buildings," by V. Schricker and G.H. Powell - Sept. 1980 (PB81 154 338)A13

UCB/EERC-80/39 "Dynamic Response of Embankment, Concrete-Gravity and Arch Dams Including Hydrodynamic Interaction," by J.F. Hall and A.K. Chopra - October 1980(PB81 152 324)A11

UCB/EERC-80/40 "Inelastic Buckling of Steel Struts Under Cyclic Load Reversal," by R.G. Black, W.A. Wenger and E.P. Popov - October 1980(PB81 154 312)A08

UCB/EERC-80/41 "Influence of Site Characteristics on Building Damage During the October 3, 1974 Lima Earthquake," by P. Repetto, I. Arango and H.B. Seed - Sept. 1980(PB81 161 739)A05

UCB/EERC-80/42 "Evaluation of a Shaking Table Test Program on Response Behavior of a Two Story Reinforced Concrete Frame," by J.M. Blondet, R.W. Clough and S.A. Mahin

UCB/EERC-80/43 "Modelling of Soil-Structure Interaction by Finite and Infinite Elements," by F. Medina - December 1980(PB81 229 270)A04

UCB/EERC-81/01 "Control of Seismic Response of Piping Systems and Other Structures by Base Isolation," edited by J.M. Kelly - January 1981 (PB81 200 735)A05

UCB/EERC-81/02 "OPTNSR - An Interactive Software System for Optimal Design of Statically and Dynamically Loaded Structures with Nonlinear Response," by M.A. Bhatti, V. Ciampi and K.S. Pister - January 1981 (PB81 218 851)A09

UCB/EERC-81/03 "Analysis of Local Variations in Free Field Seismic Ground Motions," by J.-C. Chen, J. Lysmer and H.B. Seed - January 1981 (AD-A099508)A13

UCB/EERC-81/04 "Inelastic Structural Modeling of Braced Offshore Platforms for Seismic Loading," by V.A. Zayas, P.-S.B. Shing, S.A. Mahin and E.P. Popov - January 1981(PB82 138 777)A07

UCB/EERC-81/05 "Dynamic Response of Light Equipment in Structures," by A. Der Kiureghian, J.L. Sackman and B. Nour-Omid - April 1981 (PB81 218 497)A04

UCB/EERC-81/06 "Preliminary Experimental Investigation of a Broad Base Liquid Storage Tank," by J.G. Bouwkamp, J.P. Kollegger and R.M. Stephen - May 1981(PB82 140 385)A03

UCB/EERC-81/07 "The Seismic Resistant Design of Reinforced Concrete Coupled Structural Walls," by A.E. Aktan and V.V. Bertero - June 1981(PB82 113 358)A11

UCB/EERC-81/08 "The Undrained Shearing Resistance of Cohesive Soils at Large Deformations," by M.R. Pyles and H.B. Seed - August 1981

UCB/EERC-81/09 "Experimental Behavior of a Spatial Piping System with Steel Energy Absorbers Subjected to a Simulated Differential Seismic Input," by S.F. Stiemer, W.G. Godden and J.M. Kelly - July 1981

UCB/EERC-81/10 "Evaluation of Seismic Design Provisions for Masonry in the United States," by B.I. Sveinsson, R.L. Mayes and H.D. McNiven - August 1981 (PB82 166 075)A08

UCB/EERC-81/11 "Two-Dimensional Hybrid Modelling of Soil-Structure Interaction," by T.-J. Tzong, S. Gupta and J. Penzien - August 1981(PB82 142 118)A04

UCB/EERC-81/12 "Studies on Effects of Infills in Seismic Resistant R/C Construction," by S. Brokken and V.V. Bertero - September 1981 (PB82 166 190)A09

UCB/EERC-81/13 "Linear Models to Predict the Nonlinear Seismic Behavior of a One-Story Steel Frame," by H. Valdimarsson, A.H. Shah and H.D. McNiven - September 1981(PB82 138 793)A07

UCB/EERC-81/14 "TLUSH: A Computer Program for the Three-Dimensional Dynamic Analysis of Earth Dams," by T. Kagawa, L.H. Mejia, H.B. Seed and J. Lysmer - September 1981(PB82 139 940)A06

UCB/EERC-81/15 "Three Dimensional Dynamic Response Analysis of Earth Dams," by L.H. Mejia and H.B. Seed - September 1981 (PB82 137 274)A12

UCB/EERC-81/16 "Experimental Study of Lead and Elastomeric Dampers for Base Isolation Systems," by J.M. Kelly and S.B. Hodder - October 1981 (PB82 166 182)A05

UCB/EERC-81/17 "The Influence of Base Isolation on the Seismic Response of Light Secondary Equipment," by J.M. Kelly - April 1981 (PB82 255 266)A04

UCB/EERC-81/18 "Studies on Evaluation of Shaking Table Response Analysis Procedures," by J. Marcial Blondet - November 1981 (PB82 197 278)A10

UCB/EERC-81/19 "DELIGHT.STRUCT: A Computer-Aided Design Environment for Structural Engineering," by R.J. Balling, K.S. Pister and E. Polak - December 1981 (PB82 218 496)A07

UCB/EERC-81/20 "Optimal Design of Seismic-Resistant Planar Steel Frames," by R.J. Balling, V. Ciampi, K.S. Pister and E. Polak - December 1981 (PB82 220 179)A07

UCB/EERC-82/01 "Dynamic Behavior of Ground for Seismic Analysis of Lifeline Systems," by T. Sato and A. Der Kiureghian - January 1982 (PB82 218 926)A05

UCB/EERC-82/02 "Shaking Table Tests of a Tubular Steel Frame Model," by Y. Ghanaat and R. W. Clough - January 1982 (PB82 220 161)A07

UCB/EERC-82/03 "Behavior of a Piping System under Seismic Excitation: Experimental Investigations of a Spatial Piping System supported by Mechanical Shock Arrestors and Steel Energy Absorbing Devices under Seismic Excitation," by S. Schneider, H.-M. Lee and W. G. Godden - May 1982 (PB83 172 544)A09

UCB/EERC-82/04 "New Approaches for the Dynamic Analysis of Large Structural Systems," by E. L. Wilson - June 1982 (PB83 148 080)A05

UCB/EERC-82/05 "Model Study of Effects of Damage on the Vibration Properties of Steel Offshore Platforms," by F. Shahrivar and J. G. Bouwkamp - June 1982 (PB83 148 742)A10

UCB/EERC-82/06 "States of the Art and Practice in the Optimum Seismic Design and Analytical Response Prediction of R/C Frame-Wall Structures," by A. E. Aktan and V. V. Bertero - July 1982 (PB83 147 736)A05

UCB/EERC-82/07 "Further Study of the Earthquake Response of a Broad Cylindrical Liquid-Storage Tank Model," by G. C. Manos and R. W. Clough - July 1982 (PB83 147 744)A11

UCB/EERC-82/08 "An Evaluation of the Design and Analytical Seismic Response of a Seven Story Reinforced Concrete Frame - Wall Structure," by F. A. Charney and V. V. Bertero - July 1982(PB83 157 628)A09

UCB/EERC-82/09 "Fluid-Structure Interactions: Added Mass Computations for Incompressible Fluid," by J. S.-H. Kuo - August 1982 (PB83 156 281)A07

UCB/EERC-82/10 "Joint-Opening Nonlinear Mechanism: Interface Smeared Crack Model," by J. S.-H. Kuo - August 1982 (PB83 149 195)A05

UCB/EERC-82/11 "Dynamic Response Analysis of Techi Dam," by R. W. Clough, R. M. Stephen and J. S.-H. Kuo - August 1982 (PB83 147 496)A06

UCB/EERC-82/12 "Prediction of the Seismic Responses of R/C Frame-Coupled Wall Structures," by A. E. Aktan, V. V. Bertero and M. Piazza - August 1982 (PB83 149 203)A09

UCB/EERC-82/13 "Preliminary Report on the SMART 1 Strong Motion Array in Taiwan," by B. A. Bolt, C. H. Loh, J. Penzien, Y. B. Tsai and Y. T. Yeh - August 1982 (PB83 159 400)A10

UCB/EERC-82/14 "Shaking-Table Studies of an Eccentrically X-Braced Steel Structure," by M. S. Yang - September 1982 (PB83 260 778)A12

UCB/EERC-82/15 "The Performance of Stairways in Earthquakes," by C. Roha, J. W. Axley and V. V. Bertero - September 1982 (PB83 157 693)A07

UCB/EERC-82/16 "The Behavior of Submerged Multiple Bodies in Earthquakes," by W.-G. Liao - Sept. 1982 (PB83 158 709)A07

UCB/EERC-82/17 "Effects of Concrete Types and Loading Conditions on Local Bond-Slip Relationships," by A. D. Cowell, E. P. Popov and V. V. Bertero - September 1982 (PB83 153 577)A04

UCB/EERC-82/18 "Mechanical Behavior of Shear Wall Vertical Boundary Members: An Experimental Investigation," by M. T. Wagner and V. V. Bertero - October 1982 (PB83 159 764)A05

UCB/EERC-82/19 "Experimental Studies of Multi-support Seismic Loading on Piping Systems," by J. M. Kelly and A. D. Cowell - November 1982

UCB/EERC-82/20 "Generalized Plastic Hinge Concepts for 3D Beam-Column Elements," by P. F.-S. Chen and G. H. Powell - November 1982 (PB83 247 981)A13

UCB/EERC-82/21 "ANSR-III: General Purpose Computer Program for Nonlinear Structural Analysis," by C. V. Oughourlian and G. H. Powell - November 1982 (PB83 251 330)A12

UCB/EERC-82/22 "Solution Strategies for Statically Loaded Nonlinear Structures," by J. W. Simons and G. H. Powell - November 1982 (PB83 197 970)A06

UCB/EERC-82/23 "Analytical Model of Deformed Bar Anchorages under Generalized Excitations," by V. Ciampi, R. Eligehausen, V. V. Bertero and E. P. Popov - November 1982 (PB83 169 532)A06

UCB/EERC-82/24 "A Mathematical Model for the Response of Masonry Walls to Dynamic Excitations," by H. Sucuoğlu, Y. Mengi and H. D. McNiven - November 1982 (PB83 169 011)A07

UCB/EERC-82/25 "Earthquake Response Considerations of Broad Liquid Storage Tanks," by F. J. Cambra - November 1982 (PB83 251 215)A09

UCB/EERC-82/26 "Computational Models for Cyclic Plasticity, Rate Dependence and Creep," by B. Mosaddad and G. H. Powell - November 1982 (PB83 245 829)A08

UCB/EERC-82/27 "Inelastic Analysis of Piping and Tubular Structures," by M. Mahasuverachai and G. H. Powell - November 1982 (PB83 249 987)A07

UCB/EERC-83/01 "The Economic Feasibility of Seismic Rehabilitation of Buildings by Base Isolation," by J. M. Kelly - January 1983 (PB83 197 988)A05

UCB/EERC-83/02 "Seismic Moment Connections for Moment-Resisting Steel Frames," by E. P. Popov - January 1983 (PB83 195 412)A04

UCB/EERC-83/03 "Design of Links and Beam-to-Column Connections for Eccentrically Braced Steel Frames," by E. P. Popov and J. O. Malley - January 1983 (PB83 194 811)A04

UCB/EERC-83/04 "Numerical Techniques for the Evaluation of Soil-Structure Interaction Effects in the Time Domain," by E. Bayo and E. L. Wilson - February 1983 (PB83 245 605)A09

UCB/EERC-83/05 "A Transducer for Measuring the Internal Forces in the Columns of a Frame-Wall Reinforced Concrete Structure," by R. Sause and V. V. Bertero - May 1983 (PB84 119 494)A06

UCB/EERC-83/06 "Dynamic Interactions between Floating Ice and Offshore Structures," by P. Croteau - May 1983 (PB84 119 486)A16

UCB/EERC-83/07 "Dynamic Analysis of Multiply Tuned and Arbitrarily Supported Secondary Systems," by T. Igusa and A. Der Kiureghian - June 1983 (PB84 118 272)A11

UCB/EERC-83/08 "A Laboratory Study of Submerged Multi-body Systems in Earthquakes," by G. R. Ansari - June 1983 (PB83 261 842)A17

UCB/EERC-83/09 "Effects of Transient Foundation Uplift on Earthquake Response of Structures," by C.-S. Yim and A. K. Chopra - June 1983 (PB83 261 396)A07

UCB/EERC-83/10 "Optimal Design of Friction-Braced Frames under Seismic Loading," by M. A. Austin and K. S. Pister - June 1983 (PB84 119 288)A06

UCB/EERC-83/11 "Shaking Table Study of Single-Story Masonry Houses: Dynamic Performance under Three Component Seismic Input and Recommendations," by G. C. Manos, R. W. Clough and R. L. Mayes - June 1983

UCB/EERC-83/12 "Experimental Error Propagation in Pseudodynamic Testing," by P. B. Shing and S. A. Mahin - June 1983 (PB84 119 270)A09

UCB/EERC-83/13 "Experimental and Analytical Predictions of the Mechanical Characteristics of a 1/5-scale Model of a 7-story R/C Frame-Wall Building Structure," by A. E. Aktan, V. V. Bertero, A. A. Chowdhury and T. Nagashima - August 1983 (PB84 119 213)A07

UCB/EERC-83/14 "Shaking Table Tests of Large-Panel Precast Concrete Building System Assemblages," by M. G. Oliva and R. W. Clough - August 1983